

**High-valent Iron Intermediates in Nonheme Iron
Catalytic Systems Designed for Hydrocarbon Oxidations**

A THESIS

SUBMITTED TO THE FACULTY OF THE GRADUATE SCHOOL OF
THE UNIVERSITY OF MINNESOTA

By

Subhasree Kal

IN PARTIAL FULFILMENT OF THE REQUIREMENTS
FOR THE DEGREE OF
DOCTOR OF PHILOSOPHY

Prof. Lawrence Que, Jr. Advisor

May 2019

Acknowledgments

My journey through graduate school could not have been completed without the support, encouragement and guidance of a lot of people. I thank you all from the bottom of my heart. I am fortunate to have family and friends who supported me both professionally and personally throughout the past five years.

First, I will like to thank my PhD advisor, Larry Que. Larry taught me how to design experiments strategically, and extract information from not only successful experiments but also from the failed ones to learn new things. He always gave me the freedom and encouraged me to explore different areas, which prepared me to become an independent scientist. Over the past five years I have learned a lot under his mentorship and I will be grateful to him for giving me this incredible opportunity.

Next, I will like to thank all my lab mates, a group of incredible scientists passionate about chemistry. I am honored to have worked with all of you and make some wonderful friends. When I joined the lab, Dr. Caleb Allpress, Dr. Johannes Klein, Mayank Puri and Scott Kleespies taught me the ways of the Que lab and helped me in starting my lab career. I have had multiple scientific discussions with Johannes and Caleb about my projects and their inputs have played an instrumental role in the progress of my projects. I will not forget all the help I received from senior graduate students, Mayank, Scott, Andrew Jasniewski and Anna Komor for my written and oral preliminary exams. As time progressed, I had the opportunity to work with many other highly skilled chemists. Dr. Apparao Draksharapu was an expert in resonance Raman experiments and helped me in collecting resonance Raman data on many unstable intermediates. He also taught me about resonance Raman spectroscopy. My major projects in the Que lab were based on catalysis and I had many helpful discussions about catalytic reaction mechanisms with Dr. Will Oloo. Later, I became part of a spectroscopy-based project started by Dr. Jai Prakash and he patiently guided me through the initial part of the project. Two and a half years after I joined Que lab, Ang Zhou and I formed the EPR team, and I remember running EPR samples for Que

lab continuously for over 4 hours at times. Thank you, Ang for making it an easy experience. I want to thank Dr. Brent Rivard and Dr. Melanie Rogers from the Lipscomb lab for teaching me the details of an EPR spectrometer and specially how to conduct EPR at cryogenic conditions. After Ang graduated, Shuangning Xu took his place in the EPR team and it was great to work with him. Shuangning joined Que lab as an undergraduate student and was familiar with the ways of the Que lab, and so I went to him asking for help with GC, GC-MS and other instruments. He is a very kind person and helped me every time. Saikat Banerjee, Shuangning and I became Que lab graduate students at the same time. Although Saikat's and my projects were very different, he would always ask me interesting questions in my group meetings. Waqas Rasheed is one of the most energetic person in the Que lab and it was wonderful to discuss synthetic chemistry with him. I saw Patrick Crossland, Yuan Sheng and Chase Abelson join Que lab as graduate students during my time in the group. It was fun to work with them and learn about their projects. Chase, Patrick and I were in the same office and had desks next to each other for my last two years in the group. Thank you for making the office so much fun!! Chase and I were also neighbors in the lab (Kolthoff 161).

Que lab always had people from various countries and cultures, which is very exciting to me and I learned so much about these different cultures. I am not going to name all the people from various cultures and countries because that will make my acknowledgment very long, but I want to say that at a time Que lab had people from five different continents. It was very nice to meet you all and work with you. As a group, we had a lot of fun playing board games and video games on Friday evenings while sharing pizza. Patrick and Andrew introduced me to the world of Dungeons and Dragons. Thank you, Caleb, Teresa, Mayank and Nirja for hosting the Dungeons and Dragons hangouts and the summer picnics.

Many people outside Que lab have played an important role in my graduate student career. My work involved a lot of kinetic experiments, and Dr. Rahul Banerjee from Lipscomb lab is an expert on kinetic experiments. He has helped me a lot in analyzing and designing kinetic experiments. Rahul provided me ideas that were critical for the completion of my projects. Debanjan Dhar from Tolman lab was my student contact during admission and he

gave me a lot of insightful information about the various research groups in the chemistry department, which led to my decision in joining the Que lab. Thank you Debanjan! Courtney Elwell from the Tolman lab and I are batch mates and we went through the job search and thesis writing phase together. It was wonderful to share our experiences and concerns throughout the process. We went on multiple trips to ice cream shops during this time. James Moore and Bianca Ramirez from Lu lab are two awesome chemists and wonderful friends. I remember me, Bianca and James going to classes together and working on our assignments in the first year. I am fortunate to have met you two and you guys always encouraged and supported me throughout my time here.

My friends outside the Que lab or the chemistry department have also been an important part of my journey as a graduate student. I want to thank Parvathi, Rituparna and Jibu, my friends from India, who are also currently graduate students in the United States. They have supported me throughout my time as a graduate student. After coming to the US, I have made many wonderful friends in Minneapolis who made me feel at home, Amy, Teresa, Nirja, Sajna, Vaidyanathan, Meera, Kristeen, Arjun. Again, there are many more friends who have helped me during this time whose name I am not able to include to keep the length of the acknowledgment section reasonable, but I thank you all. We went on multiple small trips across the country, which gave me a chance to recharge myself and helped me focus on my work. Sajna, Vaidyanathan, and especially Karthik, another very good friend I made after coming to the US, who is in Boston now, have helped me a lot in the last year of PhD studies in connection to my transition from graduate school to the next step of my career. Thanks to all my friends for making this period of time as a graduate student fun and making me laugh!

Finally, I will like to thank my family, the most important people in my life without whom I would not have been able to reach where I am today. My mother, Sompka Kal, and my father, Santiram Kal, have always believed in me and supported me. Since I was a child, I wanted to become a scientist like my father. He always inspired me. My mother and aunt, Pompa De-Sarkar has been a constant source of strength and encouragement in my life. My elder brother, Subhadeep Kal, have always taken care of me. He lives in New York and

is my only family in the US. Whenever, I wanted a small vacation from graduate school I used to visit him. My sister-in-law, Alexandra Krawicz, is a wonderful person and has always been a source of support when I needed. I have so many fond memories from our trips together! My success as a graduate student and my PhD degree belongs to my family and friends as much as it belongs to me!!

I dedicate this thesis to my parents, Santiram Kal and Sompa Kal, and my elder brother, Subhadeep Kal for their unconditional love and support.

Abstract

Inspired by nonheme iron enzymes, synthetic chemists have developed iron complexes to catalyze hydrocarbon oxidation reactions. High-valent iron intermediates have been proposed to be the oxidant for both enzymes and synthetic catalysts. For future development of catalysts, it is critical to discover and understand pathways for forming high-valent iron oxidants that can perform difficult oxidative transformations such as alkane and aromatic hydroxylation. Additionally, understanding the pathways to generate iron-based oxidants in model synthetic systems can help in elucidating mechanisms of the enzymes.

This thesis describes a new pathway to form reactive high-valent Fe^{V} oxidants by utilizing strong Lewis and Brønsted acids. The acids facilitate heterolytic cleavage of the O–O bond in $\text{Fe}^{\text{III}}\text{–OOH}$ intermediates generated from the reaction of nonheme Fe^{II} complexes and H_2O_2 . This pathway converts an inefficient catalyst for cyclohexane hydroxylation into an efficient catalytic system, forming an Fe^{V} oxidant in the catalytic cycle that hydroxylates cyclohexane within seconds at $-40\text{ }^\circ\text{C}$. This new oxidant can also perform benzene hydroxylation equally efficiently. $\text{Fe}^{\text{III}}(\text{OTf})_3$ is one of the Lewis acids that does this chemistry, giving rise to the first synthetic example where a mononuclear $\text{Fe}^{\text{III}}\text{–OOH}$ intermediate is activated by a second iron(III) ion to form an Fe^{V} oxidant. This work introduces the idea that the second iron in diiron nonheme enzymes can also act as a Lewis acid to activate O_2 and form high-valent iron oxidants like **Q** in sMMO, which oxidizes methane to methanol.

In addition, this thesis explores the importance of ligand topology around the iron center by comparing the effect of Lewis acid on the reactivity of three different catalytic systems. The effect of ligand topology was also investigated in the case of Fe^{V} intermediates that were generated stoichiometrically via one-electron oxidation of two topological isomers of an Fe^{IV} compound. The properties of the isomeric Fe^{V} intermediates, and the effect of Lewis acid in each case were explored.

Table of Contents

| | |
|---|-----------|
| List of Tables | x |
| List of Figures and Schemes | xii |
| List of Abbreviations | xxii |
| List of Compound Abbreviations by Chapter | xxiv |
| | |
| Chapter 1: Bioinspired nonheme iron catalytic systems using H₂O₂ as the terminal oxidant | 1 |
| 1.1. Inspiration and motivation to develop nonheme iron catalysts | 2 |
| 1.2. Nonheme iron catalysts and the various mechanisms to generate the active oxidant | 4 |
| 1.2.1. Water-assisted mechanism | 7 |
| 1.2.2. Non-water-assisted mechanism | 12 |
| 1.2.3. Carboxylic-acid-assisted mechanism | 14 |
| 1.3. Nonheme iron complexes where a Fe ^V (O) oxidant is directly observed | 20 |
| 1.4. Aim and scope of thesis | 28 |
| 1.5. References | 29 |
| | |
| Chapter 2: Activation of [(β-BPMCN)Fe^{III}-OOH]²⁺ intermediate to generate a highly reactive active oxidant using redox-inactive Lewis acidic metal ions or Brønsted acids | 34 |
| 2.1 Introduction | 35 |
| 2.2 Experimental details | 37 |
| 2.3 Effect of redox-inactive Lewis acidic metal ions on catalytic reactivity of [Fe ^{II} (β-BPMCN)] ²⁺ /H ₂ O ₂ | 40 |
| 2.4 Effect of HOAc and HClO ₄ on the reactivity of [Fe ^{II} (β-BPMCN)] ²⁺ /H ₂ O ₂ | 47 |
| 2.5 Characterization of the [(β-BPMCN)Fe ^{III} -OOH] ²⁺ intermediate | 48 |
| | vii |

| | |
|--|----|
| 2.6 Kinetic analysis of the activation of $[(\beta\text{-BPMCN})\text{Fe}^{\text{III}}\text{-OOH}]^{2+}$ by Sc^{3+} and HClO_4 | 52 |
| 2.7 Spectroscopic investigation of the effect of strong Brønsted acids – leading to the choice of HClO_4 as the optimal Brønsted acid | 63 |
| 2.8 Mechanistic isotope labeling studies and the nature of the active oxidant | 65 |
| 2.9 Summary | 69 |
| 2.10 Acknowledgments | 69 |
| 2.11 References | 70 |

Chapter 3: Activation of $[(\beta\text{-BPMCN})\text{Fe}^{\text{III}}\text{-OOH}]^{2+}$ intermediate using $\text{Fe}^{\text{III}}(\text{OTf})_3$: possible implications for O_2 activation by diiron systems **76**

| | |
|---|----|
| 3.1 Introduction | 77 |
| 3.2 Experimental details | 79 |
| 3.3 Effect of $\text{Fe}^{\text{II}}(\text{OTf})_2$ and $\text{Fe}^{\text{III}}(\text{OTf})_3$ on catalytic reactivity of $[\text{Fe}^{\text{II}}(\beta\text{-BPMCN})]^{2+}/\text{H}_2\text{O}_2$ | 82 |
| 3.4 Kinetic analysis of the reaction between $[(\beta\text{-BPMCN})\text{Fe}^{\text{III}}\text{-OOH}]^{2+}$ and $\text{Fe}^{\text{III}}(\text{OTf})_3$ or $\text{Fe}^{\text{II}}(\text{OTf})_2$ | 87 |
| 3.5 Role of $\text{Fe}^{\text{III}}(\text{OTf})_3$ in the activation of the $[\text{Fe}^{\text{II}}(\beta\text{-BPMCN})]^{2+}/\text{H}_2\text{O}_2$ system and possible implications for O_2 activation by diiron enzyme | 91 |
| 3.6 Summary | 98 |
| 3.7 References | 99 |

Chapter 4: Effect of ligand topology on Sc^{3+} -assisted activation of $\text{Fe}^{\text{III}}\text{-OOH}$ intermediates to form high-valent iron-oxidants **102**

| | |
|--|-----|
| 4.1 Introduction | 103 |
| 4.2 Experimental details | 105 |
| 4.3 Effect of $\text{Sc}(\text{OTf})_3$ on the catalytic reactivity of $[\text{Fe}^{\text{II}}(\alpha\text{-BPMCN})]^{2+}/\text{H}_2\text{O}_2$ and $[\text{Fe}^{\text{II}}(\text{TPA})]^{2+}/\text{H}_2\text{O}_2$ | 108 |
| 4.4 Characterization of $[(\alpha\text{-BPMCN})\text{Fe}^{\text{III}}\text{-OOH}]^{2+}$ | 112 |
| 4.5 Kinetic analysis of the behavior of the $\text{Fe}^{\text{III}}\text{-OOH}$ intermediates | 117 |
| 4.6 Kinetic analysis of the effect of $\text{Sc}(\text{OTf})_3$ on the $\text{Fe}^{\text{III}}\text{-OOH}$ intermediates | 124 |
| 4.7 Comparison of the effect of $\text{Sc}(\text{OTf})_3$ on the reactivity of $[\text{Fe}^{\text{II}}(\alpha\text{-BPMCN})]^{2+}$, $[\text{Fe}^{\text{II}}(\beta\text{-BPMCN})]^{2+}$ and $[\text{Fe}^{\text{II}}(\text{TPA})]^{2+}$ | 128 |

| | |
|---|------------|
| 4.8 Summary | 132 |
| 4.9 Acknowledgements | 133 |
| 4.10 References | 133 |
| Chapter 5: Generation and characterization of higher-valent iron species from Fe^{IV}(O) intermediates supported by a macrocyclic ligand framework | 136 |
| 5.1 Introduction | 137 |
| 5.2 Experimental details | 140 |
| 5.3 One electron oxidation of the <i>syn</i> -[(TMC)Fe ^{IV} (O)] ²⁺ to form a formal Fe ^V species | 141 |
| 5.4 Reaction of Fe ^V species with the strong Brønsted acid HClO ₄ and the strong Lewis acid Sc(OTf) ₃ | 147 |
| 5.5 Summary | 154 |
| 5.6 Acknowledgements | 156 |
| 5.7 References | 156 |
| Chapter 6: Conclusions and Perspectives | 159 |
| 6.1 Introduction | 160 |
| 6.2 Activation of [(β-BPMCN)Fe ^{III} -OOH] ²⁺ intermediate to generate a highly reactive active oxidant using redox-inactive Lewis acidic metal ions or Brønsted acids | 162 |
| 6.3 Activation of [(β-BPMCN)Fe ^{III} -OOH] ²⁺ intermediate using Fe ^{III} (OTf) ₃ : possible implications for O ₂ activation by diiron systems | 165 |
| 6.4 Effect of ligand topology on Sc ³⁺ -assisted activation of Fe ^{III} -OOH intermediates to form high-valent iron-oxidants | 168 |
| 6.5 Generation and characterization of high-valent iron species from Fe ^{IV} (O) intermediates supported by a macrocyclic ligand framework | 170 |
| 6.6 Future directions | 173 |
| 6.7 References | 176 |
| Comprehensive list of references | 179 |
| Bibliography | 189 |

List of Tables

| | |
|------------------|---|
| Table 1.1 | Spectroscopic signatures of select Fe ^V (O) and related Fe ^{IV} (O) species (24) |
| Table 2.1 | Hydroxylation of <i>c</i> -C ₆ H ₁₂ and C ₆ H ₆ by 1 /H ₂ O ₂ (43) |
| Table 2.2 | Cyclohexane oxidation results in the presence and the absence of air (43) |
| Table 2.3 | First-row transition metal systems that can perform aromatic hydroxylation of benzene with H ₂ O ₂ as oxidant (45) |
| Table 2.4 | Spectroscopic properties of nonheme Fe ^{III} -OOH and Fe ^{III} -(η^2 -O ₂) intermediates (50) |
| Table 2.5 | Rates for decay of 2 in the presence of cyclohexane and formation of 3 in the presence of benzene with increasing [Sc ³⁺] or [HClO ₄] (57) |
| Table 2.6 | Rates of decay of Fe ^{III} -OOH intermediates at -40 °C, except where noted (61) |
| Table 2.7 | Cyclohexane oxidation rates by high-valent nonheme iron species at -40 °C (62) |
| Table 2.8 | Percentage of ¹⁸ O-incorporation into products from the oxidation of cyclohexane and benzene (66) |
| Table 3.1 | Comparing the oxidative reactivity of the 1 /90% H ₂ O ₂ combination with different acid additives (83) |
| Table 3.2 | Control reactions with Fe ^{III} (OTf) ₃ and Fe ^{II} (OTf) ₂ (85) |
| Table 3.3 | Rates for decay of 2 in the presence of cyclohexane and formation of 3 in the presence of benzene with increasing [Fe ³⁺] or [Fe ²⁺] at -40 °C (89) |
| Table 3.4 | Table comparing decay rates of select nonheme iron intermediates involved in cyclohexane oxidation and their alcohol/ketone (A/K) ratios (96) |

- Table 4.1** Comparing the oxidative reactivity of **1**, **2** and **3** with H₂O₂ in the presence or absence of Sc³⁺ (111)
- Table 4.2** EPR parameters for Fe^{III}-OOH and their related Fe^{III}-X species (116)
- Table 4.3** Spectroscopic signatures of the three Fe^{III}-OOH intermediates discussed in this chapter (117)
- Table 4.4** Rates of Fe^{III}-OPh formation upon addition of Sc³⁺ and benzene to **1/2/3-OOH** (127)
- Table 5.1** Comparison between the different Fe^V species (144)

List of Figures and Schemes

- Figure 1.1** Structures of selected iron complexes ($L = \text{CH}_3\text{CN}$) that represent nonheme iron catalysts discussed in this chapter (4)
- Figure 1.2** (Top) Time trace monitoring absorbance at 540 nm corresponding to $\text{Fe}^{\text{III}}\text{-OOH}$ formed in the oxidation of 1-octene by **1** and H_2O_2 at $-45\text{ }^\circ\text{C}$ in CH_3CN . (Bottom) Time course for formation of products (1,2-octanediol and 1,2-epoxyoctane combined) under same conditions. Black – in the presence of 100 eq H_2O and red – in the presence of 100 eq D_2O . (Reproduced with permission from ref 23; copyright 2013 American Chemical Society) (10)
- Figure 1.3** Time trace monitoring absorbance at 460 nm corresponding to $\text{Fe}^{\text{III}}(\kappa^2\text{-OOAc})$ formed from **1*** and $\text{H}_2\text{O}_2/\text{AcOH}$ in the presence of various substrates and varying concentrations of 1-octene (black half-filled circles represent different concentrations of 1-octene). A = 250 mM cyclohexadiene, B = 250 mM cyclohexene, C = 250 mM cyclooctene, D = 250 mM 1-octene, E = 125 mM 1-octene, F = 62.5 mM 1-octene, G = 250 mM cyclohexane, H = 250 mM *tert*-butyl acrylate, I = no substrate. (Reproduced with permission from ref 33; copyright 2017 American Chemical Society) (18)
- Figure 1.4** Structures of a few representative iron complexes described in this section. (20)
- Figure 1.5** a) Formation of **7a** upon addition of AcOOH to **7** monitored by UV-visible absorption spectroscopy. Inset: EPR of **7a** showing the two $S = \frac{1}{2}$ iron species at $g = 2.20, 2.19, 1.99$ ($\sim 5\%$ iron) (blue) and $g = 2.07, 2.01, 1.95$ ($\sim 40\%$ iron) (red). b) Proposed electronic structures for the two $S = \frac{1}{2}$ species observed in EPR that represents the UV-visible absorption feature

centered at 490 nm attributed to intermediate **7a**. (Reproduced with permission from ref 47; copyright 2015 American Chemical Society) (26)

- Figure 2.1** Effect of redox-inactive Lewis acids on the oxidation of cyclohexane (*c*-C₆H₁₂) and benzene (C₆H₆) by **1** (0.7 mM) and 10 eq H₂O₂ (added all at once) in the presence of 2 eq Lewis acid at r.t. under air, demonstrating that Sc³⁺ is the best of the Lewis acids tried in activating the catalyst/H₂O₂ combination. (41)
- Figure 2.2** Yields in the hydroxylation of C₆H₆ (100 eq relative to **1**) or *c*-C₆H₁₂ (1000 eq) by **1** (0.7 mM) and 10 eq 90% H₂O₂ in CH₃CN at 20 °C under air as a function of [Sc³⁺]. Xⁿ⁺ reflects the averaged results from adding 2 eq Al³⁺, Y³⁺, Yb³⁺, or Zn²⁺ (for individual results see Figure 2.1). (90% H₂O₂ was used as oxidant to minimize Lewis-acid deactivation by water present in the H₂O₂ solution.) (41)
- Figure 2.3** Competitive hydroxylations of cyclohexane (**c**) and benzene (**b**, left) or nitrobenzene (**n**, right) with 0.7 mM **1**, 10 eq H₂O₂, 2 eq Sc³⁺ and 600 eq total substrate. The numbers on the x-axis represent the substrate ratio in the competition experiments. (46)
- Figure 2.4** Yields in the hydroxylation of C₆H₆ (100 eq relative to **1**) or *c*-C₆H₁₂ (1000 eq) by **1** (0.7 mM) and 10 eq 90% H₂O₂ in CH₃CN at 20 °C under air as a function of [HClO₄]. (48)
- Figure 2.5** (a) UV-vis spectrum of **2** formed at -40 °C in CH₃CN from 1 mM **1** and 20 eq H₂O₂; (b) X-band EPR spectrum of **2** obtained at 40 dB at 2 K; (c) resonance Raman spectrum of **2** formed with 2.5 mM **1** and 20 eq H₂O₂ at -30 °C (λ_{exc} 561 nm). (49)
- Figure 2.6** The decay of **2** as monitored by resonance Raman spectroscopy at -30 °C. (λ_{exc} 561 nm). The resonance enhanced Raman peaks at 613 and 802 cm⁻¹ disappear with time along with the Raman peak for H₂O₂ at 870 cm⁻¹. (50)

- Figure 2.7** Decay of **2** in the absence of Sc^{3+} monitored at 545 nm. The reaction solution contains 185 eq cyclohexane w.r.t **1**, and **2** was generated from 0.5 mM **1** with 20 eq. H_2O_2 at $-40\text{ }^\circ\text{C}$. (53)
- Figure 2.8** Decay of **2** upon addition of various eq Sc^{3+} . The reaction solution contains 185 eq cyclohexane w.r.t **1**, and **2** was generated from 0.5 mM **1** with 20 eq. H_2O_2 at $-40\text{ }^\circ\text{C}$. (53)
- Figure 2.9** (a) Spectral changes in the visible region upon reaction of 0.5 mM **1** (dashed black line) in CH_3CN at $-40\text{ }^\circ\text{C}$ with 20 eq H_2O_2 to form **2** (dotted purple lines). Formation of **3** is observed upon subsequent addition of 1 eq Sc^{3+} to **2** (solid blue lines). (b) Time traces monitoring nearly instantaneous changes in absorbance at 545 and 800 nm after addition of 1 eq Sc^{3+} . ■: 545 nm and ○: 800 nm in the presence of C_6H_6 ; ▲: 545 nm in the presence of C_6H_{12} . (54)
- Figure 2.10** Oxidation of substituted benzene substrates with electron-withdrawing substituents upon addition of 1 eq. Sc^{3+} to the $\text{Fe}^{\text{III}}\text{-OOH}$ intermediate **2** formed from 0.5 mM **1** at $-40\text{ }^\circ\text{C}$ in CH_3CN . (a) Absorption spectra showing formation of the Fe^{III} -phenolate complexes upon addition of Sc^{3+} to **2**. (b) Time traces monitoring formation of the Fe^{III} -phenolate products at wavelengths where the Fe^{III} -phenolate complexes have absorption but not intermediate **2**. (54)
- Figure 2.11** (a) Time traces monitoring decay of **2** at 545 nm in the presence of 185 eq cyclohexane (■) and formation of **3** at 800 nm with 100 eq benzene (○) showing the effect of increasing $[\text{Sc}^{3+}]$ (green: 1 eq; red: 2 eq; black: 8 eq Sc^{3+}). (b) $[\text{Sc}^{3+}]$ dependence of k_{obs} for **2** decay with cyclohexane as substrate (■) or **3** formation (○) with benzene as substrate. (56)
- Figure 2.12** $[\text{HClO}_4]$ dependence of rates for the decay of **2** with cyclohexane as substrate (■) or the formation of **3** (○) with benzene as substrate. (56)

- Figure 2.13** Time traces monitoring formation of **3** under two different scenarios. Black: 20 eq H₂O₂ was added to the solution containing 0.5 mM **1**, 100 eq benzene and 1 eq Sc³⁺ at -40 °C. Red: 1 eq Sc³⁺ was added to a solution of pre-formed intermediate **2** generated by adding 20 eq H₂O₂ to a solution of 0.5 mM **1** and 100 eq benzene at -40 °C. (59)
- Figure 2.14** Effect of a) 4 eq HClO₄ b) 4 eq HBF₄·Et₂O and c) 4 eq HNO₃ when added to **2** in the presence of benzene. **2** is formed by reacting 20 eq H₂O₂ to 0.5 mM **1** in the presence of 100 eq benzene as substrate at -40 °C. Time traces monitor nearly instantaneous changes in absorbance at 545, 620 and 800 nm after addition of 4 eq acid in each case. (64)
- Figure 2.15** Effect of water on cyclohexane oxidation. Fe^{II}(β-BPMCN) (1 mM) + 1000 eq cyclohexane + 10 eq H₂O₂ (90%) + 2 eq Sc³⁺ + varying amounts of H₂O at 20 °C. (67)
- Figure 3.1** a) Iron complex (**1**) (L = CH₃CN) used in this study. b) The hydroperoxoiron(III) intermediate (**2**) formed with 1 mM (**1**) and 20 eq H₂O₂ at -40 °C in CH₃CN. (79)
- Figure 3.2** Effect of Fe^{III}(OTf)₃ on cyclohexane and benzene oxidation reactions catalyzed by **1** and comparisons with Sc^{III}(OTf)₃ and Fe^{II}(OTf)₂. Reaction conditions: **1** (0.7 mM), 1000 eq cyclohexane or 100 eq benzene, 10 eq 90% H₂O₂ in CH₃CN at room temperature. (82)
- Figure 3.3** Oxidation of substituted benzene analogs with electron-withdrawing substituents upon addition of 4 eq Fe³⁺ to the Fe^{III}-OOH intermediate **2** formed from 0.5 mM **1** at -40 °C in CH₃CN. Absorption spectra showing formation of the corresponding Fe^{III}-phenolate complexes upon addition of Fe³⁺ to **2**. (87)
- Figure 3.4** a) Formation of **3** upon addition of Fe³⁺ to **2**, which is formed by reacting H₂O₂ with **1** at -40 °C in CH₃CN. Dashed black trace **1**, dotted purple trace **2**, solid blue trace **3**. b) Mⁿ⁺ (Sc³⁺, Fe³⁺, Fe²⁺) concentration dependence on

rates of **3** formation or **2** decay at -40°C . Sc^{3+} (blue); Fe^{3+} (red) and Fe^{2+} (green). Open circles for benzene and filled squares for cyclohexane. (88)

Figure 3.5 Time trace monitoring absorbance at 545 nm corresponding to **2** and at 620 and 800 nm corresponding to **3** at -40°C . 800 nm is monitored for **3** because at 800 nm there is no interference from **2**. In these reactions, 4 eq $\text{Fe}^{\text{III}}(\text{OTf})_3$ (a) or 4 eq $\text{Fe}^{\text{II}}(\text{OTf})_2$ was added to a pre-formed solution of **2** containing 100 eq benzene. Intermediate **2** is generated from the reaction of **1** (0.5 mM) and 20 eq H_2O_2 . (90)

Figure 3.6 Time traces monitoring the absorbances at 545 nm corresponding to **2** and at 620 and 800 nm corresponding to **3**. In these reactions, 20 eq H_2O_2 was added to solutions of **1** (0.5 mM), 100 eq benzene and 4 eq $\text{Fe}^{\text{III}}(\text{OTf})_3$ (a) or $\text{Fe}^{\text{II}}(\text{OTf})_2$ (b) at -40°C . (91)

Figure 3.7 Effect of addition of (a) $\text{Fe}^{\text{III}}(\text{OTf})_3$ to $\text{Fe}^{\text{IV}}(\text{O})$ and (b) $\text{Sc}^{\text{III}}(\text{OTf})_3$ to $\text{Fe}^{\text{IV}}(\text{O})$ obtained from the reaction of **1** with 2-($^t\text{BuSO}_2$)- $\text{C}_6\text{H}_4\text{IO}$ in acetonitrile at -40°C containing 100 eq benzene. (94)

Figure 4.1 a) Effect of $\text{Sc}(\text{OTf})_3$ on yields of cyclohexanol (solid bars) and cyclohexanone (patterned bars) from cyclohexane oxidation catalysed by **1**, **2** and **3**. b) Effect of $\text{Sc}(\text{OTf})_3$ on yields of phenol from benzene oxidation catalysed by **1**, **2** and **3**. Reaction conditions: **1/2/3** (0.7 mM), 1000 eq cyclohexane or 100 eq benzene, 10 eq 90% H_2O_2 in CH_3CN at room temperature. Right: The three catalysts compared here. (110)

Figure 4.2 a) UV-vis spectrum of **1-OOH** formed at 15°C in CH_3CN from 1 mM **1** and 20 eq H_2O_2 . A ChemDraw representation of **1-OOH** ($\text{L} = \text{CH}_3\text{CN}$) is shown along with the UV-vis spectrum. b) X-band EPR spectrum of **1-OOH** obtained at 2K at 30 db. c) Resonance Raman spectrum of **1-OOH** after subtracting the spectrum of the decayed intermediate. **1-OOH** formed from 2.5 mM **1** and 20 eq H_2O_2 at -20°C . *denotes a solvent peak from CH_3CN .

Resonance Raman spectra were collected at -40 °C using a 561-nm laser. (114)

Figure 4.3 Time trace monitoring absorbance at 555 nm corresponding to **1-OOH** at different temperatures. Below -20 °C no accumulation of **1-OOH** was observed. **1-OOH** was obtained from the reaction of 1 mM **1** and 20 eq H₂O₂. (115)

Figure 4.4 a) Resonance Raman spectrum of **1-OOH** (red) overlaid on the spectrum obtained from the same sample after **1-OOH** decayed (black). b) Resonance Raman spectrum of **1-OOH** after subtracting the spectrum of the decayed intermediate (same as shown in Figure 4.2). **1-OOH** formed from 2.5 mM **1** and 20 eq H₂O₂ at -20 °C. Spectrum was measured at -40 °C with 561-nm laser excitation. (115)

Figure 4.5 Left: Time traces monitoring formation and decay of **1-OOH**, **2-OOH** and **3-OOH** in the absence of any substrate. All experiments were performed at 0 °C. 10 eq H₂O₂ was added to 2.5 mM solutions of **1**, **2** and **3** in CH₃CN. Right: ChemDraw representations of **1-OOH**, **2-OOH** and **3-OOH**. (118)

Figure 4.6 a) A ChemDraw structure of **2-OOH** (L = CH₃CN). (b-d) Time traces monitoring evolution of **2-OOH** upon addition of substrates. b) 1-octene was added to **2-OOH** formed from 1mM **2** and 10 eq H₂O₂ at -40 °C in CH₃CN. c) tert-butyl acrylate and d) cyclooctene was added to **2-OOH** formed from 1mM **2** and 20 eq H₂O₂ at -15 °C in CH₃CN. We have separated the plots for each concentration by adding a fixed Δ time between the individual plots for clarity of comparison. For a) 1-octene: Δ time = 200 s, b) tert-butyl acrylate: Δ time = 40 s, c) cyclooctene: Δ time = 50 s. (121)

Figure 4.7 a) A ChemDraw structure of **1-OOH** (L = CH₃CN). b) Time traces for the evolution of **1-OOH** upon addition of 1-octene. **1-OOH** was formed from 1 mM **1** and 10 eq H₂O₂ at 0 °C in CH₃CN. The plots for each concentration were each right-shifted by 100 s for clarity of comparison. (123)

Figure 4.8 a) Time trace monitoring reaction of **2-OOH** (at 545 nm) with 1 eq Sc^{3+} in the presence of cyclohexane (185 eq relative to **2**) at $-40\text{ }^{\circ}\text{C}$. b) Time trace monitoring reaction of **3-OOH** (at 540 nm) with consecutive addition of 1 eq Sc^{3+} up to 5 eq of Sc^{3+} in the presence of cyclohexane (185 eq relative to **3**) at $-40\text{ }^{\circ}\text{C}$. c) Time trace monitoring formation of **2-OPh** (at 800 nm) upon addition of 1 eq Sc^{3+} to **2-OOH** in the presence of benzene (100 eq relative to **2**) at $-40\text{ }^{\circ}\text{C}$. d) Time trace monitoring formation of **3-OPh** (at 750 nm) upon addition of 1 eq Sc^{3+} to **3-OOH** in the presence of benzene (100 eq relative to **3**) at $-40\text{ }^{\circ}\text{C}$. (125)

Figure 4.9 a) Comparison of time traces monitoring formation of **1/2/3-OOH** at their corresponding λ_{max} for the first 300 s at $-20\text{ }^{\circ}\text{C}$. b-d) Time traces monitoring formation of b) **1-OPh** (at 850 nm), c) **2-OPh** (at 800 nm) and d) **3-OPh** (at 750 nm) upon addition of 1 eq Sc^{3+} and 100 eq benzene to **1/2/3-OOH** at $-20\text{ }^{\circ}\text{C}$. Rates of formation of **1/2/3-OPh** are obtained by fitting the data with first order exponential equations. (127)

Figure 5.1 Structures of the two isomeric $[(\text{TMC})\text{Fe}^{\text{IV}}(\text{O})]^{2+}$ complexes and their crystal structures.^{14,17} Left: *anti*- $[(\text{TMC})\text{Fe}^{\text{IV}}(\text{O})]^{2+}$ (**1**) has all four methyl groups on the opposite side of the oxo unit. Right: *syn*- $[(\text{TMC})\text{Fe}^{\text{IV}}(\text{O})]^{2+}$ (**2**) has all four methyl groups on the same side as the oxo unit. (Reproduced with permission from ref 14 and ref 17; copyright 2003 American Association for the Advancement of Science and 2015 American Chemical Society) (138)

Figure 5.2 a) UV-vis absorption spectra of *syn*- $[(\text{TMC})\text{Fe}^{\text{IV}}=\text{O}]^{2+}$ (**2**) and the corresponding Fe^{V} species (**2a**) at $-40\text{ }^{\circ}\text{C}$ in CH_3CN obtained by adding $^t\text{BuOOH}$ and NBu_4OH to **2**. b) Comparison of UV-vis absorption spectra of **1**, **2**, **1a** and **2a**. (142)

Figure 5.3 a) UV-vis absorption spectra of *syn*- $[(\text{TMC})\text{Fe}^{\text{IV}}(\text{O})]^{2+}$ (**2**) and the species formed upon addition of base NBu_4OH at $-40\text{ }^{\circ}\text{C}$ in CH_3CN . Inset: Zoomed in view between 600 nm and 1000 nm. (145)

- Figure 5.4** X-band EPR spectrum of **2a** obtained at 2 K at 35 db. (146)
- Figure 5.5** Time traces monitoring the absorbance at 400 nm corresponding to **2a** in the absence of any substrate, upon addition of DHA (4 eq) (due to low solubility) and PhSMe (200 eq) at -40 °C in CH₃CN. The substrates are added upon maximum formation of **2a**. (147)
- Figure 5.6** a) UV-vis absorption spectra of **2**, **2a** and **2a-H⁺** at -40 °C in CH₃CN. b) Time traces monitoring the absorbance at 400 nm and 640 nm. At 400 nm both **2a** and **2a-H⁺** absorb, however, at 640 nm only **2a-H⁺** absorbs. The black vertical line denotes the time when HClO₄ was added to **2a**. (148)
- Figure 5.7** a) UV-vis absorption spectra of **1**, **1a** and **1a-Sc³⁺** at -40 °C in CH₃CN. b) UV-vis absorption spectra of the three Fe^V species generated from **1**. (149)
- Figure 5.8** Resonance Raman spectra of **1**, **1a-H⁺** and **1a-Sc³⁺** at 77K. Excitation source: 457 nm laser. Samples were prepared at -40 °C and frozen with liquid nitrogen. * denotes solvent peaks. For **1a** there is a shoulder peak ~1040 cm⁻¹, which has not yet been assigned. (151)
- Figure 5.9** a) UV-vis absorption spectra of **2**, **2a** and **2a-Sc³⁺** at -40 °C in CH₃CN. b) Time traces monitoring the absorbance at 400 nm and 640 nm. At 400 nm both **2a** and **2a-Sc³⁺** absorb, however, at 640 nm only **2a-Sc³⁺** absorbs. The black vertical line denotes the time when Sc³⁺ was added to **2a**. c) UV-vis absorption spectra of the three Fe^V species generated from **2**. (152)
- Figure 5.10** UV-vis absorption spectra of a) **1a** and **1a-Y³⁺** and b) **2a** and **2a-Y³⁺** at -40 °C in CH₃CN. (154)
- Figure 5.11** Proposed structures of the isomeric Fe^V intermediates **1a** and **2a**. (155)
- Figure 6.1** Effect of Sc³⁺ or HClO₄ on catalytic reactivity of [Fe^{II}(β-BPMCN)]²⁺ (**2**). (163)
- Figure 6.2** a) [Sc³⁺] dependence of *k_{obs}* for the decay of **2a** with cyclohexane as substrate (black squares) or the formation of **2b** (red circles) with benzene

as substrate. The data for HClO₄ is shown in Chapter 2. b) Proposed mechanism for the effect of Sc³⁺ or HClO₄ on the catalytic hydroxylation of cyclohexane and benzene by **2** and H₂O₂. (164)

Figure 6.3 a) Mⁿ⁺ (Sc³⁺, Fe³⁺, Fe²⁺) concentration dependence on rates of **2b** formation or **2a** decay at -40 °C. Sc³⁺ (blue); Fe³⁺ (red) and Fe²⁺ (green). Open circles for benzene and filled squares for cyclohexane. b) Comparison between the activation of **2** by Fe^{III}(OTf)₃ and the proton-activated diiron(III)-peroxo intermediate of soluble methane monooxygenase. **I**, **II** and **III** are the three plausible structures proposed for **Q**. (167)

Figure 6.4 ChemDraw representations of the three Fe^{III}-OOH intermediates compared in this chapter. (169)

Figure 6.5 The reported [(TMC)Fe^V(O)NC(O)CH₃]²⁺ **4a**³⁴ generated from the *anti* isomer of [(TMC)Fe^{IV}(O)]²⁺ **4**, and the isomeric Fe^V species **5a** studied in this work, which is generated from the *syn* isomer of [(TMC)Fe^{IV}(O)]²⁺ **5**. (171)

Scheme 1.1 Scheme showing oxidation of alkane and olefin with high-valent iron-oxygen intermediate, namely Fe^V(O)(OH) (**5**)

Scheme 1.2 Scheme for the water-assisted mechanism (**8**)

Scheme 1.3 Scheme for the non-water-assisted mechanism (**13**)

Scheme 1.4 Scheme for the carboxylic acid-assisted mechanism. (R = CH₃ for the acetic acid assisted mechanism) (**15**)

Scheme 2.1 Proposed mechanism for the effect of Sc³⁺ or HClO₄ in cyclohexane and benzene hydroxylation by **1**/H₂O₂. (**68**)

Scheme 2.2 Proposed mechanism for formation of the Fe^V oxidants in the water-assisted, acetic-acid-assisted and Sc³⁺/HClO₄-assisted mechanism. (**68**)

- Scheme 3.1** Proposed active oxidants for a) di-iron and b) mono-iron nonheme enzymes. (The hydroxide moieties bound to the high-valent iron centers are proposed to be derived from water.) (77)
- Scheme 3.2** Proposed mechanism for the activation of intermediate **2** by $\text{Fe}^{\text{III}}(\text{OTf})_3$ for the oxidation of benzene and cyclohexane by **1**/ H_2O_2 . (93)
- Scheme 3.3** Parallels between the activation of **2** by $\text{Fe}^{\text{III}}(\text{OTf})_3$ and the proton-activated diiron(III)-peroxo intermediate of soluble methane monooxygenase. **I**, **II** and **III** are the three plausible structures proposed for **Q**. (98)
- Scheme 4.1** The three nonheme iron complexes used in this study ($\text{L} = \text{CH}_3\text{CN}$). (104)
- Scheme 4.2** Proposed mechanism for Sc-assisted pathway for **1** or **2** or **3** in the hydroxylation of cyclohexane and benzene. ($\text{L} = \text{CH}_3\text{CN}$) (130)
- Scheme 5.1** Proposed reaction mechanism for one-oxidation of $\text{Fe}^{\text{IV}}(\text{O})$ intermediates (**1** or **2**) to form $\text{Fe}^{\text{V}}(\text{O})$ species (**1a** or **2a**) and their reaction with H^+ and Sc^{3+} . (143)

List of Abbreviations

| | |
|------------------------------------|--|
| ⁵ tips ³ TPA | Tris(5-(triisopropyl)silyl-2-methylpyridyl)amine |
| 6MeTPA | (6-methyl-2-pyridylmethyl)-bis(2-pyridylmethyl)amine |
| 6Me ₂ TPA | Bis(6-methyl-2-pyridylmethyl)-(2-pyridylmethyl)amine |
| 6Me ₃ TPA | Tris(6-methyl-2-pyridylmethyl)amine |
| ArIO | 2-(<i>tert</i> -butylsulfonyl)iodosylbenzene |
| BDE | Bond dissociation energy |
| BPMCN | <i>N,N'</i> -bis(pyridyl-2-methyl)- <i>N,N'</i> -dimethyl- <i>trans</i> -1,2-diaminocyclo-hexane |
| BPMEN | <i>N,N'</i> -dimethyl- <i>N,N'</i> -bis(2-pyridylmethyl)-1,2-diaminoethane |
| CPCA | cyclohexyl percarboxylic acid |
| DFT | Density functional theory |
| DHA | 9,10-dihydroanthracene |
| ESI-MS | Electrospray-ionization mass spectrometry |
| EPR | Electron paramagnetic resonance |
| EXAFS | Extended x-ray absorption fine structure |
| GC | Gas chromatography |
| GC-MS | Gas chromatography-mass spectrometry |
| HAT | Hydrogen atom transfer |
| KIE | Kinetic isotope effect |
| MeCN | Acetonitrile |
| OAT | Oxygen atom transfer |
| OTf | Triflate |

| | |
|----------------------|--|
| PDP | 2-((S)-2-[(S)-1-(pyridin-2-ylmethyl)pyrrolidin-2-yl]pyrrolidin-1-yl)methylpyridine |
| PhIO | Iodosylbenzene |
| PKIE | Product kinetic isotope effect |
| PNA | Pernonanoic acid |
| PyNMe ₃ | 3,6,9-trimethyl-3,6,9-triaza-1(2,6)-pyridinacyclo-decaphane |
| PyNMe ₃ * | 3,6,9-trimethyl-3,6,9-triaza-1(2,6)-4-methoxy-pyridinacyclo-decaphane |
| RDS | Rate determining step |
| rRaman | Resonance Raman |
| sMMO | Soluble methane monooxygenase |
| TAML | Tetraamido macrocyclic ligand |
| ^t Bu | <i>tertiary</i> -butyl |
| TMC | 1,4,8,11-tetramethyl-1,4,8,11-tetraazacyclotetradecane |
| TON | Turnover number |
| TPA | Tris(2-pyridylmethyl)amine |
| TPA* | Tris[(3,5-dimethyl-4-methoxy)pyridyl-2-methyl]amine |
| UV-vis | Ultraviolet-visible |
| XAS | X-ray absorption spectroscopy |
| δ | Isomer shift |
| ΔE _Q | Quadrupole splitting |

List of Compound Abbreviations by Chapter

Chapter 1

| | |
|-----|---|
| 1 | $[\text{Fe}^{\text{II}}(\text{TPA})]^{2+}$ |
| 1* | $[\text{Fe}^{\text{II}}(\text{TPA}^*)]^{2+}$ |
| 2 | $[\text{Fe}^{\text{II}}(\text{BPMEN})]^{2+}$ |
| 3 | $[\text{Fe}^{\text{II}}(\text{Me}^2\text{PyTACN})]^{2+}$ |
| 4 | $[\text{Fe}^{\text{III}}(\text{TAML})]^-$ |
| 5 | $[\text{Fe}^{\text{II}}(\text{TMC})]^{2+}$ |
| 6 | $[\text{Fe}^{\text{II}}(\text{PDP})]^{2+}$ |
| 7 | $[\text{Fe}^{\text{II}}(\text{PyNMe}_3)]^{2+}$ |
| 7* | $[\text{Fe}^{\text{II}}(\text{MeO-PyNMe}_3)]^{2+}$ |
| 7a | $[(\text{PyNMe}_3)\text{Fe}^{\text{V}}(\text{O})(\text{OAc})]^{2+}$ |
| 7*a | $[(\text{MeO-PyNMe}_3)\text{Fe}^{\text{V}}(\text{O})(\text{OAc})]^{2+}$ |

Chapter 2 & 3

| | |
|---|--|
| 1 | $[\text{Fe}(\beta\text{-BPMCn})]^{2+}$ |
| 2 | $[(\beta\text{-BPMCn})\text{Fe}(\text{OOH})]^{2+}$ |
| 3 | $[(\beta\text{-BPMCn})\text{Fe}(\text{OPh})]^{2+}$ |

Chapter 4

| | |
|---|---|
| 1 | $[\text{Fe}^{\text{II}}(\alpha\text{-BPMCn})]^{2+}$ |
| 2 | $[\text{Fe}^{\text{II}}(\beta\text{-BPMCn})]^{2+}$ |
| 3 | $[\text{Fe}^{\text{II}}(\text{TPA})]^{2+}$ |

| | |
|--------------|--|
| 1-OOH | $[(\alpha\text{-BPMCN})\text{Fe}^{\text{III}}(\text{OOH})]^{2+}$ |
| 2-OOH | $[(\beta\text{-BPMCN})\text{Fe}^{\text{III}}(\text{OOH})]^{2+}$ |
| 3-OOH | $[(\text{TPA})\text{Fe}^{\text{III}}(\text{OOH})]^{2+}$ |
| 1-OPh | $[(\alpha\text{-BPMCN})\text{Fe}^{\text{III}}(\text{OPh})]^{2+}$ |
| 2-OPh | $[(\beta\text{-BPMCN})\text{Fe}^{\text{III}}(\text{OPh})]^{2+}$ |
| 3-OPh | $[(\text{TPA})\text{Fe}^{\text{III}}(\text{OPh})]^{2+}$ |

Chapter 5

| | |
|-----------|---|
| 1 | <i>anti</i> - $[(\text{TMC})\text{Fe}^{\text{IV}}(\text{O})]^{2+}$ |
| 2 | <i>syn</i> - $[(\text{TMC})\text{Fe}^{\text{IV}}(\text{O})]^{2+}$ |
| 1a | <i>anti</i> - $[(\text{TMC})\text{Fe}^{\text{V}}(\text{O})(\text{NC}(\text{O})\text{CH}_3)]^{2+}$ |
| 2a | <i>syn</i> - $[(\text{TMC})\text{Fe}^{\text{V}}(\text{O})(\text{NC}(\text{O})\text{CH}_3)]^{2+}$ |

Chapter 6

| | |
|-----------------|---|
| 1 | $[\text{Fe}^{\text{II}}(\alpha\text{-BPMCN})]^{2+}$ |
| 1-OOH | $[(\alpha\text{-BPMCN})\text{Fe}^{\text{III}}(\text{OOH})]^{2+}$ |
| 2 | $[\text{Fe}^{\text{II}}(\beta\text{-BPMCN})]^{2+}$ |
| 2a/2-OOH | $[(\beta\text{-BPMCN})\text{Fe}^{\text{III}}(\text{OOH})]^{2+}$ |
| 2b | $[(\beta\text{-BPMCN})\text{Fe}^{\text{III}}(\text{OPh})]^{2+}$ |
| 3 | $[\text{Fe}^{\text{II}}(\text{TPA})]^{2+}$ |
| 3-OOH | $[(\text{TPA})\text{Fe}^{\text{III}}(\text{OOH})]^{2+}$ |
| 4 | <i>anti</i> - $[(\text{TMC})\text{Fe}^{\text{IV}}(\text{O})]^{2+}$ |
| 5 | <i>syn</i> - $[(\text{TMC})\text{Fe}^{\text{IV}}(\text{O})]^{2+}$ |
| 4a | <i>anti</i> - $[(\text{TMC})\text{Fe}^{\text{V}}(\text{O})(\text{NC}(\text{O})\text{CH}_3)]^{2+}$ |
| 5a | <i>syn</i> - $[(\text{TMC})\text{Fe}^{\text{V}}(\text{O})(\text{NC}(\text{O})\text{CH}_3)]^{2+}$ |

Chapter 1:

Bioinspired nonheme iron catalytic systems using H₂O₂ as the terminal oxidant

1.1 Inspiration and motivation to develop nonheme iron catalysts

Nonheme iron enzymes form one of the major classes of metalloenzymes that can activate O_2 or H_2O_2 to perform a broad range of oxidative transformations including hydroxylation of aromatic and aliphatic molecules, desaturation, epoxidation, *cis*-dihydroxylation, heterocyclic ring formation, halogenation as well as N-atom oxidation.^{1,2} Not only can they functionalize inert C–H bonds, but also can do so with high levels of chemo-, regio- and stereoselectivity. These attributes make nonheme iron enzymatic reactions a major topic of interest among chemists and biochemists. Significant effort is being made to elucidate the reaction mechanisms by either investigating the enzymes directly by biochemists or by synthesizing functional and spectroscopic models of the enzyme active sites by bioinorganic chemists.^{3–6} Additionally, iron is the fourth most abundant element in the earth's crust and O_2 or H_2O_2 are environmentally benign oxidants, which makes designing and developing iron-based catalysts with O_2/H_2O_2 as the oxidant a worthwhile endeavor from the perspective of sustainable economic growth.

The iron centers in nonheme iron enzymes are coordinated with nitrogen and oxygen atoms of amino acid residues such as histidine, aspartic acid and glutamic acid from the protein backbone. Most nonheme iron enzymes use O_2 , a $4e^-$ oxidant, to perform oxidative reactions. During this process the substrate is oxidized by $2e^-$, while the remaining $2e^-$ from O_2 is taken up by the enzyme co-factor that assists in forming the iron-based active intermediate. Interestingly, some enzymes can also oxidize the substrates to form the respective products, albeit not catalytically, using H_2O_2 , which is a $2e^-$ oxidant or alternatively, a $2e^-$ reduced version of O_2 . This observation suggests that similar oxidants

can be generated using O_2 as well as H_2O_2 . This pathway is commonly referred to as a peroxide shunt and has been used as a mechanistic tool to study the mechanism of various enzymes and trap reactive intermediates. Additionally, compared to O_2 , H_2O_2 is more practical and convenient to use and monitor in mechanistic investigations. Inspired by enzymes, chemists have designed iron complexes ligated with N- and O- based ligands that react with H_2O_2 to form reactive oxidants capable of performing similar oxidation reactions.⁷

In this chapter, the nonheme iron systems that work with H_2O_2 as the oxidant will be reviewed. One major complication has been that iron salts with H_2O_2 undergo Fenton chemistry^{8,9} to generate hydroxyl radicals that are powerful but highly unselective oxidants. Since the late 1990s, iron complexes supported by tetradentate and pentadentate N-based ligands have been used as catalysts for H_2O_2 -mediated hydrocarbon oxidation^{7,10-13} and found to be capable of generating high-valent iron-oxo oxidants from H_2O_2 , rather than freely diffusing hydroxyl radicals. This development has opened up the field for the design and synthesis of iron complexes capable of generating highly selective iron-oxygen oxidants that mimic iron-enzyme reactivity.^{3,10,14,15} Mechanistic analysis of these systems has led to the discovery of different pathways to form high-valent iron oxidants. Here, I will highlight the mechanistic advances with respect to generating high-valent iron oxidants and studying their reactivity.

1.2 Nonheme iron catalysts and the various mechanisms to generate the active oxidant

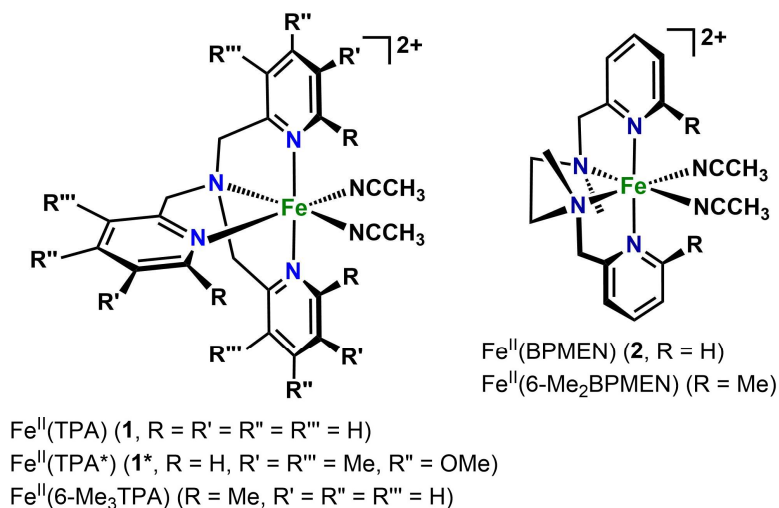
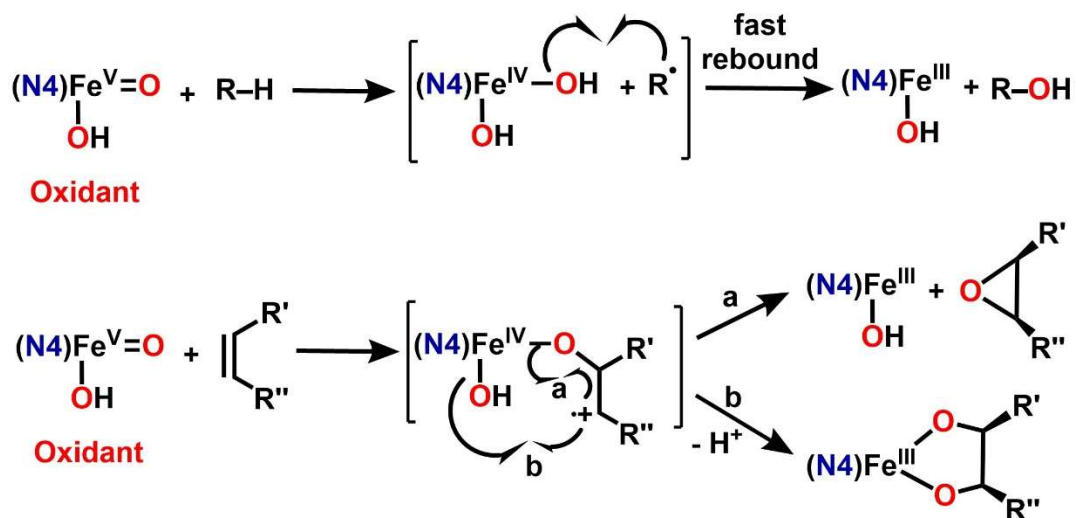


Figure 1.1. Structures of selected iron complexes (L = CH₃CN) that represent nonheme iron catalysts discussed in this chapter.

At the turn of this century, two nonheme iron complexes, [Fe^{II}(TPA)]²⁺ (**1**, TPA = tris(2-pyridylmethyl)amine) and [Fe^{II}(BPMEN)]²⁺ (**2**, BPMEN = *N,N'*-dimethyl-*N,N'*-bis(2-pyridylmethyl)-1,2-diaminoethane) were found to act as catalysts for hydrocarbon oxidations using H₂O₂ as the oxidant (Figure 1.1).^{11,13,16,17} These catalysts can perform alkane hydroxylation, alkene epoxidation and *cis*-dihydroxylation, mimicking the functions of some nonheme iron enzymes.^{14,18} Based on various mechanistic experiments on these catalytic reactions, both **1** and **2** are demonstrated to form selective metal-based oxidants as opposed to hydroxyl radicals.^{16,17} For alkane hydroxylation, the active metal-based oxidant is proposed to abstract a hydrogen atom from a C–H bond of the alkane to generate a substrate radical, which rapidly rebounds to the resulting iron-oxygen species forming alcohol with retention of stereochemistry at the hydroxylated carbon atom

(Scheme 1.1). Rapid rebound of the substrate radical does not allow the carbon-centered radical time to invert, and hence leads to retention of stereochemistry in the products. In the case of olefin oxidation, the active oxidant attacks the C=C π -bonds to form C–O bonds, leading to the formation of epoxides and *cis*-diols with retention of stereochemistry (Scheme 1.1). High-valent iron-oxygen intermediates such as $\text{Fe}^{\text{V}}=\text{O}$ in most cases and sometimes $\text{Fe}^{\text{IV}}=\text{O}$ are invoked as the oxidants responsible for the challenging oxidation of both alkanes and olefins.^{3,5,19}



Scheme 1.1. Scheme showing oxidation of alkane and olefin with high-valent iron-oxygen intermediate, namely $\text{Fe}^{\text{V}}(\text{O})(\text{OH})$.

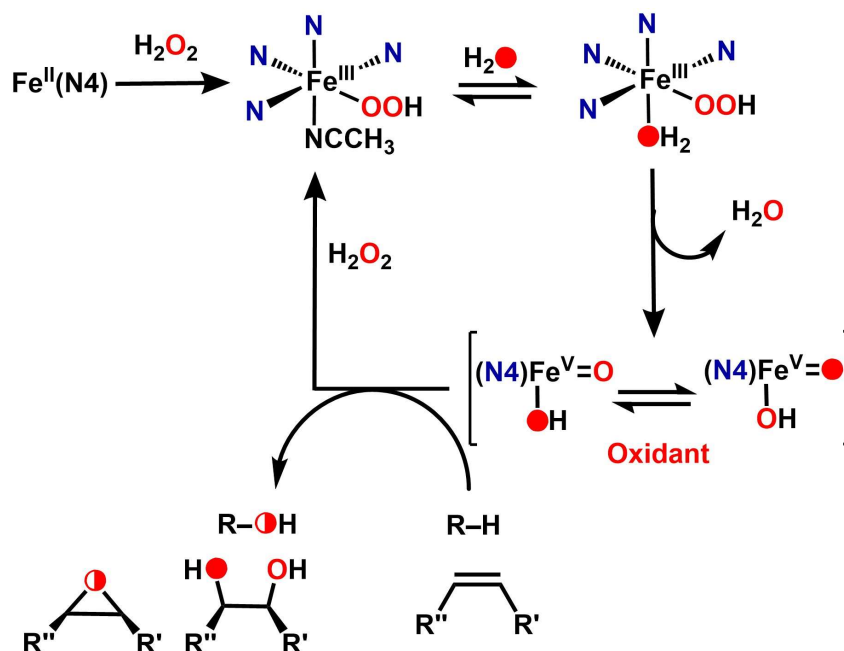
Early mechanistic results in support of a metal-based oxidant consisted of a) an alcohol-to-ketone (A/K) ratio of 5 or more in the oxidation of cyclohexane that was insensitive to the presence of O_2 , b) a kinetic isotope effect >2 for oxidation of cyclohexane-*h*₁₂ (C_6H_{12}) versus cyclohexane-*d*₁₂ (C_6D_{12}), c) a regioselectivity >15 in the oxidation of tertiary C–H

bonds over secondary C–H bonds of adamantane, and d) greater than 90% stereoretention in the hydroxylation of tertiary C–H bonds of *cis*-1,2-dimethylcyclohexane as well as for olefin oxidation.^{16,17} In alkane oxidation, the alcohol-to-ketone product ratio (A/K) has been used as a mechanistic probe to determine if the oxidant is a metal-based oxidant or hydroxyl radical. The A/K ratio gives an estimate of the lifetime of the carbon-centered radical formed after the initial H-atom abstraction from a C–H bond.¹⁰ If the radical immediately rebounds to the iron center, it forms alcohol, leading to A/K values well above 1. Some ketone is formed, probably from the subsequent oxidation of the alcohol product. On the other hand, if the radical is long-lived, it gets trapped by O₂ from air and undergoes a chain reaction involving Russell termination forming equal amounts of alcohol and ketone to afford an A/K value of 1.¹⁰ The next probe is the determination of intermolecular KIE, which tells us about the strength of the oxidant and is obtained from a competition reaction between C₆H₁₂ and C₆D₁₂.^{10,20} A KIE of 1-2 implies a powerful oxidant that does not discriminate much between weaker C–H and stronger C–D bonds of cyclohexane. Hydroxyl radicals are powerful, unselective oxidants and have a KIE around 1, whereas more selective oxidants such as metal-oxo(s) have KIE values > ~2. The third experiment is focused on the regioselectivity in adamantane oxidation. Adamantane is a substrate that contains both secondary and tertiary C–H bonds. Hence, an intramolecular competition occurs when it is oxidized. As tertiary C–H bonds are weaker than secondary C–H bonds, the tertiary C–H bonds are preferentially oxidized to tertiary alcohols over secondary C–H bonds. Now the more powerful an oxidant is, the lower is its regioselectivity in adamantane oxidation. Finally, as mentioned earlier, the observed stereoretention in the oxidation

products indicates that the substrate radicals formed during the reaction must be short-lived and immediately captured by the resulting metal-oxygen species. On the other hand, if the substrate radicals are long lived, like those generated by hydroxyl radicals, then they will invert and the products will not retain the stereochemistry of the starting reactant. The mechanistic results in the case of **1** and **2** exclude the possibility of powerful but unselective hydroxyl radicals as the oxidant, and strongly implicate a more selective iron-based oxidant.

1.2.1 Water-assisted mechanism

The water-assisted mechanism is the most in-depth studied mechanism for these nonheme iron catalysts and has been demonstrated for both **1** and **2** (Scheme 1.2).^{16,17} In this mechanism, H₂O₂ reacts with the Fe^{II} complex to form an Fe^{III}-OOH species. Water binds at the available sixth site on the iron center *cis* to the hydroperoxide ligand and hydrogen bonds to the distal oxygen atom of the hydroperoxo ligand to facilitate the breaking of the O-O bond. This sequence results in the formation of the high-valent Fe^V(O)(OH) species responsible for substrate oxidation.



Scheme 1.2. Scheme for the water-assisted mechanism.

The crucial observation that supports the proposed water-assisted mechanism is the observed label incorporation from H_2^{18}O into the products of both alkane and olefin oxidation,^{16,17} which requires the oxidant to be capable of O-atom exchange with water. This outcome rules out the possibility of the $\text{Fe}^{\text{III}}\text{-OOH}$ intermediate itself acting as the oxidant. However, there are two possible iron-based oxidants that can incorporate an O-atom by exchange with water – a) $\text{Fe}^{\text{IV}}(\text{O})$ and b) $\text{Fe}^{\text{V}}(\text{O})(\text{OH})$, which can in turn be incorporated into the products. Both of these oxidants can in principle be generated from an $\text{Fe}^{\text{III}}\text{-OOH}$ species. $\text{Fe}^{\text{IV}}(\text{O})$ is formed along with OH^\bullet via homolytic cleavage of the O–O bond in the $\text{Fe}^{\text{III}}\text{-OOH}$ intermediate. This combination of $\text{Fe}^{\text{IV}}(\text{O})$ and OH^\bullet was eliminated due to the observed high KIE, regioselectivity in adamantane oxidation and

stereoretention in the oxidized products, which cannot be achieved when an unselective OH[•] radical species is present in the reaction mixture. On the other hand, these mechanistic results could be easily rationalized by invoking a Fe^V(O)(OH) oxidant. Another route for ¹⁸O incorporation from water into the products is the formation of a carbocation, instead of a carbon radical, after the oxidant attacks the substrate. In this case the oxidant itself need not incorporate O-atom from water. But this possibility of ¹⁸O incorporation from H₂¹⁸O via a carbocation intermediate can be ruled out based on the observation that oxidation of *cis*-1,2-dimethylcyclohexane gives products with retention of configuration as opposed to epimerized alcohols that would arise from the attack of H₂¹⁸O on a carbocation intermediate. The % ¹⁸O incorporation into the alcohol product obtained from C–H bond oxidation increased with the amount of H₂¹⁸O present in the reaction mixture before reaching a plateau, and this saturation behavior indicates a preequilibrium binding of H₂¹⁸O to the iron center. The incorporation of isotopically labeled ¹⁸O-atom into the oxidant is proposed to occur via an oxo-hydroxo tautomerization mechanism, by analogy to that proposed by Bernardou and Meunier to explain the isotope label incorporation from H₂¹⁸O into the products of oxidation reactions performed by [Fe^{IV}(O)(porphyrin radical)]⁺ complexes.²¹ For olefin oxidations in the presence of H₂¹⁸O, it is observed that the epoxide products show partial label incorporation from H₂¹⁸O. In contrast, the *cis*-diol products incorporate one O-atom from H₂O and the other from H₂O₂. This outcome is rationalized by a [3+2]-cycloaddition between the Fe^V(O)(OH) oxidant and the C=C bond of the olefin substrate to form the *cis*-diol product, analogous to the mechanism generally accepted for olefin *cis*-dihydroxylation by OsO₄.²²

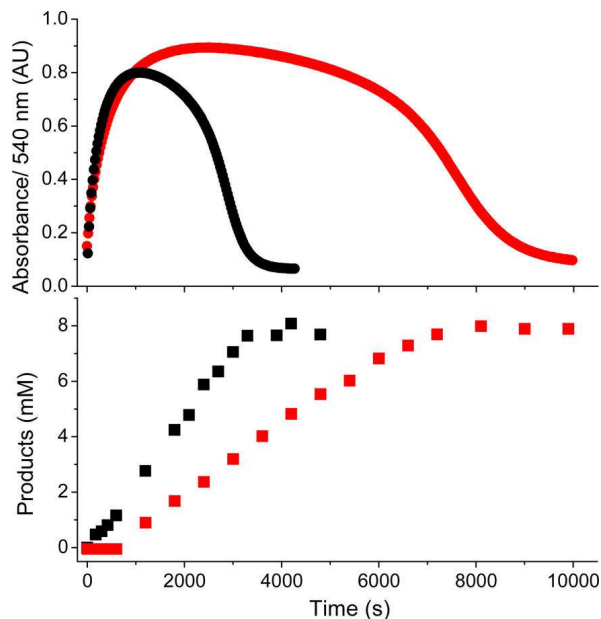


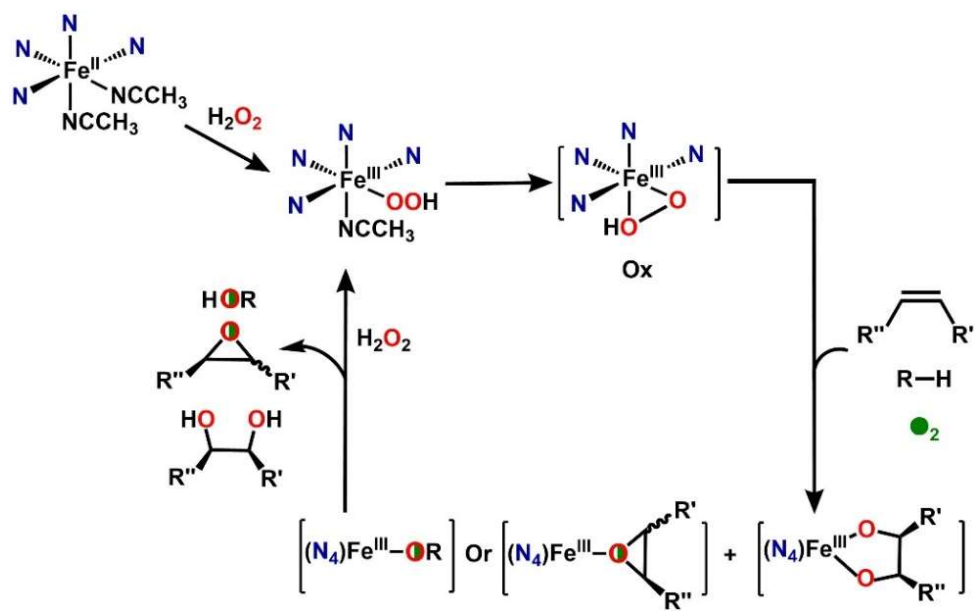
Figure 1.2. (Top) Time trace monitoring absorbance at 540 nm corresponding to $\text{Fe}^{\text{III}}\text{-OOH}$ formed in the oxidation of 1-octene by **1** and H_2O_2 at $-45\text{ }^\circ\text{C}$ in CH_3CN . (Bottom) Time course for formation of products (1,2-octanediol and 1,2-epoxyoctane combined) under same conditions. Black – in the presence of 100 eq H_2O and red – in the presence of 100 eq D_2O .²³ (Reproduced with permission from ref 23; copyright 2013 American Chemical Society)

Further support for the water-assisted mechanism comes from more recent kinetic studies.²³ Upon addition of excess (20 eq relative to **1**) H_2O_2 to a mixture of the iron catalyst (**1**) and 1-octene as a substrate in CH_3CN at $-40\text{ }^\circ\text{C}$, formation of a low spin ($S = \frac{1}{2}$) $\text{Fe}^{\text{III}}\text{-OOH}$ intermediate with a chromophore at 540 nm is observed, which can be monitored via UV-visible absorption spectroscopy. Following its formation, the $\text{Fe}^{\text{III}}\text{-OOH}$ intermediate reaches a pseudo-steady state phase that lasts for ~ 45 min, suggesting that the $\text{Fe}^{\text{III}}\text{-OOH}$ intermediate is formed at the same rate as its decay as long as there is excess H_2O_2 (Figure

1.2). Once the H_2O_2 is depleted, the $\text{Fe}^{\text{III}}\text{-OOH}$ species decays exponentially at a rate unaffected by the concentration of the substrate. This observation supports the idea that $\text{Fe}^{\text{III}}\text{-OOH}$ is not the active oxidant but is actually its precursor. The fact that the active oxidant is not observed in these reactions presumably reflects its highly reactive nature. Nevertheless, mechanistic insights can be gleaned from studying the behavior of the $\text{Fe}^{\text{III}}\text{-OOH}$ precursor of the active oxidant. The product formation rate matched the rate of exponential decay of the $\text{Fe}^{\text{III}}\text{-OOH}$ species, suggesting that the decay of the $\text{Fe}^{\text{III}}\text{-OOH}$ intermediate is directly related to the oxidation of the substrate. Together these results support a mechanism where the $\text{Fe}^{\text{III}}\text{-OOH}$ intermediate decays to form the $\text{Fe}^{\text{V}}(\text{O})(\text{OH})$ active oxidant responsible for oxidizing substrates in the rate determining step. As the concentration of water in the reaction mixture is increased, the $\text{Fe}^{\text{III}}\text{-OOH}$ species decays at faster rate and exhibits a shorter pseudo-steady state phase. Thus, it can be deduced that water facilitates the O–O bond cleavage in the $\text{Fe}^{\text{III}}\text{-OOH}$ intermediate and assists in forming the active $\text{Fe}^{\text{V}}(\text{O})(\text{OH})$ oxidant. Further evidence corroborating water assistance in cleaving the O–O bond via hydrogen bonding is provided by the observation that D_2O decreases the rate of $\text{Fe}^{\text{III}}\text{-OOH}$ decay and product formation while increasing the length of the pseudo-steady state phase (Figure 1.2). A kinetic isotope effect (KIE) of 2.5 is observed for H_2O vs D_2O . Taken together, these observations support the water-assisted mechanism for the formation of the $\text{Fe}^{\text{V}}(\text{O})(\text{OH})$ oxidant that reacts with substrates (Scheme 1.2).

1.2.2 Non-water-assisted mechanism:

The non-water-assisted mechanism has been proposed along with the water-assisted mechanism at the beginning of these studies in order to rationalize the isotope labeling results obtained for catalysts with two or more pyridines that have 6-methyl substituents in the ligand framework. However, this mechanism is not understood as well as the water-assisted mechanism and needs further investigation. The TPA and BPMEN analogs with two or more 6-Me-substituted pyridines, such as 6-Me₃TPA and 6-Me₂BPMEN (Figure 1.1), give rise to catalysts that follow a non-water-assisted mechanism.^{16,17} It has been proposed that these complexes form a high-spin ($S = 5/2$) Fe^{III}-OOH because of the steric hindrance provided by the 6-Me substituents on the ligand framework, making the Fe-N bonds longer and reducing the ligand field strength around the iron center. Evidence for longer Fe-N bond lengths has been found by comparing the crystal structures of Fe^{II}(6-Me₃TPA) and Fe^{II}(TPA).²⁴ The reduced ligand field strength is supported by the formation of ($S = 5/2$) Fe^{III}-OO^tBu species in the case of Fe^{II}(6-Me₂TPA) and Fe^{II}(6-Me₃TPA) upon addition of ^tBuOOH, whereas for Fe^{II}(TPA) and Fe^{II}(6-MeTPA) a ($S = 1/2$) Fe^{III}-OO^tBu species is observed under similar conditions.²⁴ However, the corresponding Fe^{III}-OOH species have not been observed. This is in contrast to the iron complexes such as Fe^{II}(TPA) and Fe^{II}(BPMEN) that follow the water-assisted mechanism where a ($S = 1/2$) Fe^{III}-OOH is observed to form during the reaction.^{23,25}



Scheme 1.3. Scheme for the non-water-assisted mechanism.

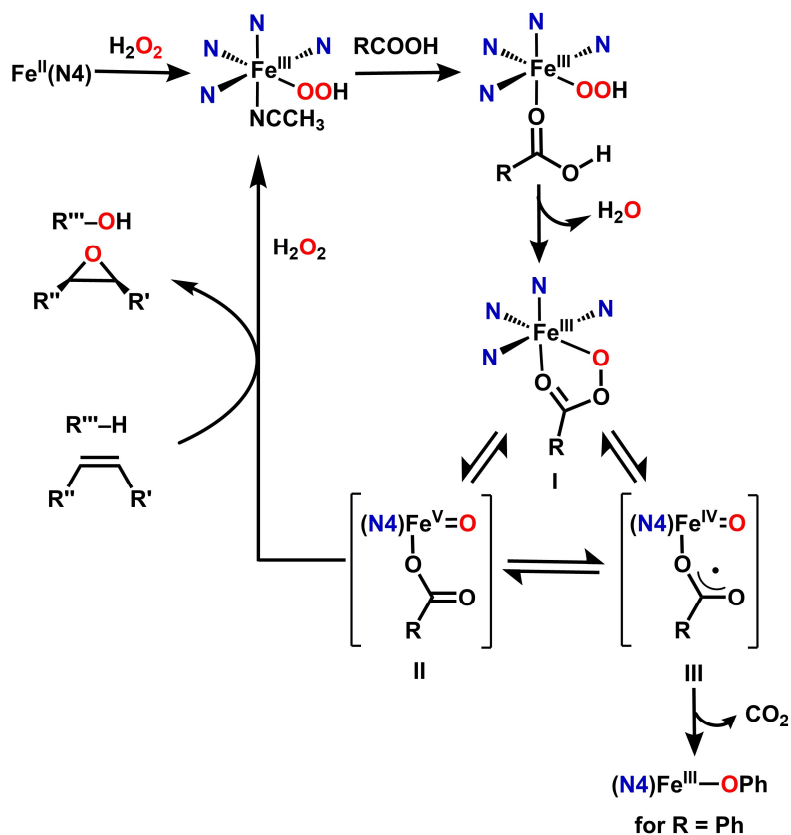
When catalysis is carried out by $\text{Fe}^{\text{II}}(6\text{-Me}_3\text{TPA})$ or $\text{Fe}^{\text{II}}(6\text{-Me}_2\text{TPA})$ in the presence of H_2^{18}O , essentially no ^{18}O -incorporation from water is observed into the *cis*-diol and epoxide products obtained from olefin oxidation.¹⁷ In these cases, both O-atoms of the *cis*-diol product are derived from H_2O_2 . These observations resulted in the development of the non-water-assisted mechanism. In contrast to catalysts following water-assisted mechanism, the catalysts following non-water-assisted mechanism favored forming *cis*-diols over epoxides in olefin oxidation. Similar to olefin oxidation, for alkane hydroxylation no ^{18}O -labeled alcohol product from H_2^{18}O is observed.¹⁶ Interestingly, a significant amount of the O-atoms in the alcohol is not derived from either H_2O_2 or H_2O , and is found to be derived from O_2 instead. The incorporation of O-atoms from O_2 into the products led to the conclusion that the substrate-based carbon radicals formed after the

initial attack of the active oxidant are long enough lived to be captured by O₂ from air. This is supported by the lower retention of configuration in the oxidation products of *cis*-1,2-dimethylcyclohexane. Additionally, these catalysts are not efficient in alkane hydroxylation. The reason for these differences in the reactivity trends is still not completely understood, but it supports the idea that different oxidants are involved in the two mechanisms. Based on these observations, an Fe^{III}-OOH intermediate with an η²-bound-OOH is favored to be the active oxidant (Scheme 1.3). The η² binding mode is proposed for the -OOH moiety to rationalize the lack of water involvement that can be caused by the unavailability of open position for water to bind to the iron center. In the non-water-assisted mechanism it is proposed that the active oxidant generates long-lived substrate radicals, which can be trapped by O₂ or can epimerize, unlike the water-assisted mechanism where the substrate radicals are short-lived.

1.2.3 Carboxylic-acid-assisted mechanism

The carboxylic-acid-assisted mechanism was added to the mechanistic picture about half a decade after the water-assisted mechanism was first proposed to rationalize observations in catalytic reactions carried out in the presence of acetic acid, the effects of which were first reported in 2001 by White *et al.*²⁶ The addition of acetic acid has a dramatic effect on the product distributions observed for **1** and **2** in the oxidation of olefins. While formation of both epoxide and *cis*-diol is observed in the absence of acetic acid, epoxide becomes the exclusive product in its presence.²⁷ Under such conditions, the O-atom of the epoxide was

derived solely from H_2O_2 , even when reactions were performed in the presence of H_2^{18}O , suggesting that the presence of carboxylic acid alters the nature of the oxidant.



Scheme 1.4. Scheme for the carboxylic acid-assisted mechanism. ($\text{R} = \text{CH}_3$ for the acetic acid assisted mechanism)

The main difference between the two mechanisms is the nature of the sixth ligand, acetic acid in place of H_2O (Scheme 1.4). Like the bound water, the carboxylic acid assists in breaking the O–O bond by protonating the terminal oxygen of the hydroperoxo moiety to form a proposed $\text{Fe}^{\text{V}}(\text{O})(\text{O}_2\text{CR})$ oxidant (II). This ligand substitution accounts for the switch in olefin oxidation product favoring epoxide formation and the lack of any ^{18}O

incorporation from labeled water.^{27,28} Moreover, in cyclooctene oxidation, careful analysis of the products showed evidence for the formation of less than one equivalent of the corresponding *cis*-1,2-hydroxoacetate derivative of cyclooctene.^{27,28} This strongly indicates that the acetate is bound to the iron center of the active oxidant as the sixth ligand, further supporting a $\text{Fe}^{\text{V}}(\text{O})(\text{O}_2\text{CR})$ oxidant (**II**).

There is evidence that the proposed $\text{Fe}^{\text{V}}(\text{O})(\text{O}_2\text{CR})$ oxidant (**II**) can tautomerize to its $\text{Fe}^{\text{IV}}(\text{O})(\bullet\text{O}(\text{O})\text{CR})$ isomer (**III**), which then undergoes decarboxylation generating an $\text{R}\bullet$ radical that is eventually trapped by either the nascent $\text{Fe}^{\text{IV}}(\text{O})$ species in a rebound step or by O_2 from air (Scheme 1.4).^{27,29} The former scenario is well documented for $\text{C}_6\text{F}_5\text{COOH}$ in place of acetic acid in which case $\text{C}_6\text{F}_5\text{OH}$ is formed catalytically. On the other hand, benzaldehyde is obtained stoichiometrically with phenylacetic acid is used in place of acetic acid, which results from the reaction of the more stable benzyl radical with O_2 . Both of these side products, benzaldehyde and phenol, are generated in competition with epoxide, depending on the relative concentrations of the olefin and the carboxylic acid.

The acetic-acid-assisted mechanism involves more intermediates compared to the water-assisted mechanism and has been extensively investigated by various other groups.^{19,27,30} In 2009, Talsi and co-workers observed a new intermediate derived from the reaction of **1** with peracetic acid or *m*-CPBA with an $S = 1/2$ EPR signal at $g = 2.71, 2.42$ and 1.53 .³¹ This spectroscopic intermediate, also referred to as the $g = 2.7$ species, was assigned to be the $\text{Fe}^{\text{V}}(\text{O})(\text{O}_2\text{CR})$ species and found to decay 5-fold faster in the presence of cyclohexene compared to its self-decay rate. However, this species represented only 7% of the iron in the sample based on EPR integration, making it difficult to ascertain the assignment of the

iron oxidation state by other methods. Subsequently, Que and co-workers found reaction conditions to produce the $g = 2.7$ EPR signal using **1** with excess H_2O_2 and AcOH and increased the yield of this intermediate.³² Additionally, the yield of the intermediate was further increased by replacing **1** with its electron-donating variant **1*** containing two methyl and one methoxy substituents on each pyridine of the ligand. Under these conditions, the $g = 2.7$ species could be generated in $\sim 50\%$ yield, allowing its characterization by Mössbauer spectroscopy. Based on information from Mössbauer and EPR spectroscopy, the $g = 2.7$ species is determined not to be the previously hoped for $S = 1/2 \text{Fe}^{\text{V}}$ species but actually an $S = 1/2 \text{Fe}^{\text{III}}$ species distinct from the $S = 1/2 \text{Fe}^{\text{III}}\text{-OOH}$ intermediate formed with H_2O_2 in the absence of AcOH. The $g = 2.7$ species has a chromophore with an absorption band at 460 nm. Kinetic studies via UV-visible spectroscopy suggest that the $g = 2.7$ species is involved in the reaction but serves as the precursor to the active oxidant, similar to the $\text{Fe}^{\text{III}}\text{-OOH}$ intermediate in the water-assisted mechanism (Scheme 1.2). In contrast to the $\text{Fe}^{\text{III}}\text{-OOH}$ species, the decay rate of this species does not show any [acid] dependence and no KIE is observed for AcOH versus AcOD.³² Based on these spectroscopic and kinetic studies, this species is proposed to be a bidentate acylperoxo-adduct $\text{Fe}^{\text{III}}\text{-O}_3\text{CR}$ (**I**) that in turn decayed to generate the $\text{Fe}^{\text{V}}(\text{O})(\text{O}_2\text{CR})$ active oxidant (**II**) (Scheme 1.4).

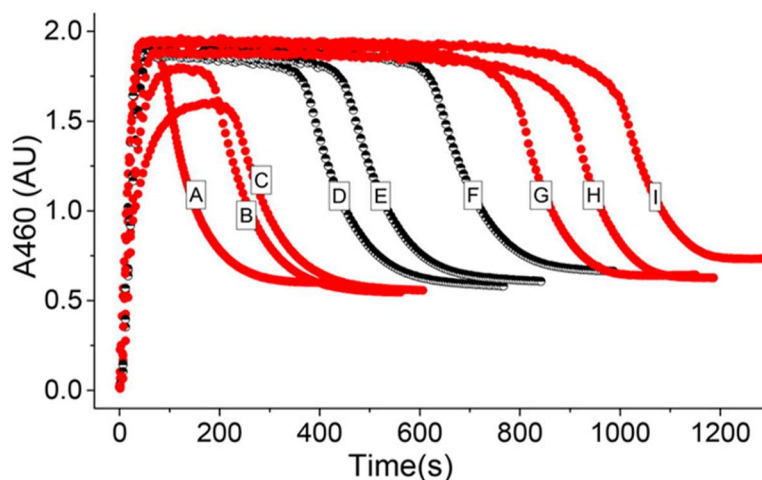


Figure 1.3. Time trace monitoring absorbance at 460 nm corresponding to $\text{Fe}^{\text{III}}(\kappa^2\text{-OOAc})$ formed from $\mathbf{1}^*$ and $\text{H}_2\text{O}_2/\text{AcOH}$ in the presence of various substrates (red filled circles) and varying concentrations of 1-octene (black half-filled circles represent different concentrations of 1-octene). A = 250 mM cyclohexadiene, B = 250 mM cyclohexene, C = 250 mM cyclooctene, D = 250 mM 1-octene, E = 125 mM 1-octene, F = 62.5 mM 1-octene, G = 250 mM cyclohexane, H = 250 mM *tert*-butyl acrylate, I = no substrate.³³ (Reproduced with permission from ref 33; copyright 2017 American Chemical Society)

Further detailed kinetic studies via UV-visible spectroscopy along with supporting EPR experiments on $\mathbf{1}^*$ using $\text{H}_2\text{O}_2/\text{AcOH}$ or AcOOH in the presence of various olefinic substrates suggest the participation of two $S = 1/2$ iron species in the mechanism. One is assigned to be an $\text{Fe}^{\text{III}}(\kappa^2\text{-OOAc})$ (**I**) with g values in the range of 2.7, 2.4, and 1.5, and the other is designated to an $\text{Fe}^{\text{V}}(\text{O})(\text{OAc})$ species (**II**) with g values of 2.07, 2.01 and 1.96.³³ AcOH binding to the $\text{Fe}^{\text{III}}\text{-OOH}$ intermediate generates the $\text{Fe}^{\text{III}}(\kappa^2\text{-OOAc})$ (**I**) and the $\text{Fe}^{\text{V}}(\text{O})(\text{OAc})$ (**II**) species, which are in equilibrium with each other. Following its formation, the $\text{Fe}^{\text{III}}(\kappa^2\text{-OOAc})$ species (**I**) reaches a steady-state phase before undergoing

an exponential decay upon depletion of H_2O_2 . Interestingly, the length of the steady-state phase of the $\text{Fe}^{\text{III}}(\kappa^2\text{-OOAc})$ species (**I**) is dependent on the nature as well as the concentration of the substrate, even though it is not directly responsible for substrate oxidation. The steady-state phase is lengthened with lower concentrations of substrates and using substrates that were more difficult to oxidize (Figure 1.3). Taken together, these results suggest that the $\text{Fe}^{\text{III}}(\kappa^2\text{-OOAc})$ (**I**) and $\text{Fe}^{\text{V}}(\text{O})(\text{OAc})$ (**II**) species are reversibly connected and that this equilibrium is modulated by the nature and concentration of the substrate as well as the electronic properties of the supporting polydentate ligand and the carboxylic acid. The $\text{Fe}^{\text{V}}(\text{O})(\text{OAc})$ (**II**) species is the active oxidant responsible for substrate oxidation, whereas the $\text{Fe}^{\text{III}}(\kappa^2\text{-OOAc})$ (**I**) acts as a reservoir. This equilibrium also involves a third component, namely the $\text{Fe}^{\text{IV}}(\text{O})(\cdot\text{OAc})$ (**III**) isomer (Scheme 1.4), which provides a pathway for the irreversible decarboxylation of the carboxylate moiety to form $\text{Fe}^{\text{IV}}(\text{O})$, alkyl radical and CO_2 . The $\text{Fe}^{\text{IV}}(\text{O})(\cdot\text{OAc})$ (**III**) species is reversibly connected to its electrophile $\text{Fe}^{\text{V}}(\text{O})(\text{OAc})$ (**II**) via valence tautomerization and to $\text{Fe}^{\text{III}}(\kappa^2\text{-OOAc})$ (**I**) via reversible O–O bond formation. Unlike the water-assisted mechanism where the rate determining step (RDS) was the O–O bond cleavage step assisted by water and did not depend on [substrate], the RDS in this case is influenced by the equilibrium as well as [substrate]. The lack of a KIE effect from AcOH/AcOD on the rate of product formation indicates that the RDS is not a carboxylic-acid-assisted step although carboxylic acid is the key player in this mechanism. Although the two mechanisms are different, one thing that is equally crucial in both water-assisted and carboxylic-acid-assisted is the cleavage of the O–O bond to generate a high-valent iron-oxo species.

1.3 Nonheme iron complexes where a $\text{Fe}^{\text{V}}(\text{O})$ oxidant is directly observed

In the previous sections, indirect mechanistic and/or kinetic evidence for involvement of the high-valent $\text{Fe}^{\text{V}}(\text{O})$ oxidant in nonheme iron catalysis has been discussed. The interesting reactivity of the proposed $\text{Fe}^{\text{V}}(\text{O})$ oxidants in the catalytic systems has inspired synthetic chemists to design model systems that can support relatively stable observable $\text{Fe}^{\text{V}}(\text{O})$ species and study them in greater detail to understand the properties of these high-valent iron oxidants. Here, I describe some of the cases where an $\text{Fe}^{\text{V}}(\text{O})$ intermediate is observed directly and studied using spectrometric and/or spectroscopic techniques.

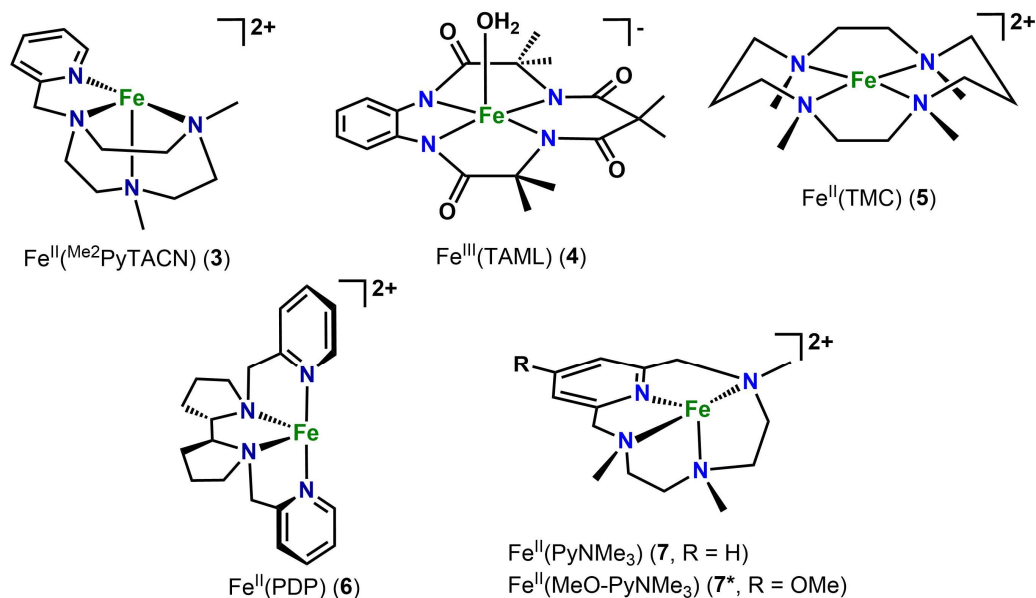


Figure 1.4. Structures of a few representative iron complexes described in this section.

The first direct evidence for the elusive $\text{Fe}^{\text{V}}(\text{O})(\text{OH})$ intermediate in the water-assisted mechanism was obtained by Costas and co-workers for the nonheme iron catalyst, $[\text{Fe}^{\text{II}}(\text{Me}_2\text{PyTACN})]^{2+}$ (**3**) (Figure 1.4), using cryospray ionization mass spectrometry at -40 °C.³⁴ A species with a prominent ion peak was found at $m/z = 486$ that could be associated with either the $\{[\text{Fe}^{\text{III}}(\text{OOH})(\text{Me}_2\text{PyTACN})](\text{OTf})\}^+$ or the $\{[\text{Fe}^{\text{V}}(\text{O})(\text{OH})(\text{Me}_2\text{PyTACN})](\text{OTf})\}^+$ ions. However, the two possibilities can be distinguished with isotope-labeling experiments. Isotope-sensitive mass spectrometry results revealed the incorporation of one O-atom from H_2O_2 and one O-atom from H_2O in the ion corresponding to $m/z = 486$, which excluded $\text{Fe}^{\text{III}}\text{-OOH}$ as a possibility. A similar isotope pattern was found for ions corresponding to the product complex obtained from olefin oxidation such as $[\text{Fe}^{\text{III}}(\text{Me}_2\text{PyTACN})(\text{cis-diolate})]^+$, which supports the intermediate at $m/z = 486$ to be the $\text{Fe}^{\text{V}}(\text{O})(\text{OH})$ active oxidant. Very recently, Perry, Que and co-workers used a different mass spectrometric technique known as transmission mode desorption electrospray ionization mass spectrometry (TM-DESI) to observe the $\text{Fe}^{\text{V}}(\text{O})(\text{OH})$ intermediates of the thoroughly studied **1** and **1*** systems at ambient temperature.³⁵ In recent years, additional mass spectrometric evidence for the $\text{Fe}^{\text{V}}(\text{O})$ species has been obtained for other catalytic systems such as $[\text{Fe}^{\text{III}}(\text{dpaq})(\text{H}_2\text{O})]^{2+}$ by Hitomi and co-workers,³⁶ and $[\text{Fe}^{\text{II}}(\text{}^5\text{tips}^3\text{TPA})]^{2+}$ (a substituted analog of TPA) in the gas phase by Costas, Roithová and co-workers.³⁷ Although mass spectrometry provides direct evidence for the existence of high-valent Fe^{V} species, but it does not give us insight into the electronic structure or the reactivity of the species.

The first spectroscopically trapped $\text{Fe}^{\text{V}}(\text{O})$ intermediate was reported by Collins and co-workers in 2007, which was supported by the tetra-anionic macrocyclic ligand TAML (4) shown in Figure 1.4.³⁸ This ligand with four strong electron-donating amido donors stabilizes the electron-deficient Fe^{V} center, allowing the formation of the $\text{Fe}^{\text{V}}(\text{O})$ species. It is associated with an $S = 1/2$ EPR signal having g values at 1.99, 1.97 and 1.74 and a Mössbauer doublet with isomer shift $\delta = -0.42(3)$ mm/s and quadrupole splitting $\Delta E_{\text{Q}} = 4.25$ mm/s (Table 1.1). Based on extended X-ray absorption fine structure (EXAFS) studies, an Fe–O distance of 1.58 Å is assigned for the Fe=O unit, which is 0.04 to 0.1 Å shorter compared to $\text{Fe}^{\text{IV}}(\text{O})$ complexes.³⁹ $[\text{Fe}^{\text{V}}(\text{O})(\text{TAML})]^-$ is reactive enough to oxidize cyclohexane at -40 °C with a rate of $2.6 \times 10^{-4} \text{ M}^{-1} \text{ s}^{-1}$.⁴⁰ The use of a modified version of the TAML ligand with an additional electron donating –NMe group in the ligand backbone (bTAML) by Sengupta and co-workers generates another $\text{Fe}^{\text{V}}(\text{O})$ species, but one that is stable at room temperature.⁴¹ It has a similar spectroscopic signature as the parent (TAML) $\text{Fe}^{\text{V}}(\text{O})$ species and reacts with cyclohexane at room temperature ($k_{\text{obs}} = 0.023 \text{ M}^{-1} \text{ s}^{-1}$). Interestingly, with bTAML both the $\text{Fe}^{\text{V}}(\text{O})$ and $\text{Fe}^{\text{IV}}(\text{O})$ intermediates can be experimentally trapped and characterized, allowing us to understand how the two high-valent intermediates differ (Table 1.1).⁴² The Mössbauer isomer shift of $[(\text{bTAML})\text{Fe}^{\text{IV}}(\text{O})]^{2-}$ is -0.12 mm/s, which is significantly different from that of the corresponding $[(\text{bTAML})\text{Fe}^{\text{V}}(\text{O})]^-$ at -0.44 mm/s. The Fe–O distance is 0.05 Å longer in the $\text{Fe}^{\text{IV}}(\text{O})$ complex than that of the $\text{Fe}^{\text{V}}(\text{O})$ species as determined by EXAFS. The longer Fe–O bond distance is also supported by the decrease of the Fe=O vibration from 862 cm^{-1} for the $\text{Fe}^{\text{V}}(\text{O})$ complex to 798 cm^{-1} for the $\text{Fe}^{\text{IV}}(\text{O})$ complex, a 64-cm^{-1} difference.

As might be expected, the oxidative reactivities of the two complexes are different. $[(bTAML)Fe^V(O)]^-$ oxidizes benzyl alcohol at pH 7 with a 2500-fold faster rate (after correcting for the pH difference) than the corresponding $Fe^{IV}(O)$ complex at pH 12. This difference can be easily rationalized by the higher redox potential of $[(bTAML)Fe^V(O)]^-$ ($Fe^{V/IV} = 1.19$ V at pH = 7 vs NHE) compared to that of $[(bTAML)Fe^{IV}(O)]^{2-}$ ($Fe^{IV/III} = 0.44$ V at pH = 12 vs NHE). Unlike for the tetra-anionic TAML ligands, neutral ligands such as TPA, BPMEN are more electron deficient, thus making it difficult to trap the elusive $Fe^V=O$ species in the latter cases.

In 2012, an $Fe^V(O)$ species supported by the neutral TMC ligand (**5**) (Figure 1.4) was generated by treating $[(TMC)Fe^{IV}(O)]^{2+}$ with $tBuOOH$ and base.⁴³ This TMC-supported Fe^V species exhibits an $S = \frac{1}{2}$ EPR signal with g values of 2.05, 2.01 and 1.97, which has an even smaller g anisotropy than found for $[Fe^V(O)(TAML)]^-$.³⁸ This complex has a Mössbauer isomer shift of $\delta = 0.10(4)$ mm/s, which is below the range of values observed for $Fe^{IV}(O)$ complexes supported by TMC (0.15 – 0.20 mm/s),^{39,44} substantiating an oxidation state higher than Fe^{IV} . Spectroscopic studies and DFT calculations on this species assign it to be a $Fe^V(O)$ species with an axial acetylimido ligand, $[(TMC)Fe^V(O)(NC(O)CH_3)]^+$. The axial anionic acetylimido ligand serves as the rationale for the weaker $Fe=O$ vibrational stretch of 789 cm^{-1} than its $Fe^{IV}(O)$ precursor (839 cm^{-1}).

Table 1.1. Spectroscopic signatures of select Fe^V(O) and related Fe^{IV}(O) species

| Complex | EPR g-values | Mössbauer (δ) (mm/s) | Fe–O (Å) from EXAFS and ν(Fe=O) (cm ⁻¹) from rR | Refs |
|--|------------------|----------------------|---|-------|
| [Fe ^V (O)(TAML)] ⁻ | 1.99, 1.97, 1.74 | -0.42 | 1.58 | 38 |
| [Fe ^V (O)(bTAML)] ⁻ | 1.98, 1.94, 1.73 | -0.44 | 1.59 Å / 862 cm ⁻¹ | 41 |
| [Fe ^{IV} (O)(bTAML)] ⁻ | | -0.12 | 1.64 Å / 798 cm ⁻¹ | 42 |
| [Fe ^V (O)(NC(O)Me)(TMC)] ⁺ | 2.05, 2.01, 1.97 | +0.10 | | 43 |
| [Fe ^{IV} (O)(TMC)] ²⁺ | | +0.17 | 1.646 (XRD) | 45 |
| [Fe ^V (O)(OAc)(TPA*)] ²⁺ | 2.07, 2.01, 1.96 | | | 46 |
| [Fe ^V (O)(OAc)(S,S-PDP*)] ²⁺ | 2.07, 2.01, 1.96 | | | 46 |
| [Fe ^V (O)(OH)(^δ tips ³ TPA)] ⁺² | | | 827 cm ⁻¹ (IRPD) | 37 |
| [Fe ^V (O)(OAc)(PyNMe ₃)] ^{2+ a} | 2.07, 2.01, 1.95 | -0.06 ^a | 1.63 Å / 815 cm ⁻¹ | 47,48 |

^a generated with cyclohexyl percarboxylic acid

An Fe^V(O) intermediate is also proposed for the acetic-acid-assisted mechanism based on mechanistic experiments (described in Section 1.2.3). In 2015, Talsi and co-workers were the first group to observe an $S = \frac{1}{2}$ EPR signal with g values around 2.07, 2.01 and 1.96 for iron complexes supported by neutral TPA- (**1** in Figure 1.1) and PDP-based (**6** in Figure 1.4) ligands containing electron-donating substituents (referred to as TPA* and PDP*) when these complexes were reacted with H₂O₂ and CH₃COOH.⁴⁶ These extremely unstable species can be trapped only at low temperatures of -75 to -85 °C. In the presence of electron-rich olefins such as 1-octene, this EPR signal decays with a second order rate constant (k_2) of 0.032 M⁻¹ s⁻¹, indicating that this species is responsible for olefin oxidation. Talsi and co-workers attributed this signal to (L⁺⁺)Fe^{IV}(O)(OAc), but later studies by Que, Lipscomb and co-workers suggested that the properties of this species are better explained

by the formulation (L)Fe^V(O)(OAc).³³ Recently, in 2018, Talsi and co-workers also demonstrated this species to be capable of performing aromatic hydroxylation of benzene and substituted benzenes.⁴⁹

In 2015, Costas and co-workers designed a nonheme iron catalyst [Fe^{II}(PyNMe₃)]²⁺ (**7**) (Figure 1.4) that along with peracetic acid (AcOOH) formed one of the most reactive catalytic systems in the nonheme iron literature to date.⁴⁷ The reaction of **7** with AcOOH at -40 °C generates a highly reactive catalytic intermediate **7a** that directly reacts with the strong C–H bonds of cyclohexane and can be monitored spectroscopically. Intermediate **7a** exhibits a [substrate] dependent decay rate and a KIE of 5 in the oxidation of C₆H₁₂ versus C₆D₁₂, which supports **7a** to be the active oxidant. This oxidant **7a** has the highest rate of cyclohexane oxidation relative to other nonheme iron oxidants.⁴⁷ More importantly, **7a** is the first example in the nonheme iron literature where the catalytic active oxidant is spectroscopically observed. Intermediate **7a** has a UV-visible absorption feature at 490 nm ($\epsilon \approx 4500 \text{ M}^{-1} \text{ cm}^{-1}$) (Figure 1.5). Its EPR spectrum shows the presence of two $S = 1/2$ species: a) one with $g = 2.20, 2.19, 1.99$ (~ 5 % iron) assigned to be the Fe^{III}(OOAc) intermediate and b) the other with $g = 2.07, 2.01, 1.95$ (~ 40 % iron) associated with an Fe^V species (Figure 1.5). The Fe^V species has been identified as Fe^V(O)(OAc) based on EPR, low temperature mass spectrometry and the observation of the *cis*-hydroxyacetato product from olefin oxidation.⁴⁷

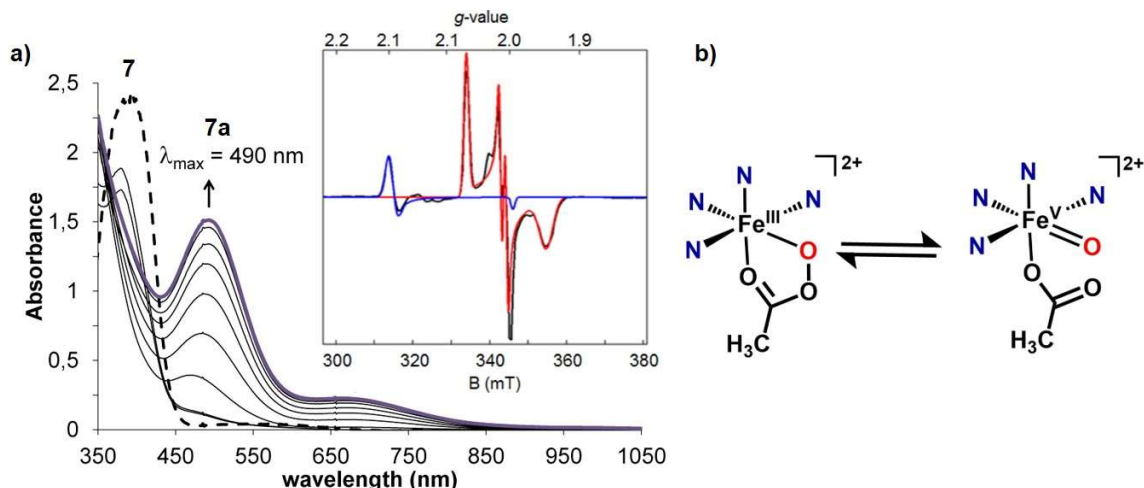


Figure 1.5. a) Formation of **7a** upon addition of AcOOH to **7** monitored by UV-visible absorption spectroscopy. Inset: EPR of **7a** showing the two $S = \frac{1}{2}$ iron species at $g = 2.20, 2.19, 1.99$ ($\sim 5\%$ iron) (blue) and $g = 2.07, 2.01, 1.95$ ($\sim 40\%$ iron) (red). b) Proposed electronic structures for the two $S = \frac{1}{2}$ species observed in EPR that represents the UV-visible absorption feature centered at 490 nm attributed to intermediate **7a**.⁴⁷ (Reproduced with permission from ref 47; copyright 2015 American Chemical Society)

Rigorous EPR, Mössbauer, XAS and resonance Raman experiments combined with DFT studies have been conducted on **7** and its electron-rich variant containing a -OMe group **7*** (Figure 1.4) to understand the electronic structure of intermediate **7a** or **7*a**.⁴⁸ Intermediate **7a** can also be generated with other peracids such as cyclohexyl percarboxylic acid (CPCA) and pernonanoic acid (PNA), and Mössbauer isomer shifts of -0.08 and -0.06 mm/s are observed for **7a**(PNA) (**7a** generated with PNA) and **7a**(CPCA) (**7a** generated with CPCA), respectively. The negative values for the Mössbauer isomer shifts, along with supporting DFT calculations, point toward an Fe^{V} oxidation state. Resonance Raman studies on **7a** generated using PNA reveal a resonance-enhanced peak at 815 cm^{-1} , which shifts to 783

cm^{-1} upon using O^{18} -PNA ($\Delta = 32 \text{ cm}^{-1}$). This 815 cm^{-1} peak is assigned to the Fe=O unit in **7a**, which has a higher frequency than the one observed for $[(\text{TMC})\text{Fe}^{\text{V}}(\text{O})(\text{NC}(\text{O})\text{CH}_3)]^+$ (798 cm^{-1}) containing an anionic ligand *trans* to the Fe=O unit, whereas for **7a** the anionic -OAc ligand is *cis* to the Fe=O unit. EXAFS analysis shows that **7a**(CPCA) has a scatterer at a distance of 1.63 \AA corresponding to the Fe=O unit. Based on DFT calculations supported by spectroscopic studies, it is concluded that **7a** and **7*a** have unique electronic structures where the O•••O distance between the oxygen of the Fe=O and the carbonyl oxygen of the acetate ligand in the Fe(O)(OAc) intermediate is calculated to be 2.04 \AA . At this O•••O distance, the iron center can exist in a facile equilibrium between $\text{Fe}^{\text{V}}(\text{O})(\text{OAc})$ and $\text{Fe}^{\text{III}}(\text{OOAc})$ species (Figure 1.5b). Intermediate **7a** is considered to have a predominant Fe^{V} character, whereas **7*a** is proposed to have a dominant Fe^{V} character along with some extent of $\text{Fe}^{\text{IV}}(\text{O})(\cdot\text{OAc})/\text{radical}$ and $\text{Fe}^{\text{III}}(\text{OOAc})$ character mixed in. The dominant Fe^{V} character of the oxidant is believed to be responsible for its unprecedented high reactivity. Quite interestingly, the three forms contributing to the electronic structure of **7*a** have also been proposed in the carboxylic acid-assisted mechanism of **1** and **1*** (Scheme 1.4). These examples highlight how slight changes in the ligand framework or reaction conditions can lead to different iron-oxo oxidants with varying degrees of reactivity.

1.4 Aim and scope of thesis

This thesis focuses on the mechanistic landscape of nonheme iron catalysts that can hydroxylate aliphatic and aromatic C–H bonds with H₂O₂ as oxidant. Nonheme iron catalysts have been shown to form high-valent iron-based oxidants from H₂O₂ with assistance from water or carboxylic acid. Chapter 2 illustrates the discovery of a new pathway to form a powerful iron(V) oxidant using H₂O₂ and Sc³⁺ or HClO₄. The nonheme iron complex [Fe^{II}(β-BPMCN)]²⁺ with H₂O₂ forms a catalytic system that has been previously reported to perform olefin oxidation but is ineffective for cyclohexane hydroxylation.⁵⁰ In this chapter, we demonstrate that redox-inactive Lewis acidic Sc³⁺ or Brønsted acid HClO₄ can form a potent oxidant that can efficiently catalyze hydroxylation of cyclohexane and benzene. Hydroxylation occurs within seconds at -40 °C, making it one of the fastest systems to date among synthetic nonheme iron complexes. Chapter 3 shows that addition of Fe^{III}(OTf)₃ can also activate the [Fe^{II}(β-BPMCN)]²⁺ and H₂O₂ combination to form a reactive oxidant, similar to Sc³⁺ or HClO₄. Fe³⁺ and Fe²⁺ are known for their redox activities, but in this study we have shown that Lewis acidic Fe³⁺ can interact with the [(β-BPMCN)Fe^{III}-OOH]²⁺ catalytic intermediate forming the oxidant that hydroxylates benzene and cyclohexane, whereas less Lewis acidic Fe²⁺ does not have the same effect. Activation of a nonheme Fe^{III}-OOH intermediate using another Fe³⁺ ion is unprecedented in synthetic bioinorganic chemistry and introduces the idea that the second iron in the diiron enzyme soluble methane monooxygenase can have an additional role as a Lewis acid to form the oxidant that oxidizes methane to methanol.

Chapter 4 examines the effect of redox-inactive Lewis-acidic Sc^{3+} on the catalytic reactivity of $[\text{Fe}^{\text{II}}(\alpha\text{-BPMCN})]^{2+}$ and $[\text{Fe}^{\text{II}}(\text{TPA})]^{2+}$ to determine how ligand topology around the iron center affects this new pathway for generating high-valent iron oxidants. The behavior of the $[\text{Fe}^{\text{II}}(\alpha\text{-BPMCN})]^{2+}$ and $[\text{Fe}^{\text{II}}(\text{TPA})]^{2+}$ systems is compared with that of $[\text{Fe}^{\text{II}}(\beta\text{-BPMCN})]^{2+}$. In contrast, Chapter 5 explores the effect of ligand topology around the iron center by comparing the relatively stable Fe^{V} species formed from one-electron oxidation of the isomeric TMC-supported $\text{Fe}^{\text{IV}}(\text{O})$ complexes where only the spatial orientations of the TMC methyl groups differ in the two isomers. Chapter 6 presents the final conclusions and future directions of the work initiated by this thesis.

1.5 References:

- (1) Kovaleva, E. G.; Lipscomb, J. D. *Nat. Chem. Biol.* **2008**, *4*, 186–193.
- (2) Kal, S.; Que, L. *J. Biol. Inorg. Chem.* **2017**, *22*, 339–365.
- (3) Olivo, G.; Cussó, O.; Borrell, M.; Costas, M. *J. Biol. Inorg. Chem.* **2017**, *22*, 425–452.
- (4) Hölzl, S. M.; Altmann, P. J.; Kück, J. W.; Kühn, F. E. *Coord. Chem. Rev.* **2017**, *352*, 517–536.
- (5) Gamba, I.; Codolà, Z.; Lloret-fillol, J.; Costas, M. *Coord. Chem. Rev.* **2017**, *334*, 2–24.
- (6) Bryliakov, K. P.; Talsi, E. P. *Coord. Chem. Rev.* **2014**, *276*, 73–96.

- (7) Costas, M.; Mehn, M. P.; Jensen, M. P.; Que, L. *Chem. Rev.* **2004**, *104*, 939–986.
- (8) Fenton, H. J. H. *J. Chem. Soc.* **1894**, *65*, 899–910.
- (9) Wardman, P.; Candeias, L. P. *Radiat. Res.* **1996**, *145*, 523–531.
- (10) Costas, M.; Chen, K.; Que, L. *Coord. Chem. Rev.* **2000**, *200–202*, 517–544.
- (11) Kim, C.; Chen, K.; Kim, J.; Que, L. *J. Am Chem. Soc.* **1997**, *119*, 5964–5965.
- (12) Chen, K.; Jr., L. Q. *Chem. Commun.* **1999**, No. 15, 1375–1376.
- (13) Chen, K.; Que, L. *Angew. Chem. Int. Ed.* **1999**, *95*, 2227–2229.
- (14) Barry, S. M.; Challis, G. L. *ACS Catal.* **2013**, *3*, 2362–2370.
- (15) Company, A.; Lloret-Fillol, J.; Costas, M. In *Comprehensive Inorganic Chemistry II*; Elsevier Ltd., 2013; p 487.
- (16) Chen, K.; Que, L. *J. Am. Chem. Soc.* **2001**, *123*, 6327–6337.
- (17) Chen, K.; Costas, M.; Kim, J.; Tipton, A. K.; Que, L. *J. Am. Chem. Soc.* **2002**, *124*, 3026–3035.
- (18) Costas, M.; Tipton, A. K.; Chen, K.; Jo, D. H.; Que L., J. *J. Am. Chem. Soc.* **2001**, *123*, 6722–6723.
- (19) Zima, A. M.; Lyakin, O. Y.; Bryliakov, K. P.; Talsi, E. P. *Mol. Catal.* **2018**, *455*, 6–13.
- (20) Simmons, E. M.; Hartwig, J. F. *Angew. Chem. Int. Ed.* **2012**, *51*, 3066–3072.

- (21) Bernadou, J.; Meunier, B. *Chem. Commun.* **1998**, 2167–2173.
- (22) Schröder, M. *Chem. Rev.* **1980**, *80*, 187–213.
- (23) Oloo, W. N.; Fielding, A. J.; Que, L. *J. Am. Chem. Soc.* **2013**, *135*, 6438–6441.
- (24) Zang, Y.; Kim, J.; Dong, Y.; Wilkinson, E. C.; Appelman, E. H.; Que, L. *J. Am. Chem. Soc.* **1997**, *119*, 4197–4205.
- (25) Makhlynets, O. V.; Rybak-Akimova, E. V. *Chem. Eur. J.* **2010**, *16*, 13995–14006.
- (26) White, M. C.; Doyle, A. G.; Jacobsen, E. N. *J. Am. Chem. Soc.* **2001**, *123*, 7194–7195.
- (27) Mas-Balleste, R.; Que, L. *J. Am. Chem. Soc.* **2007**, *129*, 15964–15972.
- (28) Mas-Balleste, R.; Fujita, M.; Que, L. *Dalton Trans.* **2008**, 1828–1830.
- (29) Das, P.; Que, L. *Inorg. Chem.* **2010**, *49*, 9479–9485.
- (30) Chen, M. S.; White, M. C. *Science* **2010**, *327*, 566–571.
- (31) Lyakin, O. Y.; Bryliakov, K. P.; Britovsek, G. J. P.; Talsi, E. P. *J. Am. Chem. Soc.* **2009**, *131*, 10798–10799.
- (32) Oloo, W. N.; Meier, K. K.; Wang, Y.; Shaik, S.; Münck, E.; Que, L. *Nat. Commun.* **2014**, *5*, 3046–3054.
- (33) Oloo, W. N.; Banerjee, R.; Lipscomb, J. D.; Que, L. *J. Am. Chem. Soc.* **2017**, *139*, 17313–17326.
- (34) Prat, I.; Mathieson, J. S.; Güell, M.; Ribas, X.; Luis, J. M.; Cronin, L.; Costas, M.

Nat. Chem. **2011**, *3*, 788–793.

(35) Xu, S.; Veach, J. J.; Oloo, W.; Peters, K. C.; Wang, J.; Perry, R. H.; Que, L. *Chem. Commun.* **2018**, *54*, 8701–8704.

(36) Hitomi, Y.; Arakawa, K.; Funabiki, T.; Kodera, M. *Angew. Chem. Int. Ed.* **2012**, *51*, 3448–3452.

(37) Borrell, M.; Andris, E.; Navrátil, R.; Roithová, J.; Costas, M. *Nat. Commun.* **2019**, *10*, 1–9.

(38) Tiago de Oliveira, F.; Chanda, A.; Banerjee, D.; Shan, X.; Mondal, S.; Que, L.; Bominaar, E. L.; Münck, E.; Collins, T. J. *Science* **2007**, *315*, 835–838.

(39) Klein, J. E. M. N.; Que, L. *Encyclopedia of Inorganic and Bioinorganic Chemistry*; 2016; DOI: 10.1002/9781119951438.eibc2344.

(40) Kundu, S.; Van Thompson, J. K.; Shen, L. Q.; Mills, M. R.; Bominaar, E. L.; Ryabov, A. D.; Collins, T. J. *Chem. Eur. J.* **2015**, *21*, 1803–1810.

(41) Ghosh, M.; Singh, K. K.; Panda, C.; Weitz, A.; Hendrich, M. P.; Collins, T. J.; Dhar, B. B.; Gupta, S. Sen. *J. Am. Chem. Soc.* **2014**, *136*, 9524–9527.

(42) Pattanayak, S.; Jasniewski, A. J.; Rana, A.; Draksharapu, A.; Singh, K. K.; Weitz, A.; Hendrich, M.; Que, L.; Dey, A.; Gupta, S. Sen. *Inorg. Chem.* **2017**, *56*, 6352–6361.

(43) Van Heuvelen, K. M.; Fiedler, A. T.; Shan, X.; De Hont, R. F.; Meier, K. K.; Bominaar, E. L.; Münck, E.; Que, L. *Proc. Natl. Acad. Sci.* **2012**, *109*, 11933–11938.

(44) McDonald, A. R.; Que, L. *Coord. Chem. Rev.* **2013**, *257*, 414–428.

- (45) Rohde, J.-U.; In, J. H.; Lim, M. H.; Brennessel, W. W.; Bukowski, M. R.; Stubna, A.; Munck, E.; Nam, W.; Que, Jr., L. *Science* **2003**, *299*, 1037–1039.
- (46) Lyakin, O. Y.; Zima, A. M.; Samsonenko, D. G.; Bryliakov, K. P.; Talsi, E. P. *ACS Catal.* **2015**, *5*, 2702–2707.
- (47) Serrano-Plana, J.; Oloo, W. N.; Acosta-Rueda, L.; Meier, K. K.; Verdejo, B.; García-España, E.; Basallote, M. G.; Münck, E.; Que, L.; Company, A.; Costas, M. *J. Am. Chem. Soc.* **2015**, *137*, 15833–15842.
- (48) Fan, R.; Serrano-Plana, J.; Oloo, W. N.; Draksharapu, A.; Delgado-pinar, E.; Company, A.; Martin-Diaconescu, V.; Borrell, M.; Lloret-Fillol, J.; García-España, E.; Guo, Y.; Bominaar, E. L.; Que, L.; Costas, M.; Munck, E. *J. Am. Chem. Soc.* **2018**, *140*, 3916–3928.
- (49) Lyakin, O. Y.; Zima, A. M.; Tkachenko, N. V.; Bryliakov, K. P.; Talsi, E. P. *ACS Catal.* **2018**, *8*, 5255–5260.
- (50) Costas, M.; Que, L. *Angew. Chem. Int. Ed.* **2002**, *41*, 2179–2181.

Chapter 2:

Activation of $[(\beta\text{-BPMCN})\text{Fe}^{\text{III}}\text{-OOH}]^{2+}$ intermediate to generate a highly reactive active oxidant using redox-inactive Lewis acidic Metal ions or Brønsted acids

Parts of the content of this chapter was published in:

Kal, S.; Draksharapu, A.; Que, L. Jr. Sc^{3+} (or HClO_4) activation of a nonheme $\text{Fe}^{\text{III}}\text{-OOH}$ intermediate for the rapid hydroxylation of cyclohexane and benzene, *J. Am. Chem. Soc.*, **2018**, *140*, 5798–5804.

2.1 Introduction

The emergence of nonheme iron enzymes as excellent biocatalysts for C–H bond functionalization^{1,2} has spurred the investigation of synthetic nonheme iron catalysts that perform hydrocarbon oxidations with H₂O₂ as the oxidant.^{3–5} Spectroscopic and mechanistic studies on some of these synthetic catalysts have provided evidence for an $S = 1/2$ Fe^{III}–OOH intermediate that then undergoes O–O bond heterolysis to generate the actual oxidant. An electrophilic oxoiron(V) species derived therefrom is proposed to be responsible for substrate oxidation.^{6–9} For Fe^{II}(TPA) and Fe^{II}(BPMEN) (TPA = tris(pyridyl-2-methyl)amine; BPMEN = *N,N'*-bis(pyridyl-2-methyl)-1,2-diaminoethane), this cleavage is promoted by a proton, delivered by a water or carboxylic acid ligand that is proposed to bind to the iron center *cis* to the HOO moiety. However, [Fe(β-BPMCNCN)]²⁺ (**1**, Figure 2.1)(BPMCNCN = *N,N'*-bis(pyridyl-2-methyl)-*N,N'*-dimethyl-*trans*-1,2-diaminocyclohexane) shows a reactivity pattern different from the well-studied Fe^{II}(TPA) and Fe^{II}(BPMEN) catalysts, and has previously been found to be a sluggish hydroxylation catalyst with H₂O₂ as the oxidant.¹⁰ We have thus investigated strategies by which to enhance the catalytic performance of **1**.

Extensive work by Fukuzumi and Nam showed that addition of Sc³⁺ and other Lewis acids can significantly enhance the oxidative reactivity of high-valent metal-oxo species, mainly by boosting the rate of electron transfer from substrate to a proposed Lewis-acid adduct of the metal-oxo center, and the electron transfer rate increased with the strength of the Lewis acid.^{11,12} In other work, Yin, Goldberg and Collins independently showed Lewis-acid activation of high-valent Mn(OH)₂ or Mn(O) centers,^{13–16} while

Fukuzumi and Nam subsequently found evidence for the formation of a Sc^{3+} -bound $\text{Mn}^{\text{V}}(\text{O})(\text{TAML})$ complex (TAML = tetraamido macrocyclic ligand) with the Lewis acid coordinated to the carbonyl oxygen of the macrocyclic ligand.¹⁷ Similarly, Lau demonstrated activation of polyoxo anions such as chromate, permanganate and ferrate by Lewis acids for the oxidation of C–H bonds.^{18–21} In a more recent effort, Lau and coworkers found that Lewis acids could activate $[\text{Os}^{\text{VI}}(\text{N})(\text{Cl})_4]^-$ by interacting with the nitride ligand to catalyze alkane oxidation with H_2O_2 or ROOH .²²

More relevant to our effort was the finding that Sc^{3+} and Y^{3+} induce cleavage of the O–O bond in $[\text{Fe}^{\text{III}}(\eta^2\text{-O}_2)(\text{TMC})]^+$ (TMC = tetramethylcyclam) to form the corresponding oxoiron(IV) complex,^{23,24} which led us to explore whether Fe-based intermediates involved in nonheme iron oxidation catalysis with peroxides as oxidants might be similarly activated. We were encouraged by recent papers that demonstrated positive effects of adding Sc^{3+} to metal-catalyzed oxidations at room temperature. Yin and coworkers found that adding Sc^{3+} tripled the olefin epoxidation yield by $\text{Fe}^{\text{II}}(\text{BPMEN})/\text{H}_2\text{O}_2$,²⁵ while Nodzevska and Watkinson showed that Sc^{3+} accelerated epoxidation rates of electron-deficient styrenes with the $[\text{Mn}_2(\mu\text{-O})_3(\text{TMTACN})_2]^{2+}/\text{H}_2\text{O}_2$ combination (TMTACN = 1,4,7-trimethyl-1,4,7-triazacyclo-nonane).²⁶ Chatterjee and Paine reported that Sc^{3+} promoted the stoichiometric hydroxylation of cyclohexane in the reaction of a nonheme iron(II)-benzilate complex with O_2 .²⁷ In all these cases, some interaction of Sc^{3+} with the putative metal-based oxidant was postulated, but no direct evidence for such an interaction was demonstrated. In this paper we focus on the sluggish catalyst **1** and report our findings that addition of Sc^{3+} or HClO_4 to the **1**/ H_2O_2 combination generates a powerful

hydroxylating agent. We have trapped a transient $S = \frac{1}{2}$ $\text{Fe}^{\text{III}}-(\eta^1\text{-OOH})$ intermediate **2** at cryogenic temperatures and demonstrate its activation by interaction with Sc^{3+} or HClO_4 to form a species that hydroxylates cyclohexane and benzene at -40 °C within a few seconds.

2.2 Experimental details

All materials were purchased from Sigma-Aldrich and used as received unless noted otherwise. H_2^{18}O (97% ^{18}O -enriched) and $\text{H}_2^{18}\text{O}_2$ (90% ^{18}O -enriched, 10% solution in H_2^{16}O) were obtained from Berry & Associates-ICON Isotopes. Cyclohexane, benzene and nitrobenzene were passed through alumina and silica gel before the reactions. 90% H_2O_2 was obtained from FMC Corporation. **Caution:** 90% H_2O_2 is potentially explosive and should be handled with proper safety precautions.^{28,29} The ligand BPMCN and the complex $[\text{Fe}^{\text{II}}(\beta\text{-BPMCN})](\text{OTf})_2$ were synthesized according to previously published procedures.^{10,30}

Product analyses were performed on a Perkin-Elmer Sigma 3 gas chromatograph (AT-1701 column) with a flame-ionization detector. GC mass spectral analyses were performed on a HP 6890 GC (HP-5 column) using an Agilent 5973 mass detector. For chemical ionization analyses, NH_3/CH_4 (4%) was used as the ionization gas. UV-visible absorption spectra were recorded on a HP8453A diode array spectrometer equipped with a cryostat from Unisoku, Scientific Instruments (Osaka, Japan). Resonance Raman spectra were obtained at -30 °C with excitation at 561 nm (100 mW at source, Cobolt Lasers) through the sample in a flat bottom NMR tube using a 90° backscattering arrangement

(parallel to the slit direction). The collimated Raman scattering was collected using two Plano convex lenses ($f = 12$ cm, placed at an appropriate distance) through appropriate long pass edge filters (Semrock) into an Acton AM-506M3 monochromator equipped with a Princeton Instruments ACTON PyLON LN/CCD-1340x400 detector. The detector was cooled to -120 °C prior to the experiments. Spectral calibration was performed using the Raman spectrum of acetonitrile/toluene 50:50 (v:v).³¹ Each spectrum was accumulated, typically 60 times with 1 s acquisition time, resulting in a total acquisition time of 1 min per spectrum. The collected data was processed using Spekwinn32,³² and a multi-point baseline correction was performed for all spectra. X-band EPR spectra were recorded on a Bruker Elexsys E-500 spectrometer equipped with an Oxford ESR 910 liquid helium cryostat and an Oxford temperature controller.

Catalytic reaction conditions – All experiments reported in this work were performed in the presence of air. In a typical reaction, 70 μ L of a 0.2 M H_2O_2 solution (diluted from 90% $\text{H}_2\text{O}_2/\text{H}_2\text{O}$ solution) in CH_3CN (10 eq H_2O_2 relative to $\mathbf{1}(\text{OTf})_2$) was added all at once to a vigorously stirred CH_3CN solution (1.93 mL) containing the iron catalyst $\mathbf{1}(\text{OTf})_2$, the substrate and $\text{Sc}(\text{OTf})_3$ or HClO_4 and stirred for 30 min at room temperature. The final concentration of the iron catalyst in the reaction mixture was 0.7 mM with 1000 eq cyclohexane/ 100 eq benzene/ 600 eq nitrobenzene and 0.5–8 eq $\text{Sc}(\text{OTf})_3$ or HClO_4 . After the reaction was over, 0.1 mL 1-methylimidazole and 1 mL acetic anhydride were added to the reaction solution to esterify the alcohol/phenol. An internal standard (naphthalene) was added after this and then the products were extracted into CH_2Cl_2 and the solution was then subjected to GC and/or GC-MS analysis. In experiments

with H₂¹⁸O₂, 10 eq or 70 μL of a 0.2 M H₂¹⁸O₂ solution (diluted from the 10% H₂¹⁸O₂/H₂O solution) relative to **1**(OTf)₂ was added instead of H₂O₂. In experiments with H₂¹⁸O, 68 μL of a 3.5-M H₂¹⁸O solution in CH₃CN (170 eq H₂¹⁸O relative to **1**(OTf)₂, which is about the same amount of H₂O that would be introduced from a 10% H₂O₂ solution) was added to the reaction mixture before adding H₂O₂.

Isotope-labeling studies – Similar conditions were used as described for catalytic reaction conditions above except for the following details. In experiments with H₂¹⁸O₂, 10 eq or 70 μL of a 0.2 M H₂¹⁸O₂ (diluted from 10% H₂¹⁸O₂/H₂O solution) relative to **1**(OTf)₂ was added instead of H₂O₂. In experiments with H₂¹⁸O, 68 μL of 3.5 M H₂¹⁸O solution in CH₃CN (170 eq H₂¹⁸O relative to **1**(OTf)₂ which is about the same amount of H₂O that would be introduced from a 10% H₂O₂ solution) was added to the reaction mixture before adding H₂O₂. The products were analyzed using GC/CI-MS or GC/EI-MS. The percent ¹⁸O-incorporation into the products was calculated on the basis of the ¹⁸O-enrichments of the reagents containing the isotope.

Competition experiments – Conditions similar to the general catalytic reactions were used except that a total of 600 eq substrate relative to **1**(OTf)₂ was present. The amount(s) of benzene/cyclohexane (in equivalents relative to **1**(OTf)₂) used were 600/0, 300/300, 100/500, 50/550, 0/600. The amount(s) of nitrobenzene/cyclohexane used were 300/300, 500/100, 550/50, 600/0.

Kinetic isotope effect (KIE) experiments – Conditions similar to what was described for the general catalytic reactions were used except for the following details. A ratio of 1:3 was used for cyclohexane/cyclohexane-d₁₂ in the KIE experiment to improve

the accuracy of the results. For benzene oxidation a 1:1 ratio of benzene/benzene- d_6 was used. H_2O_2 was added in a controlled fashion using a syringe pump to obtain results under similar conditions as reported in literature^{6,10} for the purpose of comparison. It was previously done using a syringe pump to enhance the yields of the products, but same results were obtained in the experiments with additives described in this paper with and without syringe pumping.

2.3 Effect of redox-inactive Lewis acidic metal ions on the catalytic reactivity of $[Fe^{II}(\beta\text{-BPMCN})]^{2+}/H_2O_2$

The oxidation of cyclohexane using **1** and 90% H_2O_2 (10 eq relative to **1**) in CH_3CN at 20 °C affords 0.5 eq cyclohexanol and 0.6 eq cyclohexanone as products (Figure 2.1 and Table 2.1). The apparent stoichiometric oxidation of cyclohexane and the low alcohol-to-ketone ratio (A/K) of 0.8 together indicate an unpromising catalyst/oxidant combination. These values do not change much upon addition of 2 eq Al^{3+} , Y^{3+} , Yb^{3+} , or Zn^{2+} relative to **1** (Figure 2.1), but treatment with 2 eq Sc^{3+} elicits a 10-fold increase in both the cyclohexanol yield and the A/K ratio (Figure 2.1 and Table 2.1). This observation can be rationalized by noting that H_2O_2 solutions contain water, and Lewis acidic metal salts such as $Al(OTf)_3$ and $Zn(OTf)_2$ are known to react with water and decompose. However, $Sc(OTf)_3$ is a relatively stable Lewis acid in water and a much stronger Lewis acid than the other water-stable Lewis acids tried like $Y(OTf)_3$ and $Yb(OTf)_3$.^{12,33} The increase in the alcohol TON (turnover number) is dependent on $[Sc^{3+}]$ and this effect starts to plateau at

ca. 2 eq Sc^{3+} . These results suggest that addition of Sc^{3+} changes the nature of the active oxidant formed in the reaction (Figure 2.2).

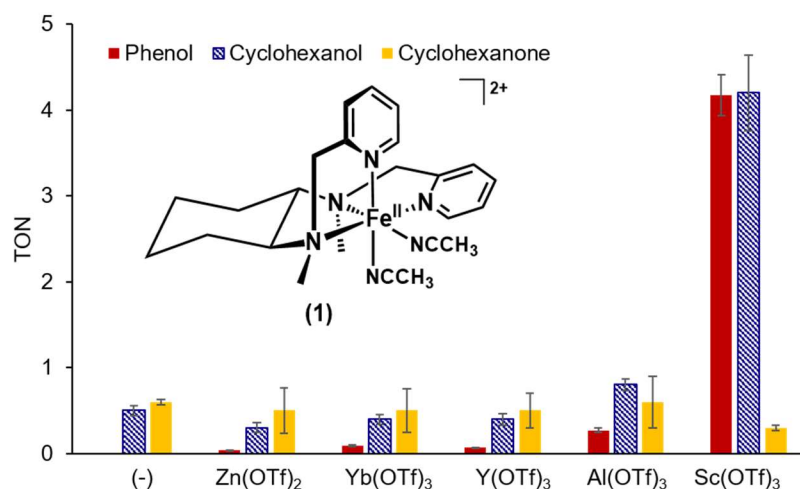


Figure 2.1. Effect of redox-inactive Lewis acids on the oxidation of cyclohexane (*c*-C₆H₁₂) and benzene (C₆H₆) by **1** (0.7 mM) and 10 eq H₂O₂ (added all at once) in the presence of 2 eq Lewis acid at r.t. under air, demonstrating that Sc^{3+} is the best of the Lewis acids tried in activating the catalyst/H₂O₂ combination.

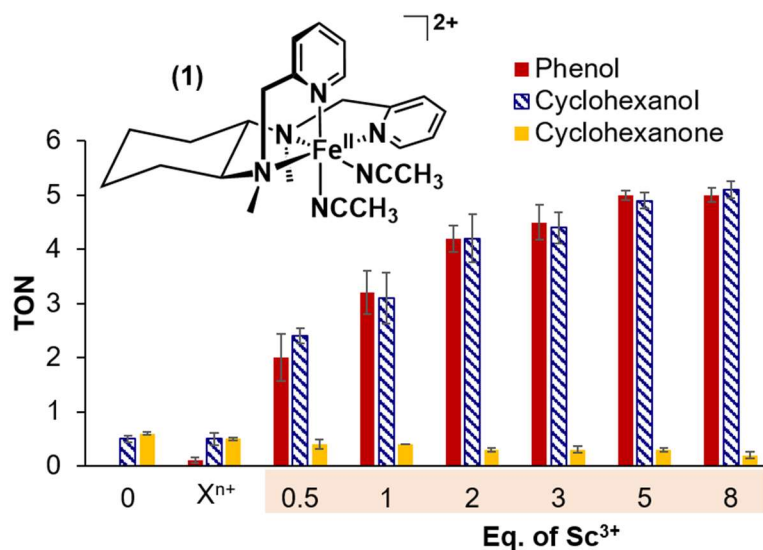


Figure 2.2. Yields in the hydroxylation of C₆H₆ (100 eq relative to **1**) or *c*-C₆H₁₂ (1000 eq) by **1** (0.7 mM) and 10 eq 90% H₂O₂ in CH₃CN at 20 °C under air as a function of [Sc³⁺].

X^{n+} reflects the averaged results from adding 2 eq Al^{3+} , Y^{3+} , Yb^{3+} , or Zn^{2+} (for individual results see Figure 2.1). (90% H_2O_2 was used as oxidant to minimize Lewis-acid deactivation by water present in the H_2O_2 solution.)

In the presence of Sc^{3+} , 50% of H_2O_2 can be converted into products versus only 11% conversion in the absence of Sc^{3+} (Figure 2.2). The high alcohol-to-ketone ratio (A/K) of 14 found for the Sc-activated reaction indicates that the alkyl radical generated after the initial H-atom abstraction must be short-lived and immediately rebounds to the oxygen attached to the metal center, which is also consistent with the absence of any significant effect of O_2 on the product TONs (Tables 2.1 and 2.2). The competitive oxidation of *c*- C_6H_{12} and *c*- C_6D_{12} in the presence of Sc^{3+} shows a product kinetic isotope effect (PKIE) of 2.5(2) versus 5(1) in the absence of Sc^{3+} (Table 2.1), suggesting the generation of a more powerful oxidant in the presence of Sc^{3+} . Taken together, the high A/K ratio, the absence of a significant effect of O_2 and a PKIE ≥ 2 point to a metal-based oxidant that forms in the presence of Sc^{3+} .

Table 2.1: Hydroxylation of *c*-C₆H₁₂ and C₆H₆ by **1**/H₂O₂^a

| | TON alcohol (A) | TON ketone (K) | A/K ^b | PKIE ^c | % H ₂ O ₂ converted ^d | TON PhOH (P) |
|------------------------|-----------------|----------------|------------------|-------------------|--|--------------|
| no Sc ³⁺ | 0.5(1) | 0.6(1) | 0.8 | 5(1) | 11 | 0 |
| 2000 eq AcOH | 2.0(1) | 0.4(1) | 5 | 4.2(4) | 24 | 0 |
| 2 eq Sc ³⁺ | 4.2(4) | 0.3(1) | 14 | 2.5(2) | 45 | 4.2(2) |
| 2 eq HClO ₄ | 4.0(2) | 0.1(1) | 40 | 2.0(1) | 40 | 4.0(3) |

^a All reactions were performed at room temperature under air; TON (Turnover Number) = moles of product/moles of **1**. ^b A/K = TON alcohol/TON ketone. ^c PKIE = kinetic isotope effect based on yields of cyclohexanol and cyclohexanol-*d*₁₁ (For PKIE experiments, H₂O₂ was added by syringe pump). ^d % conversion of H₂O₂ = (A + K)/H₂O₂ x 100 for *c*-C₆H₁₂ oxidation.

Table 2.2: Cyclohexane oxidation results in the presence and the absence of air

| | Alcohol TON (A) | Ketone TON (K) | A/K |
|--|-----------------|----------------|-----|
| 1 under air | 0.3 | 0.8 | 0.4 |
| 1 under N ₂ | 0.4 | 0.7 | 0.6 |
| 1 + Sc ³⁺ under air | 4.4 | 0.6 | 7 |
| 1 + Sc ³⁺ under N ₂ | 4.0 | 0.4 | 10 |

Reaction condition: **1**:H₂O₂:cyclohexane:Sc³⁺ = **1**(1 mM):10:1000:2 at room temperature in CH₃CN.

Interestingly, the **1**/H₂O₂/Sc³⁺ combination can also catalyze benzene hydroxylation, affording phenol in amounts comparable to cyclohexanol in cyclohexane oxidation (Figure 2.1 and 2.2). Benzene hydroxylation is observed only when Sc³⁺ is present with as much as 5 TON or 50% conversion of H₂O₂ into phenol (Figure 2.1 and

2.2), a yield comparable to or better than the other iron systems reported so far under similar conditions (Table 2.3). As found for cyclohexane hydroxylation, the phenol yield depends on $[\text{Sc}^{3+}]$ and begins to plateau at ~ 2 eq Sc^{3+} w.r.t **1** (Figure 2.2). No over-oxidation products are found, unlike for other catalytic systems in which p-benzoquinone and/or catechol were observed as byproducts.^{9,34,35} The oxidant formed is also able to attack electron-poor benzene derivatives such as bromobenzene, trifluoromethylbenzene, nitrobenzene, and even 1-chloro-2-nitrobenzene. For nitrobenzene, 3-nitrophenol and 2-nitrophenol products are obtained, with respective TONs of 1.1(1) and 0.5(1). These results point to the formation of a powerful and highly electrophilic oxidant. An inverse KIE of 0.9 is found from GC-MS analysis based on product peak intensity ratios in the oxidation of a 1:1 mixture of C_6H_6 and C_6D_6 . Such values are typically found for electrophilic aromatic substitution reactions,³⁶ implicating a metal-based electrophilic oxidant, rather than a radical-based oxidant for which the KIE is typically greater than 1.^{35,37,38}

Table 2.3: First-row transition metal systems that can perform aromatic hydroxylation of benzene with H₂O₂ as oxidant.^a

| | TON (Phenol/Fe) | KIE | T (°C) | Catalyst/ Substrate /Oxidant | Time (h) | Ref |
|--|--------------------|------------------------|-------------------------------|------------------------------------|-------------|---------------|
| KIE ≤ 1 | | | | | | |
| [Fe(β-BPMC(N)(CH ₃ CN) ₂)] ²⁺ (with 2 eq Sc ³⁺) | 4.2 | 0.9 | 25 | 1/100/10 | 0.5 | This work |
| [Fe(BPMEN)(CH ₃ CN) ₂](ClO ₄) ₂ (0.5 mM) | 1.0 | 0.8 | 25 | 1/300/10 | 0.5 | ⁹ |
| [Fe ^{III} ₂ (BPMEN) ₂ (μ-O)-(μ-OH)](ClO ₄) ₃ | 0.7 | - | 25 | 1/300/10 ^b | 0.25 | ³⁹ |
| [Fe ^{II} (di-pyridyl-di-NHC)](PF ₆) ₂ (3.05 mM) | 5.6 | 0.9 | 25 | 1/100/50 | 1 | ³⁴ |
| [Ni(TPA)] ²⁺ with 0.1 mol% triethylamine | 749 | 1.0 | 60 | 1/10000/50000 | 216 | ⁴⁰ |
| KIE > 1 | | | | | | |
| [Fe(L ₅ ²)(OOH)] ²⁺ (under single TON conditions) | (3% w.r.t Fe–OOH) | 1.05 | 21 | 1/9200 | | ³⁸ |
| [Cu ₂ (μ-OH)(6-hpa)] ²⁺ with 5 μmoles of triethylamine | 12000 | 1.04 | 50 (under N ₂) | 1/60/120 | 40 | ³⁵ |
| [Cu(MeCN)(TPA)] ²⁺ with 10 μmoles of triethylamine | 2260 | 1.40 | 50 (under N ₂) | 1/30/60 | 40 | ³⁵ |
| [Cu(MeCN)(TPA)] ²⁺ incorporated into a mesoporous material | 4320 | Radical chain reaction | 30 | - | 112 | ⁴¹ |

^a The systems listed here have undergone mechanistic investigations. ^b Based on diiron complex

Abbreviations used: BPMCN = *N,N'*-bis(pyridyl-2-methyl)-*N,N'*-dimethyl-*trans*-1,2-diaminocyclohexane; BPMEN = *N,N'*-bis(pyridyl-2-methyl)-*N,N'*-dimethyl-1,2-diaminoethane; TPA = tris(2-pyridylmethyl)amine; 6-hpa = 1,2-bis[2-[bis(2-pyridylmethyl)-aminomethyl]-6-pyridyl]ethane; di-pyridyl-di-NHC = 2-(3-((3-(pyridin-2-yl)-4H-1λ⁴,3λ⁴-imidazol-1-yl)methyl)-4H-1λ⁴,3λ⁴-imidazol-1-yl)pyridine

Despite being quite different transformations, cyclohexane and benzene oxidation by **1**/H₂O₂/Sc³⁺ show a similar dependence on [Sc³⁺] (Figure 2.2), allowing the comparison of the two distinct and relatively difficult reactions. Competitive oxidation of cyclohexane and benzene shows the oxidation of the latter to be favored by 10:1 on a per mole basis (Figure 2.3). On the other hand, oxidation of a 1:1 mixture of cyclohexane and nitrobenzene shows cyclohexane oxidation to be favored 3:1 over that of nitrobenzene. These comparisons give rise to a reactivity order of benzene > cyclohexane > nitrobenzene and, to the best of our knowledge, represent a unique opportunity for such a reactivity comparison for a first-row transition metal oxidation catalyst.

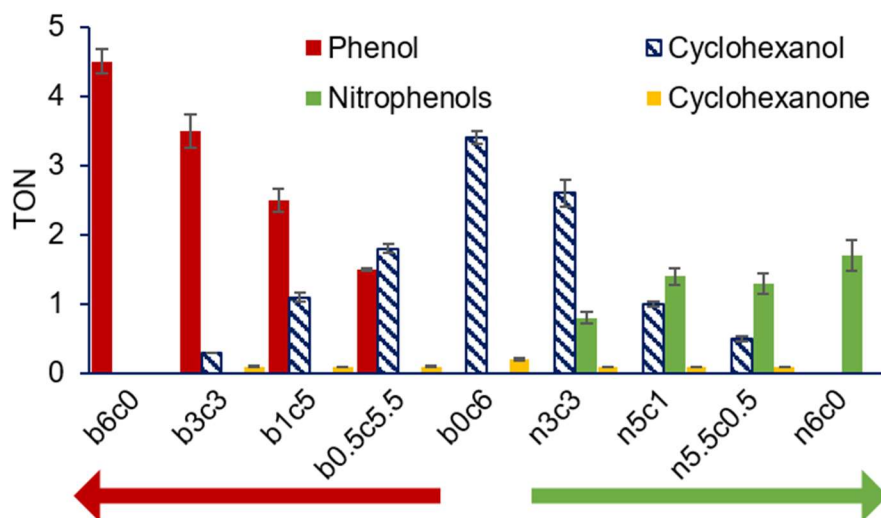


Figure 2.3. Competitive hydroxylations of cyclohexane (**c**) and benzene (**b**, left) or nitrobenzene (**n**, right) with 0.7 mM **1**, 10 eq H₂O₂, 2 eq Sc³⁺ and 600 eq total substrate. The numbers on the x-axis represent the substrate ratio in the competition experiments.

2.4 Effect of HOAc and HClO₄ on the reactivity of [Fe^{II}(β-BPMCN)]²⁺/H₂O₂

In our previous work with **1** and olefins, we showed that addition of 2000 eq HOAc to **1**/H₂O₂ switched its reactivity preference from *cis*-dihydroxylation of electron-poor olefins to epoxidation of electron-rich olefins, involving formation of a putative Fe^V(O)(OAc) oxidant.⁴² Here, we found that addition of 2000 eq HOAc to **1**/H₂O₂ only doubled the amount of cyclohexanol from cyclohexane but did not convert benzene to phenol (see Table 2.1). Additionally, the PKIE observed for HOAc addition is quite similar to the value observed without additive but different from that obtained in the presence of Sc³⁺ (Table 2.1). These results suggest that the oxidant produced by adding HOAc is less effective and quite distinct from that formed with Sc³⁺.

We have also investigated replacing Sc³⁺ with HClO₄ and found HClO₄ to have the same effect as Sc³⁺ on **1**-catalyzed oxidations (Table 2.1). At the same concentration as Sc³⁺, HClO₄ affords similar yields of cyclohexanol and phenol (Figure 2.4). Furthermore, essentially the same PKIE value is found for cyclohexane oxidation by **1**/H₂O₂/HClO₄ as **1**/H₂O₂/Sc³⁺, showing comparable selectivity for attacking the cyclohexane C–H over C–D bonds. Additionally, addition of Sc³⁺ or HClO₄ affects the lifetime of intermediate **2** similarly (*vide infra*). These results together suggest the formation of a common oxidant for HClO₄ and Sc³⁺. We have found that adding HNO₃, H₂SO₄ or HBF₄•Et₂O instead of HClO₄ to the **1**/H₂O₂/benzene mixture also leads to formation of **3** but either at a slower rate than HClO₄ or at a lower spectroscopic yield of **3**. This reactivity difference may derive from the higher pK_a's of these acids and/or possible interactions of the NO₃⁻ or SO₄²⁻ counteranion with the active oxidant. Preliminary spectroscopic experiments on acid

dependence are mentioned in Section 2.6 and show HClO₄ to have the best performance among these strong Brønsted acids. The acid dependence will be further investigated in future efforts.

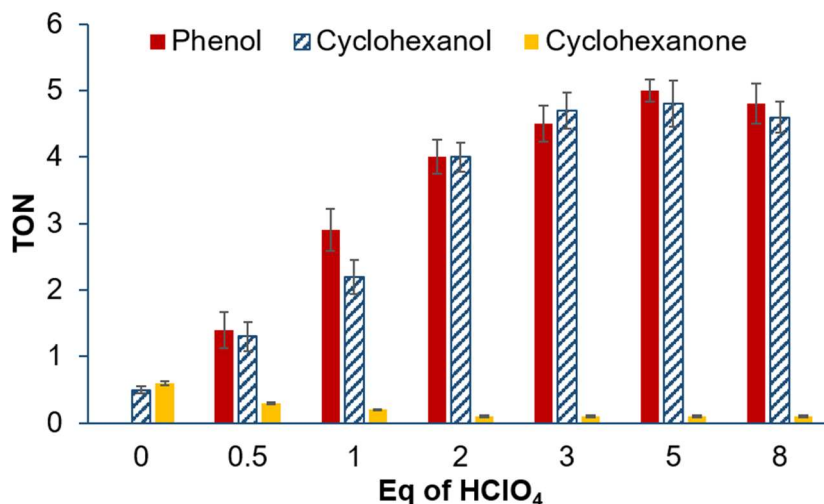


Figure 2.4. Yields in the hydroxylation of C₆H₆ (100 eq relative to **1**) or *c*-C₆H₁₂ (1000 eq) by **1** (0.7 mM) and 10 eq 90% H₂O₂ in CH₃CN at 20 °C under air as a function of [HClO₄].

2.5 Characterization of the [Fe^{III}(β-BPMCN)(OOH)]²⁺ intermediate **2**

To gain insight into this chemistry of **1**/H₂O₂ with Sc³⁺ or HClO₄, the reaction of **1** with H₂O₂ was initially investigated in the absence of Sc³⁺ and HClO₄ at -40 °C in CH₃CN. A transient purple intermediate, **2**, is observed with a λ_{max} at 545 nm, an EPR signal with g = 2.22, 2.17, and 1.96, and a resonance Raman spectrum with bands at 613 and 802 cm⁻¹ assigned to Fe–O and O–O vibrations, respectively (Figure 2.5 and 2.6). Taken together, all the spectroscopic evidence characterizes **2** as a low-spin (*S* = ½) Fe^{III}-η¹-OOH intermediate, based on literature precedents (Table 2.4).^{43,44} The corresponding [(TPA)Fe^{III}-OOH]²⁺ species has been implicated as the precursor to the electrophilic

oxidant responsible for Fe(TPA)-catalyzed alkane hydroxylation and olefin epoxidation and *cis*-dihydroxylation.⁶⁻⁸ However, despite their spectroscopic similarities, **2** is much less reactive than its TPA analog^{6,10} and requires activation by Sc³⁺ or HClO₄ to carry out electrophilic oxidations.

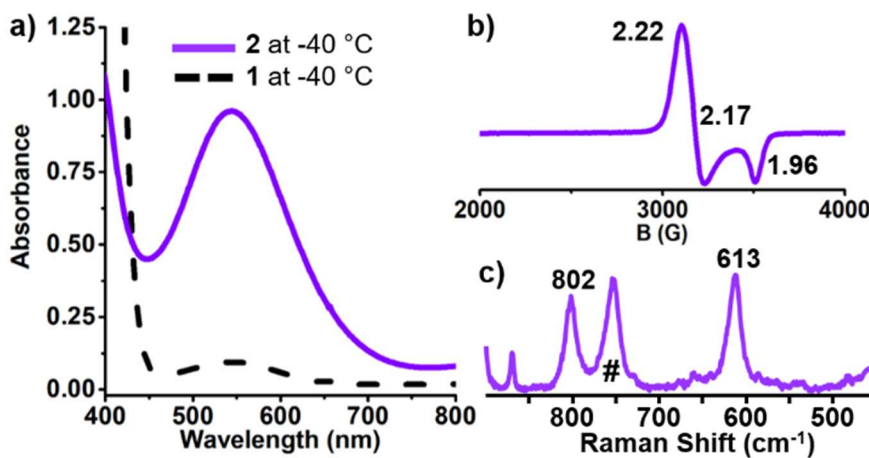


Figure 2.5. (a) UV-vis spectrum of **2** formed at -40 °C in CH₃CN from 1 mM **1** and 20 eq H₂O₂; (b) X-band EPR spectrum of **2** obtained at 40 dB at 2 K; (c) resonance Raman spectrum of **2** formed with 2.5 mM **1** and 20 eq H₂O₂ at -30 °C (λ_{exc} 561 nm).

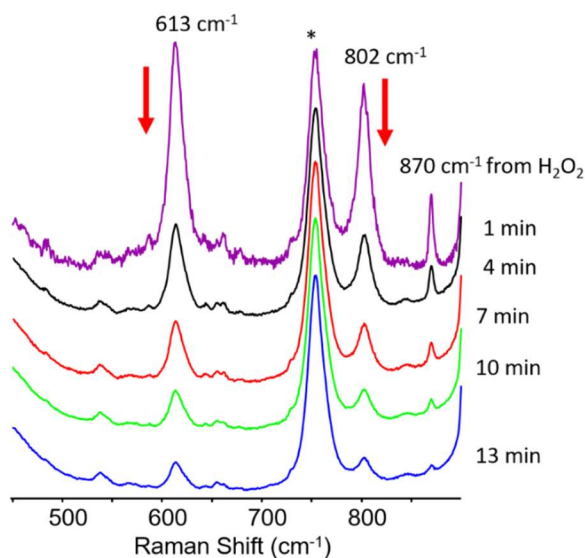


Figure 2.6. The decay of **2** as monitored by resonance Raman spectroscopy at $-30\text{ }^{\circ}\text{C}$. (λ_{exc} 561 nm). The resonance enhanced Raman peaks at 613 and 802 cm^{-1} disappear with time along with the Raman peak for H_2O_2 at 870 cm^{-1} .

Table 2.4: Spectroscopic properties of nonheme $\text{Fe}^{\text{III}}\text{-OOH}$ and $\text{Fe}^{\text{III}}\text{-(}\eta^2\text{-O}_2\text{)}$ intermediates^a

| | λ_{max} (nm) | $\nu(\text{Fe-O})$ (cm^{-1}) ($\Delta^{18}\text{O}$) | $\nu(\text{O-O})$ (cm^{-1}) ($\Delta^{18}\text{O}$) | EPR g-values | Refs |
|---|--------------------------------|---|--|------------------|-------|
| Low spin ($S = 1/2$) $\text{Fe}^{\text{III}}\text{-OOH}$ | 530-560 | 590-635 | 780-810 | 2.22-1.90 | |
| $[\text{Fe}(\text{N4Py})(\text{OOH})]^{2+}$ | 548 | 632 (16) | 790 (44) | 2.16, 2.11, 1.98 | 45,46 |
| $[\text{Fe}(\text{Py5})(\text{OOH})]^{2+}$ | 592 | 627 | 806 | 2.15, 2.13, 1.98 | 46 |
| $[\text{Fe}(\text{H-TPEN})(\text{OOH})]^{2+}$ | 531 | 625 (23) | 801 (51) | 2.19, 2.14, 1.96 | 47 |
| $[\text{Fe}(\text{Me-TPEN})(\text{OOH})]^{2+}$ | 537 | 617 (17) | 796 (45) | 2.19, 2.12, 1.95 | 47 |
| $[\text{Fe}(\text{TPEN})(\text{OOH})]^{2+}$ | 541 | 617 | 796 | 2.22, 2.15, 1.97 | 47 |
| $[\text{Fe}(\text{pb})_2(\text{OOH})]^{2+}$ | 560 | 623 | 811 | 2.18, 2.18, 1.97 | 48 |
| $[\text{Fe}(\text{TPA})(\text{OOH})]^{2+}$ | 538 | 632 (16) | 790 (44) | 2.19, 2.15, 1.97 | 45 |

| | | | | | |
|--|----------------|----------------|----------------|-------------------------------------|------------------|
| [Fe(Me-TPPN)(OOH)] ²⁺ | 550 | 609 | 799 | 2.16, 2.10, 1.92 | 49 |
| [Fe(L ^{Ph})(Tp ^{Me2})(OOH)] ₂₊ | 542 | 598 (25) | 778 (40) | 2.20, 2.16, 1.97 | 50 |
| [Fe(L ²)(OOH)] ²⁺ | 561 | 608 (24) | 804 (44) | 2.19, 2.13, 1.96 | 51 |
| [Fe(L ³)(OOH)] ²⁺ | 561 | 620 (22) | 804 (43) | 2.18, 2.12, 1.95 | 51 |
| [Fe(β -BPMCN)(OOH)] ²⁺ | 545 | 613 | 802 | 2.22, 2.17, 1.96 | <i>This work</i> |
| High spin (<i>S</i> = 5/2) Fe^{III}-OOH | 500-570 | 420-620 | 830-890 | 8.00-3.40 | |
| [Fe(H ₂ BPPA)(OOH)] ²⁺ | 568 | 621 (22) | 830 (17) | 7.54, 5.78, 4.25 | 52 |
| [Fe(TMC)(OOH)] ²⁺ | ~ 500 | 676 (24) | 870 (50) | 8.00, 5.71, 3.40 | 53 |
| [Fe(cyclam-PrS)(OOH)] ⁺ | 530 | 419 (19) | 891 (35) | 7.72, 5.40, 4.15 | 54 |
| High spin (<i>S</i> = 5/2) Fe^{III}-(η^2-O₂) | >650 | 470-500 | 810-830 | >4.3 | |
| [Fe(N4Py)(OO)] ⁺ | 685 | 495(17) | 827(47) | 8.0, 5.6 | 46 |
| [Fe(TMC)(OO)] ⁺ | 835 | 493(15) | 826(41) | 4.58, 4.38, ~4.1 | 53 |
| [Fe(Me-TPEN)(OO)] ⁺ | 740 | 470(16) | 819(45) | 7.5, 5.9 | 47 |
| [Fe(TPEN)(OO)] ⁺ | 755 | 470 | 817 | 10, 8.1, 5.6, 3.2, 2.4 ^b | 47 |

^aAbbreviations used: N4Py = *N*-(bis(2-pyridyl)methyl)-*N,N*-bis(2-pyridylmethyl)amine; Py5 = 2,6-bis(methoxy(di(2-pyridyl)methyl)pyridine); H-TPEN = [*N,N',N'*-tris(2-pyridylmethyl)ethane-1,2-diamine]; Me-TPEN = [*N*-methyl-*N,N',N'*-tris(2-pyridylmethyl)ethane-1,2-diamine]; TPEN = [*N,N,N',N'*-tetrakis(2-pyridylmethyl)ethane-1,2-diamine] (TPEN); pb = (-)4,5-pinene-2,2'-bipyridine; Me-TPPN = *N*-Methyl-*N,N',N'*-tris(2-pyridylmethyl)propane-1,3-diamine; (L^{Ph}) = [Me(Ph)B(2-Im^{*N*-Me})₂]⁻; (Tp^{Me2}) = (hydrotris(3,5-dimethylpyrazolyl)borate); L² and L³ = pentadentate bispidine derivatives; BPPA = *N,N*-bis[6-(pivaloylamino)pyridyl-2-methyl]pyridyl-2-methylamine; TMC = tetramethylcyclam; cyclam-PrS = *N*-(3-mercaptopropyl)-cyclam.

^bThe *g* = 10 signal is assigned to arise from the ground doublet, the *g* = 5.6 and 2.4 signals from the middle doublet, and the *g* = 8.1 and 3.2 signals from the upper doublet of an *S* = 5/2 system.

2.6 Kinetic analysis of the activation of $[(\beta\text{-BPMCN})\text{Fe}^{\text{III}}\text{-OOH}]^{2+}$ by Sc^{3+} and HClO_4

Upon addition of excess H_2O_2 to **1** in the presence of cyclohexane, **2** forms and reaches a pseudo-steady-state phase and then decays over the course of 90 min at $-40\text{ }^\circ\text{C}$ (Figure 2.7). However, addition of Sc^{3+} to this mixture upon maximum accumulation of **2** accelerates the decay of **2** by a 1000-fold (Figures 2.8 and 2.9b (green)). Similarly, **2** accumulates upon addition of H_2O_2 in the presence of benzene within the same time period as for cyclohexane. However, addition of Sc^{3+} to **2** in the presence of benzene instead of cyclohexane generates an intense blue chromophore characteristic of an Fe^{III} -phenolate species **3** (λ_{max} 620 nm),⁵⁵ which is conveniently monitored at 800 nm where there is no contribution from **2** (Figures 2.9a and 2.9b). The ability of $\mathbf{1}+\text{H}_2\text{O}_2+\text{Sc}^{3+}$ to oxidize other substituted benzene analogs was also monitored using the distinct $\text{Fe}^{\text{III}}\text{-OPh}'$ (OPh' = substituted phenol) chromophores corresponding to the respective substituted phenols formed from oxidation of the substituted benzene analogs (Figure 2.10). No formation of **3** was observed until Sc^{3+} was added to the reaction mixture containing benzene (Figure 2.9b). These observations concur with the catalytic results for $\mathbf{1}/\text{H}_2\text{O}_2$ where phenol is formed only in the presence of Sc^{3+} (Table 2.1).

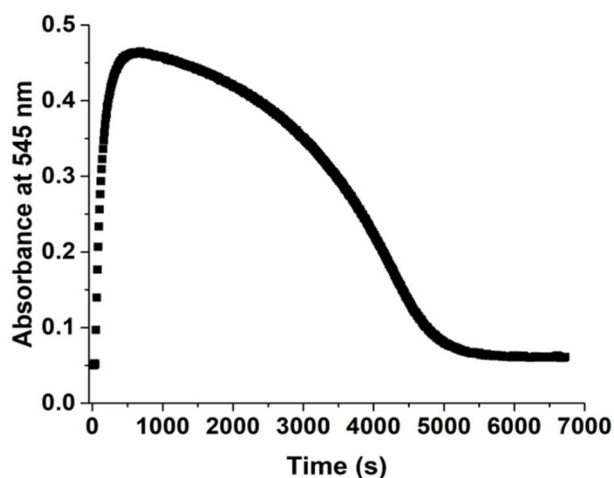


Figure 2.7. Decay of **2** in the absence of Sc^{3+} monitored at 545 nm. The reaction solution contains 185 eq cyclohexane w.r.t **1**, and **2** was generated from 0.5 mM **1** with 20 eq. H_2O_2 at $-40\text{ }^\circ\text{C}$.

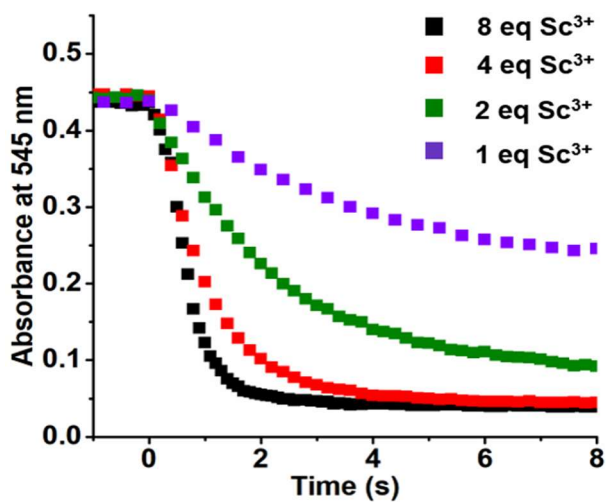


Figure 2.8. Decay of **2** upon addition of various eq Sc^{3+} . The reaction solution contains 185 eq cyclohexane w.r.t **1**, and **2** was generated from 0.5 mM **1** with 20 eq. H_2O_2 at $-40\text{ }^\circ\text{C}$.

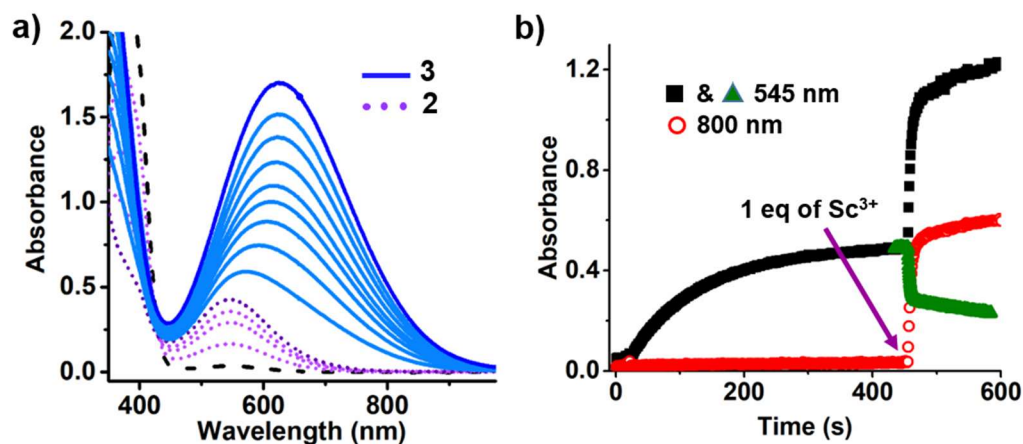


Figure 2.9. (a) Spectral changes in the visible region upon reaction of 0.5 mM **1** (dashed black line) in CH₃CN at -40 °C with 20 eq H₂O₂ to form **2** (dotted purple lines). Formation of **3** is observed upon subsequent addition of 1 eq Sc³⁺ to **2** (solid blue lines). (b) Time traces monitoring nearly instantaneous changes in absorbance at 545 and 800 nm after addition of 1 eq Sc³⁺. ■: 545 nm and ○: 800 nm in the presence of C₆H₆; ▲: 545 nm in the presence of C₆H₁₂.

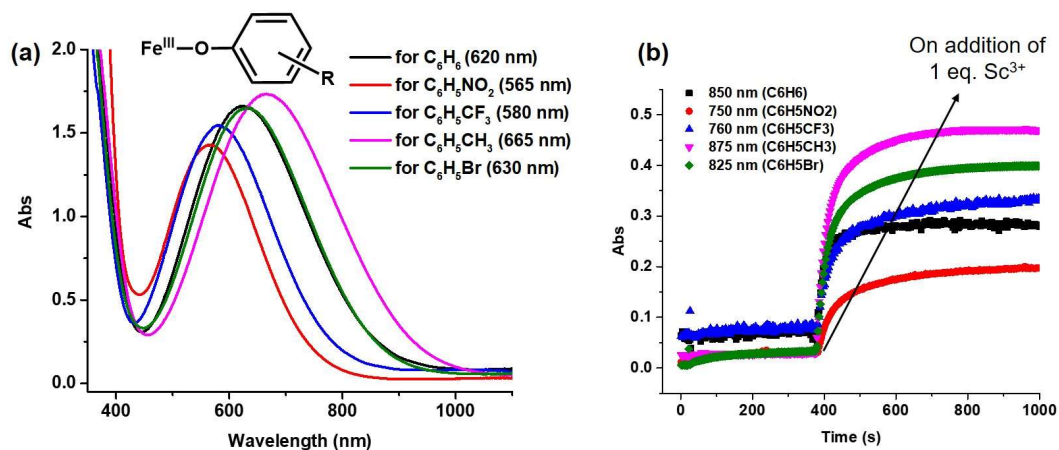


Figure 2.10. Oxidation of substituted benzene substrates with electron-withdrawing substituents upon addition of 1 eq. Sc³⁺ to the Fe^{III}-OOH intermediate **2** formed from 0.5 mM **1** at -40 °C in CH₃CN. (a) Absorption spectra showing formation of the Fe^{III}-phenolate complexes upon addition of Sc³⁺ to **2**. (b) Time traces monitoring formation of the Fe^{III}-

phenolate products at wavelengths where the Fe^{III} -phenolate complexes have absorption but not intermediate **2**.

Very interestingly, upon addition of Sc^{3+} to **2**, the rate of **3** formation in the presence of benzene matches the decay rate of **2** in the presence of cyclohexane (Figure 2.9b and 2.11). At the same concentration as Sc^{3+} , HClO_4 causes **2** to decay (in the presence of cyclohexane) or **3** to form (in the presence of benzene) at essentially the same rates as Sc^{3+} (Figure 2.12 and Table 2.5), supporting our earlier inference that Sc^{3+} and HClO_4 activate **2** in a similar fashion to form a common active oxidant. Importantly, the rates of **2** decay and **3** formation both increase as a function of $[\text{Sc}^{3+}]/[\text{HClO}_4]$ (Figure 2.11 and Figure 2.12) but do not depend on either [cyclohexane] or [benzene] (Table 2.5). Taken together, these observations suggest that **2** is not the actual oxidant, but instead interacts with $\text{Sc}^{3+}/\text{HClO}_4$ to form **Ox**, the species responsible for substrate oxidation, and the substrate oxidation step must be faster than the oxidant forming step.

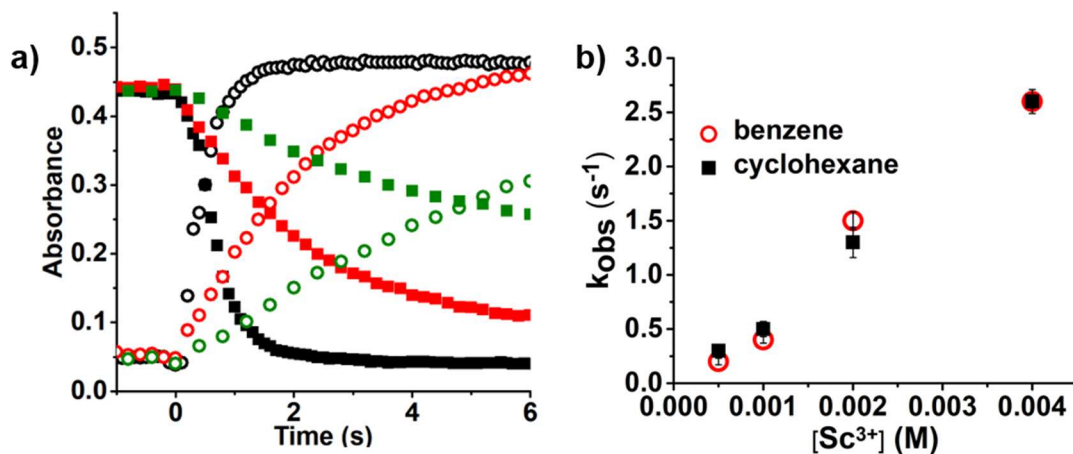


Figure 2.11. (a) Time traces monitoring decay of **2** at 545 nm in the presence of 185 eq cyclohexane (■) and formation of **3** at 800 nm with 100 eq benzene (○) showing the effect of increasing [Sc³⁺] (green: 1 eq; red: 2 eq; black: 8 eq Sc³⁺). (b) [Sc³⁺] dependence of k_{obs} for **2** decay with cyclohexane as substrate (■) or **3** formation (○) with benzene as substrate.

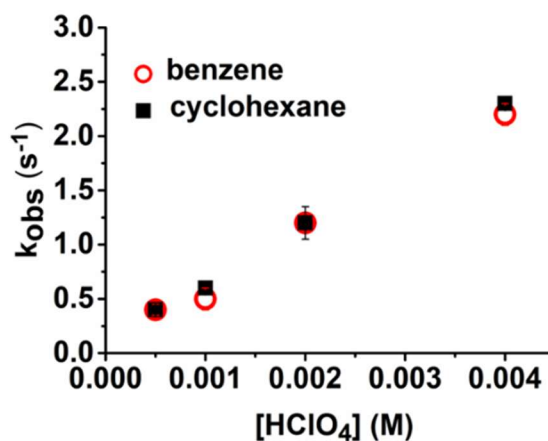


Figure 2.12. [HClO₄] dependence of rates for the decay of **2** with cyclohexane as substrate (■) or the formation of **3** (○) with benzene as substrate.

Table 2.5. Rates for decay of **2** in the presence of cyclohexane and formation of **3** in the presence of benzene with increasing $[\text{Sc}^{3+}]$ or $[\text{HClO}_4]$ ^a

| Benzene | k_{obs} (s^{-1}) | Cyclohexane | k_{obs} (s^{-1}) |
|--|--------------------------------------|--|--------------------------------------|
| Varying $[\text{Sc}^{3+}]$ | | | |
| <i>With 100 eq benzene</i> | | <i>With 185 eq cyclohexane</i> | |
| Benzene+8 eq Sc^{3+} | 2.6 ± 0.11 | Cyclohexane + 8 eq Sc^{3+} | 2.5 ± 0.06 |
| Benzene+4 eq Sc^{3+} | 1.5 ± 0.08 | Cyclohexane + 4 eq Sc^{3+} | 1.4 ± 0.14 |
| Benzene+2 eq Sc^{3+} | 0.4 ± 0.03 | Cyclohexane + 2 eq Sc^{3+} | 0.5 ± 0.07 |
| Benzene+1 eq Sc^{3+} | 0.2 ± 0.03 | Cyclohexane + 1 eq Sc^{3+} | 0.3 ± 0.04 |
| Varying $[\text{HClO}_4]$ | | | |
| <i>With 100 eq benzene</i> | | <i>With 185 eq cyclohexane</i> | |
| Benzene + 8 eq H^+ | 2.2 ± 0.10 | Cyclohexane + 8 eq H^+ | 2.3 ± 0.05 |
| Benzene + 4 eq H^+ | 1.2 ± 0.15 | Cyclohexane + 4 eq H^+ | 1.2 ± 0.15 |
| Benzene + 2 eq H^+ | 0.5 ± 0.10 | Cyclohexane + 2 eq H^+ | 0.6 ± 0.03 |
| Benzene + 1 eq H^+ | 0.4 ± 0.05 | Cyclohexane + 1 eq H^+ | 0.4 ± 0.04 |
| Varying [substrate] | | | |
| <i>With 2 eq Sc^{3+}</i> | | <i>With 2 eq Sc^{3+}</i> | |
| 50 eq benzene | 0.4 ± 0.1 | 92.5 eq cyclohexane | 0.4 ± 0.1 |
| 100 eq benzene | 0.5 ± 0.1 | 185 eq cyclohexane | 0.4 ± 0.1 |
| 200 eq benzene | 0.4 ± 0.1 | 370 eq cyclohexane | 0.4 ± 0.1 |
| 400 eq benzene | 0.4 ± 0.1 | | |
| <i>With 4 eq HClO_4</i> | | <i>With 4 eq HClO_4</i> | |
| 100 eq benzene | 1.3 ± 0.1 | 185 eq cyclohexane | 1.2 ± 0.1 |
| 400 eq benzene | 1.2 ± 0.1 | 370 eq cyclohexane | 1.3 ± 0.1 |

^a The data were fitted using exponential functions and first order rate constants were derived from the fitting.

We have demonstrated that addition of Sc^{3+} to **2** leads to the formation of the potent oxidant responsible for the observed reactivity. In the experiments described so far, intermediate **2** was pre-formed at $-40\text{ }^{\circ}\text{C}$ and the effect of Sc^{3+} (or HClO_4) on **2** was investigated. Parallel studies of the reaction were conducted in which H_2O_2 was added to a solution containing **1**, benzene and Sc^{3+} at $-40\text{ }^{\circ}\text{C}$ (Figure 2.13). It should be noted that this is the reaction sequence used to perform the catalytic reactions at room temperature. In this alternative scenario where Sc^{3+} is already present in the reaction mixture before addition of H_2O_2 , we observed that **3** forms directly upon addition of H_2O_2 and no accumulation of **2** was observed. This observation suggests that **2** is formed upon addition of H_2O_2 and immediately reacts with Sc^{3+} to generate the oxidant that oxidizes benzene to form **3**. Interestingly, we found the rate of formation of **3** in this case to be $7 \times 10^{-3}\text{ s}^{-1}$ at $-40\text{ }^{\circ}\text{C}$ with 1 eq Sc^{3+} , which was two orders of magnitude slower compared to the rate of formation of **3** when 1 eq Sc^{3+} was added to **2** ($2 \times 10^{-1}\text{ s}^{-1}$ at $-40\text{ }^{\circ}\text{C}$) (Figure 2.13). Taken together, these results suggest that the pivotal step of forming the oxidant from the reaction between **2** and Sc^{3+} is not the slowest step in the overall catalytic reaction. Additionally, as mentioned earlier we found the substrate oxidation step to be faster than the oxidant forming step. Hence from the above kinetic observations, neither the step forming the oxidant nor the step where the oxidant reacts with the substrate seems to be the slowest step of the reaction. We propose that the formation or accumulation of **2** is possibly the slowest step in this overall reaction, even though the most crucial step is the formation of the oxidant. This hypothesis is supported by the observation that the rate of accumulation of **2** is similar to the rate of formation of **3** when H_2O_2 was added to the reaction mixture

containing **1**, benzene and Sc^{3+} . It should be noted that all the studies were performed under catalytic conditions, that is, with excess H_2O_2 . Unfortunately, we could not study this reaction under single turnover conditions, as **2** does not accumulate under single turnover conditions due to its instability, which limits the extent of the kinetic studies that can be performed. As mentioned earlier, all the collected kinetic data suggest that we are observing the oxidant formation step. We cannot rule out the involvement of other steps of the catalytic cycle in the rates we observe, but the rates being dependent on $[\text{Sc}^{3+}]$ and independent of the concentration of substrate or its identity suggest that the kinetic rates we measure here predominantly reflect the formation of the active oxidant from the reaction of **2** and Sc^{3+} . Further kinetic studies might shed light on the intricate details of the various steps of the catalytic cycle.

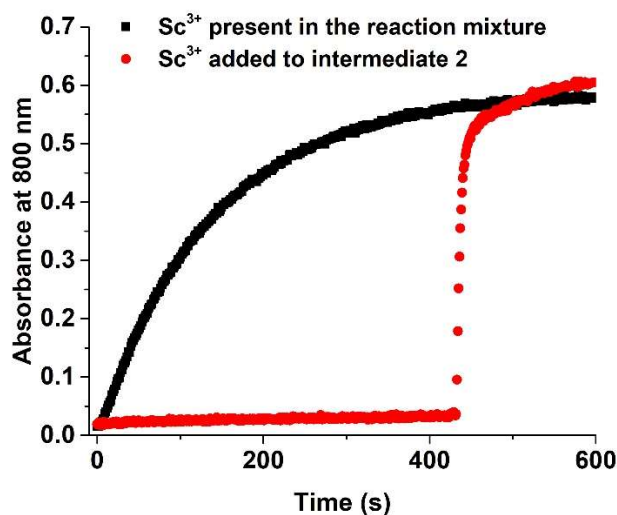


Figure 2.13. Time traces monitoring formation of **3** under two different scenarios. Black: 20 eq H_2O_2 was added to the solution containing 0.5 mM **1**, 100 eq benzene and 1 eq Sc^{3+} at $-40\text{ }^\circ\text{C}$. Red: 1 eq Sc^{3+} was added to a solution of pre-formed intermediate **2** generated by adding 20 eq H_2O_2 to a solution of 0.5 mM **1** and 100 eq benzene at $-40\text{ }^\circ\text{C}$.

Addition of Sc^{3+} or HClO_4 allows $\mathbf{1}/\text{H}_2\text{O}_2$ to perform previously unachievable reactions, such as aromatic hydroxylations, as well as accelerates the reaction step responsible for the formation of the active oxidant. $\text{Fe}^{\text{III}}\text{-OOH}$ intermediates have also been trapped for other nonheme iron catalysts and found to serve as precursors to the actual oxidant in their reactions, where the step to form the actual oxidant can be accelerated by addition of water/acids (Table 2.6). For $[\text{Fe}^{\text{III}}(\text{TPA})(\text{OOH})]^{2+}$, we showed that it underwent water-assisted O–O bond cleavage to generate an epoxidation agent,⁸ wherein substitution of H_2O with D_2O resulted in a 2.5-fold decrease in the rates of intermediate decay and epoxide product formation. Addition of 200 eq HOAc increased the reaction rate about 100-fold.⁵⁶ Similarly, Rybak-Akimova concluded that for $\text{Fe}^{\text{II}}(\text{BPMEN})/\text{H}_2\text{O}_2$ the observed $\text{Fe}^{\text{III}}\text{-OOH}$ intermediate serves as precursor to the actual oxidant.⁹ Hydroxylation of benzene to form $\text{Fe}^{\text{III}}\text{-OPh}$ occurs at a [benzene]-independent rate of 0.03 s^{-1} at $20 \text{ }^\circ\text{C}$, which increases to 0.5 s^{-1} with 1 eq HOAc. Serrano-Plana et al. found $[\text{Fe}^{\text{III}}(\text{PyNMe}_3)(\text{OOH})]^{2+}$ to be quite unreactive but could be activated by adding 1.1 eq HOTf to generate an oxidant capable of hydroxylating cyclohexane.⁵⁷ When adjusted to a common temperature of $-40 \text{ }^\circ\text{C}$, the decay rate constants of these $(\text{L})\text{Fe}^{\text{III}}\text{-OOH}$ species increase in the order: $\text{L} = \text{BPMEN}$,⁹ TPA ,⁸ $\text{BPMEN} + 1 \text{ eq HOAc}$,⁹ $\text{PyNMe}_3 + 1.1 \text{ eq HOTf}$,⁵⁷ $\text{TPA} + 200 \text{ eq HOAc}$,⁵⁶ and $\beta\text{-BPMCNCN} + 1\text{-}8 \text{ eq Sc}^{3+}$ or HClO_4) (Table 2.6). This comparison places the $\mathbf{1}/\text{H}_2\text{O}_2/(\text{Sc}^{3+}$ or $\text{HClO}_4)$ combination among the fastest in the conversion of an $\text{Fe}^{\text{III}}\text{-OOH}$ intermediate into a highly reactive oxidant for oxidation catalysis.

Table 2.6. Rates of decay of Fe^{III}-OOH intermediates at -40 °C, except where noted.

| Iron complex + additive | k_{obs} (s ⁻¹) | Ref |
|---|-------------------------------------|-----------|
| Fe ^{III} (BPMEN)(OOH) (20 °C) ^a | 0.03 | 9 |
| Fe ^{III} (BPMEN)(OOH) + 1 eq HOAc (20 °C) ^a | 0.5 | 9 |
| Fe ^{III} (TPA)(OOH) ^b | 0.002 | 8 |
| Fe ^{III} (TPA)(OOH) + 200 eq HOAc | 0.17 | 56 |
| Fe ^{III} (PyNMe ₃)(OOH) + 1.1 eq HOTf ^c | 0.02 | 57 |
| Fe ^{III} (β-BPMCN)(OOH) + 1-8 eq Sc ³⁺ /H ⁺ ^d | 0.3–2.6 | This work |

^a In the presence of benzene. ^b In the presence of 1-octene. ^c PyNMe₃ = 3,6,9-trimethyl-3,6,9-triaza-1(2,6)-pyridinacyclo-decaphane. ^d In the presence of cyclohexane or benzene.

We compare the oxidant generated by the 1/H₂O₂/Sc³⁺ combination with a number of high-valent nonheme iron-oxo species that have been characterized and shown to directly hydroxylate cyclohexane (Table 2.7). For the latter complexes, their reactivity is reflected by the magnitude of their second order rate constants measured at -40 °C. Unlike these complexes, **Ox**, the oxidant from our [Fe^{II}(β-BPMCN)(OTf)₂]/(Sc³⁺ or HClO₄) system cannot be directly observed, because its rate of formation upon decay of **2** is slower than that of the actual substrate oxidation step. Nevertheless, a comparison of the rate of **2** decay to the cyclohexane oxidation rates from the examples in the literature would still be informative, and these data are collected in Table 2.7. With 1 eq Sc³⁺ or HClO₄, **2** decays to form the active oxidant at 0.3 s⁻¹, which is significantly faster than the oxidation rates of 1 M cyclohexane by [Fe^V(O)(TAML)]⁻ and [Fe^{III}(13-TMC)(OIAr)]²⁺ (which could be considered to be a ‘masked Fe^V(O)’ species), but comparable to those of the oxoiron(IV) complexes, $S = 1$ [Fe^{IV}(O)(Me₃NTB)]²⁺ and $S = 2$ [Fe^{IV}(O)(TQA)]²⁺, and [Fe^{IV}(O)(TDCPP)]⁺ (a synthetic analog for Compound I).^{58–61} The decay rate of **2** is 10-

fold slower than that of the fastest cyclohexane oxidation rate reported thus far, which is found for the putative $[\text{Fe}^{\text{V}}(\text{O})(\text{O}_2\text{CR})(\text{PyNMe}_3)]^{2+}$ oxidant generated from the reaction of $[\text{Fe}^{\text{II}}(\text{PyNMe}_3)(\text{OTf})_2]$ with excess peracid;^{62,63} however increasing the amount of added Sc^{3+} or HClO_4 to 8 eq makes the rates of the two systems comparable. Interestingly, the fastest rates in this series match, or perhaps even exceed, the 13 s^{-1} rate for oxidation of the C3-H bond of taurine by the $S = 2 \text{ Fe}^{\text{IV}}=\text{O}$ intermediate of taurine dioxygenase at $5 \text{ }^\circ\text{C}$, after correction for the 45° temperature difference.⁶⁴ Thus, the $1/\text{H}_2\text{O}_2/(\text{Sc}^{3+} \text{ or } \text{HClO}_4)$ combination can generate a highly reactive oxidant for the hydroxylation of challenging hydrocarbon substrates like cyclohexane and benzene.

Table 2.7. Cyclohexane oxidation rates by high-valent nonheme iron species at $-40 \text{ }^\circ\text{C}$.

| | $k_2 \text{ (M}^{-1}\text{s}^{-1}\text{)}$ | Ref |
|--|---|-----------|
| $[\text{Fe}^{\text{V}}(\text{O})(\text{TAML})]^-$ | 0.00026 | 58 |
| $[\text{Fe}^{\text{III}}(13\text{-TMC})(\text{OIAr})]^{2+}$ | 0.011 | 59 |
| $[\text{Fe}^{\text{IV}}(\text{O})(\text{TDCPP}^*)]^+$ | 0.11 | 60 |
| $S = 1 \text{ } [\text{Fe}^{\text{IV}}(\text{O})(\text{Me}_3\text{NTB})]^{2+}$ | 0.25 | 60 |
| $S = 2 \text{ } [\text{Fe}^{\text{IV}}(\text{O})(\text{TQA})]^{2+}$ | 0.37 | 61 |
| $[\text{Fe}^{\text{V}}(\text{O})(\text{O}_2\text{CR})(\text{PyNMe}_3)]^{2+}$ | 2.8 | 62 |
| $[\text{Fe}^{\text{III}}(\beta\text{-BPMC N})(\text{OOH})]^{2+} \text{ (2) + 1-8 eq } \text{Sc}^{3+}/\text{H}^+$ | $k_{\text{obs}} \text{ (s}^{-1}\text{)} = 0.3\text{-}2.6$ | This work |

Abbreviations used: TAML = tetraaza macrocyclic ligand; H_2TDCPP = *meso*-tetrakis(2,6-dichlorophenyl)porphin; 13-TMC = 1,4,7,10-tetramethyl-1,4,7,10-tetraazacyclotridecane; Me_3NTB = tris(benzimidazolyl-2-methyl)-amine; TQA = tris(quinolyl-2-methyl)amine.

2.7 Spectroscopic investigation of the effect of strong Brønsted acids – leading to the choice of HClO₄ as the optimal Brønsted acid

The various strong Brønsted acids explored for this study are HClO₄, H₂SO₄, HNO₃ and HBF₄•Et₂O. All the acids mentioned above interact with **2** and are able to hydroxylate benzene forming phenol, which is monitored via UV-Visible absorption spectroscopy. However, H₂SO₄, HNO₃ and HBF₄•Et₂O behaved differently from HClO₄, likely due to differences in their pK_a values in CH₃CN and/or in the interaction between the respective counter-anions and the iron center of the catalyst. In this section, why HClO₄ is the optimal acid for this study will be discussed.

Relative to HClO₄, HNO₃ was found to react about 2 orders of magnitude more slowly than HClO₄ (with 4 eq of acid: $k_{\text{obs}}(\text{HClO}_4) = 1.2 \text{ s}^{-1}$; $k_{\text{obs}}(\text{HNO}_3) = 0.01 \text{ s}^{-1}$) (Figure 2.14). Similar to Sc³⁺ and HClO₄, HNO₃ did not kill the catalytic system, which was verified by adding a second round of 20 eq H₂O₂ to the warmed solution of the reaction. Upon warming the reaction mixture after the first round of addition of 20 eq H₂O₂, the phenolate product dissociates from the iron center, resulting in a decrease in the absorbance corresponding to the Fe^{III}-OPh chromophore. Then the reaction mixture was cooled down to -40 °C again and another 20 eq H₂O₂ was added to verify whether the catalytic system was still active and can form Fe^{III}-OPh. For HNO₃ and HClO₄, Fe^{III}-OPh formation was observed upon addition of the second round of H₂O₂. On the other hand, with both H₂SO₄ and HBF₄•Et₂O no formation of Fe^{III}-OPh was observed upon addition of the second round of H₂O₂, and thus the catalytic system was no longer active. Additionally, with HBF₄•Et₂O the Fe^{III}-OPh chromophore started decaying immediately after formation, unlike HClO₄

and HNO₃ (Figure 2.14). With H₂SO₄, the spectroscopic yield of the Fe^{III}-OPh (**3**) formed upon addition of the acid to **2** was 5-times lower compared to HClO₄. Hence, HClO₄ is the optimal strong Brønsted acid to activate the catalytic system **1**+H₂O₂ and its effect was comparable to that of Sc³⁺. The difference in the behavior of the other Brønsted acids should be further investigated in future efforts.

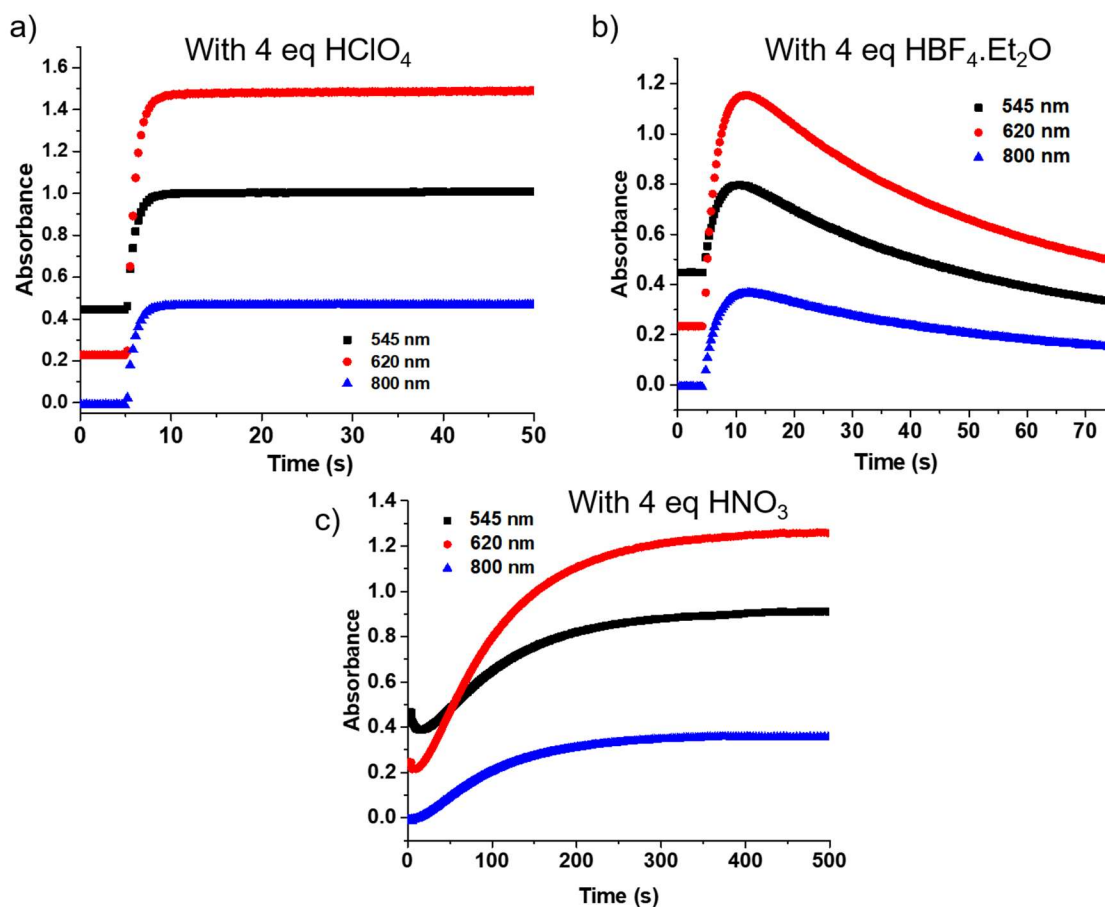


Figure 2.14. Effect of a) 4 eq HClO₄ b) 4 eq HBF₄.Et₂O and c) 4 eq HNO₃ when added to **2** in the presence of benzene. **2** is formed by reacting 20 eq H₂O₂ to 0.5 mM **1** in the presence of 100 eq benzene as substrate at -40 °C. Time traces monitor nearly instantaneous changes in absorbance at 545, 620 and 800 nm after addition of 4 eq acid in each case.

2.8 Mechanistic isotope labeling studies and the nature of the active oxidant (Ox)

^{18}O -labeling experiments have been shown to be the key to shedding mechanistic light on the action of oxygenases since 1955,^{65–68} and have also proven useful in providing insight into the nature of the oxidants formed upon O–O cleavage of $\text{Fe}^{\text{III}}\text{–OOH}$ intermediates in bio-inspired metal-catalyzed reactions.^{6,7,69} For the well-studied $\text{Fe}(\text{BPMEN})$ and $\text{Fe}(\text{TPA})$ catalysts, the accumulated evidence supports the rate determining H_2O -assisted cleavage of the O–O bond of the *cis*- $\text{H}_2\text{O}\text{–Fe}^{\text{III}}\text{–OOH}$ intermediate to form an $(\text{HO})\text{–Fe}^{\text{V}}\text{=O}$ oxidant. Oxo-hydroxo tautomerism rationalizes the observed partial incorporation of ^{18}O from added H_2^{18}O into the oxidation products (Table 2.8).^{6–9}

For the case of **1**/ H_2O_2 in the absence of additives, ^{18}O from H_2^{18}O is partially incorporated into the products. However a significant fraction of the O-atom incorporated into the products is derived from O_2 , unlike for $\text{Fe}(\text{TPA})$ and $\text{Fe}(\text{BPMEN})$ (Table 2.8).¹⁰ The observed incorporation of an O-atom from O_2 suggests that the alkyl radical formed after initial hydrogen atom abstraction by the iron oxidant is sufficiently long lived to be captured by O_2 . In contrast, no ^{18}O -incorporation from added H_2^{18}O into the cyclohexanol and phenol products is observed in the **1**-catalyzed oxidation of cyclohexane and benzene in the presence of Sc^{3+} or HClO_4 , which is confirmed by complementary experiments with a 10% aqueous solution of $\text{H}_2^{18}\text{O}_2$ showing essentially quantitative ^{18}O -label incorporation into the cyclohexanol and phenol products in the Sc^{3+} experiments (Table 2.8). Furthermore, the absence of O-atom incorporation from O_2 in the presence of Sc^{3+} indicates the formation of short-lived alkyl radicals that undergo fast rebound, as we deduced from

the reactivity studies mentioned earlier. These results thereby exclude the H₂O-assisted mechanism associated with the Fe^{II}(TPA) and Fe^{II}(BPMEN) catalysts^{6,7} to account for the labeling results observed for the 1/H₂O₂/(Sc³⁺ or HClO₄) system.

Table 2.8. Percentage of ¹⁸O-incorporation into products from the oxidation of cyclohexane and benzene^a

| | H ₂ ¹⁸ O ₂ | H ₂ ¹⁸ O | Ref |
|---|---|--------------------------------|-----------|
| <i>Cyclohexanol</i> | | | |
| Fe ^{II} (β-BPMCN) + Sc ³⁺ | 97 | 1 | This work |
| Fe ^{II} (β-BPMCN) | 34 | 10 | 10 |
| Fe ^{II} (TPA) | 70 | 27 | 6 |
| Fe ^{II} (BPMEN) | 84 | 18 | 6 |
| <i>Phenol</i> | | | |
| Fe ^{II} (β-BPMCN) + Sc ³⁺ | 99 | 2 | This work |
| Fe ^{II} (BPMEN) | 81 | 22 | 9 |

^a All experiments reported in this work were performed in the presence of air. The percentage incorporation values were calculated based on the ¹⁸O-content of the reagents. The H₂¹⁸O₂ labeling experiments were performed with 10% H₂¹⁸O₂. The larger amount of H₂O present in 10% H₂¹⁸O₂ relative to that in 90% H₂¹⁶O₂ reduced the product yield by 50% but the effect of Sc³⁺ is still present (Figure 2.15).

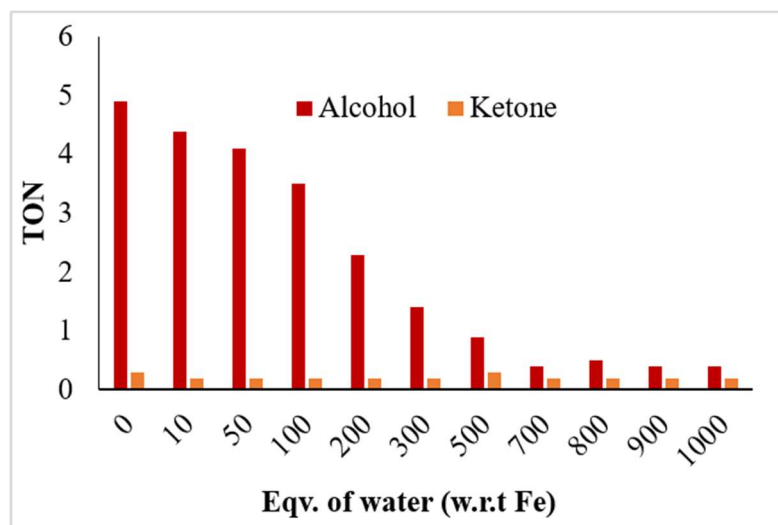
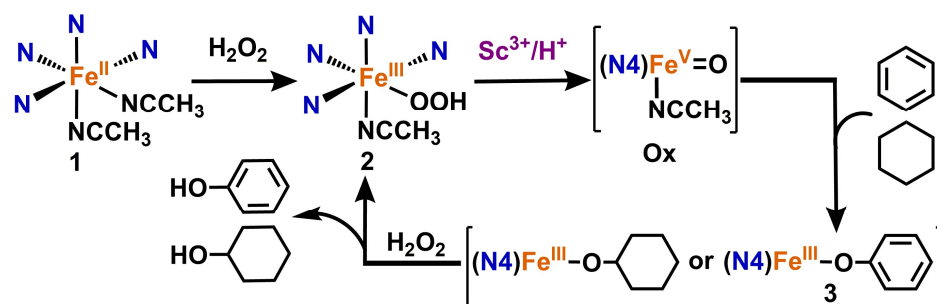


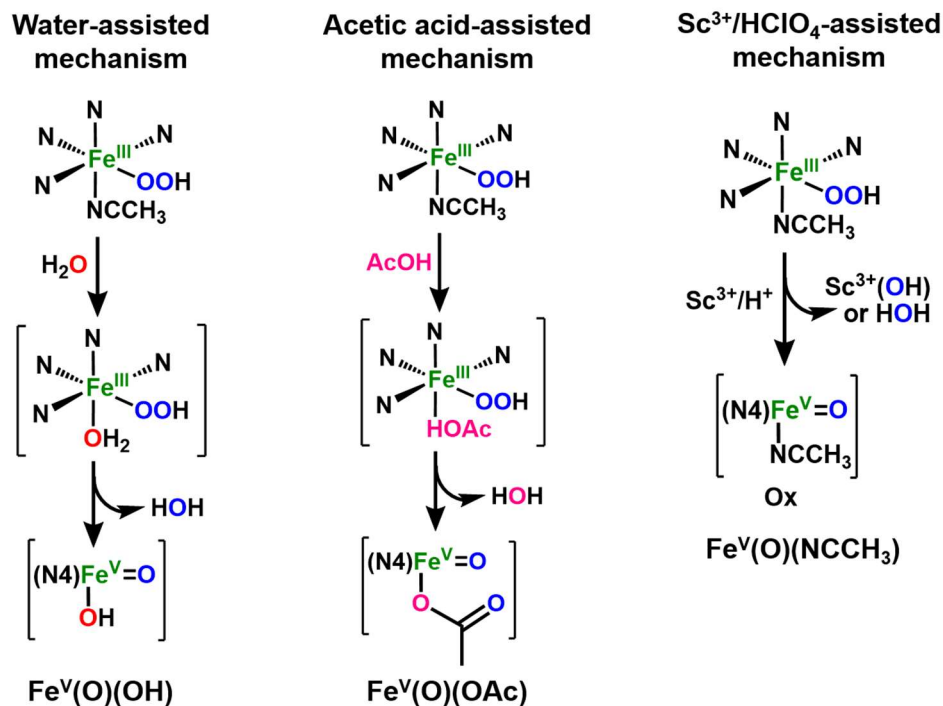
Figure 2.15. Effect of water on cyclohexane oxidation. $\text{Fe}^{\text{II}}(\beta\text{-BPMCN})$ (1 mM) + 1000 eq cyclohexane + 10 eq H_2O_2 (90%) + 2 eq Sc^{3+} + varying amounts of H_2O at 20 °C.

Instead, we propose the mechanism shown in Scheme 2.1, which rationalizes the similar reactivity patterns observed upon addition of Sc^{3+} or HClO_4 , the equivalent kinetic effects of adding Sc^{3+} or HClO_4 to **2** and the ^{18}O -labeling results. Both these additives facilitate O–O bond heterolysis in the $\text{Fe}^{\text{III}}\text{-OOH}$ intermediate **2** to form a distinct and highly electrophilic oxidant **Ox** that hydroxylates cyclohexane and benzene at high rates. As the hydroxide formed in this cleavage combines with Sc^{3+} or the proton from HClO_4 , the nascent $\text{Fe}^{\text{V}}=\text{O}$ center in this case no longer has a bound hydroxide, which should make it much more electrophilic than the proposed $\text{Fe}^{\text{V}}(\text{O})(\text{OH})$ oxidant associated with the water-assisted mechanism (Scheme 2.2). This $\text{Sc}^{3+}/\text{HClO}_4$ -assisted mechanism parallels that proposed by Serrano-Plana *et al.* for the activation of $[\text{Fe}^{\text{III}}(\text{PyNMe}_3)(\text{OOH})]^{2+}$ by strong acid,⁵⁷ which is supported by DFT calculations. Furthermore, in contrast to **Ox**, the presence of the anionic acetate ligand in the putative $\text{Fe}^{\text{V}}(\text{O})(\text{OAc})$ oxidant (Scheme 2.2)

formed from $1/H_2O_2$ in the presence of HOAc presumably reduces the electrophilicity of the $Fe^V(O)$ unit, rationalizing its inability to perform benzene hydroxylation.



Scheme 2.1. Proposed mechanism for the effect of Sc^{3+} or $HClO_4$ in cyclohexane and benzene hydroxylation by $1/H_2O_2$.



Scheme 2.2. Proposed mechanism for formation of the Fe^V oxidants in the water-assisted, acetic-acid-assisted and $Sc^{3+}/HClO_4$ -assisted mechanism.

2.9 Summary

In summary, we have shown that addition of a redox-inactive strong Lewis acid like $\text{Sc}(\text{OTf})_3$ or a Brønsted acid like HClO_4 to the reaction mixture of the nonheme iron catalyst **1** and H_2O_2 leads to the formation of a highly electrophilic oxidant capable of hydroxylating cyclohexane and benzene with comparable catalytic efficiency, a combination of transformations rarely observed for synthetic nonheme iron catalysts.^{3,4,44} This highly reactive species compares well in C–H bond cleaving ability with the fastest nonheme iron-oxo oxidants reported thus far (Table 2.7). Catalyst **1** is unique as the nature of the active oxidant that is formed can be tuned by various additives to perform four distinct reactions. The *cis*-dihydroxylation of electron-deficient C=C bonds in the absence of any additive and the epoxidation of electron-rich C=C bonds in the presence of acetic acid have been reported previously.^{10,42} In this paper, we demonstrate its ability to hydroxylate benzene and cyclohexane within seconds at $-40\text{ }^\circ\text{C}$ upon addition of Sc^{3+} or HClO_4 and identify a new route for accessing a powerful electrophilic oxidant in this fascinating landscape of high-valent nonheme oxoiron oxidants.

2.10 Acknowledgments

Dr. Apparao Draksharapu conducted the resonance Raman experiments. We thank Prof. John D. Lipscomb and Dr. Rahul Banerjee for their very helpful advice in the kinetic analysis.

2.11 References

- (1) Kovaleva, E. G.; Lipscomb, J. D. *Nat. Chem. Biol.* **2008**, *4*, 186–193.
- (2) Kal, S.; Que, L. *J. Biol. Inorg. Chem.* **2017**, *22*, 339–365.
- (3) Olivo, G.; Cussó, O.; Borrell, M.; Costas, M. *J. Biol. Inorg. Chem.* **2017**, *22*, 425–452.
- (4) Bryliakov, K. P.; Talsi, E. P. *Coord. Chem. Rev.* **2014**, *276*, 73–96.
- (5) Oloo, W. N.; Que, L. *Acc. Chem. Res.* **2015**, *48*, 2612–2621.
- (6) Chen, K.; Que, L. *J. Am. Chem. Soc.* **2001**, *123*, 6327–6337.
- (7) Chen, K.; Costas, M.; Kim, J.; Tipton, A. K.; Que, L. *J. Am. Chem. Soc.* **2002**, *124*, 3026–3035.
- (8) Oloo, W. N.; Fielding, A. J.; Que, L. *J. Am. Chem. Soc.* **2013**, *135*, 6438–6441.
- (9) Makhlynets, O. V.; Rybak-Akimova, E. V. *Chem. Eur. J.* **2010**, *16*, 13995–14006.
- (10) Costas, M.; Que, L. *Angew. Chem. Int. Ed.* **2002**, *41*, 2179–2181.
- (11) Fukuzumi, S. *Coord. Chem. Rev.* **2013**, *257*, 1564–1575.
- (12) Fukuzumi, S.; Ohkubo, K.; Lee, Y. M.; Nam, W. *Chem. Eur. J.* **2015**, *21*, 17548–17559.
- (13) Dong, L.; Wang, Y.; Lv, Y.; Chen, Z.; Mei, F.; Xiong, H.; Yin, G. *Inorg. Chem.* **2013**, *52*, 5418–5427.
- (14) Leeladee, P.; Baglia, R. A.; Prokop, K. A.; Lati, R.; Visser, S. P. De; Goldberg, D. P. *J. Am. Chem. Soc.* **2012**, *134*, 10397–10400.
- (15) Baglia, R. A.; Krest, C. M.; Yang, T.; Leeladee, P.; Goldberg, D. P. *Inorg. Chem.*

- 2016**, *55*, 10800–10809.
- (16) Miller, C. G.; Gordon-Wylie, S. W.; Horwitz, C. P.; Strazisar, S. A.; Peraino, D. K.; Clark, G. R.; Weintraub, S. T.; Collins, T. J. *J. Am. Chem. Soc.* **1998**, *120*, 11540–11541.
- (17) Hong, S.; Lee, Y.; Sankaralingam, M.; Vardhaman, A. K.; Park, Y. J.; Cho, K.-B.; Ogura, T.; Sarangi, R.; Fukuzumi, S.; Nam, W. *J. Am. Chem. Soc.* **2016**, *138*, 8523–8532.
- (18) Lam, W. W. Y.; Yiu, S. M.; Lee, J. M. N.; Yau, S. K. Y.; Kwong, H. K.; Lau, T.; Liu, D.; Lin, Z. *J. Am. Chem. Soc.* **2006**, *128*, 2851–2858.
- (19) Du, H.; Lo, P.; Hu, Z.; Liang, H.; Lau, K.; Wang, Y.-N.; Lam, W. W. Y.; Lau, T. *Chem. Commun.* **2011**, *47*, 7143–7145.
- (20) Ho, C.; Lau, T. *New J. Chem.* **2000**, *24*, 587–590.
- (21) Lau, T.; Wu, Z.; Bai, Z.; Mak, C. *J. Chem. Soc. Dalton Trans.* **1995**, *4*, 695–696.
- (22) Yiu, S.; Man, W.; Lau, T. *J. Am. Chem. Soc.* **2008**, *130*, 10821–10827.
- (23) Li, F.; Van Heuvelen, K. M.; Meier, K. K.; Münck, E.; Que, L. *J. Am. Chem. Soc.* **2013**, *135*, 10198–10201.
- (24) Lee, Y.-M.; Bang, S.; Kim, Y. M.; Cho, J.; Hong, S.; Nomura, T.; Ogura, T.; Troeppner, O.; Ivanović-Burmazović, I.; Sarangi, R.; Fukuzumi, S.; Nam, W. *Chem. Sci.* **2013**, *4*, 3917–3923.
- (25) Zhang, J.; Wei, W.-J.; Lu, X.; Yang, H.; Chen, Z.; Liao, R.-Z.; Yin, G. *Inorg. Chem.* **2017**, *56*, 15138–15149.

- (26) Nodzewska, A.; Watkinson, M. *Chem. Commun.* **2018**, *54*, 1461–1464.
- (27) Chatterjee, S.; Paine, T. K. *Angew. Chem Int. Ed.* **2015**, *54*, 9338–9342.
- (28) <https://www.cdc.gov/niosh/ipcsneng/neng0164.html>.
- (29) <http://msdsviewer.fmc.com/private/document.aspx?prd=7722-84-1--90~~PDF~~MTR~~CPNA~~EN~~1/1/0001%2012:00:00%20AM~~HYDROGEN%20PEROXIDE%2090%~~>.
- (30) Jo, D. H.; Chiou, Y. M.; Que, J. *Inorg. Chem.* **2001**, *40*, 3181–3190.
- (31) ASTM E1840-96(2007)Standard Guide for Raman Shift Standards for Spectrometer Calibration ASTM International DOI:10.1520/E1840-96R07. .
- (32) Menges, F. “Spekwin32 - optical spectroscopy software” Version 1.72.0, 2015 <http://www.ffmpeg2.de/spekwin/>. .
- (33) Kobayashi, S. *European J. Org. Chem.* **1999**, *1999*, 15–27.
- (34) Raba, A.; Cokoja, M.; Herrmann, W. A.; Kühn, F. E. *Chem. Commun.* **2014**, *50*, 11454–11457.
- (35) Tsuji, T.; Zaoputra, A. A.; Hitomi, Y.; Mieda, K.; Ogura, T.; Shiota, Y.; Yoshizawa, K.; Sato, H.; Koder, M. *Angew. Chem Int. Ed.* **2017**, *56*, 7779–7782.
- (36) Olah, G. A. *Acc. Chem. Res.* **1971**, *4*, 240–248.
- (37) Augusti, R.; Dias, A. O.; Rocha, L. L.; Lago, R. M. *J. Phys. Chem. A* **1998**, *102*, 10723–10727.
- (38) Thibon, A.; Jollet, V.; Ribal, C.; Sénéchal-David, K.; Billon, L.; Sorokin, A. B.; Banse, F. *Chem. Eur. J.* **2012**, *18*, 2715–2724.

- (39) Kejriwal, A.; Bandyopadhyay, P.; Biswas, A. N. *Dalton Trans.* **2015**, *44*, 17261–17267.
- (40) Morimoto, Y.; Bunno, S.; Fujieda, N.; Sugimoto, H.; Itoh, S. *J. Am. Chem. Soc.* **2015**, *137*, 5867–5870.
- (41) Yamada, M.; Karlin, K. D.; Fukuzumi, S. *Chem. Sci.* **2016**, *7*, 2856–2863.
- (42) Iyer, S. R.; Javadi, M. M.; Feng, Y.; Hyun, M. Y.; Oloo, W. N.; Kim, C.; Que, L. *Chem. Commun.* **2014**, *50*, 13777–13780.
- (43) Costas, M.; Mehn, M. P.; Jensen, M. P.; Que, L. *Chem. Rev.* **2004**, *104*, 939–986.
- (44) Company, A.; Lloret-Fillol, J.; Costas, M. In *Comprehensive Inorganic Chemistry II*; Elsevier Ltd., 2013; p 487.
- (45) Ho, R. Y. N.; Roelfes, G.; Feringa, B. L.; Que, L. *J. Am. Chem. Soc.* **1999**, *121*, 264–265.
- (46) Roelfes, G.; Vrajmasu, V.; Chen, K.; Ho, R. Y. N.; Rohde, J. U.; Zondervan, C.; La Crois, R. M.; Schudde, E. P.; Lutz, M.; Spek, A. L.; Hage, R.; Feringa, B. L.; Münck, E.; Que, L. *Inorg. Chem.* **2003**, *42*, 2639–2653.
- (47) Simaan, A. J.; Döpner, S.; Banse, F.; Bourcier, S.; Bouchoux, G.; Boussac, A.; Hildebrandt, P.; Girerd, J.-J. *Eur. J. Inorg. Chem.* **2000**, *2000*, 1627–1633.
- (48) Mekmouche, Y.; Hummel, H.; Ho, R. Y. N.; Que Jr., L.; Schünemann, V.; Thomas, F.; Trautwein, A. X.; Lebrun, C.; Gorgy, K.; Leprêtre, J.-C.; Collomb, M.-N.; Deronzier, A.; Fontecave, M.; Ménage, S. *Chem. Eur. J.* **2002**, *8*, 1196–1204.
- (49) Balland, V.; Banse, F.; Anxolabéhère-Mallart, E.; Ghiladi, M.; Mattioli, T. A.;

- Philouze, C.; Blondin, G.; Girerd, J. J. *Inorg. Chem.* **2003**, *42*, 2470–2477.
- (50) Oddon, F.; Chiba, Y.; Nakazawa, J.; Ohta, T.; Ogura, T.; Hikichi, S. *Angew. Chem. Int. Ed.* **2015**, *54*, 7336–7339.
- (51) Bukowski, M. R.; Comba, P.; Limberg, C.; Merz, M.; Que, L.; Wistuba, T. *Angew. Chem. Int. Ed.* **2004**, *43*, 1283–1287.
- (52) Wada, A.; Ogo, S.; Nagatomo, S.; Kitagawa, T.; Watanabe, Y.; Jitsukawa, K.; Masuda, H. *Inorg. Chem.* **2002**, *41*, 616–618.
- (53) Li, F.; Meier, K. K.; Cranswick, M. A.; Chakrabarti, M.; Van Heuvelen, K. M. .; Münck, E.; Que, L. *J. Am. Chem. Soc.* **2011**, *133*, 7256–7259.
- (54) Kitagawa, T.; Dey, A.; Lugo-Mas, P.; Benedict, J. B.; Kaminsky, W.; Solomon, E.; Kovacs, J. A. *J. Am. Chem. Soc.* **2006**, *128*, 14448–14449.
- (55) Pyrz, J. W.; Roe, A. L.; Stern, L. J.; Que, L. *J. Am. Chem. Soc.* **1985**, *107*, 614–620.
- (56) Oloo, W. N.; Banerjee, R.; Lipscomb, J. D.; Que, L. *J. Am. Chem. Soc.* **2017**, *139*, 17313–17326.
- (57) Serrano-Plana, J.; Acuña-Parés, F.; Dantignana, V.; Oloo, W. N.; Castillo, E.; Draksharapu, A.; Whiteoak, C. J.; Martin-Diaconescu, V.; Basallote, M. G.; Luis, J. M.; Que, L.; Costas, M.; Company, A. *Chem. Eur. J.* **2018**, *24*, 5331–5340.
- (58) Kundu, S.; Van Thompson, J. K.; Shen, L. Q.; Mills, M. R.; Bominaar, E. L.; Ryabov, A. D.; Collins, T. J. *Chem. Eur. J.* **2015**, *21*, 1803–1810.
- (59) Hong, S.; Wang, B.; Seo, M. S.; Lee, Y. M.; Kim, M. J.; Kim, H. R.; Ogura, T.; Garcia-Serres, R.; Clémancey, M.; Latour, J. M.; Nam, W. *Angew. Chem. Int. Ed.*

- 2014**, *53*, 6388–6392.
- (60) Seo, M. S.; Kim, N. H.; Cho, K.-B.; So, J. E.; Park, S. K.; Clémancey, M.; Garcia-Serres, R.; Latour, J.-M.; Shaik, S.; Nam, W. *Chem. Sci.* **2011**, *2*, 1039–1045.
- (61) Biswas, A. N.; Puri, M.; Meier, K. K.; Oloo, W. N.; Rohde, G. T.; Bominaar, E. L.; Münck, E.; Que, L. *J. Am. Chem. Soc.* **2015**, *137*, 2428–2431.
- (62) Serrano-Plana, J.; Oloo, W. N.; Acosta-Rueda, L.; Meier, K. K.; Verdejo, B.; García-España, E.; Basallote, M. G.; Münck, E.; Que, L.; Company, A.; Costas, M. *J. Am. Chem. Soc.* **2015**, *137*, 15833–15842.
- (63) Fan, R.; Serrano-Plana, J.; Oloo, W. N.; Draksharapu, A.; Delgado-pinar, E.; Company, A.; Martin-Diaconescu, V.; Borrell, M.; Lloret-Fillol, J.; García-España, E.; Guo, Y.; Bominaar, E. L.; Que, L.; Costas, M.; Munck, E. *J. Am. Chem. Soc.* **2018**, *140*, 3916–3928.
- (64) Price, J. C.; Barr, E. W.; Glass, T. E.; Krebs, C.; Bollinger, J. M. *J. Am. Chem. Soc.* **2003**, *125*, 13008–13009.
- (65) Mason, H. S.; Fowlks, W. L.; Peterson, E. *J. Am. Chem. Soc.* **1955**, *77*, 2914–2915.
- (66) Hayaishi, O.; Katagiri, M.; Rothberg, S. *J. Am. Chem. Soc.* **1955**, *77*, 5450–5451.
- (67) Wackett, L. P.; Kwart, L. D.; Gibson, D. T. *Biochemistry* **1988**, *27*, 1360–1367.
- (68) Banerjee, R.; Proshlyakov, Y.; Lipscomb, J. D.; Proshlyakov, D. A. *Nature* **2015**, *518*, 431–434.
- (69) Prat, I.; Mathieson, J. S.; Güell, M.; Ribas, X.; Luis, J. M.; Cronin, L.; Costas, M. *Nat. Chem.* **2011**, *3*, 788–793.

Chapter 3:

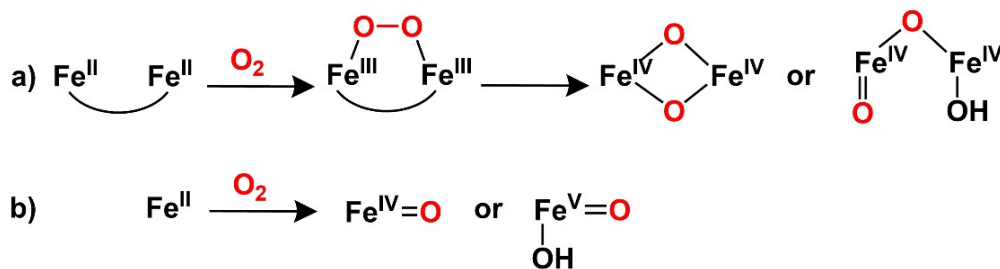
Activation of $[(\beta\text{-BPMCN})\text{Fe}^{\text{III}}\text{-OOH}]^{2+}$ intermediate using $\text{Fe}^{\text{III}}(\text{OTf})_3$: possible implications for O_2 activation by diiron systems

Parts of the content of this chapter was published in:

Kal, S.; Que, L. Jr. Activation of a nonheme $\text{Fe}^{\text{III}}\text{-OOH}$ by a second Fe^{III} to hydroxylate strong C–H bonds: possible implications for sMMO, *Angew. Chem. Int. Ed.*, **2019**, DOI: 10.1002/anie.201903465.

3.1 Introduction

Nonheme iron oxygenases form a major class of oxygen activating metalloenzymes.¹ It can be further divided into two subgroups based on the number of iron atoms in the active site: monoiron and diiron enzymes.^{2,3} Both iron atoms in the active site of diiron enzymes are responsible for activating O₂. Soluble methane monooxygenase (sMMO) belongs to this subgroup of enzymes and is one of the best-studied diiron enzyme.^{4,5} sMMO performs the challenging oxidation of methane (C–H BDE = 105 kcal/mol) to form methanol and does so via a diiron(III)-peroxo species that is converted to the diiron(IV)-oxo oxidant that cleaves the strong C–H bond of methane (Scheme 3.1). On the other hand, in mono-iron enzymes, a single iron atom is responsible for activating O₂ and forming the active oxidant (Scheme 3.1).^{2,6} This raises the intriguing question - what is the role of the second iron in diiron enzymes?



Scheme 3.1. Proposed active oxidants for a) di-iron and b) mono-iron nonheme enzymes. (The hydroxide moieties bound to the high-valent iron centers are proposed to be derived from water.)

Lewis acidic metal ions can be used for tuning the redox potentials of metal-oxygen intermediates. For example, redox-inactive metal ions have been shown to increase the Fe^{III/IV} redox potential of mononuclear nonheme Fe^{IV}=O species.^{7,8} Similarly, in the oxygen

evolving complex of photosystem II, Ca^{2+} is proposed to raise the redox potential of the manganese oxo cluster.⁹⁻¹¹ Lewis acids can also assist in cleaving O–O bonds in peroxy(hydro) intermediates to form high-valent metal-oxo species. For $[(\text{TMC})\text{Fe}^{\text{III}}-\eta^2\text{-O}_2]^+$, Lewis acids such as Sc^{3+} and Y^{3+} induce cleavage of the O–O bond to form the $[(\text{TMC})\text{Fe}^{\text{IV}}(\text{O})]^{2+}$.^{12,13} Recently, we have demonstrated that Lewis acidic Sc^{3+} activates the $[\text{Fe}^{\text{III}}(\beta\text{-BPMCN})(\text{OOH})]^{2+}$ intermediate to form a reactive $\text{Fe}^{\text{V}}=\text{O}$ oxidant that cleaves strong C–H bonds within seconds at $-40\text{ }^\circ\text{C}$.¹⁴ Fe^{3+} and Fe^{2+} are generally known for their redox properties but can potentially act as Lewis acids as well. However, neither Fe^{3+} nor Fe^{2+} has to date been reported to activate Fe^{III} -peroxy or hydroperoxy species. Here we report the activation of the $[\text{Fe}^{\text{III}}(\beta\text{-BPMCN})(\text{OOH})]^{2+}$ intermediate by a second iron(III) ion to form a strong oxidant that hydroxylates both cyclohexane and benzene efficiently.

$[\text{Fe}^{\text{II}}(\beta\text{-BPMCN})]^{2+}$ (**1**) (BPMCN = *N,N'*-bis(pyridyl-2-methyl)-*N,N'*-dimethyl-*trans*-1,2-diaminocyclo-hexane) (Figure 3.1) is a nonheme iron complex that along with H_2O_2 can form a catalytic system for olefin oxidation. However, it is not efficient in cyclohexane oxidation and can only perform stoichiometric oxidation of cyclohexane (Table 3.1).¹⁵ In the previous chapter, we showed that the redox-inactive Lewis acid Sc^{3+} can activate this catalytic system to form a powerful oxidant that can efficiently catalyze cyclohexane oxidation within seconds at $25\text{ }^\circ\text{C}$.¹⁴ Additionally, under these conditions it was able to carry out catalytic electrophilic substitution of benzene and benzene analogs with electron-withdrawing substituents. Both redox-inactive Lewis acidic Sc^{3+} and perchloric acid activated the $[\text{Fe}^{\text{III}}(\beta\text{-BPMCN})(\text{OOH})]^{2+}$ (**2**) (Figure 3.1)

intermediate to similar extents, supporting the role of Sc^{3+} as a strong acid in activating an $\text{Fe}^{\text{III}}\text{-OOH}$ species.

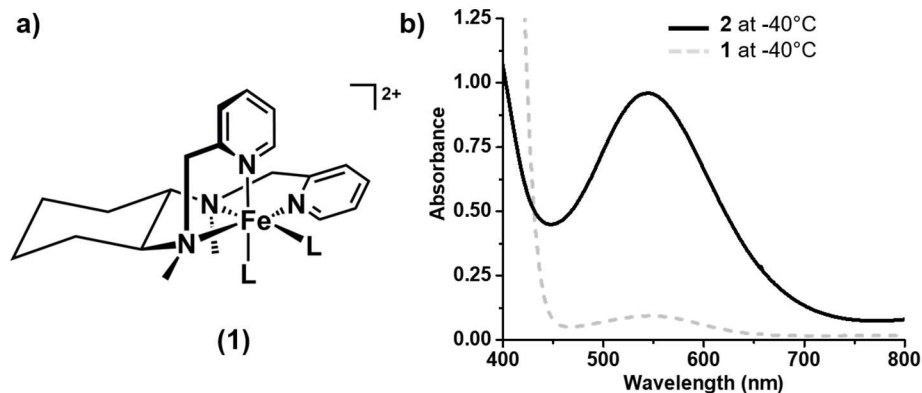


Figure 3.1. a) Iron complex (1) ($L = \text{CH}_3\text{CN}$) used in this study. b) The hydroperoxoiron(III) intermediate (2) formed with 1 mM (1) and 20 eq H_2O_2 at -40°C in CH_3CN .

3.2 Experimental details

All materials were purchased from Sigma-Aldrich and used as received unless noted otherwise. H_2^{18}O (97% ^{18}O -enriched) and $\text{H}_2^{18}\text{O}_2$ (90% ^{18}O -enriched, 10% solution in H_2^{16}O) were obtained from Berry & Associates-ICON Isotopes. Cyclohexane, benzene and nitrobenzene were passed through alumina and silica gel before the reactions. 90% H_2O_2 was obtained from FMC Corporation. **Caution:** 90% H_2O_2 is potentially explosive and should be handled with proper safety precautions.^{16,17} The ligand BPMCN and the complex $[\text{Fe}^{\text{II}}(\beta\text{-BPMCN})](\text{OTf})_2$ were synthesized according to previously published procedures.^{15,18}

Product analyses were performed on a Perkin-Elmer Sigma 3 gas chromatograph (AT-1701 column) with a flame-ionization detector. GC mass spectral analyses were performed on a HP 6890 GC (HP-5 column) using an Agilent 5973 mass detector. For chemical ionization analyses, NH_3/CH_4 (4%) was used as the ionization gas. UV-visible absorption spectra were recorded on a HP8453A diode array spectrometer equipped with a cryostat from Unisoku, Scientific Instruments (Osaka, Japan).

Catalytic reaction conditions – All experiments reported in this work were performed in the presence of air. In a typical reaction, 70 μL of a 0.2 M H_2O_2 solution (diluted from 90% $\text{H}_2\text{O}_2/\text{H}_2\text{O}$ solution) in CH_3CN (10 eq H_2O_2 relative to $\mathbf{1}(\text{OTf})_2$) was added all at once to a vigorously stirred CH_3CN solution (1.93 mL) containing the iron catalyst $\mathbf{1}(\text{OTf})_2$, the substrate and $\text{Fe}^{\text{III}}(\text{OTf})_3$ or $\text{Fe}^{\text{II}}(\text{OTf})_2$ and stirred for 30 min at room temperature. The final concentration of the iron catalyst in the reaction mixture was 0.7 mM with 1000 eq cyclohexane/ 100 eq benzene and 0.5–8 eq $\text{Fe}^{\text{III}}(\text{OTf})_3$. After the reaction was over, 0.1 mL 1-methylimidazole and 1 mL acetic anhydride were added to the reaction solution to esterify the alcohol/phenol. An internal standard (naphthalene) was added after this and then the products were extracted into CHCl_3 and the solution was then subjected to GC and/or GC-MS analysis.

Isotope-labeling studies – Similar conditions were used as described for catalytic reaction conditions above except for the following details. In experiments with $\text{H}_2^{18}\text{O}_2$, 10 eq of $\text{H}_2^{18}\text{O}_2$ from 10% $\text{H}_2^{18}\text{O}_2/\text{H}_2\text{O}$ solution (90% ^{18}O -enrichment) relative to $\mathbf{1}(\text{OTf})_2$ was added instead of $\text{H}_2^{16}\text{O}_2$. In experiments with H_2^{18}O , 68 μL of 3.5 M H_2^{18}O solution (97% ^{18}O -enrichment) in CH_3CN (170 eq H_2^{18}O relative to $\mathbf{1}(\text{OTf})_2$ which is about the same

amount of H₂O that would be introduced from a 10% H₂O₂ solution) was added to the reaction mixture before adding H₂O₂. The products were analyzed using GC/CI-MS or GC/EI-MS. The percent ¹⁸O-incorporation into the products was calculated on the basis of the ¹⁸O-enrichments of the reagents containing the isotope.

Competition experiments – Conditions similar to the general catalytic reactions were used except that a total of 600 eq substrate relative to **1**(OTf)₂ was present. The amount(s) of benzene/cyclohexane (in equivalents relative to **1**(OTf)₂) used were 300/300 and 50/550.

Kinetic isotope effect (KIE) experiments – Conditions similar to what was described for the general catalytic reactions were used except for the following details. A ratio of 1:3 was used for cyclohexane/cyclohexane-d₁₂ in the KIE experiment to improve the accuracy of the results. For benzene oxidation a 1:1 ratio of benzene/benzene-*d*₆ was used. H₂O₂ was added in a controlled fashion using a syringe pump to obtain results under similar conditions as reported in literature^{15,19} for the purpose of comparison. It was previously done using a syringe pump to enhance the yields of the products, but same results were obtained in the experiments with additives described in this paper with and without syringe pumping.

3.3 Effect of $\text{Fe}^{\text{II}}(\text{OTf})_2$ and $\text{Fe}^{\text{III}}(\text{OTf})_3$ on catalytic reactivity of $[\text{Fe}^{\text{II}}(\beta\text{-BPMCN})]^{2+}/\text{H}_2\text{O}_2$

In the absence of any additive, the oxidation of cyclohexane by **1** and 10 eq 90% H_2O_2 affords 0.5 eq cyclohexanol and 0.6 eq cyclohexanone. The use of $\text{Fe}^{\text{II}}(\text{OTf})_2$ as an additive does not affect the amount of cyclohexane oxidized relative to that obtained in its absence yield, but the alcohol-to-ketone (A/K) ratio is increased (Figure 3.2). Furthermore, with benzene as substrate, no phenol formation is detected upon $\text{Fe}^{\text{II}}(\text{OTf})_2$ addition, just like **1** in the absence of any additive. These results suggest that Fe^{2+} cannot activate the **1**/ H_2O_2 combination for catalysis.

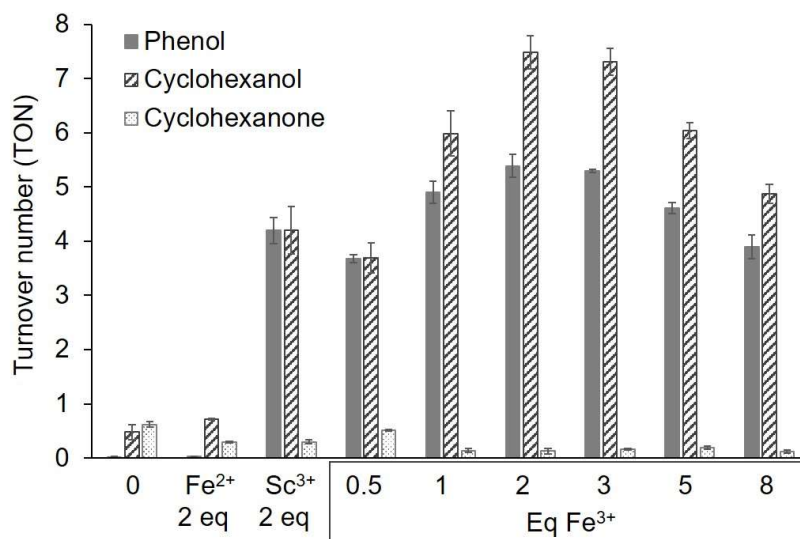


Figure 3.2. Effect of $\text{Fe}^{\text{III}}(\text{OTf})_3$ on cyclohexane and benzene oxidation reactions catalyzed by **1** and comparisons with $\text{Sc}^{\text{III}}(\text{OTf})_3$ and $\text{Fe}^{\text{II}}(\text{OTf})_2$. Reaction conditions: **1** (0.7 mM), 1000 eq cyclohexane or 100 eq benzene, 10 eq 90% H_2O_2 in CH_3CN at room temperature.

In significant contrast, the addition of 2 eq $\text{Fe}^{\text{III}}(\text{OTf})_3$ relative to **1** to the reaction mixture containing cyclohexane as substrate results in 7.5 turnovers (TON) of cyclohexanol, a 15-fold increase compared to that obtained without additives (Table 3.1 and Figure 3.2). Additionally, very little cyclohexanone (0.1 TON) is formed, resulting in a remarkably large alcohol-to-ketone (A/K) ratio of 75 (Table 3.1). Furthermore, unlike for $\text{Fe}^{\text{II}}(\text{OTf})_2$, benzene is converted to phenol in the presence of $\text{Fe}^{\text{III}}(\text{OTf})_3$ with a turnover number (TON) of 5.4. As shown in Figure 3.2, the yields of cyclohexanol and phenol grow with increasing $[\text{Fe}^{3+}]$, plateau at 2-3 eq $\text{Fe}^{\text{III}}(\text{OTf})_3$, and then decrease beyond 3 eq $\text{Fe}^{\text{III}}(\text{OTf})_3$. The latter behavior might be attributed to unproductive side reactions involving $\text{Fe}^{\text{III}}(\text{OTf})_3$ and H_2O_2 . These observations demonstrate that $\text{Fe}^{\text{III}}(\text{OTf})_3$ is able to activate the **1**/ H_2O_2 combination to generate a powerful oxidant that can perform both cyclohexane and benzene hydroxylation.

Table 3.1. Comparing the oxidative reactivity of the **1**/90% H_2O_2 combination with different acid additives.^a

| | No Additive | 2 eq Sc^{3+} | 2 eq HClO_4 | 2 eq Fe^{3+} |
|--|-------------|-----------------------|----------------------|-----------------------|
| TON cyclohexanol (A) | 0.5(1) | 4.2(4) | 4.0(2) | 7.5(3) |
| TON cyclohexanone (K) | 0.6(1) | 0.3(1) | 0.1(1) | 0.10(5) |
| A/K ^[b] | 0.8 | 14 | 40 | 75 |
| PKIE ^[c] (<i>c</i> - C_6H_{12} vs <i>c</i> - C_6D_{12}) | 5(1) | 2.5(2) | 2.0(1) | 2.1(1) |
| % H_2O_2 converted into cyclohexane products | 11 | 45 | 41 | 76 |
| % ^{18}O in $\text{C}_6\text{H}_{11}\text{OH}$ from $\text{H}_2^{18}\text{O}_2/\text{H}_2^{18}\text{O}$ ^[d] | 34/10 | 97/1 | 98/2 | 100/2 |

| | | | | |
|---|---|--------------------------|--------------------------|--------------------------|
| TON phenol | 0 | 4.2(2) | 4.0(3) | 5.4(2) |
| PKIE (C ₆ H ₆ vs C ₆ D ₆) | – | 0.9 | 0.9 | 0.9 |
| k_2 for Fe ^{III} -OOH decay with added acid (M ⁻¹ s ⁻¹) | | 6.7(4) x 10 ² | 5.5(1) x 10 ² | 2.7(2) x 10 ² |

[a] All reactions at room temperature under air with 10 eq 90% H₂O₂; TON (turnover number) = moles of product / moles of **1**. [b] A/K = TON alcohol / TON ketone. [c] PKIE = product kinetic isotope effect based on the yields of cyclohexanol and cyclohexanol-*d*₁₁. [d] ¹⁸O incorporated into cyclohexanol when H₂¹⁸O₂ is used or when the reaction is carried out in the presence of H₂¹⁸O.

Control experiments show that neither Fe^{III}(OTf)₃ nor Fe^{II}(OTf)₂ alone leads to the observed reactivity under similar reaction conditions (Table 3.2). When the results of Fe^{III}(OTf)₃ activation of the **1** + H₂O₂ system are compared to those previously reported for Sc³⁺ and HClO₄ activation,¹⁴ it is clear that Fe³⁺ is more effective than either Sc³⁺ or HClO₄ in substrate oxidation (Table 3.1 and Figure 3.2). For benzene hydroxylation, a turnover number of 5.4 is obtained with 2 eq Fe³⁺, which is about 30% higher than the effect of Sc^{III}(OTf)₃ or HClO₄. For cyclohexane oxidation with 2 eq Fe^{III}(OTf)₃, a TON of 7.5 is observed for cyclohexanol, which is almost two-fold higher than that reported for Sc^{III}(OTf)₃ or HClO₄. Furthermore, the A/K selectivity for Fe^{III}(OTf)₃ is two-fold higher than for HClO₄ and five-fold higher than for Sc^{III}(OTf)₃.

Table 3.2: Control reactions with Fe^{III}(OTf)₃ and Fe^{II}(OTf)₂

| | | Cyclohexanol yield (μmoles) | Cyclohexanone yield (μmoles) | Phenol yield (μmoles) |
|---|--|--------------------------------|------------------------------------|-----------------------------|
| 1 | Fe ^{III} (OTf) ₃ | 0.1(1) | 0.4(1) | 0 |
| 2 | Fe ^{II} (OTf) ₂ | 0.5(1) | 0.8(1) | 0 |
| 3 | 1 + Fe ^{III} (OTf) ₃ | 10.5(4) | 0.2(1) | 7.5(3) |
| 4 | 1 + Fe ^{II} (OTf) ₂ | 1.0(1) | 0.4(1) | trace |

Reaction conditions – For entry 3 and 4, **1**:H₂O₂:cyclohexane/benzene: Mⁿ⁺ = **1**(0.7 mM):10:1000/100:2 at room temperature. For control reactions (entry 1 and 2), the reaction conditions are the same as mentioned for the catalytic reactions (entry 3 and 4) except that for entry 1 and 2 the iron catalyst **1** is not added in the reaction mixture.

A product kinetic isotope effect (PKIE) of 2.1(1) is observed for the competitive oxidation of *c*-C₆H₁₂ versus *c*-C₆D₁₂ in the presence of 2 eq Fe³⁺. This result is similar to those found for cyclohexane hydroxylation by the **1**/H₂O₂ combination in the presence of either Sc^{III}(OTf)₃ or HClO₄ and points toward the formation of quite a powerful oxidant that is less discriminating in its preference for cleaving C–H versus C–D bonds (Table 3.1). The high A/K ratio suggests that the alkyl radical formed in this reaction must be quite short-lived and immediately rebounds to the oxygen attached to the iron center after the initial H-atom abstraction by the iron-based oxidant.

For the hydroxylation of benzene, an inverse product kinetic isotope effect of 0.9 is observed in the presence of Fe³⁺, comparable to values found for both Sc³⁺ and HClO₄ (Table 3.1). These results support an electrophilic aromatic substitution mechanism involving a metal-based electrophile.^{20–22} Additionally, the oxidant formed in the presence

of Fe^{3+} can oxidize electron-poor benzene analogs such as nitrobenzene, bromobenzene and trifluorotoluene, as revealed by the appearance of chromophores of the corresponding $\text{Fe}^{\text{III}}\text{-OAr}$ products, which are blue shifted relative to that of **3** (Figure 3.3). These results suggest that the oxidant is quite a potent electrophile. For both cyclohexane and benzene oxidation, essentially quantitative ^{18}O incorporation from $\text{H}_2^{18}\text{O}_2$ is observed, which is confirmed by the complementary experiment using H_2^{18}O ($\sim 2\%$ ^{18}O incorporation detected from H_2^{18}O). No incorporation from O_2 is observed, unlike in the absence of any additive (Table 1). This observation is similar to what has been observed for Sc^{3+} or HClO_4 . In a competitive oxidation between benzene and cyclohexane, it is observed that hydroxylation of benzene is favored by 10-fold over that for cyclohexane, as found for Sc^{3+} and HClO_4 . Cumulatively, these results suggest that $\text{Fe}^{\text{III}}(\text{OTf})_3$ behaves mechanistically similar to $\text{Sc}^{\text{III}}(\text{OTf})_3$ and HClO_4 in forming a metal-based oxidant; however, $\text{Fe}^{\text{III}}(\text{OTf})_3$ is 80% more effective than either $\text{Sc}^{\text{III}}(\text{OTf})_3$ or HClO_4 in converting cyclohexane to cyclohexanol.

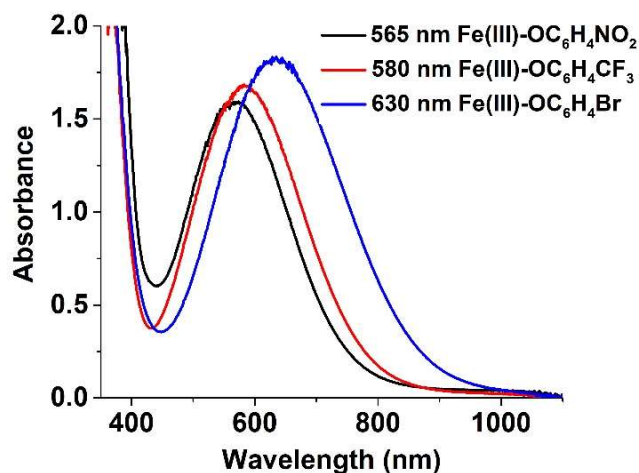


Figure 3.3. Oxidation of substituted benzene analogs with electron-withdrawing substituents upon addition of 4 eq Fe^{3+} to the $\text{Fe}^{\text{III}}\text{-OOH}$ intermediate **2** formed from 0.5 mM **1** at $-40\text{ }^{\circ}\text{C}$ in CH_3CN . Absorption spectra showing formation of the corresponding Fe^{III} -phenolate complexes upon addition of Fe^{3+} to **2**.

3.4 Kinetic analysis of the reaction between $[(\beta\text{-BPMCNCN})\text{Fe}^{\text{III}}\text{-OOH}]^{2+}$ and $\text{Fe}^{\text{III}}(\text{OTf})_3$ or $\text{Fe}^{\text{II}}(\text{OTf})_2$

At $-40\text{ }^{\circ}\text{C}$, **1** reacts with H_2O_2 to form the hydroperoxo-iron(III) species **2** with a λ_{max} of 545 nm.¹⁴ Addition of $\text{Fe}^{\text{III}}(\text{OTf})_3$ to **2** in the presence of benzene as the substrate elicits within seconds the formation of an absorption band centered at 620 nm corresponding to the blue-colored $\text{Fe}^{\text{III}}\text{-OPh}$ species **3** (Figure 3.4a). On the other hand, the Fe^{III} -cyclohexanol product does not have a visible chromophore, allowing us to see the effect of $\text{Fe}^{\text{III}}(\text{OTf})_3$ on accelerating **2** decay. In the presence of cyclohexane as the substrate, intermediate **2** decays within 10 s upon addition of 8 eq $\text{Fe}^{\text{III}}(\text{OTf})_3$, whereas it takes 90 min for **2** to decay without $\text{Fe}^{\text{III}}(\text{OTf})_3$. Notably, the decay rate of **2** in the presence of cyclohexane matches that for the formation of **3** in the presence of benzene. These

observations strongly suggest the formation of a common oxidant in the reaction of **2** with $\text{Fe}^{\text{III}}(\text{OTf})_3$ that is responsible for the hydroxylation of both benzene and cyclohexane (Figure 3.4). As observed for the reaction of **1** with $\text{Sc}^{\text{III}}(\text{OTf})_3$ or HClO_4 , increasing $[\text{Fe}^{3+}]$ accelerates the reaction rates proportionately, further connecting Fe^{3+} addition with the formation of the oxidant (Figure 3.4 and Table 3.3). However, the decay rate of **2** or formation rate of **3** with $\text{Fe}^{\text{III}}(\text{OTf})_3$ is three-fold slower than corresponding rates upon the addition of Sc^{3+} or HClO_4 . With 8 eq Sc^{3+} or HClO_4 , the rate is $2.6(1) \text{ s}^{-1}$, whereas the rate is $0.9(1) \text{ s}^{-1}$ for 8 eq Fe^{3+} . The second order rate constants derived from varying $[\text{Lewis acid}]$ are $6.7(4) \times 10^2 \text{ M}^{-1} \text{ s}^{-1}$ for Sc^{3+} and $2.7(2) \times 10^2 \text{ M}^{-1} \text{ s}^{-1}$ for Fe^{3+} at -40°C . Thus, the nature of the Lewis acid affects the activation of **2** to form the active species.

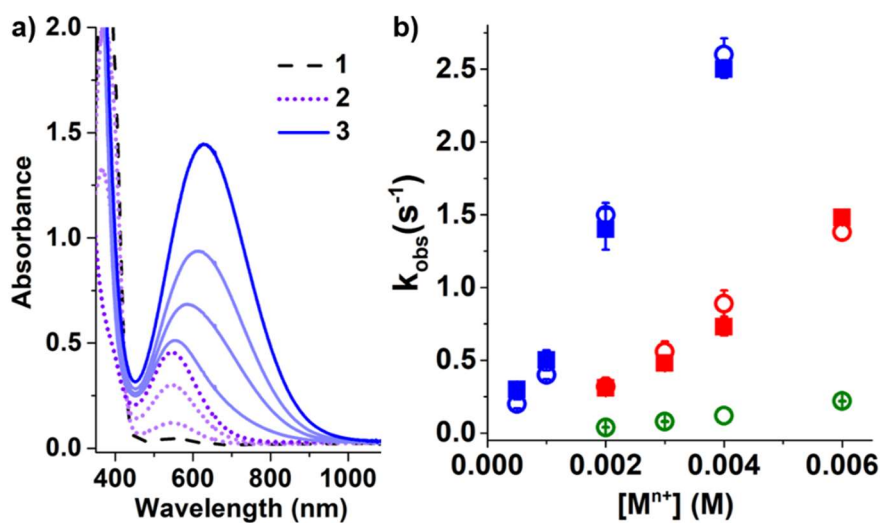


Figure 3.4. a) Formation of **3** upon addition of Fe^{3+} to **2**, which is formed by reacting H_2O_2 with **1** at -40°C in CH_3CN . Dashed black trace **1**, dotted purple trace **2**, solid blue trace **3**. b) M^{n+} (Sc^{3+} , Fe^{3+} , Fe^{2+}) concentration dependence on rates of **3** formation or **2** decay at -40°C . Sc^{3+} (blue); Fe^{3+} (red) and Fe^{2+} (green). Open circles for benzene and filled squares for cyclohexane.

Table 3.3: Rates for decay of **2** in the presence of cyclohexane and formation of **3** in the presence of benzene with increasing $[\text{Fe}^{3+}]$ or $[\text{Fe}^{2+}]$ at $-40\text{ }^\circ\text{C}$

| Benzene | From fitting $k\text{ (s}^{-1}\text{)}$ | Cyclohexane | From fitting $k\text{ (s}^{-1}\text{)}$ |
|---|--|--------------------------------------|--|
| Varying $[\text{Fe}^{3+}]$ | | | |
| <i>With 100 eq benzene</i> | | <i>With 185 eq cyclohexane</i> | |
| Benzene+12 eq Fe^{3+} | 1.38 ± 0.05 | Cyclohexane + 12 eq Fe^{3+} | 1.48 ± 0.04 |
| Benzene+8 eq Fe^{3+} | 0.89 ± 0.09 | Cyclohexane + 8 eq Fe^{3+} | 0.73 ± 0.06 |
| Benzene+6 eq Fe^{3+} | 0.56 ± 0.07 | Cyclohexane + 6 eq Fe^{3+} | 0.48 ± 0.02 |
| Benzene+4 eq Fe^{3+} | 0.32 ± 0.06 | Cyclohexane + 4 eq Fe^{3+} | 0.31 ± 0.01 |
| Varying $[\text{Fe}^{2+}]$ | | | |
| <i>With 100 eq benzene (just the initial decay of 2 upon addition of $\text{Fe}^{\text{II}}(\text{OTf})_2$ was fitted)</i> | | | |
| Benzene+12 eq Fe^{2+} | 0.22 ± 0.003 | | |
| Benzene+8 eq Fe^{2+} | 0.12 ± 0.001 | | |
| Benzene+6 eq Fe^{2+} | 0.08 ± 0.003 | | |
| Benzene+4 eq Fe^{2+} | 0.04 ± 0.003 | | |

The data was fitted using exponential functions to obtain the observed rate constants.

In contrast, addition of $\text{Fe}^{\text{II}}(\text{OTf})_2$ to **2** in the presence of benzene simply results its decay without forming **3**, indicating that it does not activate **2**. However, the rate of **2** decay is found to depend on $[\text{Fe}^{2+}]$, affording a second order rate constant of $4.5(3) \times 10^1 \text{ M}^{-1} \text{ s}^{-1}$ that is six-fold slower than the decay rate for **2** upon addition of $\text{Fe}^{\text{III}}(\text{OTf})_3$ in the presence of cyclohexane (Figure 3.4b). We suggest that this reaction corresponds to the oxidation of $\text{Fe}^{\text{II}}(\text{OTf})_2$ by **2**. Indeed, when this reaction is monitored beyond the initial 100-s time period where rapid decay of **2** occurs, a small amount of **3** can be observed spectroscopically to form over the next 1000 s (Figure 3.5). This outcome likely derives

from the reaction of the nascent Fe^{3+} formed *in situ* with residual **2** to form a small amount of **3**.

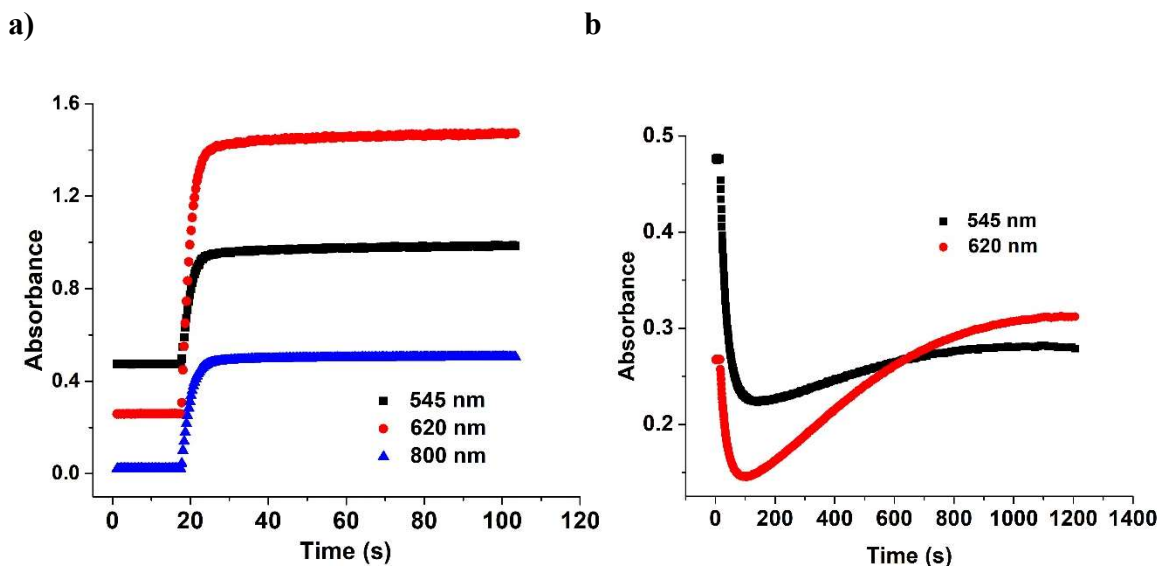


Figure 3.5: Time trace monitoring absorbance at 545 nm corresponding to **2** and at 620 and 800 nm corresponding to **3** at $-40\text{ }^{\circ}\text{C}$. 800 nm is monitored for **3** because at 800 nm there is no interference from **2**. In these reactions, 4 eq $\text{Fe}^{\text{III}}(\text{OTf})_3$ (a) or 4 eq $\text{Fe}^{\text{II}}(\text{OTf})_2$ was added to a pre-formed solution of **2** containing 100 eq benzene. Intermediate **2** is generated from the reaction of **1** (0.5 mM) and 20 eq H_2O_2 .

A further comparison of the differing effects of $\text{Fe}^{\text{III}}(\text{OTf})_3$ and $\text{Fe}^{\text{II}}(\text{OTf})_2$ is presented in Figure 3.6, in which H_2O_2 is added to a solution containing **1**, benzene and either $\text{Fe}^{\text{III}}(\text{OTf})_3$ or $\text{Fe}^{\text{II}}(\text{OTf})_2$ at $-40\text{ }^{\circ}\text{C}$, instead of adding $\text{Fe}^{\text{II}}(\text{OTf})_2$ or $\text{Fe}^{\text{III}}(\text{OTf})_3$ to a solution of pre-formed **2** and benzene at $-40\text{ }^{\circ}\text{C}$ as presented in earlier paragraphs. For $\text{Fe}^{\text{III}}(\text{OTf})_3$, exponential formation of **3** occurs within 100 s (Figure 3.6a). However, for $\text{Fe}^{\text{II}}(\text{OTf})_2$, a small amount of **2** is observed to form initially, followed by a much slower appearance of **3** over 1000 s with an A_{620} value corresponding to less than 0.2 eq **3** formed

(Figure 3.6b). This sequence of spectroscopic changes demonstrates that $\text{Fe}^{\text{III}}(\text{OTf})_3$ interacts with **2** to form the oxidant for benzene hydroxylation, whereas $\text{Fe}^{\text{II}}(\text{OTf})_2$ must first be oxidized to Fe^{3+} by **2** before any phenol can be formed.

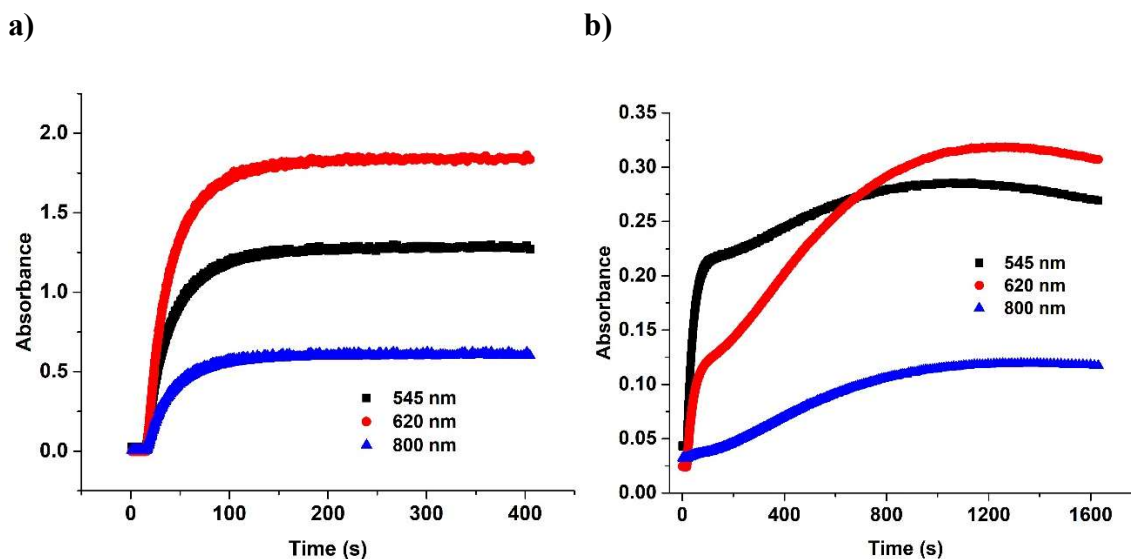


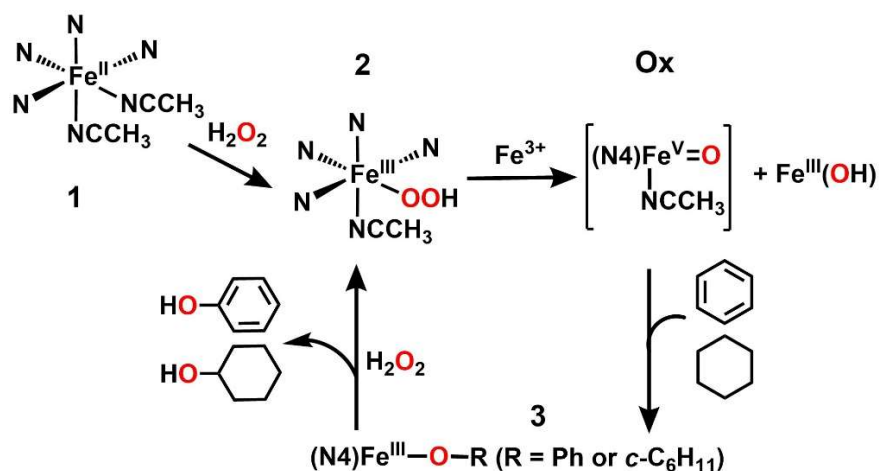
Figure 3.6: Time traces monitoring the absorbances at 545 nm corresponding to **2** and at 620 and 800 nm corresponding to **3**. In these reactions, 20 eq H_2O_2 was added to solutions of **1** (0.5 mM), 100 eq benzene and 4 eq $\text{Fe}^{\text{III}}(\text{OTf})_3$ (a) or $\text{Fe}^{\text{II}}(\text{OTf})_2$ (b) at $-40\text{ }^\circ\text{C}$.

3.5 Role of $\text{Fe}^{\text{III}}(\text{OTf})_3$ in the activation of the $[\text{Fe}^{\text{II}}(\beta\text{-BPMCN})]^{2+}/\text{H}_2\text{O}_2$ system and possible implications for O_2 activation by diiron enzyme

The Lewis acidities of $\text{M}^{\text{n}+}(\text{H}_2\text{O})_x$ ions decrease in the order Fe^{3+} (2.2) > Sc^{3+} (4.3) > Fe^{2+} (9.5),²³ with Fe^{2+} being much less Lewis acidic than either Fe^{3+} or Sc^{3+} . Thus, it is not surprising to find Fe^{2+} is unable to convert **2** into an oxidant that is capable of

hydroxylating benzene or cyclohexane. Furthermore, among the three ions, $\text{Fe}^{\text{II}}(\text{OTf})_2$ is the most likely to undergo one-electron oxidation and deactivate **2** by reduction. In contrast, $\text{Fe}^{\text{III}}(\text{OTf})_3$ can act as a strong Lewis acid like $\text{Sc}^{\text{III}}(\text{OTf})_3$ to activate **2**, generating a powerful oxidant that can perform both cyclohexane and benzene oxidation. In fact, $\text{Fe}^{\text{III}}(\text{OTf})_3$ appears to be more effective than $\text{Sc}(\text{OTf})_3$, affording a 30% higher yield of phenol from benzene oxidation and an 80% higher yield of cyclohexanol from cyclohexane hydroxylation in experiments at room temperature. However the rate at which $\text{Fe}^{\text{III}}(\text{OTf})_3$ reacts with **2** to form the active oxidant at $-40\text{ }^\circ\text{C}$ is only one-third as fast as that for $\text{Sc}^{\text{III}}(\text{OTf})_3$, clearly suggesting some differences in the way these two metal ions interact with **2**. Furthermore, we found that the use of $\text{Fe}^{\text{III}}\text{Cl}_3$ in place of $\text{Fe}^{\text{III}}(\text{OTf})_3$ does not result in the formation of the $\text{Fe}^{\text{III}}\text{-OPh}$ chromophore. However, both $\text{Fe}^{\text{III}}\text{Cl}_3$ and $\text{Fe}^{\text{II}}\text{Cl}_2$ made **2** decay, which is likely due to chloride binding to **1**, hence inhibiting the iron center from binding H_2O_2 . This was verified by adding NBu_4Cl to **2**, which also led to its decay. Thus, the counter-anion also plays a significant role in the activation of **2** and requires to be a noncoordinating anion.

In Scheme 3.2, we propose that the Lewis acidic Fe^{3+} interacts with the distal oxygen atom of the hydroperoxo ligand of **2** to facilitate the heterolytic cleavage of the O–O bond to form the powerful $\text{Fe}^{\text{V}}(\text{O})$ oxidant (**Ox**). Such a potent oxidant rationalizes the hydroxylation of cyclohexane with a very high A/K ratio, a relatively low PKIE of ~ 2 and the hydroxylation of benzene with an inverse KIE of 0.9.



Scheme 3.2. Proposed mechanism for the activation of intermediate **2** by $\text{Fe}^{\text{III}}(\text{OTf})_3$ for the oxidation of benzene and cyclohexane by **1**/ H_2O_2 .

An alternative possibility is O–O bond homolysis forming $(\beta\text{-BPMCN})\text{Fe}^{\text{IV}}(\text{O})$ and $\cdot\text{OH}$ radical. Hydroxyl radicals cannot give rise to the selective cyclohexane hydroxylation chemistry we observe here, reducing the probability of this pathway, but some $\text{Fe}^{\text{IV}}=\text{O}$ complexes reported to date are capable of oxidizing cyclohexane.²⁴ Nevertheless, the $\text{Fe}^{\text{IV}}(\text{O})$ may be activated by formation of an $\text{Fe}^{\text{IV}}(\text{O})\cdots\text{Fe}^{\text{III}}(\text{OTf})_3$ adduct by analogy to the Lewis acid adducts of $\text{Fe}^{\text{IV}}=\text{O}$ complexes investigated by Fukuzumi and Nam, which have been found to exhibit enhanced electron transfer properties.^{7,8} We have tested this hypothesis by adding $\text{Fe}^{\text{III}}(\text{OTf})_3$ to a solution containing $(\beta\text{-BPMCN})\text{Fe}^{\text{IV}}(\text{O})$ (Figure 3.7), which was generated in situ from the reaction of **1** and 2-($t\text{BuSO}_2$)- $\text{C}_6\text{H}_4\text{IO}$ in acetonitrile at $-40\text{ }^\circ\text{C}$. When done in the presence of benzene, no formation of phenol was observed. Similarly, addition of $\text{Sc}^{\text{III}}(\text{OTf})_3$ to a solution containing $(\beta\text{-BPMCN})\text{Fe}^{\text{IV}}(\text{O})$ in the presence of benzene did not elicit its hydroxylation, excluding the likelihood of Lewis acid activation of the $\text{Fe}^{\text{IV}}(\text{O})$ unit to

generate a powerful electrophilic oxidant. Therefore, we eliminate $\text{Fe}^{\text{IV}}(\text{O})\text{M}^{\text{III}}$ ($\text{M} = \text{Fe}$ or Sc) adducts or $\text{Fe}^{\text{V}}(\text{O})$ generated from $\text{Fe}^{\text{IV}}(\text{O})$ and Fe^{III} as possibilities, and **Ox** is assigned to be an $\text{Fe}^{\text{V}}(\text{O})$ species formed by Fe^{3+} -assisted heterolytic cleavage of the O–O bond of **2**.

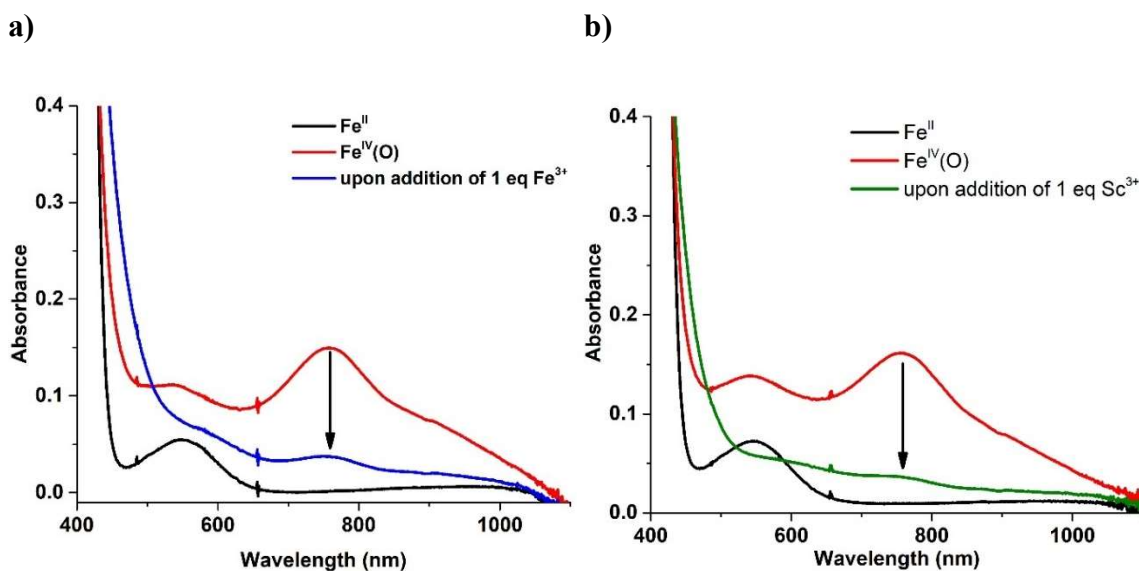


Figure 3.7: Effect of addition of (a) $\text{Fe}^{\text{III}}(\text{OTf})_3$ to $\text{Fe}^{\text{IV}}(\text{O})$ and (b) $\text{Sc}^{\text{III}}(\text{OTf})_3$ to $\text{Fe}^{\text{IV}}(\text{O})$ obtained from the reaction of **1** with 2-($t\text{BuSO}_2$)- $\text{C}_6\text{H}_4\text{IO}$ in acetonitrile at $-40\text{ }^\circ\text{C}$ containing 100 eq benzene.

We have compared our results with those of previously reported nonheme iron oxidants capable of oxidizing cyclohexane (Table 3.4). For all other cases listed in this table, the high-valent iron oxidants can be directly observed and decay upon addition of cyclohexane at rates dependent on substrate concentration. However, for our experiments with $[\text{Fe}(\beta\text{-BPMCNCN)OOH}]^{2+}$, the oxidant **Ox** cannot be observed directly because the

formation of **Ox** is slower than its subsequent reaction with substrate. The rate of **Ox** formation thus represents the lower limit for the rate of substrate oxidation, which is why the decay rate of **2** in the presence of cyclohexane matches the rate of **3** formation with benzene, even though hydroxylation of benzene is favored 10-fold over that of cyclohexane in mixed-substrate competition experiments. To compare the rates listed for **2** in the bottom half of Table 3.4 with previously reported rates for cyclohexane oxidation by high-valent iron oxidants listed in the upper half of Table 3.4, we have calculated first-order rate constants for those in the top half assuming the presence of 1 M cyclohexane in the reaction solution. Thus the rate found for the reaction of **2** with 8 eq Sc^{3+} (2.5 s^{-1}) is comparable to that of $[\text{Fe}^{\text{V}}(\text{O})(\text{O}_2\text{CR})(\text{PyNMe}_3)]^{2+}$ (2.8 s^{-1}), the fastest nonheme iron system for cyclohexane hydroxylation documented to date,²⁵ followed by **2** with 8 eq of Fe^{3+} (0.7 s^{-1}), which is in turn two-fold faster than $S = 1$ $[\text{Fe}^{\text{IV}}(\text{O})(\text{Me}_3\text{NTB})]^{2+}$ (0.25 s^{-1})²⁶ and $S = 2$ $[\text{Fe}^{\text{IV}}(\text{O})(\text{TQA})]^{2+}$ (0.37 s^{-1})²⁷ the two most reactive $\text{Fe}^{\text{IV}}(\text{O})$ complexes characterized thus far. It should be noted that the rates associated with **2** are dependent on $[\text{Sc}^{3+}$ or Fe^{3+} or H^+]; hence increasing the concentrations of these additives results in higher rates, potentially allowing substrate oxidation by **2** to be faster than by $[\text{Fe}^{\text{V}}(\text{O})(\text{O}_2\text{CR})(\text{PyNMe}_3)]^{2+}$. From a comparison of the products formed by these systems, it is clear that the **2**/ Fe^{3+} combination affords the best cyclohexanol yield and the highest cyclohexanol/cyclohexanone product ratio, making the oxidant formed by this combination a fast and highly selective oxidant for hydroxylating cyclohexane.

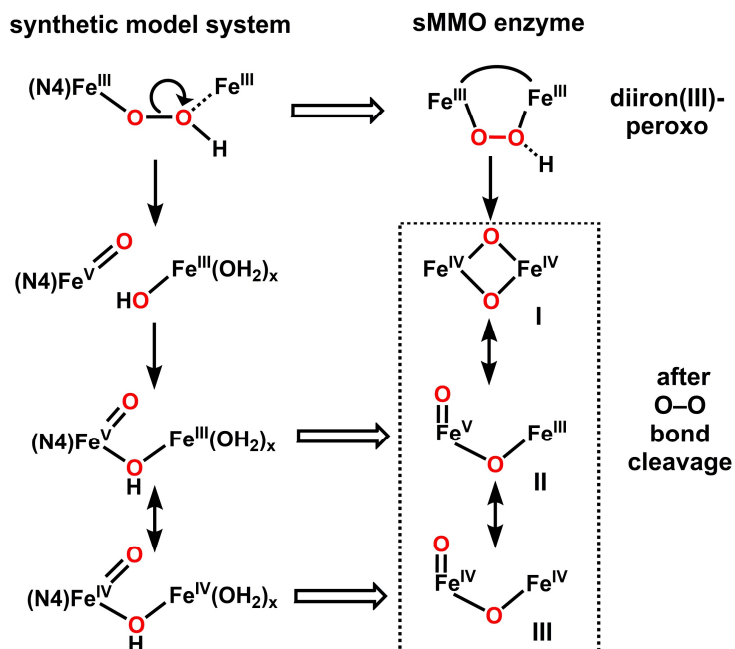
Table 3.4: Table comparing decay rates of select nonheme iron intermediates involved in cyclohexane oxidation and their alcohol/ketone (A/K) ratios.

| | k_2 ($M^{-1}s^{-1}$) measured at $-40\text{ }^\circ\text{C}$ | A/K | Ref |
|--|---|--------------------|-----------|
| $[\text{Fe}^{\text{V}}(\text{O})(\text{TAML})]^-$ | 0.00026 | | 28 |
| $S = 1$ $[\text{Fe}^{\text{IV}}(\text{O})(\text{Me}_3\text{NTB})]^{2+}$ | 0.25 | | 26 |
| $S = 2$ $[\text{Fe}^{\text{IV}}(\text{O})(\text{TQA})]^{2+}$ | 0.37 | only ketone formed | 27 |
| $[\text{Fe}^{\text{V}}(\text{O})(\text{O}_2\text{CR})(\text{PyNMe}_3)]^{2+}$ | 2.8 | 5 | 25 |
| | k_{obs} (s^{-1}) | | |
| $[\text{Fe}^{\text{III}}(\beta\text{-BPMCN})(\text{OOH})]^{2+}$ (2) | $t_{1/2} \approx 1\text{ h}$ | 0.8 | 14 |
| + 8 eq $\text{Sc}^{\text{III}}(\text{OTf})_3$ | 2.5 | 14 | 14 |
| + 8 eq HClO_4 | 2.3 | 40 | 14 |
| + 8 eq $\text{Fe}^{\text{III}}(\text{OTf})_3$ | 0.7 | 75 | This work |

Abbreviations used: TAML = tetraaza macrocyclic ligand; 13-TMC = 1,4,7,10-tetramethyl-1,4,7,10-tetraazacyclotridecane; Me_3NTB = tris(benzimidazolyl-2-methyl)-amine; TQA = tris(quinolyl-2-methyl)amine; PyNMe_3 = 3,6,9-trimethyl-3,6,9-triaza-1(2,6)-pyridina-cyclo-decaphane

The observations we have described above may also shed some light on how the diiron center of soluble methane monooxygenase (sMMO) could act to hydroxylate methane. The efforts of Lipscomb^{5,29,30} and Lippard^{4,31} have shown that reduced sMMO has a diiron(II) active center that reacts with O_2 to form a diiron(III)-peroxo intermediate called **P**, which in turn converts into **Q**, the diiron(IV) oxidant responsible for methane hydroxylation (Scheme 3.1). The conversion of **P** to **Q** has been demonstrated to exhibit a pH dependence implicating a water-derived proton with a $\text{pK}_a \sim 7.6$ that facilitates O–O bond cleavage.^{32,33} Parallels may be drawn between the structures of the protonated **P** intermediate and the Fe^{III} -adduct with **2** postulated in Scheme 3.3. In the latter case, we have proposed that Lewis acidic Fe^{3+} facilitates heterolytic O–O bond cleavage to form an

oxidant **Ox** formulated simply as $[(L)Fe^V=O]^{3+}$. However, it is possible that the Lewis acidic Fe^{III} center could interact with the nascent $[(L)Fe^V=O]^{3+}$ species to form an $O=Fe^V-OH-Fe^{III}$ adduct. This structure would then be related to the high-valent diiron structures formed after O–O bond cleavage as shown in the sMMO column in Scheme 3.3. At present, there is resonance Raman evidence supporting the diamond core structure **I** for sMMO-**Q**³⁴ but recent EXAFS studies favor the open core structure **III**.^{35,36} The putative $O=Fe^V-O(H)-Fe^{III}$ species proposed in this study can be thought of as an electromer of **III** and provide a mechanism to concentrate the oxidizing power of **Q** onto one iron center in order to cleave the very strong C–H bond of methane.^{35,36} Hence, the second iron in diiron sMMO can have an additional role as a Lewis acid that is positioned in the active center to activate the O–O bond and form a highly reactive oxidant.



Scheme 3.3. Parallels between the activation of **2** by $Fe^{III}(OTf)_3$ and the proton-activated diiron(III)-peroxo intermediate of soluble methane monooxygenase. **I**, **II** and **III** are the three plausible structures proposed for **Q**.

3.6 Summary

In summary, we show that Fe^{III} can act as a Lewis acid and activate a synthetic nonheme $Fe^{III}-OOH$ intermediate **2** to form a powerful electrophilic oxidant **Ox** that can perform the hydroxylation of benzene and cyclohexane within seconds even at $-40\text{ }^\circ\text{C}$. Such activation of an iron(III) peroxo or hydroperoxo intermediate using another iron(III) center is unprecedented in bioinspired nonheme iron chemistry and raises the possibility that the second iron in soluble methane monooxygenase may be required not only for its redox capabilities but additionally to act as a strong Lewis acid to form the powerful oxidant **Q** for the hydroxylation of methane.

3.7 References

- (1) Que, L.; Tolman, W. B. *Nature* **2008**, *455*, 333–340.
- (2) Kal, S.; Que, L. *J. Biol. Inorg. Chem.* **2017**, *22*, 339–365.
- (3) Jasniewski, A. J.; Que, L. *Chem. Rev.* **2018**, *118*, 2554–2592.
- (4) Tinberg, C. E.; Lippard, S. J. *Acc. Chem. Res.* **2011**, *44*, 280–288.
- (5) Wallar, B. J.; Lipscomb, J. D. *Chem. Rev.* **1996**, *96*, 2625–2657.
- (6) Krebs, C.; Fujimori, D. G.; Walsh, C. T.; Bollinger, J. M. *Acc. Chem. Res.* **2007**, *40*, 484–492.
- (7) Fukuzumi, S.; Ohkubo, K.; Lee, Y. M.; Nam, W. *Chem. Eur. J.* **2015**, *21*, 17548–17559.
- (8) Fukuzumi, S. *Coord. Chem. Rev.* **2013**, *257*, 1564–1575.
- (9) Lee, C.-I.; Lakshmi, K. V.; Brudvig, G. W. *Biochemistry* **2007**, *46*, 3211–3223.
- (10) Tsui, E. Y.; Tran, R.; Yano, J.; Agapie, T. *Nat. Chem.* **2013**, *5*, 293–299.
- (11) Herbert, D. E.; Lionetti, D.; Rittle, J.; Agapie, T. *J. Am. Chem. Soc.* **2013**, *135*, 19075–19078.
- (12) Li, F.; Van Heuvelen, K. M.; Meier, K. K.; Münck, E.; Que, L. *J. Am. Chem. Soc.* **2013**, *135*, 10198–10201.
- (13) Lee, Y.-M.; Bang, S.; Kim, Y. M.; Cho, J.; Hong, S.; Nomura, T.; Ogura, T.; Troepfner, O.; Ivanović-Burmazović, I.; Sarangi, R.; Fukuzumi, S.; Nam, W. *Chem. Sci.* **2013**, *4*, 3917–3923.
- (14) Kal, S.; Draksharapu, A.; Que, L. *J. Am. Chem. Soc.* **2018**, *140*, 5798–5804.

- (15) Costas, M.; Que, L. *Angew. Chem. Int. Ed.* **2002**, *41*, 2179–2181.
- (16) <https://www.cdc.gov/niosh/ipcsneng/neng0164.html>.
- (17) <http://msdsviewer.fmc.com/private/document.aspx?prd=7722-84-1--90~PDF~MTR~CPNA~EN~1/1/0001%2012:00:00%20AM~HYDROGEN%20PEROXIDE%2090%~>.
- (18) Jo, D. H.; Chiou, Y. M.; Que, J. *Inorg. Chem.* **2001**, *40*, 3181–3190.
- (19) Chen, K.; Que, L. *J. Am. Chem. Soc.* **2001**, *123*, 6327–6337.
- (20) Olah, G. A. *Acc. Chem. Res.* **1971**, *4*, 240–248.
- (21) Augusti, R.; Dias, A. O.; Rocha, L. L.; Lago, R. M. *J. Phys. Chem. A* **1998**, *102*, 10723–10727.
- (22) Tsuji, T.; Zaoputra, A. A.; Hitomi, Y.; Mieda, K.; Ogura, T.; Shiota, Y.; Yoshizawa, K.; Sato, H.; Kodera, M. *Angew. Chem Int. Ed.* **2017**, *56*, 7779–7782.
- (23) Gilson, R.; Durrant, M. C. *Dalt. Trans.* **2009**, 10223–10230.
- (24) McDonald, A. R.; Que, L. *Coord. Chem. Rev.* **2013**, *257*, 414–428.
- (25) Serrano-Plana, J.; Oloo, W. N.; Acosta-Rueda, L.; Meier, K. K.; Verdejo, B.; García-España, E.; Basallote, M. G.; Münck, E.; Que, L.; Company, A.; Costas, M. *J. Am. Chem. Soc.* **2015**, *137*, 15833–15842.
- (26) Seo, M. S.; Kim, N. H.; Cho, K.-B.; So, J. E.; Park, S. K.; Clémancey, M.; Garcia-Serres, R.; Latour, J.-M.; Shaik, S.; Nam, W. *Chem. Sci.* **2011**, *2*, 1039–1045.
- (27) Biswas, A. N.; Puri, M.; Meier, K. K.; Oloo, W. N.; Rohde, G. T.; Bominaar, E. L.; Münck, E.; Que, L. *J. Am. Chem. Soc.* **2015**, *137*, 2428–2431.
- (28) Kundu, S.; Van Thompson, J. K.; Shen, L. Q.; Mills, M. R.; Bominaar, E. L.; Ryabov,

- A. D.; Collins, T. J. *Chem. Eur. J.* **2015**, *21*, 1803–1810.
- (29) Banerjee, R.; Komor, A. J.; Lipscomb, J. D. *Methods Enzymol.* **2017**, *596*, 239–289.
- (30) Lipscomb, J. D. *J. Biol. Chem.* **2014**, *289*, 15141–15153.
- (31) Sazinsky, M. H.; Lippard, S. J. *Sustaining Life on Planet Earth: Metalloenzymes Mastering Dioxygen and Other Chewy Gases*; Sigel, A., Sigel, H., Sigel, R. K. O., Kroneck, P. M. H., Sosa Torres, M. E., Eds.; Springer Berlin Heidelberg, 2015; Vol. 15.
- (32) Lee, S.-K.; Lipscomb, J. D. *Biochemistry* **1999**, *38*, 4423–4432.
- (33) Tinberg, C. E.; Lippard, S. J. *Biochemistry* **2009**, *48*, 12145–12158.
- (34) Banerjee, R.; Proshlyakov, Y.; Lipscomb, J. D.; Proshlyakov, D. A. *Nature* **2015**, *518*, 431–434.
- (35) Castillo, R. G.; Banerjee, R.; Allpress, C. J.; Rohde, G. T.; Bill, E.; Que, L.; Lipscomb, J. D.; DeBeer, S. *J. Am. Chem. Soc.* **2017**, *139*, 18024–18033.
- (36) Cutsail III, G. E.; Banerjee, R.; Zhou, A.; Que, L.; Lipscomb, J. D.; DeBeer, S. *J. Am. Chem. Soc.* **2018**, *140*, 16807–16820.

Chapter 4:

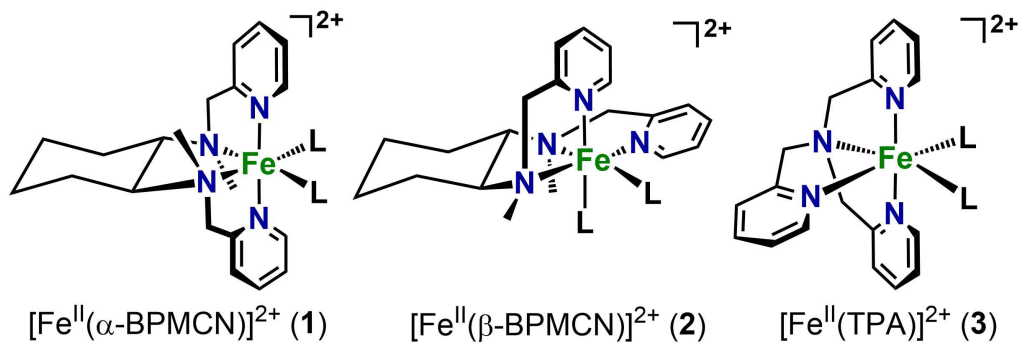
Effect of ligand topology on Sc³⁺-assisted activation of Fe^{III}-OOH intermediates to form high-valent iron oxidants

4.1 Introduction

Inspired by nonheme iron enzymes that catalyze the difficult reaction of functionalizing inert C–H bonds of hydrocarbons, many synthetic iron catalysts have been designed in the last two decades for hydrocarbon oxidations using H₂O₂ as the oxidant.^{1–4} Nonheme iron complexes supported by nitrogen-based tetradentate ligands has been developed to perform catalytic alkane hydroxylation (including cyclohexane with strong C–H bonds, BDE = 99.5 kcal mol⁻¹) as well as olefin epoxidation and cis-dihydroxylation, similar to the enzymes.^{2,3,5,6} [Fe^{II}(TPA)]²⁺ (TPA = tris(pyridyl-2-methyl)amine), [Fe^{II}(BPMEN)]²⁺ (BPMEN = N,N'-bis(pyridyl-2-methyl)-1,2-diaminoethane) and their substituted analogs have been extensively studied both mechanistically and spectroscopically.^{7–10} An S = 1/2 Fe^{III}–OOH species was trapped and characterized for [Fe^{II}(TPA)]²⁺, which was demonstrated to undergo water-assisted O–O bond cleavage to form a high valent iron(V) oxidant responsible for oxidizing alkanes and olefins.^{9,11} This mechanism is found to be common among nonheme iron catalysts as more and more synthetic iron catalysts are developed.^{2,12,13}

O–O bond cleavage in [(TPA)Fe^{III}–OOH]²⁺ leading to the formation of the iron(V) oxidant is found to be assisted by a proton that is derived from water.^{2,10} Unlike the well-known [Fe^{II}(TPA)]²⁺ or [Fe^{II}(BPMEN)]²⁺, [Fe^{II}(β-BPMCN)]²⁺ reported in 2002 was inefficient in performing cyclohexane oxidation.¹⁴ However, in 2018, we demonstrated that Lewis acidic Sc(OTf)₃ or HClO₄ can interact with the [(β-BPMCN)Fe^{III}–OOH]²⁺ intermediate to form a powerful oxidant that oxidizes both cyclohexane and benzene within seconds at -40 °C (Chapter 2).¹⁵ We propose that in this case the Sc(OTf)₃ or HClO₄ assists

in breaking the O–O bond of the $[(\beta\text{-BPMCN})\text{Fe}^{\text{III}}\text{-OOH}]^{2+}$ forming the iron(V) oxidant - a new route to access a reactive iron(V) oxidant. In 2013, Sc^{3+} and Y^{3+} were reported to induce O–O bond cleavage in $[(\text{TMC})\text{Fe}^{\text{III}}(\eta^2\text{-O}_2)]^+$ supported by the macrocyclic TMC ligand (tetramethylcyclam) to form the corresponding $\text{Fe}^{\text{IV}}(\text{O})$ species.^{16,17} These reports indicate that Lewis acids can interact with $\text{Fe}^{\text{III}}\text{-OO}(\text{H})$ species leading to the formation of high-valent iron oxidants by breaking the O–O bonds. In Chapter 2, we focussed on the effect of Sc^{3+} on the catalytic reactivity of $[\text{Fe}^{\text{II}}(\beta\text{-BPMCN})]^{2+}$. In this chapter, we study the effect of $\text{Sc}(\text{OTf})_3$ on the catalytic reactivity of two other nonheme iron complexes, $[\text{Fe}^{\text{II}}(\alpha\text{-BPMCN})]^{2+}$ and $[\text{Fe}^{\text{II}}(\text{TPA})]^{2+}$, and compare it with that of $[\text{Fe}^{\text{II}}(\beta\text{-BPMCN})]^{2+}$. Additionally, we compare the behaviour of the catalytically relevant $\text{Fe}^{\text{III}}\text{-OOH}$ intermediates generated in the three cases.



Scheme 4.1. The three nonheme iron complexes used in this study ($\text{L} = \text{CH}_3\text{CN}$).

The tetradentate ligand BPMCN (BPMCN = N,N'-bis(pyridyl-2-methyl)-N,N'-dimethyl-trans-1,2-diaminocyclohexane)) can bind the iron center in two different topologies (*cis*- α and *cis*- β) forming two distinct iron complexes with very different

reactivities – $[\text{Fe}^{\text{II}}(\alpha\text{-BPMCN})]^{2+}$ (**1**) and $[\text{Fe}^{\text{II}}(\beta\text{-BPMCN})]^{2+}$ (**2**) (Scheme 4.1).¹⁴ $[\text{Fe}^{\text{II}}(\alpha\text{-BPMCN})]^{2+}$ (**1**) was reported to be an efficient catalyst for cyclohexane hydroxylation similar to $[\text{Fe}^{\text{II}}(\text{BPMEN})]^{2+}$ and $[\text{Fe}^{\text{II}}(\text{TPA})]^{2+}$ (**3**), whereas $[\text{Fe}^{\text{II}}(\beta\text{-BPMCN})]^{2+}$ (**2**) was inefficient in cyclohexane hydroxylation. Furthermore, in olefin oxidation, **1** and **3** favored oxidizing electron-rich olefins over electron-poor ones, whereas **2** favored oxidizing electron-poor olefins.^{18,19} Based on these reactivity trends, it was concluded that **2** forms a nucleophilic oxidant, in contrast to **1** and **3**, which form oxidants with electrophilic character.^{18,19} For olefin *cis*-dihydroxylation, in the cases of **1** and **3**, one O-atom in the *cis*-diol was obtained from H_2O_2 and the other from H_2O . However, for **2** both O-atoms in the *cis*-diol product were derived from H_2O_2 .¹⁴ These observations together suggest that the ligand topology around the iron center can play a crucial role in the reactivity of nonheme iron catalysts, and that **1** and **2**, although being supported by the same ligand, follows different mechanisms involving most likely different oxidants. In this chapter, we have studied the effect of Sc^{3+} on the topological isomeric complexes **1** and **2** to see if ligand topology plays a significant role on the Sc^{3+} -assisted mechanism.

4.2 Experimental details

All materials were purchased from Sigma-Aldrich and used as received unless noted otherwise. H_2^{18}O (97% ^{18}O -enriched) and $\text{H}_2^{18}\text{O}_2$ (90% ^{18}O -enriched, 10% solution in H_2^{16}O) were obtained from Berry & Associates-ICON Isotopes. Cyclohexane, benzene and nitrobenzene were passed through alumina and silica gel before the reactions. 90% H_2O_2 was obtained from FMC Corporation. Caution: 90% H_2O_2 is potentially explosive

and should be handled with proper safety precautions.^{20,21} The ligand BPMCN, TPA and the complexes $[\text{Fe}^{\text{II}}(\beta\text{-BPMCN})](\text{OTf})_2$, $[\text{Fe}^{\text{II}}(\alpha\text{-BPMCN})](\text{OTf})_2$ and $[\text{Fe}^{\text{II}}(\text{TPA})](\text{OTf})_2$ were synthesized according to previously published procedures.^{7,14,22}

Product analyses were performed on a Perkin-Elmer Sigma 3 gas chromatograph (AT-1701 column) with a flame-ionization detector. GC mass spectral analyses were performed on a HP 6890 GC (HP-5 column) using an Agilent 5973 mass detector. For chemical ionization analyses, NH_3/CH_4 (4%) was used as the ionization gas. UV-visible absorption spectra were recorded on a HP8453A diode array spectrometer equipped with a cryostat from Unisoku, Scientific Instruments (Osaka, Japan). Resonance Raman spectra were obtained at $-30\text{ }^\circ\text{C}$ with excitation at 561 nm (100 mW at source, Cobolt Lasers) through the sample in a flat bottom NMR tube using a 90° backscattering arrangement (parallel to the slit direction). The collimated Raman scattering was collected using two Plano convex lenses ($f = 12\text{ cm}$, placed at an appropriate distance) through appropriate long pass edge filters (Semrock) into an Acton AM-506M3 monochromator equipped with a Princeton Instruments ACTON PyLON LN/CCD-1340x400 detector. The detector was cooled to $-120\text{ }^\circ\text{C}$ prior to the experiments. Spectral calibration was performed using the Raman spectrum of acetonitrile/toluene 50:50 (v:v).²³ Each spectrum was accumulated, typically 60 times with 1 s acquisition time, resulting in a total acquisition time of 1 min per spectrum. The collected data was processed using Spekwin32,²⁴ and a multi-point baseline correction was performed for all spectra. X-band EPR spectra were recorded on a Bruker Elexsys E-500 spectrometer equipped with an Oxford ESR 910 liquid helium cryostat and an Oxford temperature controller.

Catalytic reaction conditions – All experiments reported in this work were performed in the presence of air. In a typical reaction, 70 μL of a 0.2 M H_2O_2 solution (diluted from 90% $\text{H}_2\text{O}_2/\text{H}_2\text{O}$ solution) in CH_3CN (10 eq H_2O_2 relative to $\mathbf{1/2/3}(\text{OTf})_2$) was added all at once to a vigorously stirred CH_3CN solution (1.93 mL) containing the iron catalyst $\mathbf{1/2/3}(\text{OTf})_2$, the substrate and $\text{Sc}^{\text{III}}(\text{OTf})_3$ and stirred for 30 min at room temperature. The final concentration of the iron catalyst in the reaction mixture was 0.7 mM with 1000 eq cyclohexane/ 100 eq benzene and 0.5–8 eq $\text{Sc}^{\text{III}}(\text{OTf})_3$. After the reaction was over, 0.1 mL 1-methylimidazole and 1 mL acetic anhydride were added to the reaction solution to esterify the alcohol/phenol. An internal standard (naphthalene) was added after this and then the products were extracted into CHCl_3 and the solution was then subjected to GC and/or GC-MS analysis.

Isotope-labeling studies – Similar conditions were used as described for catalytic reaction conditions above except for the following details. In experiments with $\text{H}_2^{18}\text{O}_2$, 10 eq of $\text{H}_2^{18}\text{O}_2$ from 10% $\text{H}_2^{18}\text{O}_2/\text{H}_2\text{O}$ solution (90% ^{18}O -enrichment) relative to $\mathbf{1/2/3}(\text{OTf})_2$ was added instead of $\text{H}_2^{16}\text{O}_2$. In experiments with H_2^{18}O , 68 μL of 3.5 M H_2^{18}O solution (97% ^{18}O -enrichment) in CH_3CN (170 eq H_2^{18}O relative to $\mathbf{1/2/3}(\text{OTf})_2$ which is about the same amount of H_2O that would be introduced from a 10% H_2O_2 solution) was added to the reaction mixture before adding H_2O_2 . The products were analyzed using GC/CI-MS or GC/EI-MS. The percent ^{18}O -incorporation into the products was calculated on the basis of the ^{18}O -enrichments of the reagents containing the isotope.

Kinetic isotope effect (KIE) experiments – Conditions similar to what was described for the general catalytic reactions were used except for the following details. A

ratio of 1:3 was used for cyclohexane/cyclohexane-d₁₂ in the KIE experiment to improve the accuracy of the results. For benzene oxidation a 1:1 ratio of benzene/benzene-d₆ was used. H₂O₂ was added in a controlled fashion using a syringe pump to obtain results under similar conditions as reported in literature^{7,14} for the purpose of comparison. It was previously done using a syringe pump to enhance the yields of the products, but same results were obtained in the experiments with additives described in this paper with and without syringe pumping.

4.3 Effect of Sc(OTf)₃ on the catalytic reactivity of [Fe^{II}(α -BPMCN)]²⁺/H₂O₂ and [Fe^{II}(TPA)]²⁺/H₂O₂

In previous literature reports^{7,14} on these catalytic systems **1**, **2** and **3**, H₂O₂ was added slowly at a controlled rate using a syringe pump to reduce unproductive side reactions such as Fenton chemistry, and increase the yield of the desired products. As shown in Figure 4.1, the yields decrease when we move from controlled addition of H₂O₂ using a syringe pump to all-at-once addition of H₂O₂. Interestingly, for Sc³⁺-assisted catalytic reactions of **2**, we previously observed that addition of H₂O₂ via syringe pump does not affect the yields, suggesting that the desired reactions occur much faster than the unproductive side reactions. Here, we have performed the catalytic reactions by adding H₂O₂ all at once at the beginning of the reactions and compared the effect of Sc³⁺ in **1**-, **2**- and **3**-catalyzed oxidations of cyclohexane and benzene.

Upon addition of Sc(OTf)₃ to a reaction mixture of **1**+H₂O₂+cyclohexane, a three-fold increase in the yield of cyclohexanol is observed relative to that the absence of any

Sc(OTf)₃, when H₂O₂ is added all at once (Figure 4.1a). For **3**, a similar three-fold increase in the yield of cyclohexanol is observed in the presence of Sc³⁺. However, it takes 3-5 eq Sc³⁺ for **3** compared to only 1 eq Sc³⁺ required for **1**. Interestingly, for both **1** and **3** the maximum yields of cyclohexanol observed in the presence of Sc³⁺ are the same as observed with controlled addition of H₂O₂ via syringe pump. In contrast, for **2** the presence of Sc³⁺ enhances the yield of cyclohexanol by 10-fold compared to controlled addition of H₂O₂. These observations suggest that the oxidants formed in the presence of Sc³⁺ for **1** and **3** are equally efficient as the one formed in the absence of Sc³⁺. On the other hand, for **2** the oxidant formed in the presence of Sc³⁺ is much more reactive than that formed in its absence.

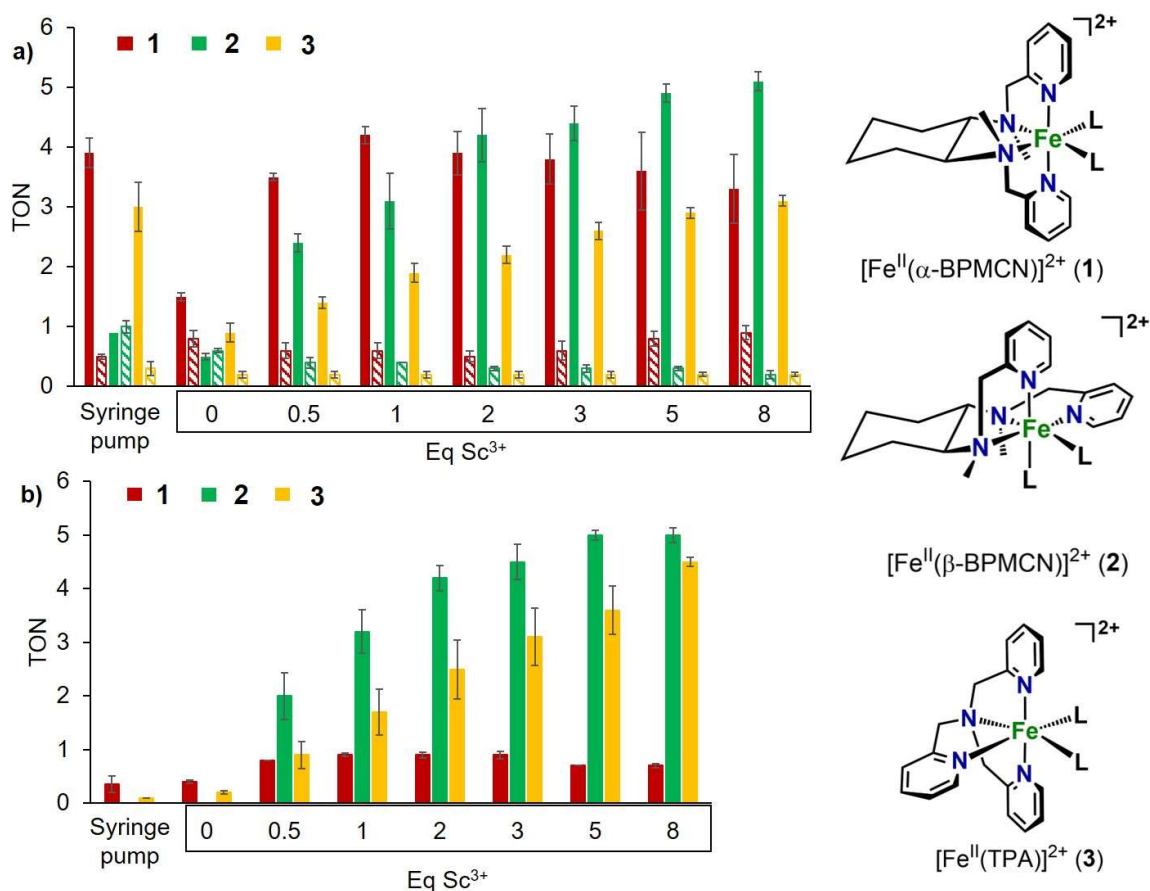


Figure 4.1. Left: a) Effect of Sc(OTf)₃ on yields of cyclohexanol (solid bars) and cyclohexanone (patterned bars) from cyclohexane oxidation catalysed by **1**, **2** and **3**. b) Effect of Sc(OTf)₃ on yields of phenol from benzene oxidation catalysed by **1**, **2** and **3**. Reaction conditions: **1/2/3** (0.7 mM), 1000 eq cyclohexane or 100 eq benzene, 10 eq 90% H₂O₂ in CH₃CN at room temperature. Right: The three catalysts compared here.

In the case of benzene hydroxylation, **1** is able to convert benzene to phenol without addition of Sc³⁺, unlike **2**. Addition of Sc³⁺ increases the yield of phenol three-fold from 0.3 TON to 1 TON, but increasing the concentration of Sc³⁺ does not have any effect on phenol yields, unlike for **2** (Figure 4.1b). On the other hand, for **3** as the concentration of

Sc³⁺ is increased the phenol yields also increase, similar to **2**. Although the trend observed on phenol formation in the presence of Sc³⁺ is similar for both **2** and **3**, the effect is more prominent for **2** (Figure 4.1b).

Table 4.1. Comparing the oxidative reactivity of **1**, **2** and **3** with H₂O₂ in the presence or absence of Sc³⁺.^a

| | Fe ^{II} (β-BPMCN) (2) | Fe ^{II} (α-BPMCN) (1) | Fe ^{II} (TPA) (3) |
|--|---|---|-------------------------------------|
| A/K ^[b] (with no Sc ³⁺) | 0.8 | 9 | 5 |
| (with 2 eq Sc ³⁺) | 14 | 8 | 11 |
| (c-C ₆ H ₁₂ vs c-C ₆ D ₁₂) ^[c] | | | |
| PKIE (with no Sc ³⁺) | 5(1) | 3.2 | 3.5 |
| (with 2 eq Sc ³⁺) | 2.5(2) | 2.3(1) | 2.6(5) |
| PKIE (C ₆ H ₆ vs C ₆ D ₆) with 2 eq Sc ³⁺ | 0.9 | 0.8 | 0.9 |

[a] All reactions at room temperature under air with 10 eq 90% H₂O₂; TON (turnover number) = moles of product/moles of **1/2/3**. [b] A/K = TON alcohol/TON ketone. [c] PKIE = product kinetic isotope effect based on the yields of cyclohexanol-*h*₁₁ and cyclohexanol-*d*₁₁

Even though the effect of Sc³⁺ on these three systems varies, they all show lower KIE values in the presence of Sc³⁺ compared to that observed in its absence for the oxidation of C₆H₁₂ versus C₆D₁₂ (Table 4.1). The lower KIE value indicates the formation of a more powerful oxidant that is less discriminating between C–H and C–D bonds. In the case of benzene oxidation, an inverse KIE is observed for all three systems in the presence of Sc³⁺, hinting that all of them proceed via an electrophilic aromatic substitution

mechanism involving a metal-based oxidant instead of hydroxyl radicals (Table 4.1). These results along with the high alcohol-to-ketone (A/K) ratios suggest that the oxidant is a metal-based oxidant in all the three cases in the presence of Sc^{3+} .

Cumulatively, these results strongly suggest that the effects of Sc^{3+} on **1**- and **2**-catalyzed oxidation reactions are very different, although they are supported by the same ligand and shows that ligand topology has a significant effect on the Sc^{3+} -assisted mechanism. Furthermore, the mechanistically most extensively studied system **3** appears to behave yet differently from **1** and **2**, in the presence of Sc^{3+} .

4.4 Characterization of $[(\alpha\text{-BPMCN})\text{Fe}^{\text{III}}\text{-OOH}]^{2+}$

Iron(III) hydroperoxo intermediates are considered to be the precursors to the high-valent iron oxidants formed in nonheme iron catalytic systems.^{2,10} Our goal is to compare the properties of the $\text{Fe}^{\text{III}}\text{-OOH}$ intermediates formed in the cases of **1**, **2** and **3** to see if they behave differently and give rise to different oxidants and reactivities. The first $\text{Fe}^{\text{III}}\text{-OOH}$ intermediate to be characterized among the three complexes discussed here was $[(\text{TPA})\text{Fe}^{\text{III}}(\text{OOH})]^{2+}$ (**3-OOH**) in 1997,^{11,25} which was trapped at $-40\text{ }^{\circ}\text{C}$ in CH_3CN . In Chapter 2 of this thesis, characterization was presented for the $[(\beta\text{-BPMCN})\text{Fe}^{\text{III}}(\text{OOH})]^{2+}$ (**2-OOH**) intermediate at $-40\text{ }^{\circ}\text{C}$ in CH_3CN .¹⁵ However, the $[(\alpha\text{-BPMCN})\text{Fe}^{\text{III}}(\text{OOH})]^{2+}$ (**1-OOH**) species has not yet been observed. In this section, we describe the successful trapping and characterization of **1-OOH** ($\lambda_{\text{max}} = 550\text{ nm}$) at temperatures of $-20\text{ }^{\circ}\text{C}$ or higher in CH_3CN (Figure 4.2). This species does not form at temperatures below $-20\text{ }^{\circ}\text{C}$, unlike other $\text{Fe}^{\text{III}}\text{-OOH}$ intermediates including **2-OOH** and **3-OOH**. Interestingly, the

spectroscopic yield of **1-OOH** at the time of its maximum accumulation increased with increasing temperature (Figure 4.3) unlike **2-OOH**, **3-OOH** and most other intermediates where higher yields are obtained at lower temperatures. A similar behavior was observed by Rybak-Akimova and co-workers for the closely related (BPMEN)Fe^{III}-OOH species, which also adopts the same *cis-α* topology around the iron center as **1-OOH**.²⁶ It is plausible that complexes with a *cis-α* topology bind CH₃CN solvent strongly below -20 °C, which hinders H₂O₂ binding to the iron center to form the iron(III) hydroperoxide species such as the case of **1-OOH**.

Fe^{III}-OOH intermediates have diagnostic EPR signals.^{27,28} We collected the EPR spectrum of **1-OOH** to verify its identity. The EPR spectrum of **1-OOH** contains two sets of low-spin Fe^{III} signals – a) $g = 2.23, 2.15, 1.96$ and b) $g = 2.47, 2.18, 1.90$ (Figure 4.2). Consistent with other Fe^{III}-OOH intermediates, the signal at $g = 2.23, 2.15, 1.96$ can be assigned to **1-OOH**, while the signal at $g = 2.47, 2.18, 1.90$ is assigned to Fe^{III}-L (where L = OH, H₂O) based on literature precedents (Table 4.2).²⁶⁻³¹ A similar EPR spectrum was also observed in the case of [(BPMEN)Fe^{III}-OOH]²⁺.²⁶ **1-OOH** forms in higher yield at temperatures above -20°C, but it also decays faster as the temperature is increased, which makes this fleeting intermediate difficult to characterize. Nevertheless, we have been able to obtain the resonance Raman spectrum of **1-OOH** in solution. Two peaks are observed at 792 cm⁻¹ and 613 cm⁻¹, which are assigned to O–O and Fe–O stretching vibrations, respectively, based on literature precedents^{15,27,28} (Figure 4.2 and 4.4). Cumulatively, all the spectroscopic evidence identifies **1-OOH** to be a $S = 1/2$ Fe^{III}-OOH species (Tables 2.4 and 4.2).

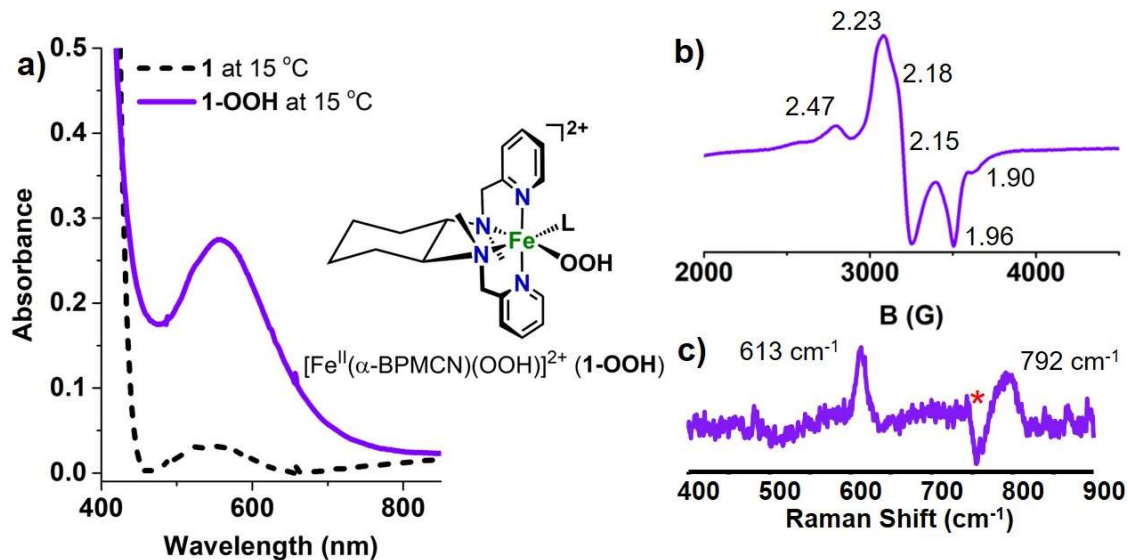


Figure 4.2. a) UV-vis spectrum of **1-OOH** formed at 15 °C in CH₃CN from 1 mM **1** and 20 eq H₂O₂. A ChemDraw representation of **1-OOH** (L = CH₃CN) is shown along with the UV-vis spectrum. b) X-band EPR spectrum of **1-OOH** obtained at 2 K at 30 db. c) Resonance Raman spectrum of **1-OOH** after subtracting the spectrum of the decayed intermediate. **1-OOH** formed from 2.5 mM **1** and 20 eq H₂O₂ at -20 °C. *denotes a solvent peak from CH₃CN. Resonance Raman spectra were collected at -40 °C using a 561-nm laser.

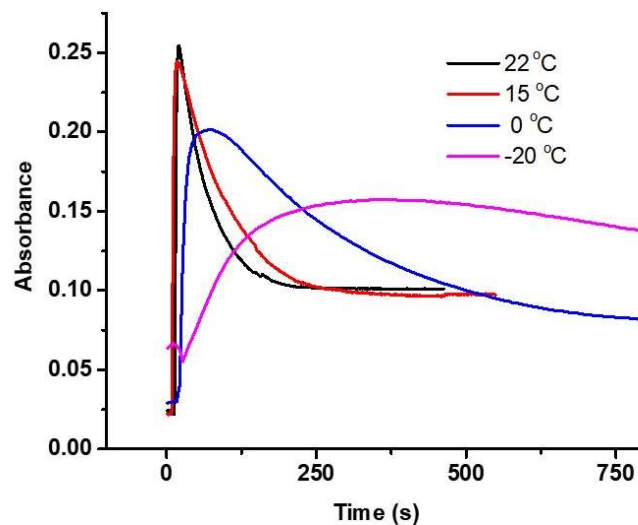


Figure 4.3. Time trace monitoring absorbance at 555 nm corresponding to **1-OOH** at different temperatures. Below $-20\text{ }^{\circ}\text{C}$ no accumulation of **1-OOH** was observed. **1-OOH** was obtained from the reaction of 1 mM **1** and 20 eq H_2O_2 .

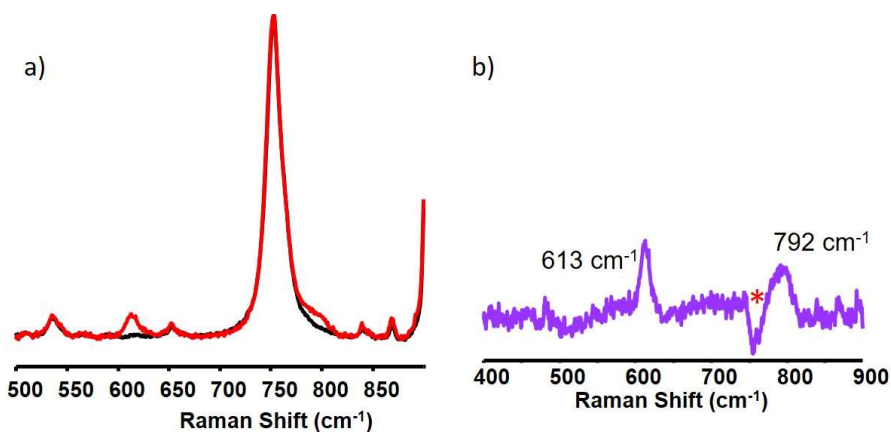


Figure 4.4: a) Resonance Raman spectrum of **1-OOH** (red) overlaid on the spectrum obtained from the same sample after **1-OOH** decayed (black). b) Resonance Raman spectrum of **1-OOH** after subtracting the spectrum of the decayed intermediate (same as shown in Figure 4.1). **1-OOH** formed from 2.5 mM **1** and 20 eq H_2O_2 at $-20\text{ }^{\circ}\text{C}$. Spectrum was measured at $-40\text{ }^{\circ}\text{C}$ with 561-nm laser excitation.

Table 4.2: EPR parameters for Fe^{III}-OOH and their related Fe^{III}-X species. Only those Fe^{III}-OOH species are listed here that also have an Fe^{III}-X species that is observed by EPR. For other EPR parameters of other Fe^{III}-OOH species please refer to Table 2.4.

| | EPR g-values | Reference |
|--|------------------|-----------|
| Low spin (S = 1/2) Fe ^{III} -OOH | 2.22-1.93 | |
| [Fe(BPMEN)(OOH)] ²⁺ | 2.21, 2.14, 1.96 | 26 |
| [Fe(Bn-TPEN)(OOH)] ²⁺ | 2.20, 2.16, 1.96 | 30 |
| [Fe(PMA)(OOH)] ²⁺ | 2.21, 2.18, 1.93 | 29 |
| [Fe(L ²)(OOH)] ²⁺ | 2.19, 2.12, 1.95 | 31 |
| [Fe(α -BPMCN)(OOH)] ²⁺ (1-OOH) | 2.23, 2.15, 1.96 | This work |
| Low spin (S = 1/2) Fe ^{III} -X | 2.47-1.90 | |
| Fe(BPMEN)(X) {X = Cl ⁻ , OMe ⁻ , OH ⁻ , MeOH, H ₂ O} | 2.41, 2.17, 1.90 | 26 |
| [Fe(Bn-TPEN)(X)] ²⁺ {X = Cl ⁻ , OH ⁻ , OR ⁻ } | 2.32, 2.14, 1.93 | 30 |
| [Fe(PMA)(OMe)] ²⁺ | 2.28, 2.18, 1.93 | 29 |
| Fe(L ²)(X) {X = Cl ⁻ , Br ⁻ , OMe ⁻ , OH ⁻ , MeOH, H ₂ O} | 2.30, 2.12, 1.92 | 31 |
| [Fe(α -BPMCN)(X)] ²⁺ {X = OH ⁻ , H ₂ O} (1-OOH) | 2.47, 2.18, 1.90 | This work |

PMAH = (2-[[N-(aminoethyl)amino]methyl]-4-[N-[2-(4-imidazolyl)ethyl]-carbonyl]-5-bromopyrimidine); BnTPEN = [N-benzyl-N,N',N'-tris(pyridyl-2-methyl)-1,2-diaminoethane]; BPMEN = N,N'-bis(pyridyl-2-methyl)-1,2-diaminoethane; BPMCN = N,N'-bis(pyridyl-2-methyl)-N,N'-dimethyl-trans-1,2-diaminocyclohexane; L² = N-methyl-N,N',N'-tris(2-pyridylmethyl)-1,2-diamino-ethane.

Table 4.3. Spectroscopic signatures of the three Fe^{III}-OOH intermediates discussed in this chapter.

| | λ_{\max} (nm) | g-values | ν (cm ⁻¹) ^a | Refs |
|--------------|-----------------------|------------------|--|------------------------------|
| 1-OOH | 550 | 2.23, 2.15, 1.96 | 792 (O–O) 613 (Fe–O) | This work |
| 2-OOH | 545 | 2.22, 2.17, 1.96 | 802 (O–O) 613 (Fe–O) | ¹⁵ |
| 3-OOH | 540 | 2.19, 2.15, 1.97 | 805 (O–O) 632 (Fe–O) | ^{11,27} , This work |

Raman data were obtained in CH₃CN solution with 561-nm excitation.

4.5 Kinetic analysis of the behavior of the Fe^{III}-OOH intermediates

First, we have compared the evolution of the three Fe^{III}-OOH intermediates in the absence of any substrate. At 0 °C, addition of 10 eq of H₂O₂ to a 2.5 mM solution of **1**, **2** or **3** in the absence of any substrate elicits formation of **1-OOH**, **2-OOH** or **3-OOH**, respectively (Figure 4.5). **2-OOH** and **3-OOH** accumulate to similar absorbances at their respective λ_{\max} ; however, **1-OOH** accumulates to less than 30% of the absorbance of **2-OOH** or **3-OOH**. Between **2-OOH** and **3-OOH**, **2-OOH** decays in less than half the time compared to **3-OOH** (Figure 4.5). These observations indicate that the three Fe^{III}-OOH intermediates have different kinetic behaviors.

Interestingly, upon addition of H₂O₂ to **2** in the absence of any substrate, a species appears with a broad absorption band in the NIR region beyond 800 nm along with **2-OOH**, which grows as **2-OOH** decays. This species is not a catalytically relevant intermediate and appears to be a novel side product with significant absorbance in the near-

IR region. Our preliminary investigation based on EPR and Mössbauer spectroscopy suggests that this species is a diferric complex. This species is unique to **2** and is not observed for **1** and **3**. Further efforts are required to identify and characterize this species.

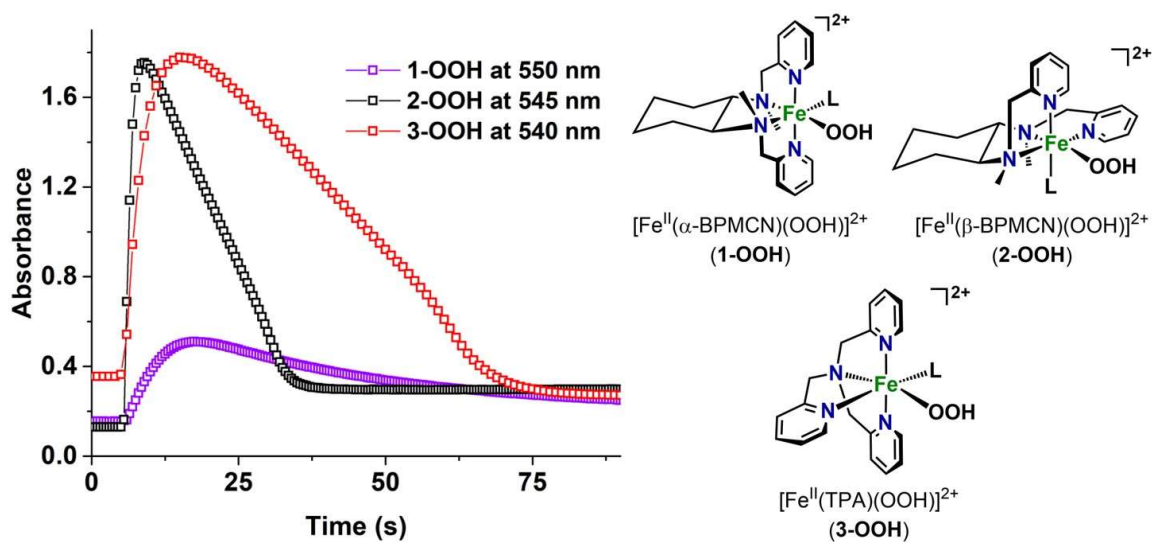


Figure 4.5. Left: Time traces monitoring formation and decay of **1-OOH**, **2-OOH** and **3-OOH** in the absence of any substrate. All experiments were performed at 0 °C. 10 eq H₂O₂ was added to 2.5 mM solutions of **1**, **2** and **3** in CH₃CN. Right: ChemDraw representations of **1-OOH**, **2-OOH** and **3-OOH**.

In 2002, it was observed that **1** and **3** had similar reactivity trends, whereas **2** exhibited a different behavior, suggesting the formation of a different type of oxidant.¹⁴ Based on mechanistic studies performed at that time,^{7,8,14} it was proposed that **1** and **3** involve a low-spin $S = 1/2$ Fe^{III}-OOH intermediate that forms the oxidant responsible for substrate oxidation. On the other hand, **2** was hypothesized to generate a high-spin $S = 5/2$ Fe^{III}-OOH that acts as the oxidant.¹⁴ However, in Chapter 2, we have demonstrated that **2**

in fact forms a low-spin $S = 1/2$ $\text{Fe}^{\text{III}}\text{-OOH}$ intermediate (**2-OOH**) upon reacting with H_2O_2 , with no evidence of an $S = 5/2$ $\text{Fe}^{\text{III}}\text{-OOH}$ species. In the following paragraphs, we demonstrate that the $\text{Fe}^{\text{III}}\text{-OOH}$ intermediate **2-OOH** generated from **2** is not the actual oxidant but is a precursor to the oxidant. In Chapters 2 and 3, so far, we have shown that **2-OOH** forms a powerful oxidant upon reacting with Sc^{3+} , Fe^{3+} or HClO_4 . Here, we have compared the chemistry of **1-OOH**, **2-OOH** and **3-OOH** in the presence of substrates but in the absence of any additive.

It was reported in 2013 that after its formation, **3-OOH** has a distinguishable pseudo-steady-state phase followed by an exponential decay phase as the H_2O_2 concentration is depleted, and varying the concentration of the substrate 1-octene did not affect the rate of decay of **3-OOH** at -40 °C.⁹ These results led to the conclusion that **3-OOH** is itself not the active oxidant but is the precursor to it.⁹ Here, we have studied the effect of [1-octene] on **2-OOH**. 1-octene is used as a substrate in these experiments because of its high solubility in CH_3CN at -40 °C and all the three catalysts studied here have been shown to oxidize 1-octene. In these studies, the chromophore of the $\text{Fe}^{\text{III}}\text{-OOH}$ intermediate is monitored via UV-vis absorption spectroscopy. It should be noted that these experiments are conducted with excess H_2O_2 under multi-turnover conditions, making kinetic analysis somewhat complex since multiple steps of the catalytic cycle can contribute to the evolution of the $\text{Fe}^{\text{III}}\text{-OOH}$ intermediate. We added varying amounts of 1-octene to a pre-formed solution of **2-OOH** at -40 °C, as was previously done with **3-OOH**⁹. Unlike **3-OOH**, **2-OOH** does not have an easily distinguishable pseudo-steady-state phase and exponential decay phase, which made fitting the data more difficult. We

have thus shown the experimental plots with various 1-octene concentrations next to each other for comparison (Figure 4.6b). As can be clearly seen from Figure 4.6b, changing [1-octene] does not affect the decay profile or decay rate of **2-OOH**. However, there is a difference between the self-decay of **2-OOH** and its decay in the presence of 1-octene, suggesting that the presence of a substrate affects the behavior of the intermediate. This likely happens because the substrate oxidation and the product release steps now contribute to the evolution of the Fe^{III}-OOH intermediate, which is not present in the case of no substrate. Attempts to fit the data highlighted by the orange box led to the same conclusion where the rates of decay of **2-OOH** were independent of [1-octene], but slightly slower (~1.5 times) than for self-decay. A similar observation was reported for **3-OOH**.⁹ Upon the addition of the *cis*-diol product to **3-OOH**, it was observed to have a decay rate similar to that observed with 1-octene but slower (~1.5 times) than the self-decay rate, which was suggested to be due to the binding of the *cis*-diol that might compete with the decay pathway in the absence of the product.⁹ The *cis*-diol product formed from olefin oxidation has been observed to bind to the iron(III) center in mass spectrometric experiments,^{8,32} suggesting that the iron(III)-*cis*-diol complex is sufficiently stable to be able to influence the kinetics of the reaction. Previous reactivity studies showed that **2** favors oxidizing electron-deficient olefins over electron-rich ones,¹⁸ and so we have further compared the effect of varying concentrations of the electron-deficient olefin *tert*-butyl acrylate and the electron-rich olefin cyclooctene on **2-OOH** under the same conditions. For both *tert*-butyl acrylate and cyclooctene, varying the concentration of the olefin does not affect the decay of **2-OOH** (Figure 4.6c and 4.6d). Together these results suggest that, like **3-OOH**, **2-OOH**

is not the actual oxidant in the catalytic reactions of **2** but leads to the formation of the oxidant, which is nucleophilic in nature, in contrast to the electrophilic oxidant derived from **3-OOH**.

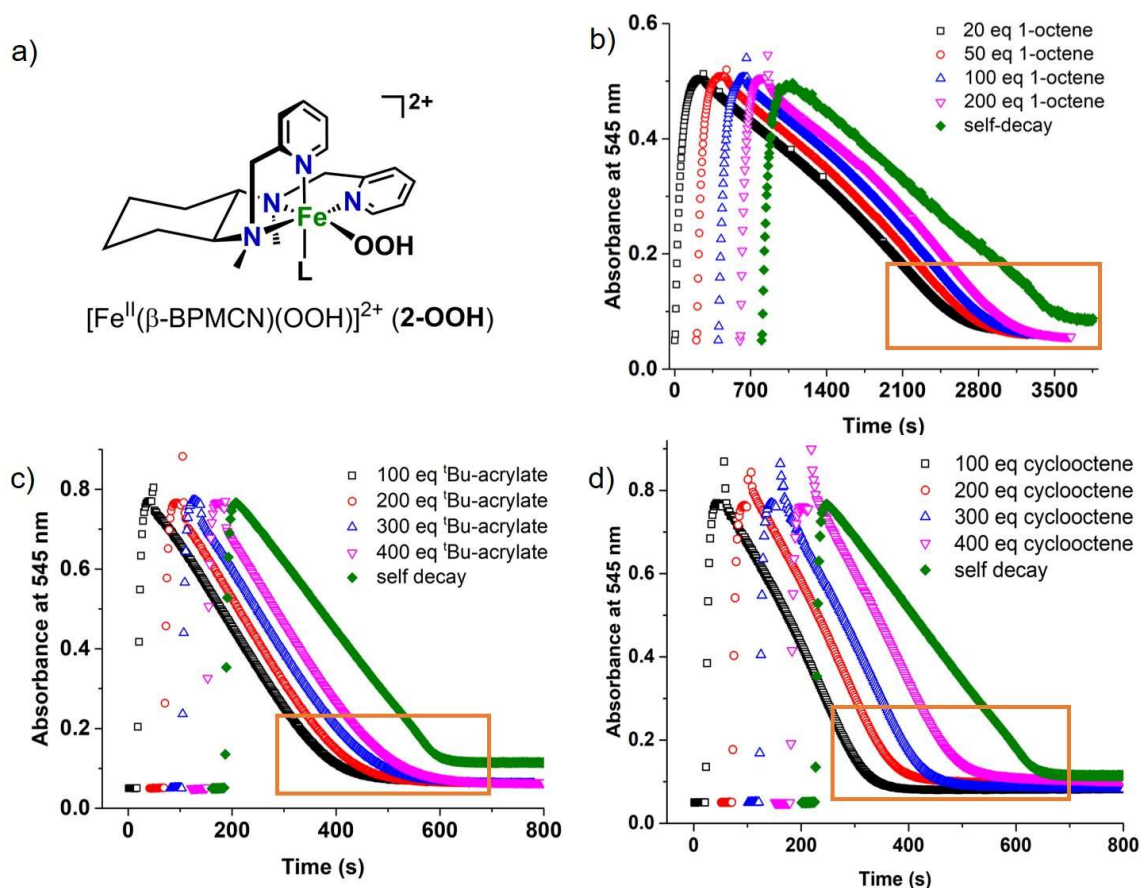


Figure 4.6. a) A ChemDraw structure of **2-OOH** ($\text{L} = \text{CH}_3\text{CN}$). (b-d) Time traces monitoring evolution of **2-OOH** upon addition of substrates. b) 1-octene was added to **2-OOH** formed from 1 mM **2** and 10 eq H_2O_2 at -40°C in CH_3CN . c) *tert*-butyl acrylate and d) cyclooctene was added to **2-OOH** formed from 1 mM **2** and 20 eq H_2O_2 at -15°C in CH_3CN . We have separated the plots for each concentration by adding a fixed Δtime between the individual plots for clarity of comparison. For a) 1-octene: $\Delta\text{time} = 200$ s, b) *tert*-butyl acrylate: $\Delta\text{time} = 40$ s, c) cyclooctene: $\Delta\text{time} = 50$ s.

Next, we have studied the effect of 1-octene on the decay of **1-OOH**. Similar to **2-OOH** and **3-OOH**, the decay of **1-OOH** is unaffected by the amount of 1-octene added, suggesting that **1-OOH** is not the oxidant responsible for substrate oxidation (Figure 4.7). However, there is a difference in its behavior upon addition of 1-octene, compared to those of **2-OOH** and **3-OOH**. For **1-OOH**, addition of 1-octene causes the absorption peak at 550 nm corresponding to **1-OOH** to grow to a certain extent before it starts decaying, which is not observed for **2-OOH** and **3-OOH**. Currently, we hypothesize that addition of the substrate 1-octene to **1-OOH** drives the reaction towards the oxidation of 1-octene that competes with the self-decay pathway of **1-OOH**, which may lead to increased accumulation of **1-OOH** if the rate of 1-octene oxidation is slower than the self-decay. The difference between the reactions in the presence and absence of the substrate is also observed from the decay profiles of **1-OOH** under the two conditions (Figure 4.7b). However, further detailed studies need to be performed to understand this interesting behavior of **1-OOH** upon addition of 1-octene.

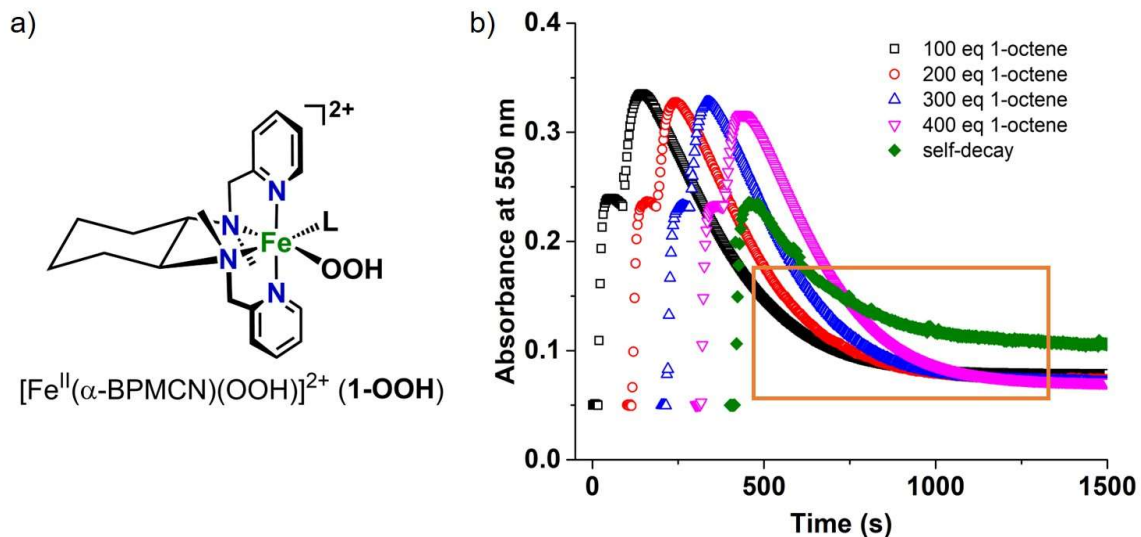


Figure 4.7. a) A ChemDraw structure of **1-OOH** ($L = \text{CH}_3\text{CN}$). b) Time traces for the evolution of **1-OOH** upon addition of 1-octene. **1-OOH** was formed from 1 mM **1** and 10 eq H_2O_2 at 0 °C in CH_3CN . The plots for each concentration were each right-shifted by 100 s for clarity of comparison.

Previous studies on **2**^{14,18} proposed the $\text{Fe}^{\text{III}}\text{-OOH}$ intermediate in this system to be the active oxidant; however, we have shown here that the hydroperoxo intermediate **2-OOH** is not the active oxidant. Based on the current results on **1-OOH** and **2-OOH**, and reported results⁹ on **3-OOH**, it is clear that none of the three $\text{Fe}^{\text{III}}\text{-OOH}$ intermediates discussed here is the actual oxidant responsible for substrate oxidation. Additionally, even though **1/2/3-OOH** look quite similar spectroscopically (Table 4.3), they exhibit different kinetic behavior and reactivity trends.

4.6 Kinetic analysis of the effect of Sc(OTf)₃ on the Fe^{III}-OOH intermediates

As both **2-OOH** and **3-OOH** form at -40 °C, the effect of Sc³⁺ on these intermediates could be investigated at -40 °C. Addition of 1 eq Sc³⁺ to **2-OOH** in the presence of cyclohexane results in its decay within 20 s (Figure 4.8a). Similarly, in the presence of benzene, **2-OOH** reacts with 1 eq Sc³⁺ to form $[(\beta\text{-BPMCN})\text{Fe}^{\text{III}}(\text{OPh})]^{2+}$ (**2-OPh**) completely within 20 s (Figure 4.8c). On the other hand, addition of 1 eq Sc³⁺ to **3-OOH** in the presence of cyclohexane leads to its decay over 400 s, a 20-fold longer time period than for **2-OOH** under similar conditions. Furthermore, there is only a 16% loss of its initial absorbance. Addition of a second equivalent of Sc³⁺ elicits a similar loss in absorbance, and full decay of **3-OOH** requires the addition of 5 aliquots containing 1 eq Sc³⁺ each (Figure 4.8b). The corresponding reaction of **3-OOH** in the presence of benzene takes ~700 s, 35-fold longer than for the reaction between **2-OOH** and 1 eq Sc³⁺. A maximum absorbance change of 0.06 a.u is observed (Figure 4.8d), which represents about a 10-fold lower yield of $[(\text{TPA})\text{Fe}^{\text{III}}(\text{OPh})]^{2+}$ (**3-OPh**) than found for the formation of **2-OPh** from the reaction between **2-OOH** and 1 eq Sc³⁺. Addition of additional aliquots containing 1 eq Sc³⁺ each results in the formation of more **3-OPh**, but the addition of 5 aliquots of 1 eq Sc³⁺ forms **3-OPh** in about half the total yield found for **2-OPh** (assuming that they have similar extinction coefficients). Taken together, these results show that **3-OOH** does not interact with Lewis acidic Sc³⁺ as effectively as **2-OOH**. Thus, it can be proposed that **2-OOH** might be more nucleophilic compared to **3-OOH**, and hence Sc³⁺ exerts a larger effect on **2-OOH** compared to **3-OOH**.

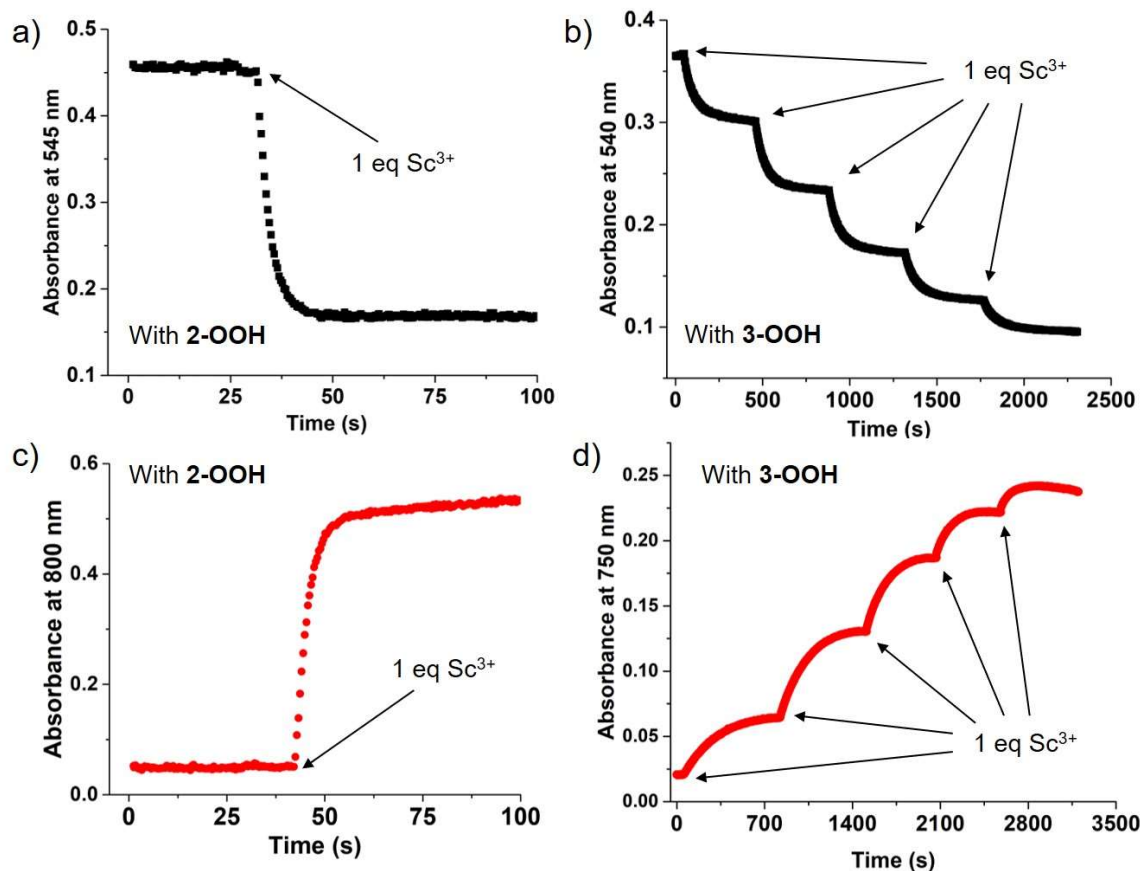


Figure 4.8. a) Time trace monitoring reaction of **2-OOH** (at 545 nm) with 1 eq Sc^{3+} in the presence of cyclohexane (185 eq relative to **2**) at $-40\text{ }^{\circ}\text{C}$. b) Time trace monitoring reaction of **3-OOH** (at 540 nm) with consecutive addition of 1 eq Sc^{3+} up to 5 eq of Sc^{3+} in the presence of cyclohexane (185 eq relative to **3**) at $-40\text{ }^{\circ}\text{C}$. c) Time trace monitoring formation of **2-OPh** (at 800 nm) upon addition of 1 eq Sc^{3+} to **2-OOH** in the presence of benzene (100 eq relative to **2**) at $-40\text{ }^{\circ}\text{C}$. d) Time trace monitoring formation of **3-OPh** (at 750 nm) upon addition of 1 eq Sc^{3+} to **3-OOH** in the presence of benzene (100 eq relative to **3**) at $-40\text{ }^{\circ}\text{C}$.

The intermediate **1-OOH** can only be generated at $-20\text{ }^{\circ}\text{C}$ and higher temperatures (Section 4.4). Therefore, to place the reactivity of **1-OOH** into the same context as the other two Fe-OOH intermediates, we have compared the reactivity of all three

intermediates at -20 °C. With benzene as the substrate, the Fe^{III}-OPh products can be easily monitored via their characteristic visible chromophores between 580 and 650 nm. It turned out that **1-OOH** can oxidize benzene even in the absence of Sc³⁺ to form [(α -BPMCN)Fe^{III}(OPh)]²⁺ (**1-OPh**). To assess the effect of Sc³⁺ on benzene hydroxylation by **1-OOH**, two parallel experiments were carried out in which the rates of **1-OPh** formation were compared for the addition of 100 eq benzene (relative to **1**) to a solution of pre-formed **1-OOH** in the first experiment and for the addition of 100 eq benzene and 1 eq Sc³⁺ together to a solution of pre-formed **1-OOH** in the second experiment. We observed that addition of 1 eq Sc³⁺ along with benzene enhances the rate of **1-OPh** formation by about two orders of magnitude at -20 °C (0.0008 s⁻¹ without Sc³⁺ versus 0.13 s⁻¹ with 1 eq Sc³⁺) and thus, Sc³⁺ increases the rate of formation of the active oxidant responsible for benzene oxidation.

Similar experiments for **2-OOH** and **3-OOH** were carried out, where 1 eq of Sc³⁺ and 100 eq benzene were added together to a pre-formed solution of **2-OOH** or **3-OOH**. In the generation of the respective Fe^{III}-OOH solutions at -20 °C, we observed that the times required to accumulate the Fe-OOH intermediates increase in the order **2-OOH** (40 s) < **3-OOH** (300 s) < **1-OOH** (16 min) (Figure 4.9a), which further supports our previous conclusion that they exhibit different kinetic behavior, although spectroscopically they look similar (Section 4.5 and Table 4.3). Upon addition of benzene and Sc³⁺, it was observed that **2-OOH** was the fastest in interacting with Sc³⁺ and forming **2-OPh**, followed by **1-OOH** which was 10-fold slower (Figure 4.9b and c). **3-OOH** was slowest among the three, and it was 10-fold slower than **1-OOH** and 100-fold slower compared to **2-OOH** (Figure 4.9b-d, Table 4.4).

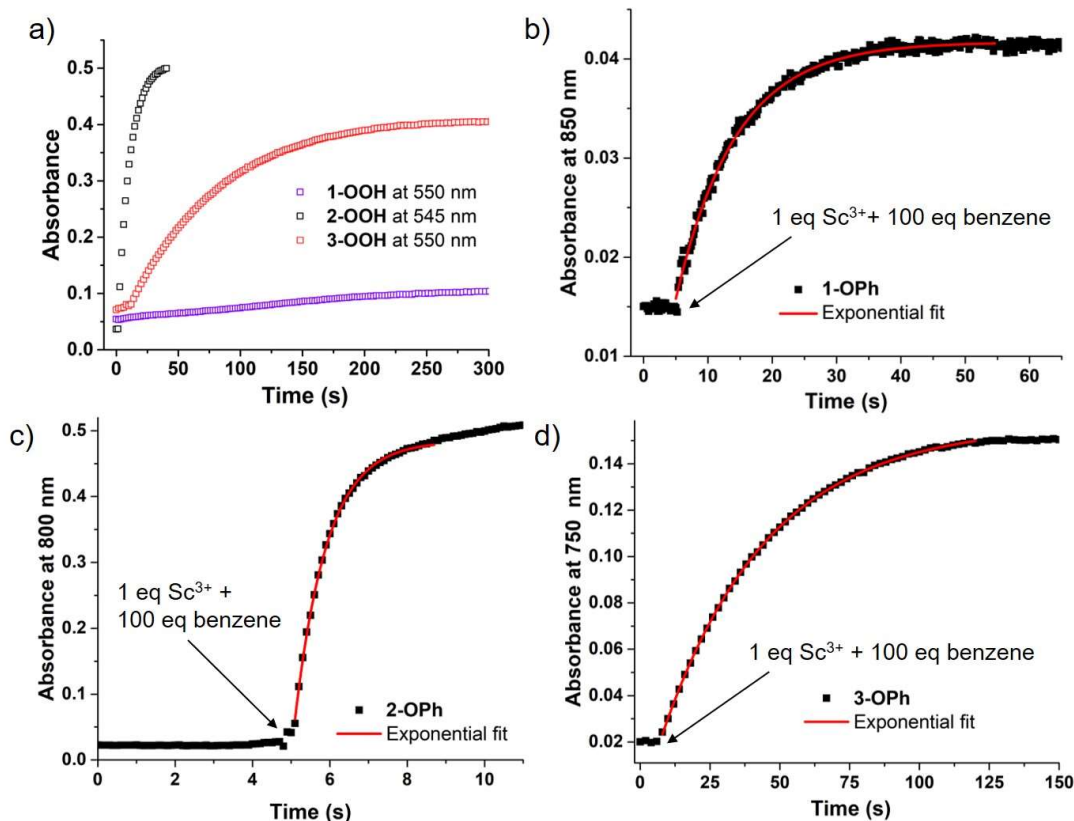


Figure 4.9. a) Comparison of time traces monitoring formation of **1/2/3-OOH** at their corresponding λ_{\max} for the first 300 s at $-20\text{ }^{\circ}\text{C}$. b-d) Time traces monitoring formation of b) **1-OPh** (at 850 nm), c) **2-OPh** (at 800 nm) and d) **3-OPh** (at 750 nm) upon addition of 1 eq Sc^{3+} and 100 eq benzene to **1/2/3-OOH** at $-20\text{ }^{\circ}\text{C}$. Rates of formation of **1/2/3-OPh** are obtained by fitting the data with first order exponential equations.

Table 4.4. Rates of $\text{Fe}^{\text{III}}\text{-OPh}$ formation upon addition of Sc^{3+} and benzene to **1/2/3-OOH**.

| | $k_{\text{obs}}\text{ (s}^{-1}\text{) at }-20\text{ }^{\circ}\text{C}^{\text{a}}$ |
|--------------|---|
| 1-OPh | $1.3(3) \times 10^{-1}$ |
| 2-OPh | 1.3(2) |
| 3-OPh | $3.0(1) \times 10^{-2}$ |

^aThe rates were obtained from exponential fits of the plots as shown in Figure 4.9.

4.7 Comparison of the effect of Sc(OTf)₃ on the reactivity of [Fe^{II}(α -BPMCN)]²⁺, [Fe^{II}(β -BPMCN)]²⁺ and [Fe^{II}(TPA)]²⁺

The reactivity results from cyclohexane and benzene oxidation reactions described in Section 4.3 and Chapter 2 together suggest that in the case of **2** the Sc-assisted pathway forms a more powerful oxidant capable of oxidizing both substrates equally efficiently, which could not be accessed in the absence of Sc³⁺.¹⁵ On the other hand, the oxidant formed for **1** and **3** upon all-at-once addition of H₂O₂ in the presence of Sc³⁺ is as efficient in oxidizing cyclohexane as the oxidant formed in the absence of Sc³⁺ with controlled addition of H₂O₂ via a syringe pump. However, the presence of Sc³⁺ eliminates the requirement of controlled addition of H₂O₂ and hence the Sc³⁺-assisted route is more efficient in forming the high-valent iron oxidant, and reducing unproductive side reactions. Next, moving to benzene hydroxylation, although both **1** and **3** were able to hydroxylate benzene in the absence of Sc³⁺, but the yields were very low or untraceable in some cases. The Sc-assisted route to form the oxidant is clearly better as it leads to higher yields of phenol in the case of **3** (TON of 0.1 in the absence of Sc³⁺ to TON of 4.5 with 8 eq Sc³⁺) (Figure 4.1). For **1**, the effect of Sc³⁺ on the yield of phenol is not significant, but Sc³⁺ does have a significant effect on the rate of **1-OPh** formation. The presence of Sc³⁺ increases the rate of **1-OPh** formation by two orders of magnitude at -20 °C. This supports the idea that the reaction to form the oxidant occurs faster in the presence of Sc³⁺, outpacing the undesired side reactions.

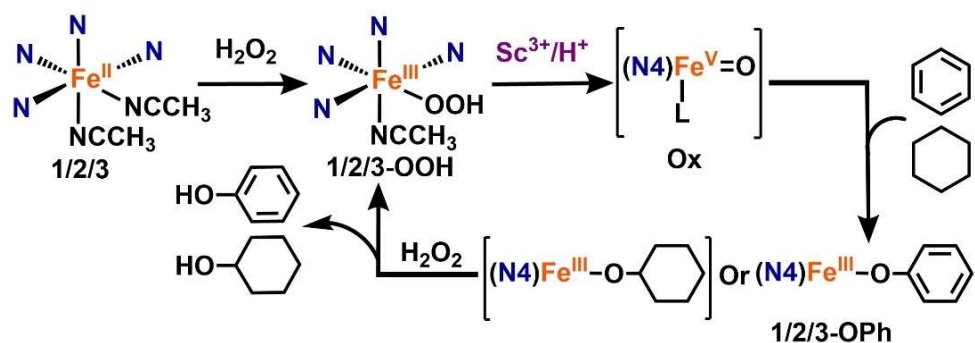
In Chapter 2, we showed that both Sc³⁺ and HClO₄ can activate the catalytic system **2**/H₂O₂ to similar extents. However for **3**/H₂O₂, it was reported in 2007 that HClO₄ has a

negative effect on its catalytic reactivity.³³ When H₂O₂ was added all at once to a reaction mixture containing **3** in the presence of 1 eq of HClO₄ it was observed that the yields of the oxidized products decreased. Thus, it appears that the catalytic system **3**/H₂O₂ is not stable in the presence of HClO₄. Hence, in this study we focussed on the effect of Sc³⁺ on the three catalytic systems, **1/2/3** with H₂O₂, and compared their behavior. The effect of HClO₄ on the catalytic reactivity of **1**/H₂O₂ should be explored in future.

Similar to **1**, the closely related [Fe^{II}(BPMEN)]²⁺ system was also observed to oxidize benzene to form phenol but not efficiently, with a TON of only 1, whereas for cyclohexane hydroxylation a TON of 5.6 was observed under similar conditions in the absence of Sc³⁺.^{7,26} This lower yield for phenol formation for **1** and [Fe^{II}(BPMEN)]²⁺ can perhaps be due to a strong binding affinity of phenol for the [Fe^{III}(α -BPMCNC)]³⁺ or [Fe^{III}(BPMEN)]³⁺ centers formed in their respective catalytic cycles, which inhibits the catalyst's ability to re-enter the cycle.

Isotope-labeling studies using H₂¹⁸O₂ show that in the case of **2**, all O-atoms in the products are essentially derived from H₂¹⁸O₂ and no O-atom from water is incorporated into the products.¹⁵ Labeling experiments using H₂¹⁸O₂ show that for **1** 88% O-atoms in phenol are derived from H₂¹⁸O₂, while ~15% are derived from H₂¹⁸O. Similarly, for **3** 82% O-atoms in phenol are derived from H₂¹⁸O₂. These results indicate that for **1** and **3** water is able to bind the iron center in the presence of Sc³⁺, resulting in some incorporation of the O-atom from water into phenol. These results can be explained based on the observations that reactions of **1-OOH** and **3-OOH** with Sc³⁺ are slower compared to **2-OOH** (Table 4.4 and Section 4.6). The relatively slower reactions might allow for water to bind to the iron

center and form an $\text{Fe}^{\text{V}}(\text{O})(\text{OH}_2)$ species, replacing the CH_3CN ligand of **Ox** in Scheme 4.2, even though the Sc^{3+} is assisting in breaking the O–O bond of the $\text{Fe}^{\text{III}}\text{--OOH}$ intermediate (Scheme 4.2). Additionally, some of the O-atoms in the products can also come from the water-assisted pathway for **1** and **3**, since we cannot exclude it when water is present in the reaction mixture (the probable source of water here is H_2O_2).



Scheme 4.2. Proposed mechanism for Sc^{3+} -assisted pathway for **1** or **2** or **3** in the hydroxylation of cyclohexane and benzene. ($\text{L} = \text{CH}_3\text{CN}$)

The intermediate **2-OOH** reacts with Sc^{3+} an order of magnitude faster than **1-OOH** and two orders of magnitude faster than **3-OOH** under the same conditions. Based on these results, it can be said that Lewis acidic Sc^{3+} has a higher affinity for **2-OOH** followed by **1-OOH** and **3-OOH**. Hence, it can be proposed that **2-OOH** is more nucleophilic compared to **1-OOH** and **3-OOH**. As mentioned earlier in this chapter, in 2014, based on the results of competitive oxidation reactions between an electron-rich and an electron-deficient olefin, it was concluded that the oxidant formed in catalytic reactions of **1** is electrophilic, whereas the oxidant formed in the reactions of **2** is nucleophilic.¹⁸

Furthermore, **3** was also said to involve an electrophilic oxidant based on competition reactions in 2003.¹⁹ In the last decade, bioinorganic chemists around the world have demonstrated that Fe^{III}-OOH intermediates lead to the formation of high-valent iron oxidants responsible for oxidizing alkanes, olefins and aromatic compounds.^{2,5,13,34} Hence, it can be perceived that the Fe^{III}-OOH precursor of the active oxidant can also have varying nucleophilic and electrophilic characters. This study supports the idea that indeed the Fe^{III}-OOH precursors of the high-valent iron oxidants have different nucleophilic and electrophilic character that make them interact differently with Lewis acidic Sc³⁺ ions. **2-OOH**, the precursor to the nucleophilic oxidant in catalytic reactions of **2**, also has a nucleophilic character, which makes it interact with Sc³⁺ at a faster rate than **1-OOH** and **3-OOH**, which are precursors of the electrophilic oxidants involved in the reactions of **1** and **3**. Alternatively, it is possible that the three systems, **1-OOH**, **2-OOH** and **3-OOH**, interact with Sc³⁺ at different rates because of significantly different kinetics of the various steps of their respective catalytic cycle. Interestingly, upon reacting with Sc³⁺, **2-OOH** forms a new electrophilic oxidant that could not be accessed previously. On the other hand, since **1-OOH** and **3-OOH** are more electrophilic, they can form a powerful oxidant via the water-assisted pathway as well and do not require a strong Lewis acid such as Sc³⁺. The oxidant formed in the presence of Sc³⁺ is as potent as the oxidant formed in the water-assisted pathway for **1** and **3**; however, the rate of the reaction to form the oxidant is increased, outpacing the undesired side reactions and resulting in higher yields of the oxidized products.

4.8 Summary

The significance of ligand topology around the iron center has been previously demonstrated by differences in the reactivities of **1** and **2**.^{14,18} In 2011, Hong et al. showed a significant influence of ligand topology on the reactivity of Fe^{IV}(O) using a different ligand framework, BQCN, which also gives rise to two isomeric complexes with *cis*- α and *cis*- β topology. Here, we have shown that even though spectroscopically **1-OOH** and **2-OOH** look similar, Sc³⁺ interacts with the two topologically isomeric complexes very differently. **2-OOH**, the putative precursor of the nucleophilic oxidant for **2**, reacts with Lewis acidic Sc³⁺ faster than **1-OOH**, the putative precursor of the electrophilic oxidant for **1**. Thus, ligand topology plays an important role in the Sc³⁺-assisted mechanism.

Furthermore, we have compared **1-OOH** and **2-OOH** with the extensively studied **3-OOH**, which interacts with Sc³⁺ more slowly than both **1-OOH** and **2-OOH**. Previously, **1**, **3** and [Fe^{II}(BPMEN)]²⁺ have been suggested to behave similarly based on mechanistic studies on alkane and olefin oxidations.^{7,14} However, the current results suggest that there are certain differences in their reactivity and kinetic behavior, even though both are suggested to form electrophilic Fe(V) oxidants. In this work, we highlight the importance of ligand topology of the iron complex in determining the behavior of the catalytically active Fe^{III}-OOH intermediates and their interactions with the Lewis acid Sc³⁺ to form high-valent iron oxidants. Furthermore, we have shown here that the interaction with Lewis acids such as Sc(OTf)₃ can be used as a probe to distinguish between these spectroscopically similar mononuclear nonheme Fe^{III}-OOH intermediates.

4.9 Acknowledgments

Dr. Apparao Draksharapu conducted the resonance Raman experiments. We thank Dr. Rahul Banerjee for his very helpful advice in the kinetic analysis.

4.10 References

- (1) Kal, S.; Que, L. *J. Biol. Inorg. Chem.* **2017**, *22*, 339–365.
- (2) Olivo, G.; Cussó, O.; Borrell, M.; Costas, M. *J. Biol. Inorg. Chem.* **2017**, *22*, 425–452.
- (3) Gamba, I.; Codolà, Z.; Lloret-Fillol, J.; Costas, M. *Coord. Chem. Rev.* **2017**, *334*, 2–24.
- (4) Jasniewski, A. J.; Que, L. *Chem. Rev.* **2018**, *118*, 2554–2592.
- (5) Barry, S. M.; Challis, G. L. *ACS Catal.* **2013**, *3*, 2362–2370.
- (6) Costas, M.; Tipton, A. K.; Chen, K.; Jo, D. H.; Que L., J. *J. Am. Chem. Soc.* **2001**, *123*, 6722–6723.
- (7) Chen, K.; Que, L. *J. Am. Chem. Soc.* **2001**, *123*, 6327–6337.
- (8) Chen, K.; Costas, M.; Kim, J.; Tipton, A. K.; Que, L. *J. Am. Chem. Soc.* **2002**, *124*, 3026–3035.
- (9) Oloo, W. N.; Fielding, A. J.; Que, L. *J. Am. Chem. Soc.* **2013**, *135*, 6438–6441.
- (10) Oloo, W. N.; Que, L. *Acc. Chem. Res.* **2015**, *48*, 2612–2621.

- (11) Ho, R. Y. N.; Roelfes, G.; Feringa, B. L.; Que, L. *J. Am. Chem. Soc.* **1999**, *121*, 264–265.
- (12) Que, L.; Tolman, W. B. *Nature* **2008**, *455*, 333–340.
- (13) Lyakin, O. Y.; Bryliakov, K. P.; Talsi, E. P. *Coord. Chem. Rev.* **2019**, *384*, 126–139.
- (14) Costas, M.; Que, L. *Angew. Chem. Int. Ed.* **2002**, *41*, 2179–2181.
- (15) Kal, S.; Draksharapu, A.; Que, L. *J. Am. Chem. Soc.* **2018**, *140*, 5798–5804.
- (16) Li, F.; Van Heuvelen, K. M.; Meier, K. K.; Münck, E.; Que, L. *J. Am. Chem. Soc.* **2013**, *135*, 10198–10201.
- (17) Lee, Y.-M.; Bang, S.; Kim, Y. M.; Cho, J.; Hong, S.; Nomura, T.; Ogura, T.; Troppner, O.; Ivanović-Burmazović, I.; Sarangi, R.; Fukuzumi, S.; Nam, W. *Chem. Sci.* **2013**, *4*, 3917–3923.
- (18) Iyer, S. R.; Javadi, M. M.; Feng, Y.; Hyun, M. Y.; Oloo, W. N.; Kim, C.; Que, L. *Chem. Commun.* **2014**, *50*, 13777–13780.
- (19) Fujita, M.; Costas, M.; Que, L. *J. Am. Chem. Soc.* **2003**, *125*, 9912–9913.
- (20) <https://www.cdc.gov/niosh/ipcsneng/neng0164.html>.
- (21) <http://msdsviewer.fmc.com/private/document.aspx?prd=7722-84-1--90~~PDF~~MTR~~CPNA~~EN~~1/1/0001%2012:00:00%20AM~~HYDROGEN%20PEROXIDE%2090%~~>.
- (22) Jo, D. H.; Chiou, Y. M.; Que, J. *Inorg. Chem.* **2001**, *40*, 3181–3190.
- (23) ASTM E1840-96(2007)Standard Guide for Raman Shift Standards for Spectrometer Calibration ASTM International DOI:10.1520/E1840-96R07. .

- (24) Menges, F. “Spekwin32 - optical spectroscopy software” Version 1.72.0, 2015
<http://www.ffmpeg2.de/spekwin/> .
- (25) Kim, C.; Chen, K.; Kim, J.; Que, L. *J. Am Chem. Soc.* **1997**, *119*, 5964–5965.
- (26) Makhlynets, O. V.; Rybak-Akimova, E. V. *Chem. Eur. J.* **2010**, *16*, 13995–14006.
- (27) Costas, M.; Mehn, M. P.; Jensen, M. P.; Que, L. *Chem. Rev.* **2004**, *104*, 939–986.
- (28) Company, A.; Lloret-Fillol, J.; Costas, M. In *Comprehensive Inorganic Chemistry II*; Elsevier Ltd., 2013; p 487.
- (29) Lippai, I.; Magliozzo, R. S.; Peisach, J. *J Am Chem Soc* **1999**, *121*, 780–784.
- (30) Jensen, K. B.; Mckenzie, C. J.; Nielsen, L. P.; Pedersen, J. Z.; Svendsen, M. H. *Chem. Commun.* **1999**, 1313–1314.
- (31) Bernal, I.; Jensen, M. I.; Jensen, B. K.; McKenzie, J. C.; Toftlund, H.; Tuchagues, J. J. *Chem. Soc. Dalton Trans.* **1995**, 3667–3675.
- (32) Prat, I.; Mathieson, J. S.; Güell, M.; Ribas, X.; Luis, J. M.; Cronin, L.; Costas, M. *Nat. Chem.* **2011**, *3*, 788–793.
- (33) Mas-Balleste, R.; Que, L. *J. Am. Chem. Soc.* **2007**, *129*, 15964–15972.
- (34) Bryliakov, K. P.; Talsi, E. P. *Coord. Chem. Rev.* **2014**, *276*, 73–96.

Chapter 5:

Generation and characterization of higher-valent iron species from Fe^{IV}(O) intermediates supported by a macrocyclic ligand framework

5.1 Introduction

Nonheme iron enzymes are proposed and in some cases demonstrated to form $\text{Fe}^{\text{IV}}(\text{O})$ and $\text{Fe}^{\text{V}}(\text{O})$ species as oxidants for hydrocarbon oxidations.¹⁻⁴ Bioinorganic chemists have been working towards generating these high-valent iron intermediates, and studying their properties and reactivities.⁵⁻⁸ One of the common ways to generate synthetic $\text{Fe}^{\text{IV}}(\text{O})$ complexes is using Fe^{II} complexes and O-atom transfer agents like iodosylbenzene (PhIO) or 2-^tBuSO₂-C₆H₄IO (ArIO). On the other hand, $\text{Fe}^{\text{V}}(\text{O})$ intermediates are mostly generated from Fe^{III} intermediates such as $\text{Fe}^{\text{III}}(\text{OOH})$ or $\text{Fe}^{\text{III}}(\text{OOAc})$ by heterolytically cleaving the O-O bond in the Fe^{III} intermediates.^{7,9} Some Fe^{V} intermediates were also generated from Fe^{III} precursor complexes using O-atom transfer reagents such as PhIO.^{10,11} Another route to form $\text{Fe}^{\text{V}}(\text{O})$ intermediate is to oxidize the high-valent $\text{Fe}^{\text{IV}}(\text{O})$ intermediate by one-electron.¹²

Tetramethylcyclam (TMC, 1,4,8,11-tetramethyl-1,4,8,11-tetrazacyclotetradecane) has been an important ligand in the field of coordination chemistry.¹³ It has been shown to coordinate various 3d-transition metal ions including copper, nickel and iron.¹³ $[\text{Fe}^{\text{II}}(\text{TMC})]^{2+}$ is considered the most important complex in the field of nonheme iron chemistry because it allowed the formation of the first crystallographically characterized $\text{Fe}^{\text{IV}}(\text{O})$ species in 2003 by Que and coworkers.¹⁴ This $[(\text{TMC})\text{Fe}^{\text{IV}}(\text{O})]^{2+}$ species was able to perform hydrogen atom abstraction and oxo-atom transfer reactions.¹⁵ Since 2003, $[(\text{TMC})\text{Fe}^{\text{IV}}(\text{O})]^{2+}$ and related complexes have been widely studied around the world as models of the $[\text{Fe}^{\text{IV}}(\text{O})]^{2+}$ intermediates involved in nonheme iron enzymes.^{5,16}

In 2012, Que and co-workers reported the generation of a formally $\text{Fe}^{\text{V}}(\text{O})$ species by one-electron oxidation of the corresponding $\text{Fe}^{\text{IV}}(\text{O})$ species supported by TMC.¹² The $S = 1$ $[(\text{TMC})\text{Fe}^{\text{IV}}(\text{O})]^{2+}$ was treated with *tert*-butylhydroperoxide and a strong base such as KO^tBu or NBu_4OH in acetonitrile at $-44\text{ }^\circ\text{C}$ to form the $\text{Fe}^{\text{V}}(\text{O})$ species. It was identified as an Fe^{V} center based on its EPR spectrum, which had an $S = \frac{1}{2}$ EPR signal similar to the previously characterized $[(\text{TAML})\text{Fe}^{\text{V}}(\text{O})]^-$ complex.¹⁰ Further characterization of the TMC-supported $\text{Fe}^{\text{V}}(\text{O})$ species revealed that it had an acetylimido ligand axial to the oxo moiety on the iron center, leading to its formulation as $[(\text{TMC})\text{Fe}^{\text{V}}(\text{O})(\text{NC}(\text{O})\text{CH}_3)]^+$.

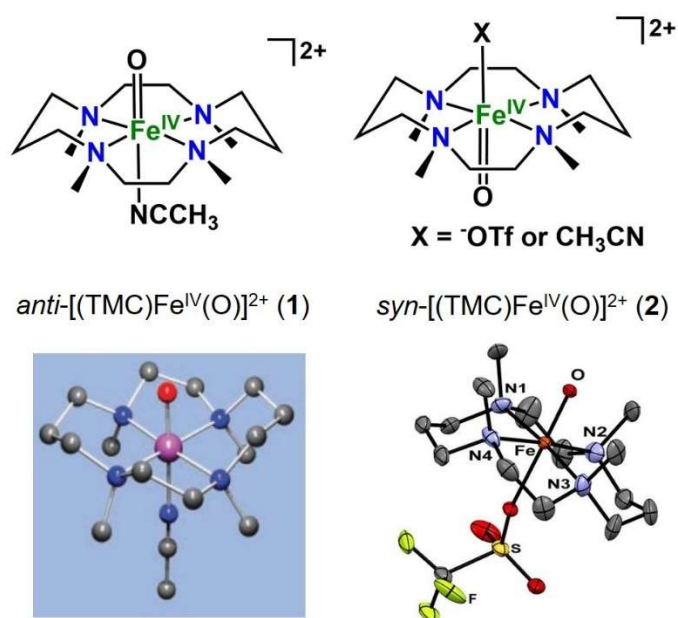


Figure 5.1. Structures of the two isomeric $[(\text{TMC})\text{Fe}^{\text{IV}}(\text{O})]^{2+}$ complexes and their crystal structures.^{14,17} Left: *anti*- $[(\text{TMC})\text{Fe}^{\text{IV}}(\text{O})]^{2+}$ (1) has all four methyl groups on the opposite side of the oxo unit. Right: *syn*- $[(\text{TMC})\text{Fe}^{\text{IV}}(\text{O})]^{2+}$ (2) has all four methyl groups on the same side as the oxo unit. (Reproduced with permission from ref 14 and ref 17; copyright 2003 American Association for the Advancement of Science and 2015 American Chemical Society)

The crystal structure of the $[(\text{TMC})\text{Fe}^{\text{IV}}(\text{O})]^{2+}$ complex reported in 2003 shows that all the four methyl groups of the TMC ligand are on one side of the TMC macrocycle opposite to the side where the oxo unit is situated (Figure 5.1).¹⁴ This arrangement will be referred to as *anti* (**1**) as the oxo unit is on the opposite side of the methyl groups. After the discovery of this structure, chemists started investigating the possibility of making the other isomeric $\text{Fe}^{\text{IV}}(\text{O})$ where the oxo moiety is on the same side as the methyl groups of the TMC framework. The search ended in 2015, when Que and co-workers reported the crystal structure of the *syn*-isomer of the $[(\text{TMC})\text{Fe}^{\text{IV}}(\text{O})]^{2+}$ (Figure 5.1).¹⁷ The two isomers have distinct spectroscopic characteristics that help to identify which isomer is formed or present in the solution. It turns out that the *syn*-isomer is the kinetic product and converts to form the *anti*-isomer with time, which is the thermodynamic product¹⁸ via H_2O -facilitated oxo-hydroxo tautomerism first described by Muenier.^{19,20}

The previously reported TMC-supported Fe^{V} species was generated starting from the *anti*-isomer of the $[(\text{TMC})\text{Fe}^{\text{IV}}(\text{O})]^{2+}$ (**1**). The goal of this study is to see if we can generate the isomeric Fe^{V} species starting from the *syn*-isomer of the $[(\text{TMC})\text{Fe}^{\text{IV}}(\text{O})]^{2+}$ (**2**), and then study the differences between the two corresponding Fe^{V} species. The only difference between the two precursor $\text{Fe}^{\text{IV}}\text{O}$ intermediates is the topology of the ligand framework around the iron center and our goal is to explore the effect of ligand topology on the formation and properties of the two Fe^{V} species.

5.2 Experimental details

All materials were purchased from commercial sources and used as received unless noted otherwise. The complex $[\text{Fe}^{\text{II}}(\text{TMC})](\text{OTf})_2$, PhIO and 2-^tBuSO₂-C₆H₄IO (ArIO) were synthesized according to previously published procedures.^{14,21,22}

UV-visible absorption spectra were recorded on a HP8453A diode array spectrometer equipped with a cryostat from Unisoku, Scientific Instruments (Osaka, Japan). Resonance Raman spectra were obtained with excitation at 457 nm (50 mW at source, Cobolt Lasers). The collimated Raman scattering was collected using two Plano convex lenses ($f = 12$ cm, placed at an appropriate distance) through appropriate long pass edge filters (Semrock) into an Acton AM-506M3 monochromator equipped with a Princeton Instruments ACTON PyLON LN/CCD-1340x400 detector. The detector was cooled to -120 °C prior to the experiments. Spectral calibration was performed using the Raman spectrum of acetonitrile/toluene 50:50 (v:v).²³ X-band EPR spectra were recorded on a Bruker Elexsys E-500 spectrometer equipped with an Oxford ESR 910 liquid helium cryostat and an Oxford temperature controller.

Conditions for generating $[(\text{TMC})\text{Fe}^{\text{IV}}(\text{O})]^{2+}$ isomers (1 and 2) – The *anti*-isomer of the $[(\text{TMC})\text{Fe}^{\text{IV}}(\text{O})]^{2+}$ complex (**1**) is generated by adding 1.2 eq PhIO to a 1mM solution of $(\text{TMC})\text{Fe}^{\text{II}}(\text{OTf})_2$ in CH₃CN at room temperature and then cooling down to -40 °C. The *syn*-isomer of the $[(\text{TMC})\text{Fe}^{\text{IV}}(\text{O})]^{2+}$ (**2**) complex is generated by adding 1 eq ArIO at -40 °C to a 1 mM solution of $(\text{TMC})\text{Fe}^{\text{II}}(\text{OTf})_2$ in CH₃CN.

5.3 One-electron oxidation of the *syn*-[(TMC)Fe^{IV}(O)]²⁺ to form a formal Fe^V species

Upon addition of 1 eq ArIO to a 1 mM solution of [(TMC)Fe^{II}]²⁺ in CH₃CN at -40 °C, the *syn*-[(TMC)Fe^{IV}(O)]²⁺ (**2**) forms within 20 s. To the solution of **2**, 3 eq *tert*-butylhydroperoxide (^tBuOOH) (relative to **2**) is added, followed by 2 eq of a strong base (NBu₄OH or KO^tBu). While addition of ^tBuOOH does not cause any change in the optical absorption spectrum of **2**, the introduction of the base elicits the formation of a new species (**2a**) with absorption bands at 400 nm and 805 nm (Figure 5.2a). The formation of **2a** upon addition of NBu₄OH takes 15 s and it decays completely within 250 s at -40 °C. The procedure used to form **2a** from **2** is the same used in the case of **1** to generate the corresponding Fe^V species **1a**.¹² **1a** is reported to have absorption bands around 410 nm and 780 nm.¹² Species **2a** can be assigned to be the putative Fe^V species obtained from one-electron oxidation of **2** based on the similarities in the UV-vis absorption spectra of **1a** and **2a** (Figure 5.2b and Table 5.1).

We have found that **1a** forms within 2 s at -40 °C, while **2a** takes 15 s to form under similar conditions. This difference can be explained based on the structures of **1** and **2** (Figure 5.1) and the proposed reaction mechanism for the formation of the Fe^V intermediates (Scheme 5.1). It is proposed that the ^tBuOOH gets deprotonated in the presence of the base and attacks the acetonitrile molecule bound to the Fe^{IV}(O) center, following which the O–O bond in the ^tBuOO- moiety undergoes homolytic cleavage to form the Fe^V species (Scheme 5.1). In the case of **1**, the acetonitrile is on the more accessible side of the TMC macrocycle, allowing facile attack by ^tBuOOH, whereas for **2**, the acetonitrile is on the less accessible face of the TMC macrocycle replacing the triflate

anion in the crystal structure (Figure 5.1), which likely makes it difficult for the ^tBuOOH to attack the acetonitrile. Compared to a half-life of 60 min for **1a** at -44 °C,¹² **2a** has a half-life of 53 s and completely decays within 250 s at -40 °C. Thus, in comparison to **1a**, **2a** seems to be more unstable under similar conditions (Table 5.1). Due to its unstable nature, we were not able to perform ESI-MS experiment. The instability of **2a** may be due to the oxo moiety being on the more accessible side of the TMC macrocycle, and thus more reactive.

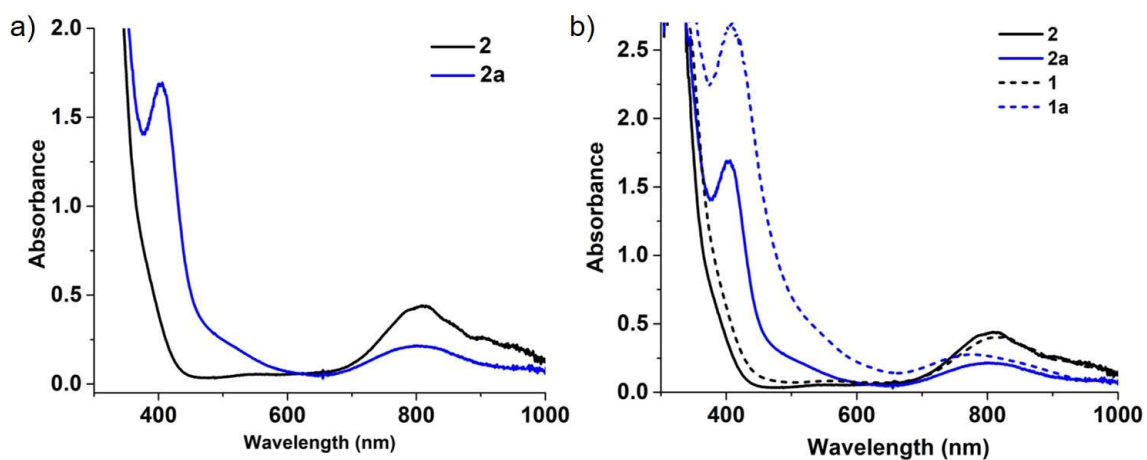
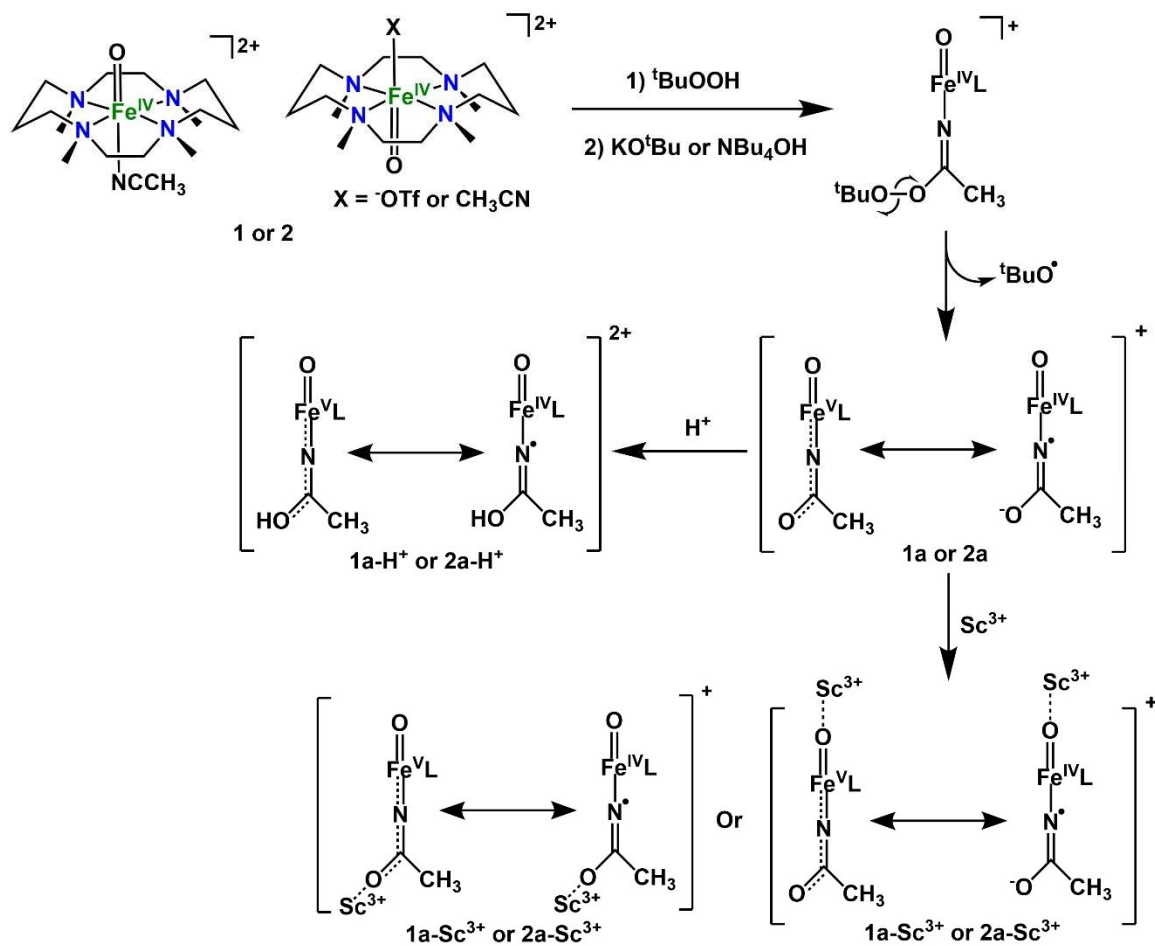


Figure 5.2. a) UV-vis absorption spectra of *syn*-[(TMC)Fe^{IV}=O]²⁺ (**2**) and the corresponding Fe^V species (**2a**) at -40 °C in CH₃CN obtained by adding ^tBuOOH and NBu₄OH to **2**. b) Comparison of UV-vis absorption spectra of **1**, **2**, **1a** and **2a**.



Scheme 5.1. Proposed reaction mechanism for one-oxidation of Fe^{IV}(O) intermediates (**1** or **2**) to form Fe^V(O) species (**1a** or **2a**) and their reaction with H⁺ and Sc³⁺.

Table 5.1. Comparison between the different Fe^V species.^a

| | λ_{\max} (nm) | EPR g values, $\nu(\text{Fe}=\text{O})^b$ | Half-life (lifetime) ^c | Ref |
|---|-----------------------|--|--------------------------------------|---------------------------------|
| <i>anti</i> - [(TMC)Fe ^V (O)(NC(O)CH ₃)] ²⁺ 1a | 410, 780 | 2.05, 2.01, 1.97 797 cm ⁻¹ | 60 min ^d | ¹² , This work |
| <i>syn</i> - [(TMC)Fe ^V (O)(NC(O)CH ₃)] ²⁺ 2a | 400, 805 | 2.05, 2.01, 1.97 | 53 s (250 s) | This work |
| 1a-H⁺ | 425, 600, 750 | 2.05, 2.01, 1.98 812 cm ⁻¹ | 30 min ^d | ¹² , this work |
| 2a-H⁺ | 420, 625, 810 | 2.05, 2.01, 1.98 | 7 s (50 s) | This work |
| 1a-Sc³⁺ | 425, 580, 760 | 2.05, 2.01, 1.98 805 cm ⁻¹ | 20 min | This work |
| 2a-Sc³⁺ | 425, 595, 805 | | 37 s (200 s) | This work |

^aFor this work, all reactions were carried out in CH₃CN at -40 °C. ^bFrom resonance Raman data obtained by excitation at 457 nm. ^cNumbers in parenthesis denote lifetimes ^d measured at -44 °C.

The sequence of addition of the reagents ^tBuOOH (oxidant) and NBu₄OH (base) is very important for the formation of **2a**. Addition of the base (NBu₄OH) to the Fe^{IV}=O species **2** before addition of the oxidant makes it decay, leading to the formation of what we propose to be the hydroxide bound form of **2** (Figure 5.3), based on the similarity of its UV-vis spectrum with that reported for *anti*-[(TMC)Fe^{IV}(O)(OH)]²⁺ generated in water using buffers in the pH range of 6.0 and 8.0.²⁴ **1** in CH₃CN was not stable upon addition of NBu₄OH and decomposed to form a precipitate. The proposed reaction mechanism for formation of **1a** and **2a** shown in Scheme 5.1 rationalizes the importance of the addition sequence of the reagents. If the base is added first then it can bind to the iron center.

However, if added in the presence of ^tBuOOH, the base then deprotonates ^tBuOOH, which can in turn attack the CH₃CN bound to the iron center.

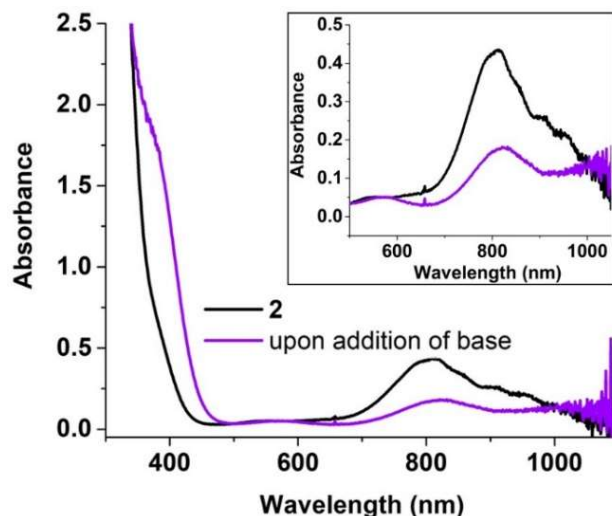


Figure 5.3. a) UV-vis absorption spectra of *syn*-[(TMC)Fe^{IV}(O)]²⁺ (**2**) and the species formed upon addition of base NBu₄OH at -40 °C in CH₃CN. Inset: Zoomed in view between 600 nm and 1000 nm.

The key spectroscopic evidence for assigning **2a** to be an Fe^V species comes from EPR spectroscopy. An Fe^V center should contain an odd number of unpaired electrons, and thus can be detected by perpendicular mode X-band EPR, unlike Fe^{IV} centers. As expected, **2a** exhibits a *S* = 1/2 EPR signal with *g*-values of 2.05, 2.01 and 1.97 suggesting that the Fe^{IV} center in **2** is oxidized to an Fe^V center (Figure 5.4). This signal matches well with that of **1a** with *g*-values¹² of 2.053, 2.010 and 1.971 (Table 5.1). Hence, we assigned **2a** to be an Fe^V species generated from the *syn* isomer of [(TMC)Fe^{IV}(O)]²⁺ **2**. **2a** and **1a** are proposed to be isomeric Fe^V species similar to **1** and **2**, based on the similarities in their

EPR and UV-vis spectroscopies as well as the same method of generation. However, the lower stability of **2a** compared to **1a** suggests that there are differences in their kinetic properties, similar to **1** and **2**.

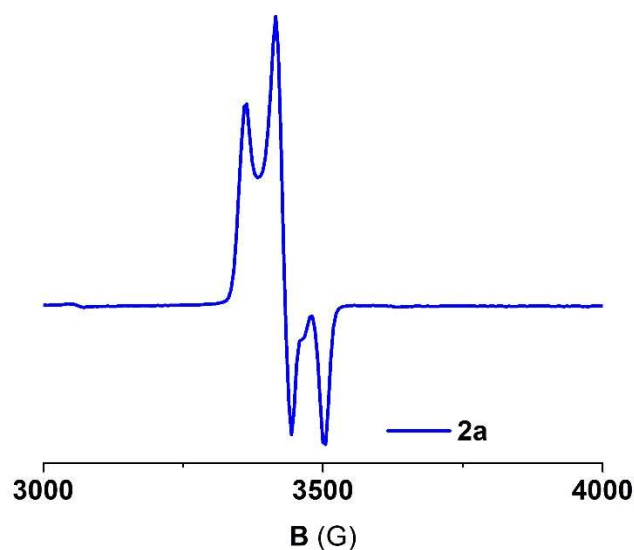


Figure 5.4. X-band EPR spectrum of **2a** obtained at 2 K at 35 db.

Previous work in the Que Lab suggests that **1a** is not reactive (unpublished). **2a** is less stable than **1a**, and thus presumed to be more reactive. Preliminary screening of reactivity suggests that this surmise is correct, as **2a** reacts with dihydroanthracene (DHA), a substrate probe for HAT (hydrogen atom abstraction or transfer), and thioanisole (PhSMe), a substrate probe for OAT (oxygen atom transfer) (Figure 5.5). Further experiments are needed to understand the reactivity of **2a**.

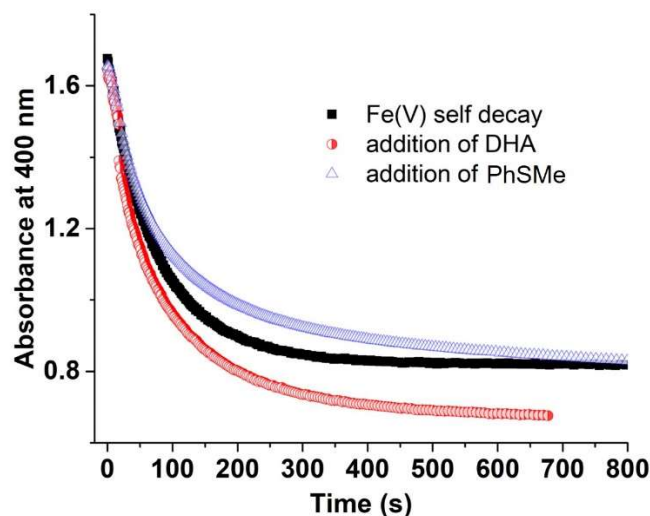


Figure 5.5. Time traces monitoring the absorbance at 400 nm corresponding to **2a** in the absence of any substrate, upon addition of DHA (4 eq) (due to low solubility) and PhSMe (200 eq) at $-40\text{ }^{\circ}\text{C}$ in CH_3CN . The substrates are added upon maximum formation of **2a**.

5.4 Reaction of Fe^{V} species with the strong Brønsted acid HClO_4 and the strong Lewis acid $\text{Sc}(\text{OTf})_3$

Intermediate **1a** is reported to form its conjugate acid **1a-H⁺** upon introduction of a strong Brønsted acid such as HClO_4 (Scheme 5.1).¹² **1a-H⁺** has absorption bands at 425 nm, 600 nm and 750 nm and a half-life of 30 min at $-44\text{ }^{\circ}\text{C}$ in CH_3CN . Here we have successfully trapped the conjugate acid **2a-H⁺** of **2a** using HClO_4 (Figure 5.6). Addition of 2 eq HClO_4 (relative to the starting $[\text{Fe}^{\text{II}}(\text{TMC})]^{2+}$ complex) to **2a** at $-40\text{ }^{\circ}\text{C}$ in CH_3CN generates a new species **2a-H⁺**, which has absorption bands at 420, 625 and 810 nm, similar to those of **1a-H⁺** (Figure 5.6 and Table 5.1). Furthermore, **2a-H⁺** exhibits an $S = 1/2$ EPR signal with g values of 2.05, 2.01 and 1.98, like **1a-H⁺**, indicating that **2a-H⁺** contains an Fe^{V} center (Table 5.1). Based on similarities between **1a-H⁺** and **2a-H⁺**, we assigned **2a-**

H^+ as the conjugate acid of **2a**. We monitored the evolution of **2a** and **2a-H⁺** at 400 nm and 640 nm (where only **2a-H⁺** has contribution) and found that **2a-H⁺** decayed exponentially within 50 s at a rate of 0.1 s^{-1} at $-40 \text{ }^\circ\text{C}$ (Figure 5.6). **2a-H⁺** has a half-life of 7 s at $-40 \text{ }^\circ\text{C}$, in contrast to **1a-H⁺**, which has a half-life of 30 min under similar conditions. Thus, we have successfully generated the isomeric *syn*- Fe^{V} intermediates, **2a** and **2a-H⁺**, starting from the *syn*- $\text{Fe}^{\text{IV}}(\text{O})$ complex **2**. Here, we have observed that the *syn*- Fe^{V} intermediates are more unstable compared to their *anti*- Fe^{V} counterparts, similar to the pair of corresponding starting $\text{Fe}^{\text{IV}}(\text{O})$ complexes (unpublished work in the Que lab).

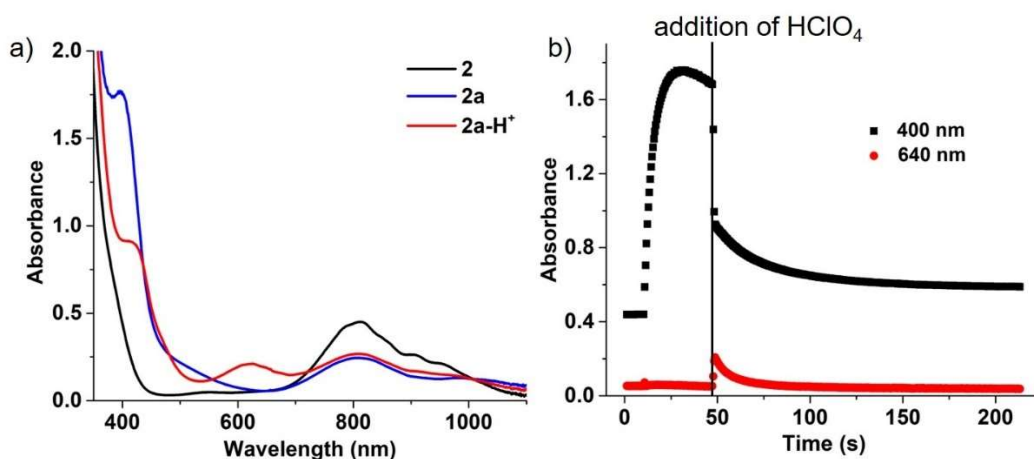


Figure 5.6. a) UV-vis absorption spectra of **2**, **2a** and **2a-H⁺** at $-40 \text{ }^\circ\text{C}$ in CH_3CN . b) Time traces monitoring the absorbance at 400 nm and 640 nm. At 400 nm both **2a** and **2a-H⁺** absorbs, however, at 640 nm only **2a-H⁺** absorbs. The black vertical line denotes the time when HClO_4 was added to **2a**.

Nam and Fukuzumi have extensively studied the interaction of Lewis acids with $\text{Fe}^{\text{IV}}(\text{O})$ complexes;^{25,26} however, little is known about interaction of $\text{Fe}^{\text{V}}(\text{O})$ species with

Lewis acids. Here we have explored the effect of Lewis acidic Sc^{3+} on the Fe^{V} intermediates **1a** and **2a**. Upon addition of 1 eq Sc^{3+} to **1a** at $-40\text{ }^{\circ}\text{C}$ in CH_3CN , the formation of a new species **1a-Sc³⁺** can be observed via UV-vis absorption spectroscopy (Figure 5.7a). This species has absorption bands at 425, 580 and 760 nm, somewhat shifted from those of **1a-H⁺**, suggesting that they are different species (Figure 5.7b and Table 5.1). **1a-Sc³⁺** has a half-life of 20 min at $-40\text{ }^{\circ}\text{C}$, similar to **1a-H⁺**. From EPR spectroscopy, **1a-Sc³⁺** has an $S = 1/2$ signal at $g = 2.05, 2.01, 1.98$ indicating the presence of an Fe^{V} center. Hence, we propose **1a-Sc³⁺** to be a Sc^{3+} adduct of **1a**.

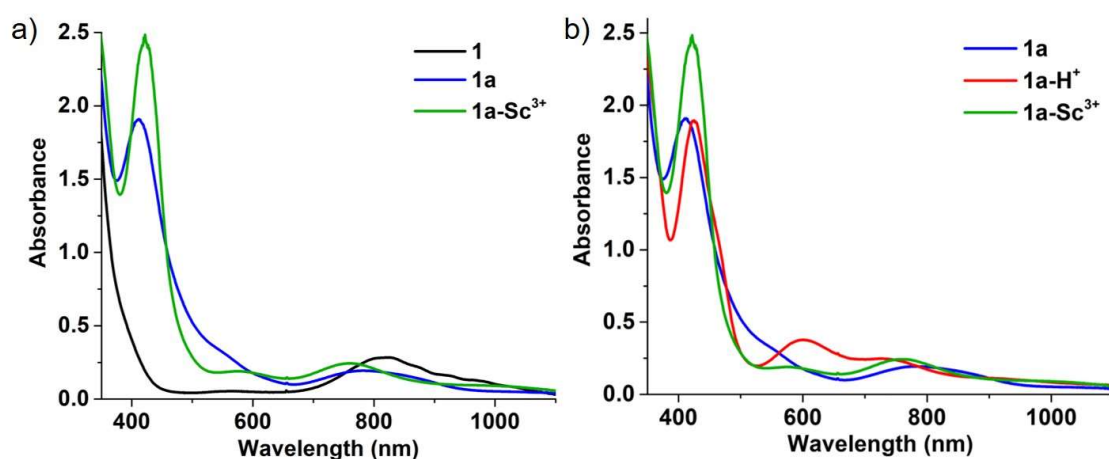


Figure 5.7. a) UV-vis absorption spectra of **1**, **1a** and **1a-Sc³⁺** at $-40\text{ }^{\circ}\text{C}$ in CH_3CN . b) UV-vis absorption spectra of the three Fe^{V} species generated from **1**.

From resonance Raman spectroscopy, the $\text{Fe}^{\text{V}}=\text{O}$ unit of **1a** was found to have a vibrational feature at 798 cm^{-1} when excited using a 413 nm laser source,¹² and **1a-H⁺** was found to have a vibrational feature at 811 cm^{-1} . These values for the $\text{Fe}=\text{O}$ vibrations of **1a** and **1a-H⁺** were lower than that of the related $\text{Fe}^{\text{IV}}=\text{O}$ unit of **1** at 839 cm^{-1} and its analogs

with axial ligands, with a minimum of 814 cm^{-1} for the $\text{Fe}^{\text{IV}}=\text{O}$ complex containing an azide as the axial *trans* ligand.⁵ Based on rigorous DFT studies supported with spectroscopic studies by Münck, Que and co-workers, it was concluded that the anionic *trans* acetylimido ligand weakens the $\text{Fe}^{\text{V}}=\text{O}$ bond and lowers the $\text{Fe}=\text{O}$ vibrational frequency.¹² Protonating **1a** reduces the electron-donating ability of the *trans* ligand in **1a-H⁺** resulting in an increase in the vibrational frequency. We obtained the resonance Raman spectrum of **1a-Sc³⁺** and compared it with **1a** and **1a-H⁺** (Table 5.1). Unfortunately, we were unable to obtain the resonance Raman spectra for **2a**, **2a-H⁺** and **2a-Sc³⁺**. We tried to collect spectra both in frozen as well as solution states, but we were not able to detect any resonance enhanced peaks. The intermediates might have decayed thermally before any data could be collected or they might have been photoreduced. Another possibility is that the peaks originating from the intermediates overlap with the solvent-derived peaks. Further attempts to collect the data should be made in a different solvent. Additionally, attempts to generate the species at lower temperatures to prolong the lifetimes are worth exploring.

We have found that **1a-Sc³⁺** has a vibrational feature at 805 cm^{-1} (with 457-nm laser excitation), which is assigned to the $\text{Fe}=\text{O}$ unit in **1a-Sc³⁺** (Figure 5.8). This vibration can be compared to those for **1** and **1a-H⁺** under similar conditions and excitation source, with respective vibrational features at 797 and 812 cm^{-1} for **1a** and **1a-H⁺**. Hence, the $\text{Fe}=\text{O}$ unit in **1a-Sc³⁺** was stronger than in **1** but weaker than in **1a-H⁺**, which suggests that Sc^{3+} interacts with **1a** in a different fashion compared to H^+ . Sc^{3+} can potentially interact with the acetylimido ligand like H^+ , or it can interact with the oxo-moiety of the $\text{Fe}=\text{O}$ unit

(Scheme 5.1). If Sc^{3+} interacts with the acetylimido ligand like H^+ , then the $\text{Fe}=\text{O}$ vibration would probably have remained the same. On the other hand, if Sc^{3+} interacts with the $\text{Fe}=\text{O}$ unit, then the ligand *trans* to the oxo unit is still anionic with a higher electron donating ability than the protonated form, which may result in a $\text{Fe}=\text{O}$ vibration frequency that lies between **1a** and **1a-H⁺**, as is observed for **1a-Sc³⁺**. Furthermore, introduction of Sc^{3+} and H^+ affects different parts of the absorption spectrum of **1a**. Sc^{3+} affects the higher energy band at ~ 400 nm, whereas H^+ barely affects that band but instead forms a new band at 625 nm (Figure 5.7). This might indicate that H^+ and Sc^{3+} interact with different parts of **1a** affecting different electronic transitions of the absorption spectrum, further supporting the idea that Sc^{3+} does not interact with the acetylimido ligand like H^+ .

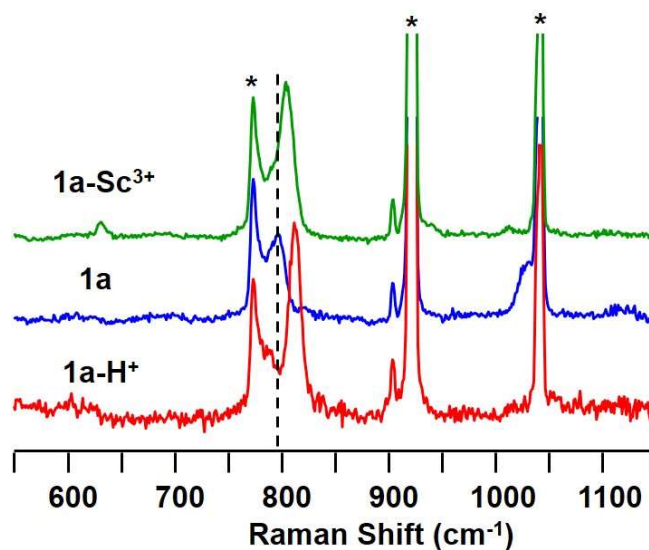


Figure 5.8. Resonance Raman spectra of **1**, **1a-H⁺** and **1a-Sc³⁺** at 77K. Excitation source: 457 nm laser. Samples were prepared at -40 °C and frozen with liquid nitrogen. * denotes solvent peaks. For **1a** there is a shoulder peak ~ 1040 cm^{-1} , which has not yet been assigned.

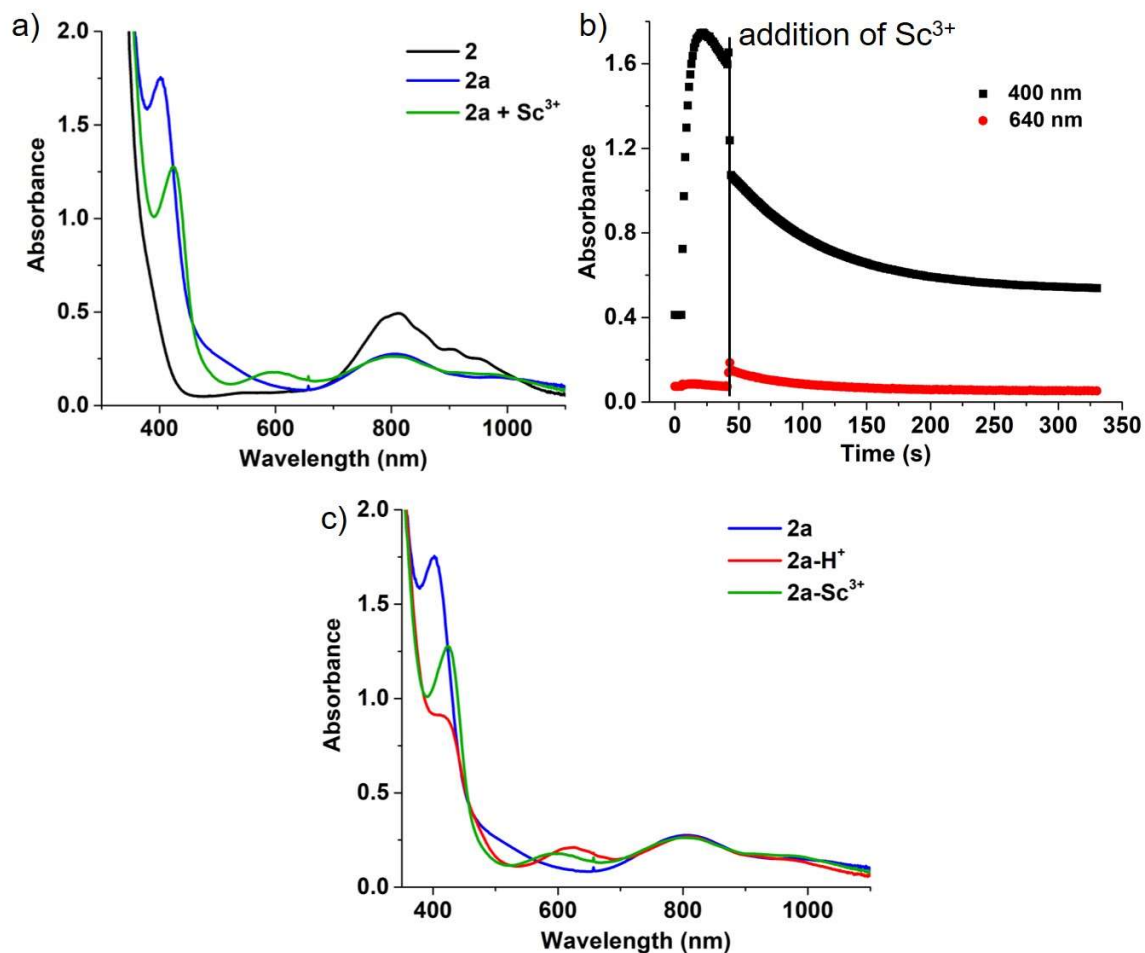


Figure 5.9. a) UV-vis absorption spectra of **2**, **2a** and **2a-Sc³⁺** at -40 °C in CH₃CN. b) Time traces monitoring the absorbance at 400 nm and 640 nm. At 400 nm both **2a** and **2a-Sc³⁺** absorbs, however, at 640 nm only **2a-Sc³⁺** absorbs. The black vertical line denotes the time when Sc³⁺ was added to **2a**. c) UV-vis absorption spectra of the three Fe^V species generated from **2**.

Addition of 1 eq Sc³⁺ (relative to [Fe^{II}(TMC)]²⁺) to **2a** at -40 °C in CH₃CN results in the formation a new species **2a-Sc³⁺** with absorption bands at 425, 595 and 805 nm (Figure 5.9a). The intermediate **2a-Sc³⁺** is different from **2a-H⁺**, as can be seen by overlaying their respective spectra (Figure 5.9c and Table 5.1). **2a-Sc³⁺** persists for about

200 s with a half-life of 37 s versus **2a-H⁺** that lives for ~ 50 s with a half-life of 7 s under similar conditions (Figure 5.9b). We were not able to get the EPR spectrum of **2a-Sc³⁺** due to an unfortunate event where the sample decayed. However, based on the similarity with **1a-Sc³⁺**, we assigned **2a-Sc³⁺** to be the isomeric Sc³⁺ adduct of **2a**. Hence, two different species are formed depending on whether a Lewis acid or a Brønsted acid is added to **2a**, similar to what is observed for **1a**. This further supports that the possibility that H⁺ and Sc³⁺ interact with different parts of the [(TMC)Fe^V(O)(NC(O)CH₃)⁺ intermediate irrespective of which isomer is present.

Lewis acidic Y³⁺ is also known to enhance the rate of electron transfer reactions for Fe^{IV}(O) complexes.^{25,26} We explored the effect of adding Y³⁺ to **1a** and **2a**. The spectrum of **1a** changed upon addition of 1 eq Y³⁺ (relative to [Fe^{II}(TMC)]²⁺) to **1a**, indicating that Y³⁺ interacts with **1a**. The 780 nm peak of **1a** shifts to 770 nm and the absorbance at 530 nm decreases in intensity (Figure 5.10a). However, no new peak is formed in the 580-600 nm region, unlike H⁺ and Sc³⁺. When 1 eq Y³⁺ (relative to [Fe^{II}(TMC)]²⁺) is added to **2a**, no peak shift or new peak is observed, rather the peaks of **2a** at 400 and 805 nm decrease in absorbance along with a decrease in the absorbance of the 500 nm shoulder (Figure 5.10b). The effects of Y³⁺ vary between the two isomers **1a** and **2a**, as is observed earlier for H⁺ and Sc³⁺. Preliminary studies suggest that Y³⁺ interacts with **1a** and **2a**, but the effect is not as significant as in the case of Sc³⁺, which may be due to the lower Lewis acidity of Y³⁺ compared to Sc³⁺. Further detailed investigation needs to be done.

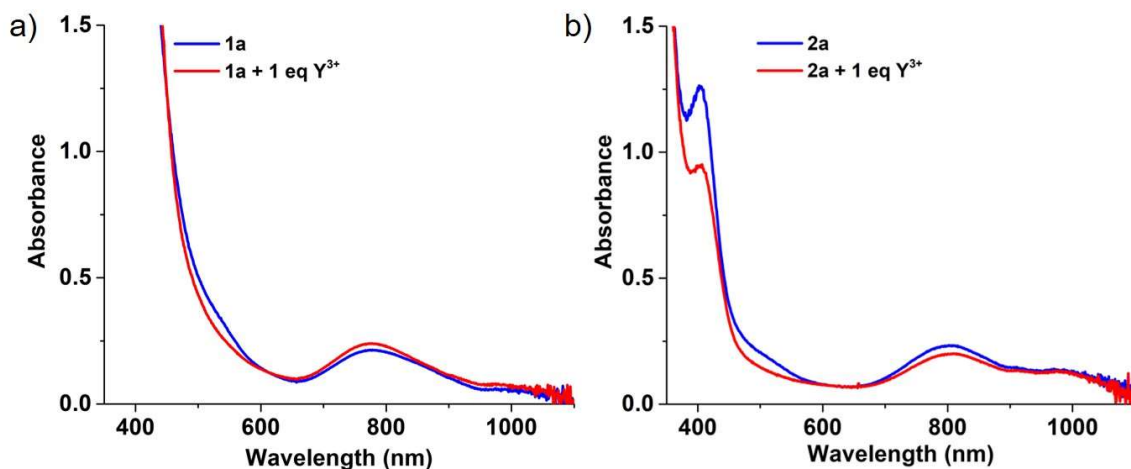


Figure 5.10. UV-vis absorption spectra of a) **1a** and **1a-Y³⁺** and b) **2a** and **2a-Y³⁺** at -40 °C in CH₃CN.

5.5 Summary

In this work, our first goal was to generate a Fe^V(O) species from the recently discovered *syn* isomer of [(TMC)Fe^{IV}(O)]²⁺ (**2**), similar to the one generated from the well-known *anti* isomer of [(TMC)Fe^{IV}(O)]²⁺ (**1**). We were able to successfully generate the Fe^V species (**2a**) from **2** by oxidizing it with one-electron using ^tBuOOH in the presence of a base at -40 °C. We ascertained its Fe(V) oxidation state using EPR spectroscopy. We observed an S = 1/2 EPR signal with g values of 2.05, 2.01, 1.97, similar to the Fe(V) species **1a** generated from **1**.¹² Intermediate **2a** (half-life = 53 s) is less stable than **1a** (half-life = 60 min), and preliminary results suggest that it can perform HAT and OAT reactions. We are also able to generate the conjugate acid of **2a**, **2a-H⁺**, which has an even shorter half-life (7s) than **2a**.

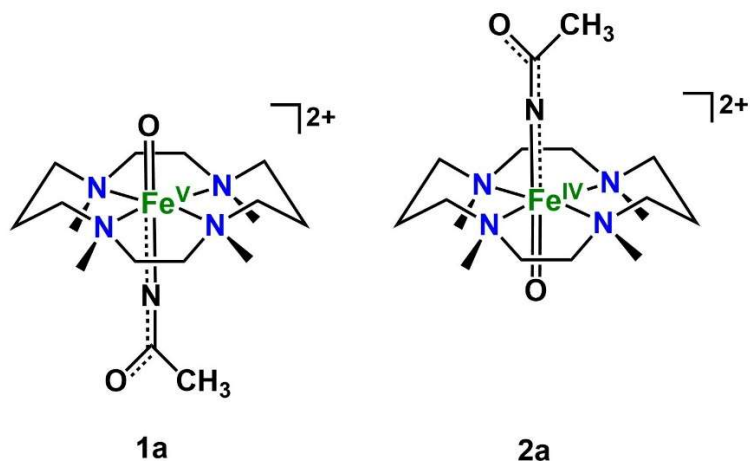


Figure 5.11. Proposed structures of the isomeric Fe^{V} intermediates **1a** and **2a**.

Both Fe^{V} intermediates **1a** and **2a** are supported by the same ligand. The only difference is the topology of the precursor $\text{Fe}^{\text{IV}}(\text{O})$ complex (Figure 5.1). For **1a**, all the methyl groups are on the opposite side of the oxo-moiety, while for **2a** all the methyl groups are on the same side of the oxo unit (Figure 5.11). This difference in ligand topology leads to the formation of two distinct Fe^{V} species, which look similar spectroscopically, but are kinetically different. This further supports our conclusion in Chapter 4 that ligand topology has a significant effect on the reactivity and kinetic behavior of iron-oxygen intermediates, even though spectroscopically they might look similar.

In the literature, scientists all around the world have studied the effect of Lewis acids on $\text{Fe}^{\text{IV}}(\text{O})$ intermediates,^{25,26} but very little is known about their effect on Fe^{V} species. Here, we have explored the effect of Lewis acidic Sc^{3+} on the Fe^{V} intermediates and found that Sc^{3+} can interact with the Fe^{V} species **1a** and **2a** to form two new species, **1a-Sc³⁺** and **2a-Sc³⁺**. These species spectroscopically look different from the conjugate

acids of the corresponding Fe^V intermediates, **1a-H⁺** and **2a-H⁺**. This comparison leads us to propose that Sc³⁺ interacts at a site of the Fe^V species different from H⁺, which has been previously demonstrated to bind to the anionic acetylimido ligand. Perhaps Sc³⁺ might interact with the oxo moiety of the Fe^V center in **1a** and **2a**. At this point, we cannot completely rule out the possibility that Sc³⁺ can also interact with the anionic acetylimido ligand, like H⁺, but the interaction is weaker than H⁺, giving rise to a different species. Further spectroscopic techniques such as extended X-ray absorption fine structure spectroscopy (EXAFS) and Mössbauer spectroscopy will be helpful in gaining insight into the nature of the interaction of Sc³⁺ with the Fe^V intermediates.

5.6 Acknowledgments

We thank Dr. Jai Prakash for his initial observations and help in designing some of the initial experiments. Patrick Crossland helped in our attempts to obtain resonance Raman spectra of **2a**, **2a-H⁺** and **2a-Sc³⁺**.

5.7 References

- (1) Kal, S.; Que, L. *J. Biol. Inorg. Chem.* **2017**, *22*, 339–365.
- (2) Barry, S. M.; Challis, G. L. *ACS Catal.* **2013**, *3*, 2362–2370.
- (3) Lipscomb, J. D. *J. Biol. Chem.* **2014**, *289*, 15141–15153.
- (4) Krebs, C.; Fujimori, D. G.; Walsh, C. T.; Bollinger, J. M. *Acc. Chem. Res.* **2007**, *40*, 484–492.

- (5) Klein, J. E. M. N.; Que, L. *Encyclopedia of Inorganic and Bioinorganic Chemistry*; 2016; DOI: 10.1002/9781119951438.eibc2344.
- (6) Olivo, G.; Cussó, O.; Borrell, M.; Costas, M. *J. Biol. Inorg. Chem.* **2017**, *22*, 425–452.
- (7) Lyakin, O. Y.; Bryliakov, K. P.; Talsi, E. P. *Coord. Chem. Rev.* **2019**, *384*, 126–139.
- (8) Gamba, I.; Codolà, Z.; Lloret-Fillol, J.; Costas, M. *Coord. Chem. Rev.* **2017**, *334*, 2–24.
- (9) Oloo, W. N.; Que, L. *Acc. Chem. Res.* **2015**, *48*, 2612–2621.
- (10) Tiago de Oliveira, F.; Chanda, A.; Banerjee, D.; Shan, X.; Mondal, S.; Que, L.; Bominaar, E. L.; Münck, E.; Collins, T. J. *Science* **2007**, *315*, 835–838.
- (11) Ghosh, M.; Singh, K. K.; Panda, C.; Weitz, A.; Hendrich, M. P.; Collins, T. J.; Dhar, B. B.; Gupta, S. Sen. *J. Am. Chem. Soc.* **2014**, *136*, 9524–9527.
- (12) Van Heuvelen, K. M.; Fiedler, A. T.; Shan, X.; De Hont, R. F.; Meier, K. K.; Bominaar, E. L.; Münck, E.; Que, L. *Proc. Natl. Acad. Sci.* **2012**, *109*, 11933–11938.
- (13) Barefield, E. K. *Coord. Chem. Rev.* **2010**, *254*, 1607–1627.
- (14) Rohde, J.-U.; In, J. H.; Lim, M. H.; Brenessel, W. W.; Bukowski, M. R.; Stubna, A.; Münck, E.; Nam, W.; Que, Jr., L. *Science* **2003**, *299*, 1037–1039.
- (15) Sastri, C. V.; Lee, J.; Oh, K.; Lee, Y. J.; Lee, J.; Jackson, T. A.; Ray, K.; Hirao, H.; Shin, W.; Halfen, J. A.; Kim, J.; Que, L.; Shaik, S.; Nam, W. *Proc. Natl. Acad. Sci.* **2007**, *104*, 19181–19186.
- (16) McDonald, A. R.; Que, L. *Coord. Chem. Rev.* **2013**, *257*, 414–428.

- (17) Prakash, J.; Rohde, G. T.; Meier, K. K.; Münck, E.; Que, L. *Inorg. Chem.* **2015**, *54*, 11055–11057.
- (18) Prakash, J.; Sheng, Y.; Draksharapu, A.; Klein, J. E. M. N.; Cramer, C. J.; Que, L. *Angew. Chem. Int. Ed.* **2019**, *58*, 1995–1999.
- (19) Meunier, B.; Bernadou, J. *Struct. Bond.* **2000**, *97*, 1–35.
- (20) Bernadou, J.; Meunier, B. *Chem. Commun.* **1998**, 2167–2173.
- (21) Saltzman, H.; Sharefkin, J. G. *Org. Synth.* **1963**, *43*, 60–61.
- (22) Macikenas, D.; Skrzypczak-Jankun, E.; Protasiewicz, J. D. *J. Am. Chem. Soc.* **1999**, *121*, 7164–7165.
- (23) ASTM E1840-96(2007)Standard Guide for Raman Shift Standards for Spectrometer Calibration ASTM International DOI:10.1520/E1840-96R07. .
- (24) Klein, J. E. M. N.; Draksharapu, A.; Shokri, A.; Cramer, C. J.; Que, L. *Chem. Eur. J.* **2017**, *24*, 5373–5378.
- (25) Fukuzumi, S. *Coord. Chem. Rev.* **2013**, *257*, 1564–1575.
- (26) Fukuzumi, S.; Ohkubo, K.; Lee, Y. M.; Nam, W. *Chem. Eur. J.* **2015**, *21*, 17548–17559.

Chapter 6:

Conclusions and Perspective

Parts of the content of this chapter was published in:

1) Kal, S.; Draksharapu, A.; Que, L. Jr. Sc^{3+} (or HClO_4) activation of a nonheme Fe^{III} -OOH intermediate for the rapid hydroxylation of cyclohexane and benzene, *J. Am. Chem. Soc.*, **2018**, *140*, 5798–5804.

2) Kal, S.; Que, L. Jr. Activation of a nonheme Fe^{III} -OOH by a second Fe^{III} to hydroxylate strong C–H bonds: possible implications for sMMO, *Angew. Chem. Int. Ed.*, **2019**, DOI: 10.1002/anie.201903465.

Reprinted with permission from the American Chemical Society and Wiley-VCH.

Copyright © 2018 American Chemical Society and © 2019 Wiley-VCH.

6.1 Introduction

In Nature, nonheme iron enzymes generate powerful metal-based oxidants that are capable of performing a wide range of oxidative transformations such as C–H bond hydroxylation, electrophilic aromatic substitution, *cis*-dihydroxylation, oxidative cyclization, desaturation, N-oxidation and halogenation.^{1–6} While biochemists directly investigate these enzymes extensively, bioinorganic chemists design synthetic structural and functional models of these enzymes to understand their mechanism and develop catalysts to perform similar oxidative transformations.^{7,8} Biochemical engineers are now using some of these nonheme iron oxygenases to design biocatalysts that can perform difficult oxidative transformations.^{9,10} Iron being the fourth most abundant element in the earth's crust further fuels interest among scientists to develop iron-based catalysts for organic transformations.^{11–13} Nonheme iron enzymes capable of performing oxidative chemistry are proposed and in some cases shown to involve high-valent iron-oxidants.^{1,2} For future development of catalysts, we need to design pathways to form high-valent iron oxidants synthetically and understand their characteristics. Understanding the high-valent iron oxidants in synthetic systems in turn helps us to solve the mechanisms of complex enzymatic systems.

About two decades ago, nonheme iron complexes supported by tetradentate nitrogen-based ligands were shown to form metal-based oxidants upon reacting with H₂O₂ in catalytic reactions.^{14,15} Since then, chemists around the world have designed many nonheme iron complexes that can catalyze hydrocarbon oxidation reactions under ambient conditions.^{7,16} Extensive studies have been performed to understand the various pathways

followed by such nonheme iron catalysts. In Chapter 1, I have provided a description of the various mechanisms to generate high-valent iron-oxidants that are reported in the literature to date. In Chapter 2, I have described a new pathway to form high-valent Fe^{V} oxidants from $\text{Fe}^{\text{III}}\text{-OOH}$ intermediates with assistance from strong Lewis acidic $\text{Sc}(\text{OTf})_3$ or Brønsted acid HClO_4 . Here we used a relatively inefficient nonheme iron catalyst $[\text{Fe}^{\text{II}}(\beta\text{-BPMCN})]^{2+}$ to demonstrate the ability of the Sc^{3+} - or HClO_4 -assisted pathway to generate a potent metal-based oxidant that can perform hydroxylation of difficult substrates such as cyclohexane and benzene at $-40\text{ }^\circ\text{C}$ within seconds. Next, I described that Fe^{III} ions can also act as a Lewis acid to activate an $\text{Fe}^{\text{III}}\text{-OOH}$ intermediate resulting in the formation of a potent Fe^{V} oxidant in Chapter 3. In Chapter 4, I compared the effect of Lewis acidic $\text{Sc}(\text{OTf})_3$ on the catalytic reactivity of two other nonheme iron complexes, one of them being a topological isomer of $[\text{Fe}^{\text{II}}(\beta\text{-BPMCN})]^{2+}$ and the other is one of most well-studied nonheme iron catalyst. So far, I have described high-valent iron oxidants in catalytic systems that are not directly observed due to their high reactivity. In Chapter 5, I described the formation of Fe^{V} intermediates in a stoichiometric fashion via one-electron oxidation of $\text{Fe}^{\text{IV}}(\text{O})$ intermediates. The goal was to generate Fe^{V} species for the unstable isomer of a pair of topological isomers and compare their characteristics. We further explored the effect of Lewis acidic Sc^{3+} on this pair of Fe^{V} intermediates. Finally, here in Chapter 6, I present a summary of these results and future directions for the work presented in this thesis.

6.2 Activation of $[(\beta\text{-BPMCN})\text{Fe}^{\text{III}}\text{-OOH}]^{2+}$ intermediate to generate a highly reactive active oxidant using redox-inactive Lewis acidic Metal ions or Brønsted acids

$[\text{Fe}^{\text{II}}(\beta\text{-BPMCN})]^{2+}$ (**2**) reported in 2002 is an inefficient catalyst for alkane hydroxylation that oxidizes cyclohexane only stoichiometrically.¹⁷ Here, we have found that the introduction of $\text{Sc}(\text{OTf})_3$ or HClO_4 in the catalytic reaction mixture, allows **2** to perform catalytic cyclohexane hydroxylation with 10-fold higher yields for cyclohexanol. Additionally, the selectivity to form alcohol (A) over ketone (K), denoted by the A/K ratio, increases from 0.8 in the absence of any additive to 14 with 2 eq Sc^{3+} , and 40 with 2 eq HClO_4 , suggesting that very little amount of ketone is produced in the reaction. We have found that about 50 % H_2O_2 is being converted to products in the presence of Sc^{3+} or HClO_4 compared to only 11 % in the absence of any additive (Figure 6.1). Thus, a new oxidant is proposed to form in the presence of Sc^{3+} or HClO_4 . This oxidant is also equally efficient in oxidizing benzene to form phenol, a reaction that does not occur in the absence of Sc^{3+} or HClO_4 . Furthermore, this oxidant oxidizes electron-deficient benzene analogs such as nitrobenzene. All mechanistic experiments indicate towards the formation of a potent metal-based electrophilic oxidant in the presence of Sc^{3+} or HClO_4 (Figure 6.1).

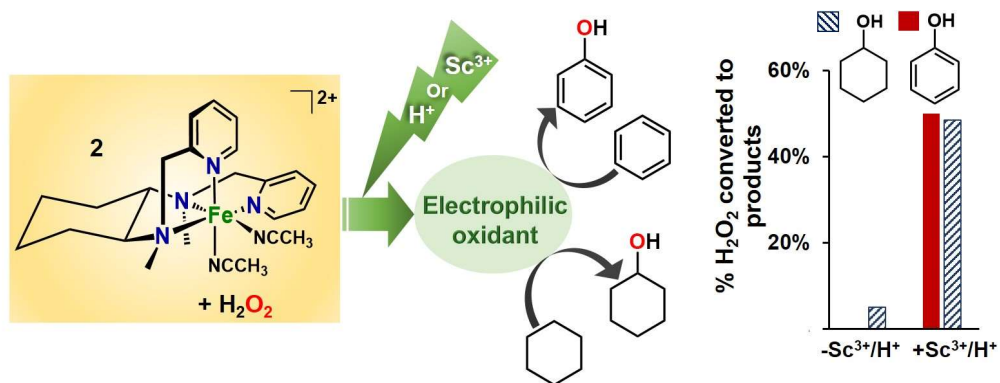


Figure 6.1 Effect of Sc^{3+} or HClO_4 on catalytic reactivity of $[\text{Fe}^{\text{II}}(\beta\text{-BPMCN})]^{2+}$ (**2**).

We have characterized the $[(\beta\text{-BPMCN})\text{Fe}^{\text{III}}(\text{OOH})]^{2+}$ intermediate (**2a**) at $-40\text{ }^\circ\text{C}$ and have demonstrated that Sc^{3+} and HClO_4 interact with it. In the presence of cyclohexane as the substrate, addition of Sc^{3+} or HClO_4 enhances the decay rate of **2a**. On the other hand, in the presence of benzene, addition of Sc^{3+} or HClO_4 elicits the formation of the Fe^{III} -phenolate adduct (**2b**). The rate of formation of **2b** matches the decay rate of **2a** and increases with increasing concentration of Sc^{3+} or HClO_4 but is independent of substrate identity and concentration. Cumulatively, these kinetic results suggest that Sc^{3+} and HClO_4 interact with **2a** to form the actual oxidant responsible for substrate oxidation, and the substrate oxidation step is faster than oxidant formation. This system can oxidize substrates within seconds at $-40\text{ }^\circ\text{C}$, and has a cyclohexane oxidation rate comparable to the fastest rate reported in the literature for the $[(\text{PyNMe}_3)\text{Fe}^{\text{V}}(\text{O})(\text{OAc})]^{2+}$ intermediate.¹⁸ Isotope labelling experiments reveal that essentially all O-atoms in the cyclohexanol and phenol products are derived from H_2O_2 in the presence of Sc^{3+} or HClO_4 . In the absence of any additive, about 50% O-atoms in cyclohexanol are derived from O_2 ,¹⁷ whereas no O-atom

incorporation from O₂ is observed in presence of Sc³⁺ or HClO₄. Additionally, for the most extensively studied water-assisted mechanism, O-atom from water is incorporated into the products,^{17,19} which is not the case in the presence of Sc³⁺ or HClO₄. Based on all the mechanistic and kinetic results, it is proposed that Sc³⁺ or HClO₄ facilitates heterolytic O–O bond cleavage in the Fe^{III}–OOH intermediate **2a** to form the actual oxidant in the Sc³⁺-/HClO₄-assisted mechanism (Figure 6.2). This work has added a new pathway to form a potent electrophilic Fe^V-oxo oxidant in the mechanistic landscape of nonheme iron catalysis.

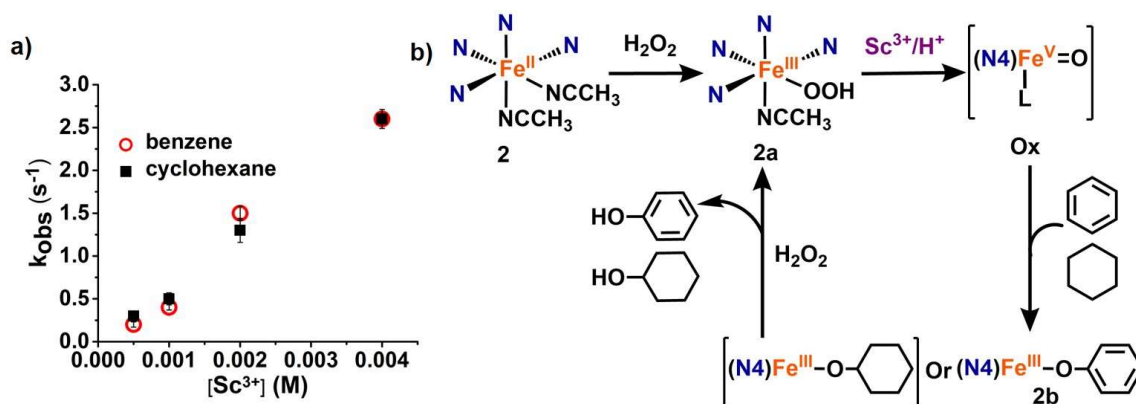


Figure 6.2 a) [Sc³⁺] dependence of k_{obs} for the decay of **2a** with cyclohexane as substrate (black squares) or the formation of **2b** (red circles) with benzene as substrate. The data for HClO₄ is shown in Chapter 2. b) Proposed mechanism for the effect of Sc³⁺ or HClO₄ on the catalytic hydroxylation of cyclohexane and benzene by **2** and H₂O₂.

6.3 Activation of $[(\beta\text{-BPMCN})\text{Fe}^{\text{III}}\text{-OOH}]^{2+}$ intermediate using $\text{Fe}^{\text{III}}(\text{OTf})_3$: possible implications for O_2 activation by diiron systems

In Chapter 3, we have demonstrated that $\text{Fe}^{\text{III}}(\text{OTf})_3$ can act as a Lewis acid to activate the catalytic system of $[\text{Fe}^{\text{II}}(\beta\text{-BPMCN})]^{2+}$ (**2**) and H_2O_2 to form a reactive high-valent iron-oxidant. In the presence of 2 eq of $\text{Fe}^{\text{III}}(\text{OTf})_3$ (relative to **2**), a 15-fold increase is observed in the cyclohexanol yield compared to that obtained in the absence of any additive. Additionally, very little cyclohexanone is formed, leading to a high alcohol-to-ketone (A/K) ratio value of 75. $\text{Fe}^{\text{III}}(\text{OTf})_3$ is 50% more effective than $\text{Sc}^{\text{III}}(\text{OTf})_3$ or HClO_4 in cyclohexane hydroxylation. In the case of benzene hydroxylation also, $\text{Fe}^{\text{III}}(\text{OTf})_3$ is about 30 % more effective from $\text{Sc}^{\text{III}}(\text{OTf})_3$ or HClO_4 . Mechanistic experiments support the formation of a metal-based oxidant from **2** and H_2O_2 in the presence of $\text{Fe}^{\text{III}}(\text{OTf})_3$, similar to $\text{Sc}^{\text{III}}(\text{OTf})_3$ and HClO_4 . Hence, it is concluded that $\text{Fe}^{\text{III}}(\text{OTf})_3$ is acting as a Lewis acid similar to $\text{Sc}^{\text{III}}(\text{OTf})_3$, and activates the otherwise inefficient catalytic system of **2** and H_2O_2 . The higher Lewis acidity of Fe^{3+} (2.2) than Sc^{3+} (4.3) explains the more significant effect of Fe^{3+} on the catalytic reactivity of **2**. On the other hand, Fe^{2+} (9.5) has a much lower Lewis acidity compared to both Fe^{3+} and Sc^{3+} and is found to be ineffective in activating the catalytic reactivity of **2** and H_2O_2 .

We performed kinetic studies to understand the effect of Fe^{3+} and Fe^{2+} on the $\text{Fe}^{\text{III}}\text{-OOH}$ intermediate **2a**. Similar to Sc^{3+} , the addition of Fe^{3+} to **2a** in the presence of benzene results in the formation of the $\text{Fe}^{\text{III}}\text{-OPh}$ adduct (**2b**) within seconds, the rate of which matches the decay rate of **2a** upon addition of Fe^{3+} in the presence of cyclohexane (Figure 6.3a). Kinetic results suggest that Fe^{3+} reacts with the intermediate **2a** to form the active

oxidant, similar to Sc^{3+} . However, the rate of reaction of Fe^{3+} with **2a** is about 3-fold slower than Sc^{3+} , indicating that the nature of the Lewis acid influences its interaction with **2a** (Figure 6.3a). The addition of Fe^{2+} to **2a** in the presence of benzene does not result in the formation of **2b**, instead **2a** decays, when the reaction is monitored for the same time duration as for the reaction with Fe^{3+} or Sc^{3+} (for ~ 100 s). However, upon monitoring the reaction for a longer duration of 20–30 min, we have observed that after the initial decay of **2a** within 100 s, a small amount of **2b** forms. Hence, Fe^{2+} first deactivates **2a** by reducing it to form Fe^{3+} , which then can form phenol. In contrast, Fe^{3+} activates **2a** directly by breaking the O–O bond in **2a** to form the potent Fe^{V} oxidant.

Diiron enzymes use two iron atoms to activate O_2 and form the active oxidant, whereas monoiron enzymes can activate O_2 using a single iron atom (with the help of co-factors and substrates), which raises question about the role of the second iron in the former.^{1,2} The diiron enzyme sMMO has been proposed to form a diiron(III) peroxo intermediate **P**, which in turn forms the oxidant **Q** that oxidizes methane to methanol.^{6,20} The cleavage of the O–O bond in **P** to form **Q** involves a proton with a $\text{pK}_a \sim 7.6$.^{21,22} Our work in this chapter shows that a second Fe^{III} center can act as a Lewis acid and activate an $\text{Fe}^{\text{III}}\text{-OOH}$ intermediate to form an Fe^{V} oxidant. The protonated intermediate **P** can be considered similar to an Fe^{III} -adduct of the $\text{Fe}^{\text{III}}\text{-OOH}$ species **2a** (Figure 6.3b). Furthermore, in our studies, we propose the oxidant to be a nascent $[(\text{L})\text{Fe}^{\text{V}}=\text{O}]^{3+}$ species. However, it can be envisioned that the Lewis acidic Fe^{III} ion interacts with the Fe^{V} oxidant to form an $\text{O}=\text{Fe}^{\text{V}}\text{-OH-Fe}^{\text{III}}$ adduct, which can then be related to the oxidant **Q** (Figure 6.3). This $\text{O}=\text{Fe}^{\text{V}}\text{-OH-Fe}^{\text{III}}$ adduct is an electromer of the two proposed structures (**I** and

III) for **Q**^{23–25} (Figure 6.3). This work on activating an Fe^{III}–OOH intermediate by a second Fe^{III} ion is unprecedented in nonheme iron chemistry, and introduces the idea that the second iron in the active site of sMMO is not only present for its redox capabilities, but can also act as a Lewis acid to promote the O–O bond cleavage in the intermediate **P**, forming the oxidant **Q** that oxidizes methane to methanol.

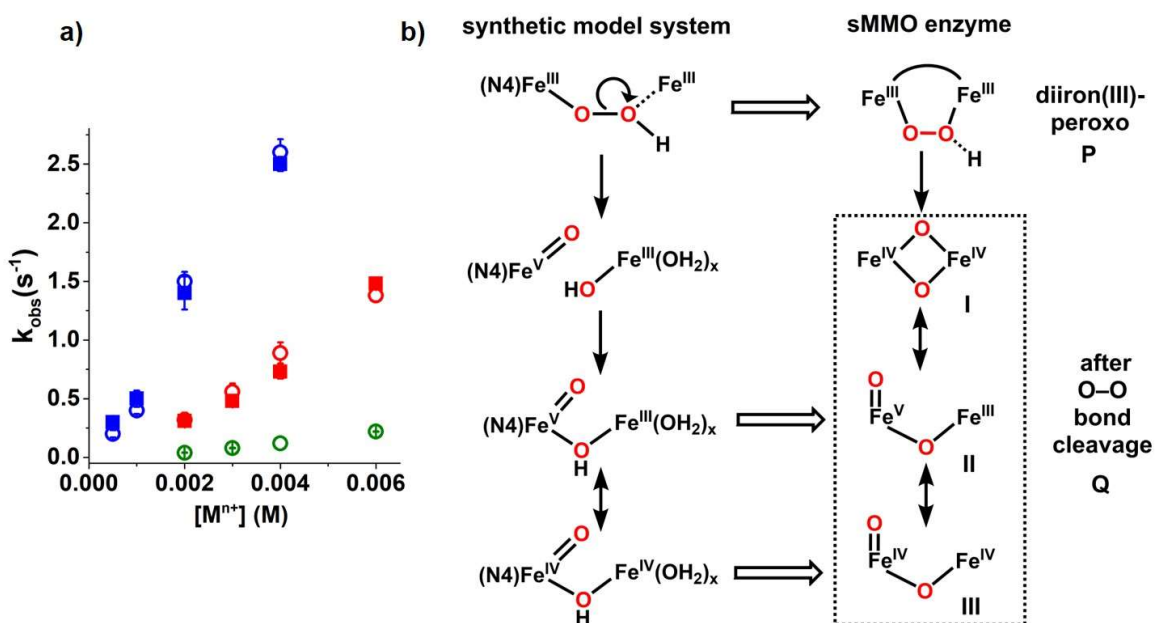


Figure 6.3 a) M^{n+} (Sc^{3+} , Fe^{3+} , Fe^{2+}) concentration dependence on rates of **2b** formation or **2a** decay at $-40\text{ }^\circ\text{C}$. Sc^{3+} (blue); Fe^{3+} (red) and Fe^{2+} (green). Open circles for benzene and filled squares for cyclohexane. b) Comparison between the activation of **2** by $\text{Fe}^{\text{III}}(\text{OTf})_3$ and the proton-activated diiron(III)-peroxo intermediate of soluble methane monooxygenase. **I**, **II** and **III** are the three plausible structures proposed for **Q**.

6.4 Effect of ligand topology on Sc³⁺-assisted activation of Fe^{III}-OOH intermediates to form high-valent iron-oxidants

[Fe^{II}(β -BPMCN)]²⁺ (**2**) has a topological isomer [Fe^{II}(α -BPMCN)]²⁺ (**1**), which was reported along with **2** in 2002.¹⁷ **1** and **2** have very different reactivity trends, and in contrast to **2**, **1** is found to be an efficient catalyst for cyclohexane hydroxylation. In Chapter 4, we have compared the effect of Sc³⁺ on the catalytic reactivity of **1**/H₂O₂ with that of **2**/H₂O₂. Furthermore, we also studied the effects of Sc³⁺ on the catalytic reactivity of [Fe^{II}(TPA)]²⁺ (**3**), one of the most extensively studied nonheme iron catalysts.^{19,26,27}

Lewis acidic Sc(OTf)₃ affects the reactivity of both **1** and **3** but the effects are very different from that of **2**. For both **1** and **3**, the desired oxidation reaction occurs faster than the unproductive side reactions in the presence of Sc³⁺, but the oxidants formed under both conditions are equally efficient in oxidizing cyclohexane, forming the same amount of cyclohexanol. On the other hand, for **2** the oxidant formed in the presence of Sc³⁺ enhances the yield of cyclohexanol by 10-fold. Furthermore, the oxidant formed in the presence of Sc³⁺ also allows **2**/H₂O₂ to hydroxylate benzene, which does not occur in its absence. Also in the case of **3**, Sc³⁺ enhances the yield of phenol by up to 20-fold. On contrary, for **1**-catalyzed benzene hydroxylation, the presence of Sc³⁺ does not have a significant effect on the yield of phenol, but the reaction occurs about two orders of magnitude faster than in the absence of Sc³⁺. The differences between **1** and **2** show the importance of ligand topology in the Sc³⁺-assisted mechanism. Additionally, these results suggest that **1** and **3** behave differently in the presence of Sc³⁺, even though they have been previously proposed to follow the same water-assisted mechanism and form similar oxidants.¹⁷

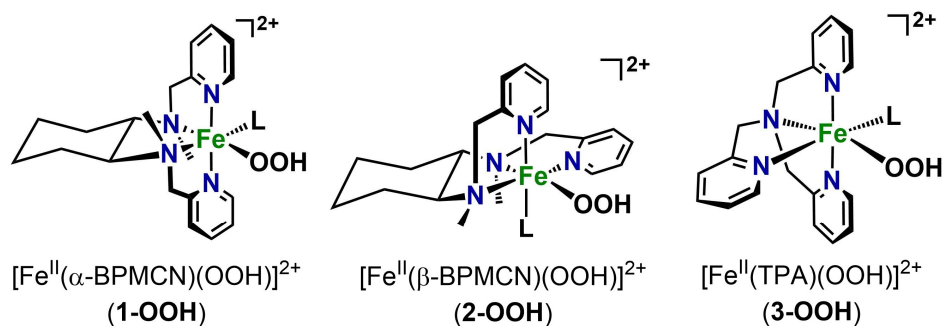


Figure 6.4 ChemDraw representations of the three $\text{Fe}^{\text{III}}\text{-OOH}$ intermediates compared in this chapter.

Here, we have characterized the $S = 1/2$ $\text{Fe}^{\text{III}}\text{-OOH}$ intermediate (**1-OOH**) generated from the reaction of **1** and H_2O_2 , and spectroscopically **1-OOH** looks similar to **2-OOH**²⁸ (Chapter 2) and **3-OOH**^{14,29}, the $\text{Fe}^{\text{III}}\text{-OOH}$ species formed from **2** and **3**, respectively (Figure 6.4). However, the kinetics of their formation and decay differ from each other, suggesting that the ligand topology influences the reactivity of the $\text{Fe}^{\text{III}}\text{-OOH}$ intermediates. Here, we have shown that both **1-OOH** and **2-OOH** are not the actual oxidants but are precursors to the actual oxidants in their respective catalytic systems, similar to the case of **3-OOH**²⁷. Previously, in Chapters 2 and 3, we have demonstrated that the $\text{Fe}^{\text{III}}\text{-OOH}$ species reacts with Lewis acid to form the active oxidant. Here, in Chapter 4, we show that **2-OOH** reacts with Sc^{3+} 10-fold faster than **1-OOH** and 100-fold faster than **3-OOH** at -20 °C. Thus, it implies that **2-OOH** is most nucleophilic followed by **1-OOH** and **3-OOH**. This electronic character of the $\text{Fe}^{\text{III}}\text{-OOH}$ species can be further extended to the oxidant formed from these intermediates in the absence of any additive, suggesting that the oxidant formed from **2-OOH** will be more nucleophilic than the one

derived from **1-OOH**. This idea is indeed supported by the reactivity trends reported for **1** and **2** in 2014,³⁰ where it was concluded that **2** forms a nucleophilic oxidant and **1** forms an electrophilic oxidant in the absence of any additive. This work highlights the importance of ligand topology in tuning the reactivity of the catalyst and its effect on the Sc³⁺-assisted mechanism. Thus, even if two Fe^{III}-OOH intermediates look spectroscopically similar, they might have different electronic nature leading to different oxidants. Additionally, this work shows that reaction of Fe^{III}-OOH species with Lewis acidic Sc(OTf)₃ can be used as a probe to determine its electronic nature and predict the nature of the oxidant formed thereof.

6.5 Generation and characterization of high-valent iron species from Fe^{IV}(O) intermediates supported by a macrocyclic ligand framework

High-valent Fe^V intermediates are proposed to be the oxidant in many synthetic nonheme iron catalytic systems developed so far.^{7,16,31,32} Additionally, Rieske oxygenases have been proposed to involve Fe^V oxidants in their mechanisms.⁸ Scientists have been trying to trap and characterize Fe^V intermediates in order to study their reactivity for a long time. Over the past two decades, more than 80 nonheme Fe^{IV}(O) intermediates have been characterized synthetically.³³ However, less than 10 nonheme Fe^V(O) species have been trapped in the same time.^{18,31} In most catalytic systems that invoke Fe^V(O) oxidants, the Fe^V(O) species is too reactive to be observed spectroscopically. In 2012, a nonheme Fe^V(O)³⁴ intermediate supported by the neutral macrocyclic ligand TMC was generated

from the corresponding $\text{Fe}^{\text{IV}}(\text{O})^{35}$ complex, which was the first crystallographically characterized $\text{Fe}^{\text{IV}}(\text{O})$ species. There are two topological isomers of the TMC-supported $\text{Fe}^{\text{IV}}(\text{O})$ complex, one with the oxo unit on the opposite side as the methyl groups of TMC, the *anti* isomer (**4**) reported in 2003,³⁵ and the other with the oxo moiety on the same side as the methyl groups of TMC, the *syn* isomer (**5**) reported in 2015.³⁶ The *syn* isomer is less stable than the *anti* isomer. The Fe^{V} species (**4a**) (Figure 6.5) reported in 2012 was generated from the more stable *anti* isomer **4**. Here, our goal was to trap the Fe^{V} species from the less stable *syn* isomer **5**.

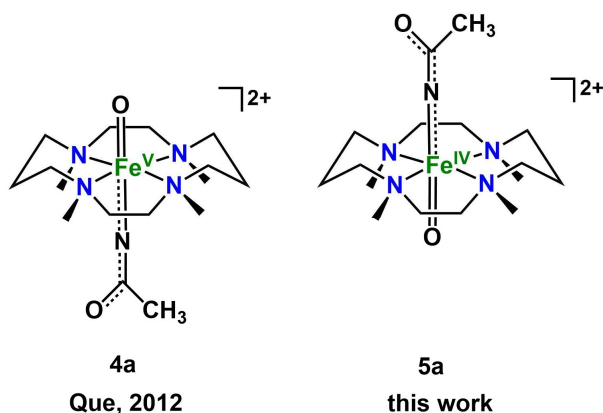


Figure 6.5 The reported $[(\text{TMC})\text{Fe}^{\text{V}}(\text{O})\text{NC}(\text{O})\text{CH}_3]^{2+}$ **4a**³⁴ generated from the *anti* isomer of $[(\text{TMC})\text{Fe}^{\text{IV}}(\text{O})]^{2+}$ **4**, and the isomeric Fe^{V} species **5a** studied in this work, which is generated from the *syn* isomer of $[(\text{TMC})\text{Fe}^{\text{IV}}(\text{O})]^{2+}$ **5**.

We have successfully generated the Fe^{V} species (**5a**) (Figure 6.5) from the *syn* isomer of the $[(\text{TMC})\text{Fe}^{\text{IV}}(\text{O})]^{2+}$ (**5**) complex via one-electron oxidation of the $\text{Fe}^{\text{IV}}(\text{O})$ precursor **5** using ¹BuOOH and a base in a stoichiometric fashion. The intermediate **5a** exhibits an $S = 1/2$ EPR signal with g values of 2.05, 2.01, 1.97 confirming the +5 oxidation

state of the iron center. From UV-visible and EPR spectroscopies, the two isomeric Fe^V intermediates **4a** and **5a** look similar, however, **5a** is more reactive (half life of 53 s at -40 °C) than **4a** (half-life of 60 min at -44 °C). An acetylimido ligand is bound *trans* to the oxo unit in **4a**, which can be protonated to form a conjugate acid complex **4a-H⁺**.³⁴ Here we have generated the conjugate acid of **5a** (**5a-H⁺**) with HClO₄. **5a-H⁺** is less stable (half life of 7 s at -40 °C) than **4a-H⁺** (half-life of 30 min at -44 °C). This work shows that the Fe^V species **5a** and **5a-H⁺**, generated from the *syn* isomer of the Fe^{IV}(O) complex (**5**), have spectroscopic features similar to **4a** and **4a-H⁺**, derived from the *anti* isomer of the Fe^{IV}(O) species (**4**). However, **5a** and **5a-H⁺** are observed to be kinetically more reactive compared to **4a** and **4a-H⁺**.

The interaction of Lewis acids with Fe^{IV}(O) complexes is well documented in the literature,^{37,38} however, little is known about the effect of Lewis acids on Fe^V complexes. Upon addition of Sc³⁺ to **4a**, a new Fe^V species is observed to form **4a-Sc³⁺**. The Fe=O vibration frequency for **4a-Sc³⁺** (805 cm⁻¹) lies between **4a** (797 cm⁻¹) and **4a-H⁺** (812 cm⁻¹). Based on the differences between **4a-Sc³⁺** and **4a-H⁺**, we propose that the Sc³⁺ in **4a-Sc³⁺** might be interacting with a different site like the oxo moiety on **4a** than the H⁺ in **4a-H⁺**, which interacts with the anionic acetylimido ligand bound *trans* to the oxo unit. Further experiments are needed to identify the site of interaction of the Sc³⁺. We also trapped the Sc³⁺ adduct of **5a**, **5a-Sc³⁺** and like before **5a-Sc³⁺** (half life of 37 s at -40 °C) was less stable than **4a-Sc³⁺** (half life of 20 min at -40 °C). Interestingly, the Sc³⁺-adduct **5a-Sc³⁺** is more stable compared to the conjugate acid **5a-H⁺**. The difference in the reactivity between the two set of isomeric Fe^V complexes can attributed to the different accessibility of the

oxo moiety in the two topological settings. This work shows that the topology around the iron center affects the reactivity of the Fe^V centers, and thus we should remember the importance of topology while developing reactive high-valent iron intermediates for oxidizing organic substrates.

6.6 Future directions

The study of nonheme high-valent iron intermediates and the different pathways to form them will continue to be a topic of great interest in bioinorganic chemistry as we develop nonheme iron catalysts for performing oxidative transformations. Iron being the most abundant metal on earth will remain a metal of choice for designing catalysts for oxidation reactions. Furthermore, examples of nonheme iron enzymes performing a wide range of difficult oxidative transformations using environmentally friendly oxidant O₂ inspire scientists and make the field of nonheme iron chemistry an important area of research in science.

This work developed a new route for accessing a powerful electrophilic oxidant in the interesting landscape of high-valent nonheme iron oxidants. We have shown that addition of a strong Lewis acid like Sc(OTf)₃ or a Brønsted acid like HClO₄ to the reaction mixture of the nonheme iron catalyst **2** and H₂O₂ leads to the formation of a highly electrophilic oxidant that can hydroxylate cyclohexane and benzene with comparable catalytic efficiency, a combination of transformations rarely observed for synthetic nonheme iron catalysts.^{7,16,32} This Sc³⁺- or HClO₄-assisted route has the ability to

hydroxylate benzene and cyclohexane within seconds at -40 °C. One question in this project that is yet to be answered is how strong is the oxidant formed in the presence of Sc^{3+} or HClO_4 . It will be interesting to see what other substrates with C–H bonds stronger than cyclohexane can be oxidized by this oxidant, and finally will it be able to oxidize methane containing the strongest aliphatic C–H bonds (105 kcal/mol).

We have demonstrated that Fe^{3+} can also act as a Lewis acid and activate the $\text{Fe}^{\text{III}}\text{-OOH}$ species **2a** to form a potent oxidant, like Sc^{3+} . In fact, Fe^{3+} is a stronger Lewis acid compared to Sc^{3+} and higher yields of cyclohexanol and phenol are observed in the presence of Fe^{3+} than Sc^{3+} . However, Sc^{3+} reacts three-fold faster with **2a** than Fe^{3+} , indicating that the nature of the Lewis acid plays a role. Thus, it will be important to determine what properties of the Lewis acid control the kinetics of their reaction with the $\text{Fe}^{\text{III}}\text{-OOH}$ intermediate **2a**.

Catalysts **1** and **2** are topological isomers with very different reactivity trends.^{17,30} Catalyst **1** forms an electrophilic oxidant like **3**, which is one of the most well-studied nonheme iron catalyst.^{17,30} On the other hand, **2** is unique as the nature of the active oxidant formed can be tuned by various additives to catalyze four distinct reactions.^{17,28,30} Here we have shown that Sc^{3+} reacts 10-fold faster with the $\text{Fe}^{\text{III}}\text{-OOH}$ species derived from **2** (**2-OOH**) than the one derived from **1** (**1-OOH**). This work highlights the importance of ligand topology around the iron center and how it affects the reactivity of the intermediates and the oxidants formed thereof. Thus, other pairs of topological isomers could be studied to understand the factors that cause this difference in the reactivity. Additionally,

computational studies should be performed on **1** and **2** to see which aspect of the iron complex, sterics, electronics or both, give rise to the observed difference in reactivity.

In Chapter 5, we have generated five new Fe^V species via one-electron oxidation of Fe^{IV}(O) complexes under different conditions. The Fe^V intermediates **5a** and **5a-H⁺** generated from the *syn* [(TMC)Fe^{IV}(O)]²⁺ complex are more reactive compared to the previously reported ones³⁴ generated from the *anti* [(TMC)Fe^{IV}(O)]²⁺ complex. Detailed studies on the reactivity of these complexes will help us understand more about the characteristics of the Fe^V intermediates and the factors that affect their reactivity. Furthermore, we have shown that Sc³⁺ interacts with the Fe^V intermediates **4a** and **5a**, forming Sc³⁺ adducts **4a-Sc³⁺** and **5a-Sc³⁺**. Further structural characterization of **4a-Sc³⁺** and **5a-Sc³⁺** will be helpful to understand the interaction of Sc³⁺ with the Fe^V intermediates. Extended X-ray absorption fine structure spectroscopy will be a good technique to understand the interaction of Sc³⁺ with **5a** since the adduct **5a-Sc³⁺** is not stable at -40 °C, unlike **4a-Sc³⁺**, for which X-ray crystallography could be used. Another strategy that could help in this study would be to prolong the lifetime of these intermediates by generating them in a different solvent system that could go to temperatures below -40 °C before freezing.

I wish all the best to the future aspiring bioinorganic chemists who decide to pursue these exciting challenges.

6.7 References

- (1) Kal, S.; Que, L. *J. Biol. Inorg. Chem.* **2017**, *22*, 339–365.
- (2) Jasniewski, A. J.; Que, L. *Chem. Rev.* **2018**, *118*, 2554–2592.
- (3) Krebs, C.; Fujimori, D. G.; Walsh, C. T.; Bollinger, J. M. *Acc. Chem. Res.* **2007**, *40*, 484–492.
- (4) Lipscomb, J. D. *J. Biol. Chem.* **2014**, *289*, 15141–15153.
- (5) Kovaleva, E. G.; Lipscomb, J. D. *Nat. Chem. Biol.* **2008**, *4*, 186–193.
- (6) Wallar, B. J.; Lipscomb, J. D. *Chem. Rev.* **1996**, *96*, 2625–2657.
- (7) Olivo, G.; Cussó, O.; Borrell, M.; Costas, M. *J. Biol. Inorg. Chem.* **2017**, *22*, 425–452.
- (8) Barry, S. M.; Challis, G. L. *ACS Catal.* **2013**, *3*, 2362–2370.
- (9) Dror, A.; Fishman, A. *Comput Struct Biotechnol J* **2012**, *2*, e201209011.
- (10) Nakashima, Y.; Mori, T.; Nakamura, H.; Awakawa, T.; Hoshino, S.; Senda, M.; Senda, T.; Abe, I. *Nat. Commun.* **2018**, *9*, 104.
- (11) Hunt, A. J.; Farmer, T. J.; Clark, J. H. In *Element Recovery and Sustainability*; 2013; pp 1–28.
- (12) Crabtree, R. H. *Chem. Rev.* **2010**, *110*, 575.
- (13) Frey, P. A.; Reed, G. H. *ACS Chem. Biol.* **2012**, *7*, 1477–1481.
- (14) Kim, C.; Chen, K.; Kim, J.; Que, L. *J. Am Chem. Soc.* **1997**, *119*, 5964–5965.
- (15) Costas, M.; Chen, K.; Que, L. *Coord. Chem. Rev.* **2000**, *200–202*, 517–544.
- (16) Company, A.; Lloret-Fillol, J.; Costas, M. In *Comprehensive Inorganic Chemistry II*; Elsevier Ltd., 2013; 487.

- (17) Costas, M.; Que, L. *Angew. Chem. Int. Ed.* **2002**, *41*, 2179–2181.
- (18) Serrano-Plana, J.; Oloo, W. N.; Acosta-Rueda, L.; Meier, K. K.; Verdejo, B.; García-España, E.; Basallote, M. G.; Münck, E.; Que, L.; Company, A.; Costas, M. *J. Am. Chem. Soc.* **2015**, *137*, 15833–15842.
- (19) Chen, K.; Que, L. *J. Am. Chem. Soc.* **2001**, *123*, 6327–6337.
- (20) Tinberg, C. E.; Lippard, S. J. *Acc. Chem. Res.* **2011**, *44*, 280–288.
- (21) Lee, S.-K.; Lipscomb, J. D. *Biochemistry* **1999**, *38*, 4423–4432.
- (22) Tinberg, C. E.; Lippard, S. J. *Biochemistry* **2009**, *48*, 12145–12158.
- (23) Banerjee, R.; Proshlyakov, Y.; Lipscomb, J. D.; Proshlyakov, D. A. *Nature* **2015**, *518*, 431–434.
- (24) Castillo, R. G.; Banerjee, R.; Allpress, C. J.; Rohde, G. T.; Bill, E.; Que, L.; Lipscomb, J. D.; DeBeer, S. *J. Am. Chem. Soc.* **2017**, *139*, 18024–18033.
- (25) Cutsail III, G. E.; Banerjee, R.; Zhou, A.; Que, L.; Lipscomb, J. D.; DeBeer, S. *J. Am. Chem. Soc.* **2018**, *140*, 16807–16820.
- (26) Chen, K.; Costas, M.; Kim, J.; Tipton, A. K.; Que, L. *J. Am. Chem. Soc.* **2002**, *124*, 3026–3035.
- (27) Oloo, W. N.; Fielding, A. J.; Que, L. *J. Am. Chem. Soc.* **2013**, *135*, 6438–6441.
- (28) Kal, S.; Draksharapu, A.; Que, L. *J. Am. Chem. Soc.* **2018**, *140*, 5798–5804.
- (29) Ho, R. Y. N.; Roelfes, G.; Feringa, B. L.; Que, L. *J. Am. Chem. Soc.* **1999**, *121*, 264–265.
- (30) Iyer, S. R.; Javadi, M. M.; Feng, Y.; Hyun, M. Y.; Oloo, W. N.; Kim, C.; Que, L. *Chem. Commun.* **2014**, *50*, 13777–13780.

- (31) Lyakin, O. Y.; Bryliakov, K. P.; Talsi, E. P. *Coord. Chem. Rev.* **2019**, *384*, 126–139.
- (32) Bryliakov, K. P.; Talsi, E. P. *Coord. Chem. Rev.* **2014**, *276*, 73–96.
- (33) Klein, J. E. M. N.; Que, L. *Encyclopedia of Inorganic and Bioinorganic Chemistry*; 2016; DOI: 10.1002/9781119951438.eibc2344.
- (34) Van Heuvelen, K. M.; Fiedler, A. T.; Shan, X.; De Hont, R. F.; Meier, K. K.; Bominaar, E. L.; Münck, E.; Que, L. *Proc. Natl. Acad. Sci.* **2012**, *109*, 11933–11938.
- (35) Rohde, J.-U.; In, J. H.; Lim, M. H.; Brenessel, W. W.; Bukowski, M. R.; Stubna, A.; Munck, E.; Nam, W.; Que, Jr., L. *Science* **2003**, *299*, 1037–1039.
- (36) Prakash, J.; Rohde, G. T.; Meier, K. K.; Münck, E.; Que, L. *Inorg. Chem.* **2015**, *54*, 11055–11057.
- (37) Fukuzumi, S. *Coord. Chem. Rev.* **2013**, *257*, 1564–1575.
- (38) Fukuzumi, S.; Ohkubo, K.; Lee, Y. M.; Nam, W. *Chem. Eur. J.* **2015**, *21*, 17548–17559.

Comprehensive list of references

At the end of each chapter, the references cited in that chapter have been listed with proper reference numbering as used in the body of each chapter. Following is a comprehensive list of all the references used in the preparation of this dissertation. Note, the reference numbers in the following list do not correspond to the reference numbers in the text of the dissertation.

- (1) Rohde, J.-U.; In, J. H.; Lim, M. H.; Brenessel, W. W.; Bukowski, M. R.; Stubna, A.; Munck, E.; Nam, W.; Que, Jr., L. *Science* **2003**, *299*, 1037–1039.
- (2) Prakash, J.; Rohde, G. T.; Meier, K. K.; Münck, E.; Que, L. *Inorg. Chem.* **2015**, *54*, 11055–11057.
- (3) Van Heuvelen, K. M.; Fiedler, A. T.; Shan, X.; De Hont, R. F.; Meier, K. K.; Bominaar, E. L.; Münck, E.; Que, L. *Proc. Natl. Acad. Sci.* **2012**, *109*, 11933–11938.
- (4) Kovaleva, E. G.; Lipscomb, J. D. *Nat. Chem. Biol.* **2008**, *4*, 186–193.
- (5) Kal, S.; Que, L. *J. Biol. Inorg. Chem.* **2017**, *22*, 339–365.
- (6) Olivo, G.; Cussó, O.; Borrell, M.; Costas, M. *J. Biol. Inorg. Chem.* **2017**, *22*, 425–452.
- (7) Hölzl, S. M.; Altmann, P. J.; Kück, J. W.; Kühn, F. E. *Coord. Chem. Rev.* **2017**, *352*, 517–536.
- (8) Gamba, I.; Codolà, Z.; Lloret-fillol, J.; Costas, M. *Coord. Chem. Rev.* **2017**, *334*, 2–24.
- (9) Bryliakov, K. P.; Talsi, E. P. *Coord. Chem. Rev.* **2014**, *276*, 73–96.
- (10) Costas, M.; Mehn, M. P.; Jensen, M. P.; Que, L. *Chem. Rev.* **2004**, *104*, 939–986.
- (11) Fenton, H. J. H. *J. Chem. Soc.* **1894**, *65*, 899–910.
- (12) Wardman, P.; Candeias, L. P. *Radiat. Res.* **1996**, *145*, 523–531.

- (13) Costas, M.; Chen, K.; Que, L. *Coord. Chem. Rev.* **2000**, *200–202*, 517–544.
- (14) Kim, C.; Chen, K.; Kim, J.; Que, L. *J. Am. Chem. Soc.* **1997**, *119*, 5964–5965.
- (15) Chen, K.; Jr., L. Q. *Chem. Commun.* **1999**, No. 15, 1375–1376.
- (16) Chen, K.; Que, L. *Angew. Chem. Int. Ed.* **1999**, *95*, 2227–2229.
- (17) Barry, S. M.; Challis, G. L. *ACS Catal.* **2013**, *3*, 2362–2370.
- (18) Company, A.; Lloret-Fillol, J.; Costas, M. In *Comprehensive Inorganic Chemistry II*; Elsevier Ltd., 2013; p 487.
- (19) Chen, K.; Que, L. *J. Am. Chem. Soc.* **2001**, *123*, 6327–6337.
- (20) Chen, K.; Costas, M.; Kim, J.; Tipton, A. K.; Que, L. *J. Am. Chem. Soc.* **2002**, *124*, 3026–3035.
- (21) Costas, M.; Tipton, A. K.; Chen, K.; Jo, D. H.; Que L., J. *J. Am. Chem. Soc.* **2001**, *123*, 6722–6723.
- (22) Zima, A. M.; Lyakin, O. Y.; Bryliakov, K. P.; Talsi, E. P. *Mol. Catal.* **2018**, *455*, 6–13.
- (23) Simmons, E. M.; Hartwig, J. F. *Angew. Chem. Int. Ed.* **2012**, *51*, 3066–3072.
- (24) Bernadou, J.; Meunier, B. *Chem. Commun.* **1998**, 2167–2173.
- (25) Schröder, M. *Chem. Rev.* **1980**, *80*, 187–213.
- (26) Oloo, W. N.; Fielding, A. J.; Que, L. *J. Am. Chem. Soc.* **2013**, *135*, 6438–6441.
- (27) Zang, Y.; Kim, J.; Dong, Y.; Wilkinson, E. C.; Appelman, E. H.; Que, L. *J. Am. Chem. Soc.* **1997**, *119*, 4197–4205.
- (28) Makhlynets, O. V.; Rybak-Akimova, E. V. *Chem. Eur. J.* **2010**, *16*, 13995–14006.
- (29) White, M. C.; Doyle, A. G.; Jacobsen, E. N. *J. Am. Chem. Soc.* **2001**, *123*, 7194–7195.
- (30) Mas-Balleste, R.; Que, L. *J. Am. Chem. Soc.* **2007**, *129*, 15964–15972.
- (31) Mas-Balleste, R.; Fujita, M.; Que, L. *Dalton Trans.* **2008**, 1828–1830.

- (32) Das, P.; Que, L. *Inorg. Chem.* **2010**, *49*, 9479–9485.
- (33) Chen, M. S.; White, M. C. *Science* **2010**, *327*, 566–571.
- (34) Lyakin, O. Y.; Bryliakov, K. P.; Britovsek, G. J. P.; Talsi, E. P. *J. Am. Chem. Soc.* **2009**, *131*, 10798–10799.
- (35) Oloo, W. N.; Meier, K. K.; Wang, Y.; Shaik, S.; Münck, E.; Que, L. *Nat. Commun.* **2014**, *5*, 3046–3054.
- (36) Oloo, W. N.; Banerjee, R.; Lipscomb, J. D.; Que, L. *J. Am. Chem. Soc.* **2017**, *139*, 17313–17326.
- (37) Prat, I.; Mathieson, J. S.; Güell, M.; Ribas, X.; Luis, J. M.; Cronin, L.; Costas, M. *Nat. Chem.* **2011**, *3*, 788–793.
- (38) Xu, S.; Veach, J. J.; Oloo, W.; Peters, K. C.; Wang, J.; Perry, R. H.; Que, L. *Chem. Commun.* **2018**, *54*, 8701–8704.
- (39) Hitomi, Y.; Arakawa, K.; Funabiki, T.; Kodera, M. *Angew. Chem. Int. Ed.* **2012**, *51*, 3448–3452.
- (40) Borrell, M.; Andris, E.; Navrátil, R.; Roithová, J.; Costas, M. *Nat. Commun.* **2019**, *10*, 1–9.
- (41) Tiago de Oliveira, F.; Chanda, A.; Banerjee, D.; Shan, X.; Mondal, S.; Que, L.; Bominaar, E. L.; Münck, E.; Collins, T. J. *Science* **2007**, *315*, 835–838.
- (42) Klein, J. E. M. N.; Que, L. *Encyclopedia of Inorganic and Bioinorganic Chemistry*; 2016; p DOI: 10.1002/9781119951438.eibc2344.
- (43) Kundu, S.; Van Thompson, J. K.; Shen, L. Q.; Mills, M. R.; Bominaar, E. L.; Ryabov, A. D.; Collins, T. J. *Chem. Eur. J.* **2015**, *21*, 1803–1810.
- (44) Ghosh, M.; Singh, K. K.; Panda, C.; Weitz, A.; Hendrich, M. P.; Collins, T. J.; Dhar, B. B.; Gupta, S. Sen. *J. Am. Chem. Soc.* **2014**, *136*, 9524–9527.
- (45) Pattanayak, S.; Jasniewski, A. J.; Rana, A.; Draksharapu, A.; Singh, K. K.; Weitz, A.; Hendrich, M.; Que, L.; Dey, A.; Gupta, S. Sen. *Inorg. Chem.* **2017**, *56*, 6352–

6361.

- (46) McDonald, A. R.; Que, L. *Coord. Chem. Rev.* **2013**, *257*, 414–428.
- (47) Lyakin, O. Y.; Zima, A. M.; Samsonenko, D. G.; Bryliakov, K. P.; Talsi, E. P. *ACS Catal.* **2015**, *5*, 2702–2707.
- (48) Serrano-Plana, J.; Oloo, W. N.; Acosta-Rueda, L.; Meier, K. K.; Verdejo, B.; García-España, E.; Basallote, M. G.; Münck, E.; Que, L.; Company, A.; Costas, M. *J. Am. Chem. Soc.* **2015**, *137*, 15833–15842.
- (49) Fan, R.; Serrano-Plana, J.; Oloo, W. N.; Draksharapu, A.; Delgado-pinar, E.; Company, A.; Martin-Diaconescu, V.; Borrell, M.; Lloret-Fillol, J.; García-España, E.; Guo, Y.; Bominaar, E. L.; Que, L.; Costas, M.; Munck, E. *J. Am. Chem. Soc.* **2018**, *140*, 3916–3928.
- (50) Lyakin, O. Y.; Zima, A. M.; Tkachenko, N. V.; Bryliakov, K. P.; Talsi, E. P. *ACS Catal.* **2018**, *8*, 5255–5260.
- (51) Costas, M.; Que, L. *Angew. Chem. Int. Ed.* **2002**, *41*, 2179–2181.
- (52) Oloo, W. N.; Que, L. *Acc. Chem. Res.* **2015**, *48*, 2612–2621.
- (53) Fukuzumi, S. *Coord. Chem. Rev.* **2013**, *257*, 1564–1575.
- (54) Fukuzumi, S.; Ohkubo, K.; Lee, Y. M.; Nam, W. *Chem. Eur. J.* **2015**, *21*, 17548–17559.
- (55) Dong, L.; Wang, Y.; Lv, Y.; Chen, Z.; Mei, F.; Xiong, H.; Yin, G. *Inorg. Chem.* **2013**, *52*, 5418–5427.
- (56) Leeladee, P.; Baglia, R. A.; Prokop, K. A.; Lati, R.; Visser, S. P. De; Goldberg, D. P. *J. Am. Chem. Soc.* **2012**, *134*, 10397–10400.
- (57) Baglia, R. A.; Krest, C. M.; Yang, T.; Leeladee, P.; Goldberg, D. P. *Inorg. Chem.* **2016**, *55*, 10800–10809.
- (58) Miller, C. G.; Gordon-Wylie, S. W.; Horwitz, C. P.; Strazisar, S. A.; Peraino, D. K.; Clark, G. R.; Weintraub, S. T.; Collins, T. J. *J. Am. Chem. Soc.* **1998**, *120*, 11540–

11541.

- (59) Hong, S.; Lee, Y.; Sankaralingam, M.; Vardhaman, A. K.; Park, Y. J.; Cho, K.-B.; Ogura, T.; Sarangi, R.; Fukuzumi, S.; Nam, W. *J. Am. Chem. Soc.* **2016**, *138*, 8523–8532.
- (60) Lam, W. W. Y.; Yiu, S. M.; Lee, J. M. N.; Yau, S. K. Y.; Kwong, H. K.; Lau, T.; Liu, D.; Lin, Z. *J. Am. Chem. Soc.* **2006**, *128*, 2851–2858.
- (61) Du, H.; Lo, P.; Hu, Z.; Liang, H.; Lau, K.; Wang, Y.-N.; Lam, W. W. Y.; Lau, T. *Chem. Commun.* **2011**, *47*, 7143–7145.
- (62) Ho, C.; Lau, T. *New J. Chem.* **2000**, *24*, 587–590.
- (63) Lau, T.; Wu, Z.; Bai, Z.; Mak, C. *J. Chem. Soc. Dalt. Trans.* **1995**, *4*, 695–696.
- (64) Yiu, S.; Man, W.; Lau, T. *J. Am. Chem. Soc.* **2008**, *130*, 10821–10827.
- (65) Li, F.; Van Heuvelen, K. M.; Meier, K. K.; Münck, E.; Que, L. *J. Am. Chem. Soc.* **2013**, *135*, 10198–10201.
- (66) Lee, Y.-M.; Bang, S.; Kim, Y. M.; Cho, J.; Hong, S.; Nomura, T.; Ogura, T.; Troeppner, O.; Ivanović-Burmazović, I.; Sarangi, R.; Fukuzumi, S.; Nam, W. *Chem. Sci.* **2013**, *4*, 3917–3923.
- (67) Zhang, J.; Wei, W.-J.; Lu, X.; Yang, H.; Chen, Z.; Liao, R.-Z.; Yin, G. *Inorg. Chem.* **2017**, *56*, 15138–15149.
- (68) Nodzevska, A.; Watkinson, M. *Chem. Commun.* **2018**, *54*, 1461–1464.
- (69) Chatterjee, S.; Paine, T. K. *Angew. Chem Int. Ed.* **2015**, *54*, 9338–9342.
- (70) <https://www.cdc.gov/niosh/ipcsneng/neng0164.html>.
- (71) <http://msdsviewer.fmc.com/private/document.aspx?prd=7722-84-1--90~~PDF~~MTR~~CPNA~~EN~~1/1/0001%2012:00:00%20AM~~HYDROGEN%20PEROXIDE%2090%~~>.
- (72) Jo, D. H.; Chiou, Y. M.; Que, J. *Inorg. Chem.* **2001**, *40*, 3181–3190.

- (73) ASTM E1840-96(2007)Standard Guide for Raman Shift Standards for Spectrometer Calibration ASTM International DOI:10.1520/E1840-96R07.
- (74) Menges, F. "Spekwin32 - optical spectroscopy software" Version 1.72.0, 2015 <http://www.ffmpeg2.de/spekwin/>.
- (75) Kobayashi, S. *European J. Org. Chem.* **1999**, 1999, 15–27.
- (76) Raba, A.; Cokoja, M.; Herrmann, W. A.; Kühn, F. E. *Chem. Commun.* **2014**, 50, 11454–11457.
- (77) Tsuji, T.; Zaoputra, A. A.; Hitomi, Y.; Mieda, K.; Ogura, T.; Shiota, Y.; Yoshizawa, K.; Sato, H.; Kodera, M. *Angew. Chem Int. Ed.* **2017**, 56, 7779–7782.
- (78) Olah, G. A. *Acc. Chem. Res.* **1971**, 4, 240–248.
- (79) Augusti, R.; Dias, A. O.; Rocha, L. L.; Lago, R. M. *J. Phys. Chem. A* **1998**, 102, 10723–10727.
- (80) Thibon, A.; Jollet, V.; Ribal, C.; Sénéchal-David, K.; Billon, L.; Sorokin, A. B.; Banse, F. *Chem. Eur. J.* **2012**, 18, 2715–2724.
- (81) Kejriwal, A.; Bandyopadhyay, P.; Biswas, A. N. *Dalton Trans.* **2015**, 44, 17261–17267.
- (82) Morimoto, Y.; Bunno, S.; Fujieda, N.; Sugimoto, H.; Itoh, S. *J. Am. Chem. Soc.* **2015**, 137, 5867–5870.
- (83) Yamada, M.; Karlin, K. D.; Fukuzumi, S. *Chem. Sci.* **2016**, 7, 2856–2863.
- (84) Iyer, S. R.; Javadi, M. M.; Feng, Y.; Hyun, M. Y.; Oloo, W. N.; Kim, C.; Que, L. *Chem. Commun.* **2014**, 50, 13777–13780.
- (85) Ho, R. Y. N.; Roelfes, G.; Feringa, B. L.; Que, L. *J. Am. Chem. Soc.* **1999**, 121, 264–265.
- (86) Roelfes, G.; Vrajmasu, V.; Chen, K.; Ho, R. Y. N.; Rohde, J. U.; Zondervan, C.; La Crois, R. M.; Schudde, E. P.; Lutz, M.; Spek, A. L.; Hage, R.; Feringa, B. L.; Münck, E.; Que, L. *Inorg. Chem.* **2003**, 42, 2639–2653.

- (87) Simaan, A. J.; Döpner, S.; Banse, F.; Bourcier, S.; Bouchoux, G.; Boussac, A.; Hildebrandt, P.; Girerd, J.-J. *Eur. J. Inorg. Chem.* **2000**, *2000*, 1627–1633.
- (88) Mekmouche, Y.; Hummel, H.; Ho, R. Y. N.; Que Jr., L.; Schünemann, V.; Thomas, F.; Trautwein, A. X.; Lebrun, C.; Gorgy, K.; Leprêtre, J.-C.; Collomb, M.-N.; Deronzier, A.; Fontecave, M.; Ménage, S. *Chem. Eur. J.* **2002**, *8*, 1196–1204.
- (89) Balland, V.; Banse, F.; Anxolabéhère-Mallart, E.; Ghiladi, M.; Mattioli, T. A.; Philouze, C.; Blondin, G.; Girerd, J. J. *Inorg. Chem.* **2003**, *42*, 2470–2477.
- (90) Oddon, F.; Chiba, Y.; Nakazawa, J.; Ohta, T.; Ogura, T.; Hikichi, S. *Angew. Chem. Int. Ed.* **2015**, *54*, 7336–7339.
- (91) Bukowski, M. R.; Comba, P.; Limberg, C.; Merz, M.; Que, L.; Wistuba, T. *Angew. Chem. Int. Ed.* **2004**, *43*, 1283–1287.
- (92) Wada, A.; Ogo, S.; Nagatomo, S.; Kitagawa, T.; Watanabe, Y.; Jitsukawa, K.; Masuda, H. *Inorg. Chem.* **2002**, *41*, 616–618.
- (93) Li, F.; Meier, K. K.; Cranswick, M. A.; Chakrabarti, M.; Van Heuvelen, K. M. .; Münck, E.; Que, L. *J. Am. Chem. Soc.* **2011**, *133*, 7256–7259.
- (94) Kitagawa, T.; Dey, A.; Lugo-Mas, P.; Benedict, J. B.; Kaminsky, W.; Solomon, E.; Kovacs, J. A. *J. Am. Chem. Soc.* **2006**, *128*, 14448–14449.
- (95) Pyrz, J. W.; Roe, A. L.; Stern, L. J.; Que, L. *J. Am. Chem. Soc.* **1985**, *107*, 614–620.
- (96) Serrano-Plana, J.; Acuña-Parés, F.; Dantignana, V.; Oloo, W. N.; Castillo, E.; Draksharapu, A.; Whiteoak, C. J.; Martin-Diaconescu, V.; Basallote, M. G.; Luis, J. M.; Que, L.; Costas, M.; Company, A. *Chem. Eur. J.* **2018**, *24*, 5331–5340.
- (97) Hong, S.; Wang, B.; Seo, M. S.; Lee, Y. M.; Kim, M. J.; Kim, H. R.; Ogura, T.; Garcia-Serres, R.; Clémancey, M.; Latour, J. M.; Nam, W. *Angew. Chem. Int. Ed.* **2014**, *53*, 6388–6392.
- (98) Seo, M. S.; Kim, N. H.; Cho, K.-B.; So, J. E.; Park, S. K.; Clémancey, M.; Garcia-Serres, R.; Latour, J.-M.; Shaik, S.; Nam, W. *Chem. Sci.* **2011**, *2*, 1039–1045.

- (99) Biswas, A. N.; Puri, M.; Meier, K. K.; Oloo, W. N.; Rohde, G. T.; Bominaar, E. L.; Münck, E.; Que, L. *J. Am. Chem. Soc.* **2015**, *137*, 2428–2431.
- (100) Price, J. C.; Barr, E. W.; Glass, T. E.; Krebs, C.; Bollinger, J. M. *J. Am. Chem. Soc.* **2003**, *125*, 13008–13009.
- (101) Mason, H. S.; Fowlks, W. L.; Peterson, E. *J. Am. Chem. Soc.* **1955**, *77*, 2914–2915.
- (102) Hayaishi, O.; Katagiri, M.; Rothberg, S. *J. Am. Chem. Soc.* **1955**, *77*, 5450–5451.
- (103) Wackett, L. P.; Kwart, L. D.; Gibson, D. T. *Biochemistry* **1988**, *27*, 1360–1367.
- (104) Banerjee, R.; Proshlyakov, Y.; Lipscomb, J. D.; Proshlyakov, D. A. *Nature* **2015**, *518*, 431–434.
- (105) Que, L.; Tolman, W. B. *Nature* **2008**, *455*, 333–340.
- (106) Jasniewski, A. J.; Que, L. *Chem. Rev.* **2018**, *118*, 2554–2592.
- (107) Tinberg, C. E.; Lippard, S. J. *Acc. Chem. Res.* **2011**, *44*, 280–288.
- (108) Wallar, B. J.; Lipscomb, J. D. *Chem. Rev.* **1996**, *96*, 2625–2657.
- (109) Krebs, C.; Fujimori, D. G.; Walsh, C. T.; Bollinger, J. M. *Acc. Chem. Res.* **2007**, *40*, 484–492.
- (110) Lee, C.-I.; Lakshmi, K. V.; Brudvig, G. W. *Biochemistry* **2007**, *46*, 3211–3223.
- (111) Tsui, E. Y.; Tran, R.; Yano, J.; Agapie, T. *Nat. Chem.* **2013**, *5*, 293–299.
- (112) Herbert, D. E.; Lionetti, D.; Rittle, J.; Agapie, T. *J. Am. Chem. Soc.* **2013**, *135*, 19075–19078.
- (113) Kal, S.; Draksharapu, A.; Que, L. *J. Am. Chem. Soc.* **2018**, *140*, 5798–5804.
- (114) Gilson, R.; Durrant, M. C. *Dalt. Trans.* **2009**, 10223–10230.
- (115) Banerjee, R.; Komor, A. J.; Lipscomb, J. D. *Methods Enzymol.* **2017**, *596*, 239–289.
- (116) Lipscomb, J. D. *J. Biol. Chem.* **2014**, *289*, 15141–15153.
- (117) Sazinsky, M. H.; Lippard, S. J. *Sustaining Life on Planet Earth: Metalloenzymes Mastering Dioxygen and Other Chewy Gases*; Sigel, A., Sigel, H., Sigel, R. K. O.,

- Kroneck, P. M. H., Sosa Torres, M. E., Eds.; Springer Berlin Heidelberg, 2015; Vol. 15.
- (118) Lee, S.-K.; Lipscomb, J. D. *Biochemistry* **1999**, *38*, 4423–4432.
- (119) Tinberg, C. E.; Lippard, S. J. *Biochemistry* **2009**, *48*, 12145–12158.
- (120) Castillo, R. G.; Banerjee, R.; Allpress, C. J.; Rohde, G. T.; Bill, E.; Que, L.; Lipscomb, J. D.; DeBeer, S. *J. Am. Chem. Soc.* **2017**, *139*, 18024–18033.
- (121) Cutsail III, G. E.; Banerjee, R.; Zhou, A.; Que, L.; Lipscomb, J. D.; DeBeer, S. *J. Am. Chem. Soc.* **2018**, *140*, 16807–16820.
- (122) Lyakin, O. Y.; Bryliakov, K. P.; Talsi, E. P. *Coord. Chem. Rev.* **2019**, *384*, 126–139.
- (123) Fujita, M.; Costas, M.; Que, L. *J. Am. Chem. Soc.* **2003**, *125*, 9912–9913.
- (124) Lippai, I.; Magliozzo, R. S.; Peisach, J. *J Am Chem Soc* **1999**, *121*, 780–784.
- (125) Jensen, K. B.; McKenzie, C. J.; Nielsen, L. P.; Pedersen, J. Z.; Svendsen, M. H. *Chem. Commun.* **1999**, 1313–1314.
- (126) Bernal, I.; Jensen, M. I.; Jensen, B. K.; McKenzie, J. C.; Toftlund, H.; Tuchagues, J. *J. Chem. Soc. Dalton Trans.* **1995**, 3667–3675.
- (127) Barefield, E. K. *Coord. Chem. Rev.* **2010**, *254*, 1607–1627.
- (128) Sastri, C. V.; Lee, J.; Oh, K.; Lee, Y. J.; Lee, J.; Jackson, T. A.; Ray, K.; Hirao, H.; Shin, W.; Halfen, J. A.; Kim, J.; Que, L.; Shaik, S.; Nam, W. *Proc. Natl. Acad. Sci.* **2007**, *104*, 19181–19186.
- (129) Prakash, J.; Sheng, Y.; Draksharapu, A.; Klein, J. E. M. N.; Cramer, C. J.; Que, L. *Angew. Chem. Int. Ed.* **2019**, *58*, 1995–1999.
- (130) Meunier, B.; Bernadou, J. *Struct. Bond.* **2000**, *97*, 1–35.
- (131) Saltzman, H.; Sharefkin, J. G. *Org. Synth.* **1963**, *43*, 60–61.
- (132) Macikenas, D.; Skrzypczak-Jankun, E.; Protasiewicz, J. D. *J. Am. Chem. Soc.* **1999**, *121*, 7164–7165.

- (133) Klein, J. E. M. N.; Draksharapu, A.; Shokri, A.; Cramer, C. J.; Que, L. *Chem. Eur. J.* **2017**, *24*, 5373–5378.
- (134) Dror, A.; Fishman, A. *Comput Struct Biotechnol J* **2012**, *2*, e201209011.
- (135) Nakashima, Y.; Mori, T.; Nakamura, H.; Awakawa, T.; Hoshino, S.; Senda, M.; Senda, T.; Abe, I. *Nat. Commun.* **2018**, *9*, 104.
- (136) Hunt, A. J.; Farmer, T. J.; Clark, J. H. In *Element Recovery and Sustainability*; 2013; pp 1–28.
- (137) Crabtree, R. H. *Chem. Rev.* **2010**, *110*, 575.
- (138) Frey, P. A.; Reed, G. H. *ACS Chem. Biol.* **2012**, *7*, 1477–1481.

Bibliography

Publications

- **Kal, S.**; Que, L. Jr. Activation of a nonheme Fe^{III}-OOH by a second Fe^{III} to hydroxylate strong C-H bonds: possible implications for sMMO, *Angew. Chem. Int. Ed.*, **2019**, DOI: 10.1002/anie.201903465.
- Magherusan, A.M.; **Kal, S.**; Nelis, D.N.; Doyle, L.M.; Farquhar, E.R.; Que, L., Jr.; McDonald, A.R., A Mn^{II}Mn^{III}-peroxide complex capable of aldehyde deformylation, *Angew. Chem. Int. Ed.*, **2019**, 58, 5718-5722.
- **Kal, S.**; Draksharapu, A.; Que, L. Jr. Sc³⁺ (or HClO₄) activation of a nonheme Fe^{III}-OOH intermediate for the rapid hydroxylation of cyclohexane and benzene, *J. Am. Chem. Soc.*, **2018**, 140, 5798-5804.
- **Kal, S.**; Que, L., Jr., Dioxygen activation by nonheme iron enzymes with the 2-His-1-carboxylate facial triad that generate high-valent oxoiron oxidants, *J. Biol. Inorg. Chem.*, **2017**, 22, 339-365.

Presentations

- **Kal, S.;** Que, L. Jr. Activation of nonheme Fe(III)-hydroperoxo intermediates for cleaving strong C–H bonds, *UMN Metalloprotein Interest Group (MPIG) - Invited Lecture*, Minneapolis, MN, 2018. **(Talk)**
- **Kal, S.;** Que, L. Jr. Bio-inspired nonheme iron catalyst: Electrophilic versus nucleophilic iron-based active oxidant – effect on alkane hydroxylation, *UMN 253rd American Chemical Society National Meeting*, San Francisco, CA, 2017. **(Talk)**
- **Kal, S.;** Que, L. Jr. Factors influencing the electronic nature of the active oxidant in a bio-inspired non-heme mononuclear iron catalyst, *UMN 253rd American Chemical Society National Meeting*, San Francisco, CA, 2017. **(Poster)**